Synthesis and Modification of [2+3] Imine Cage based on 2,7,14-Triaminotriptycene

Xinyue HU

胡心悦

Dissertation

Heidelberg

2019

Inaugural-Dissertation

Zur Erlangung der Doktorwürde der

Naturwissenschaftlichen-Mathematischen Gesamtfakultät

der Ruprecht-Karls-Universität Heidelberg

vorgelegt von

Xinyue Hu, M. Sc.

März 2019

Tag der mündlichen Prüfung: 15.03.2019

Synthesis and Modification of [2+3] Imine Cage based on 2,7,14-Triaminotriptycene

Gutachter: Prof. Dr. Michael Mastalerz

Prof. Dr. Bernd F. Straub

Eidesstattliche Versicherung gemäß § 8 der Promotionsordnung der Naturwissenschaftlich-Mathematischen Gesamtfakultät der Universität Heidelberg

1.   Bei der eingereichten Dissertation zu dem Thema „*Synthesis and Modification of [2+3] Imine Cage based on 2,7,14-Triaminotriptycene*" handelt es sich um meine eigenständig erbrachte Leistung.

2.   Ich habe nur die angegebenen Quellen und Hilfsmittel benutzt und mich keiner unzulässigen Hilfe Dritter bedient. Insbesondere habe ich wörtlich oder sinngemäß aus anderen Werken übernommene Inhalte als solche kenntlich gemacht.

3.   Die Arbeit oder Teile davon habe ich bislang nicht an einer Hochschule des In- oder Auslands als Bestandteil einer Prüfungs- oder Qualifikationsleistung vorgelegt.

4.   Die Richtigkeit der vorstehenden Erklärungen bestätige ich.

5.   Die Bedeutung der eidesstattlichen Versicherung und die strafrechtlichen Folgen einer unrichtigen oder unvollständigen eidesstattlichen Versicherung sind mir bekannt.

Ich versichere an Eides statt, dass ich nach bestem Wissen die reine Wahrheit erklärt und nichts verschwiegen habe.

_____   _____

   Ort, Datum   Unterschrift

Die vorliegende Arbeit wurde von Oktober 2015 bis Januar 2019 in dem Arbeitskreis von Prof. Dr. Michael Mastalerz an der der Ruprecht-Karls-Universität Heidelberg angefertigt

Teile dieser Arbeit wurden bereit veröffentlicht:

Xin-Yue Hu, Wen-Shan Zhang, Frank Rominger, Irene Wacker, Rasmus R. Schröder, Michael Mastalerz, *Chem. Commun.* **2017**, *53*, 8616-8619: "*Transforming a chemically labile [2+3] imine cage into a robust carbamate cage*".

Poster:

Xin-Yue Hu, Frank Rominger, Michael Mastalerz, SUPRACHEM 2017, Aachen, Germany (Febuary 13-14, 2017): "*Synthesis of a Chemically Robust Porous [2+3] Carbamate Cage*".

Acknowledgments

I have to admit that these three and half years in Heidelberg is a treasure in my life. It's really a pleasure to study in this beautiful city and to meet so many good colleagues and friends.

My deepest gratitude goes first and foremost to Prof. Dr. Michael Mastalerz, my supervisor, for his constant encouragement and guidance. Without his consistent and illuminating instruction, this thesis could not have reached its present form. Besides his professional advices in chemistry, his enthusiasm in science also encourages me a lot.

 I would thank Prof. Bernd F. Straub to be my second "Gutachter" without any hesitation. I would thank all the stuffs and technicians from the Organisch-Chemisches Institut: Dr. Jürgen Graf and his colleagues (NMR measurements), Dr. Jürgen Gross and his colleagues (MS measurements), Dr. Frank Rominger, Sonja Pfrommer and Sarah Götz (crystal structure analysis) for the technical and analytical support. I would thank Anna Widera from the Anorganisch-Chemisches Institut for measuring the PXRD. I also thank Dr Wen-Shan Zhang in the BioQuant for doing in SEM experiments.

I thank all my colleagues in the lab, Dr. Gang Zhang, Dr. Sven Elbert, Dr. Xubin Wang, Xuan Yang, Dennis Reinhard, Alex Rowse, Fabian Uhrmacher, Jochen Lauer for their kind help and discussions during my research. I would especially thank Dr. Sven Elbert, Dr. Xubin Wang, M. Chem. Alex Rowse and M. Sc. Philippe Wagner for their kindly check for this thesis. I would also thank M. Sc. Philippe Wagner and Dr. Sven Elbert for helping me to translate the abstract into German. I also thank the internship student, Shuyi Yang, for his help in synthesizing the alkene chain modified [2+3] cage. I thank Ms Ute Gärtner for her help in chemical supplies and equipment maintenance.

I would thank to all the friends I met in Heidelberg, without you it would be much harder for these three years. Especially for Wan Zhang, it's really a wonderful thing that we met in Beijing and found out we both would come to Uni Heidelberg. I would also thank my friends in China, Danya Lv, Yingying Li, Jia Ren for flying 10 hours to Germany to visit me, without your communications it would be more difficult to start living in a new country.

Finally, I would show my gratitude to my father and mother because they give me the courage to continue. Without their support and love in the past 28 years, I would not have the chance to finish this journey.
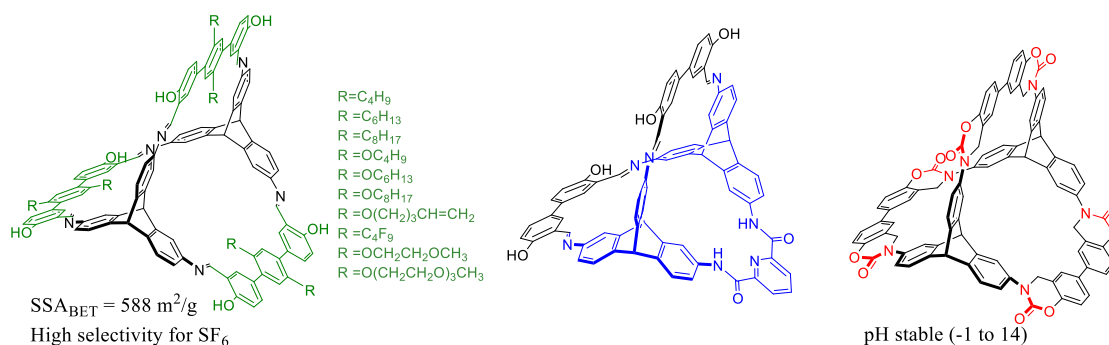
<div style="text-align: right">

Xinyue HU

胡心悦

</div>

Kurzzusammenfassung

Diese Arbeit befasst sich mit der Synthese und Modifikation von [2+3]-Iminkäfigen auf der Basis von 2,7,14-Triaminotriptycen. Aufgrund des starren 3D-Gerüsts und der D_{3h}-Symmetrie von Triptycenen wurden viele poröse Käfigverbindungen basierend auf Molekülen synthetisiert. Die Modifikation von Käfigverbindungen mit funktionellen Gruppen ist jedoch immer noch eine Herausforderung.

Im Allgemeinen sind die postsynthetische Modifikation von vorsynthetisierten Käfigen und die Modifikation molekularer Vorläufer zwei Hauptstrategien, um funktionelle Gruppen in Käfigverbindungen einzuführen. Durch Modifizierung der Aldehydbausteine wurden zehn verschiedene Seitenketten in [2+3] Terphenyliminkäfige eingeführt. Die Löslichkeit in organischen Lösungsmitteln ist für alle diese neuen Käfige im Vergleich zu den ursprünglichen verbessert. Unter diesen Käfigen weist der Perfluorbutan-modifizierte Käfig eine spezifische Oberfläche bis zu $SA_{BET} = 588$ m^2/g und hohe Henry-Selektivitäten $S_{SF_6/N_2} = 107$ für Schwefelhexafluorid gegenüber Stickstoff auf, was eine mögliche Anwendung bei Trennung von Gasgemischen aufzeigt.

Neben den Aldehydbausteinen wurde eine neue Art von Aminbausteinen aus Triaminotriptycen und Pyridindicarbonsäurechlorid aufgebaut. Dieser neue Aminobaustein wurde verwendet, um mit einer Reihe von Disalicylaldehyden mit unterschiedlichem Abstand zwischen den Aldehydgruppen Iminkäfige zu bilden. Die Ergebnisse belegen, dass die Form des Käfigs durch die Länge der Aldehydbausteine beeinflusst wird.

Im dritten Teil wurde mittels der postsynthetischen Modifikationsstrategie ein Carbamatkäfig in zwei Schritten auf Basis eines [2+3]-Iminkäfigs (gebildet aus Triaminotriptycen und Bisphenylsalicylaldehyd) synthetisiert. Dieser Carbamatkäfig zeigt eine hohe pH-Stabilität von pH = -1 bis 14, was durch NMR-Spektren, SEM- und Gassorptionsexperimente nachgewiesen wurde.

$SSA_{BET} = 588$ m^2/g
High selectivity for SF_6

R=C$_4$H$_9$
R =C$_6$H$_{13}$
R =C$_8$H$_{17}$
R =OC$_4$H$_9$
R =OC$_6$H$_{13}$
R =OC$_8$H$_{17}$
R = O(CH$_2$)$_3$CH=CH$_2$
R =C$_4$F$_9$
R =OCH$_2$CH$_2$OCH$_3$
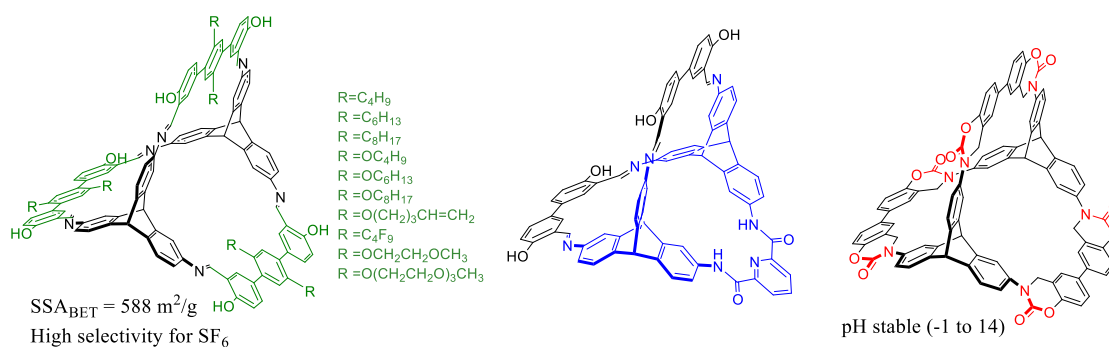R =O(CH$_2$CH$_2$O)$_3$CH$_3$

pH stable (-1 to 14)

Abstract

This thesis is focused on the synthesis and modification of [2+3] organic imine cages based on 2,7,14-triaminotriptycene. Many porous cage compounds have been synthesized based on triptycene precursors because of its rigid 3D skeleton and a D_{3h} symmetry. However, modifying the cage compounds with functional groups which may empower the cages is still challenging.

In general, post-synthetic modification in pre-synthesized cages and modification of molecular precursors are two main strategies to introduce functional groups into cage compounds. By modifying aldehyde building blocks, ten different side-chains were introduced to the [2+3] terphenyl imine cages. Solubility in organic solvent was improved for all these new cages compared with the unfunctionalized one. Among these cages, the perfluorobutyl chain modified cage exhibits specific surface area up to $SA_{BET} = 588$ m^2/g and high Henry selectivity $S_{SF6/N2} = 107$ for sulphur hexafluoride over nitrogen, which shows a potential application in the separation of sulphur hexafluoride.

Besides the aldehyde building blocks, a new amine building block was constructed by triaminotriptycene and pyridine dicarbonyl dichloride. This new amino building block was used to react with a series of salicylaldehydes with different distance between the aldehyde groups, and the results prove topologies of cage can be affected by the length of the aldehyde precursors.

In the third part, through a post-synthetic modification strategy, a carbamate cage was synthesized after two steps based on a [2+3] imine cage (formed by triaminotriptycene and bisphenyl salicylaldehyde). This carbamate cage exhibits high pH stability from pH =-1 to 14 which is proved by NMR spectra, SEM and gas sorption experiments. This is one of the most stable cage compounds reported so far

R=C$_4$H$_9$
R =C$_6$H$_{13}$
R =C$_8$H$_{17}$
R =OC$_4$H$_9$
R =OC$_6$H$_{13}$
R =OC$_8$H$_{17}$
R =O(CH$_2$)$_3$CH=CH$_2$
R =C$_4$F$_9$
R =OCH$_2$CH$_2$OCH$_3$
R =O(CH$_2$CH$_2$O)$_3$CH$_3$

SSA$_{BET}$ = 588 m^2/g
High selectivity for SF$_6$

pH stable (-1 to 14)

Table of Contents

1 Introduction

1.1 Molecular cage compounds

Molecular cages have drawn more and more interest from scientists recently because this type of compounds exhibit good properties and potential applications in the field of supramolecular chemistry [1] and porous materials.[2] According to the International Union of Pure and Applied Chemistry (IUPAC), a cage compound is a "polycyclic compound with the shape of a cage".[3] Molecular cage compounds can be divided into two classes based on their connection mode: the supramolecular cages and the organic cages.[4] The supramolecular cages are constructed by non-covalent interactions, such as hydrogen bonds [5] and coordination interactions.[6] A lot of coordination cages have been reported.[7] They not only show the possibilities to construct different kind of polyhedron by simple precursors,[7] but also exhibit the applications in host-guest chemistry.[8] For example, some coordination cages have been used as "molecular flask", which could improve the selectivity of organic reactions.[9]

The organic cage compounds are constructed by covalent bonds.[10] Compared with supramolecular cages, organic cages are relatively rare because the synthesis is more difficult.[11] The history of organic cage compounds goes back to 1964, when a platonic hydrocarbon, cubane, was successfully synthesized.[12] After nearly twenty years, dodecahedrane was also synthesized by two different research groups.[13] In 1967, Jean-Marie Lehn constructed a three-dimensional molecule, the cryptand, with a reaction similar to the one used to construct crown ethers.[14] This molecule probably was the first example of a functional cage molecule because of its recognition of cations. Since then, some other functional organic cages, like the sideropohore from the Vögtle's group [15] and the carcerand from the Cram group,[16] have been synthesized.

1.2 Synthesis of organic cages

1.2.1 Cages formed by irreversible bonds

The concept of organic cage compounds has been known for more than 50 years,[11, 17] but the properties of these compounds have not been well investigated because their synthesis is difficult. In the beginning, most organic cage compounds have been synthesized step by step by irreversible bond formations, for example, cross-coupling reactions[18] or amidation.[15] Cages synthesized by this strategy have good chemical stability, but the overall yields are

usually low even though the yields of each individual step might be high,[19] because most irreversible bonds formations are normally controlled by kinetic factors.

The amide bond formations were often used as the final cyclization step to construct the cage compounds, and a good yield could be obtained in some cases.[10] The Vögtle's group synthesized several cage compounds with different shapes through amide-bond formation, but the overall yields were around 10%.[15, 20] The Raymond group used an iron(III) cation as a template to pre-organize three catechol units. Then in the final cyclization step, the complex was reacted with triamine to get the final amide cage with a relatively high yield of 70%.[21] Davis and co-workers synthesized a macrotricyclic cage with 62% yield in the final cyclization step.[22]

Nucleophilic substitution reactions are also used to form covalent bonds of cages.[23] The big caesium cation was used as the template to pre-organize the pyridine precursor **2** before reacting with triol precursor **1** (Scheme 1). The yield of this cage product **3** is 95%, but because of the limitation of the size of metal cations, larger structures could not be obtained by this strategy.
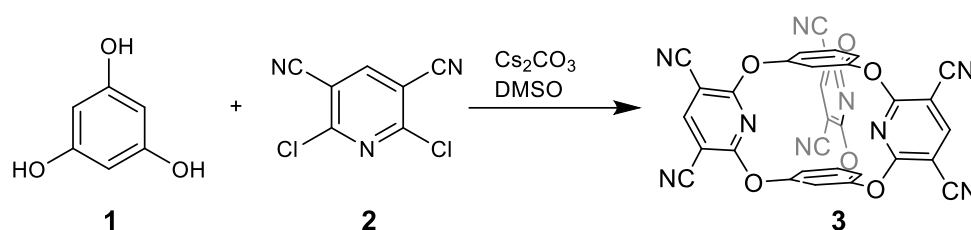
Scheme 1. Synthesis of small cage by irreversible C-O bonds formation via nucleophilic aromatic substitution.[23]

Organic cages with a carbon-carbon backbone are quite attractive. Besides the chemical and thermal stability, the scaffold of the carbon-carbon cage can be considered as a precursor to synthesize fullerene.[24] The first example of a carbon-carbon cage was obtained by Wennerström and co-workers in 1977.[25] They used mesitylaldehyde and a bisphosphonium salt *via* a sixfold Wittig reaction to obtain the final cage compound in 1.7% yield. The Vögtle group reported a seven-step synthesis of a tetrahedral hydrocarbon cage with the overall yield of 3%.[24] Starting from hexabromobenzene and furan, the Stoddart group successfully synthesized the trinacrene in four steps, but the overall yield was lower than 0.01%.[26]

1.2.2   Cages formed by reversible bonds

The other useful way to synthesize cage compounds is to use dynamic covalent bond formation. Dynamic covalent chemistry (DCC) is "the combinatorial molecular chemistry under

thermodynamic control."[27] It relates to the chemical reactions carried out reversibly under conditions of equilibrium control.[28] The products distributions in DCC reactions depend on the relative stabilities of the final products.[28a] So the percentage of the products in dynamic chemical systems can be controlled by introducing certain features into the starting materials which can make the desired product more stable, or by removing the condensation products to lead the reaction equilibrium toward the desired products.[28a] Until now, more than twenty kinds of dynamic covalent reactions,[28] for instance, the Aldol reaction,[29] phenol/aldehyde condensation,[30] imine formation[31] and boronic ester condensation,[32] have been reported. A series of organic cages have been synthesized through dynamic covalent reactions with high yield.[33] Among all the dynamic covalent reactions, boronic acid condensations[34] and imine condensations[35] are the two most commonly reactions used to synthesize organic cage compounds (Scheme 2).
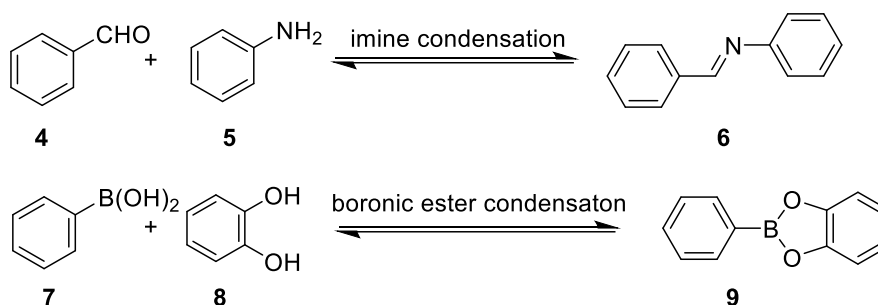
Scheme 2. Dynamic covalent reactions based on the imine condensation and boronic ester condensation.

1.2.2.1 Cages formed by imine condensation

The first example of a cage formed via imine condensation, the hemicarcerand, was reported by Cram and co-worker in 1991.[36] This cage was obtained by reaction of diaminobenzene and resorcinarene functionalized with aldehydes. After that, a number of organic cage compounds were obtained through condensation of different amines and aldehydes.[37]

In 2006, the Warmuth group reported a [6+12] octahedral cage (compound **12** in Figure 1). This cage was obtained by condensation reaction between the four formyl-substituted cavitand **10** and the ethylendiamine **11** in a one-pot syntheses with a yield of 82%.[38] Later, they successfully synthesized a [6+8] rhombicuboctahedral nanocapsule by condensation of the same tetracavitand **10** and 1,3,5-tris-(p-aminophenyl) benzene.[39] DOSY NMR spectrum showed the solvodynamic diameter of the nanocapsule was 3.9 nm. They also observed that the solvents used in this reaction would affect the size of the cages.[40] With the same tetracavitand **10** and diamine **11**, octahedral [6+12], tetrahedral [4+8] and square antiprismatic

[8+16] shaped products were obtained as main product in $CHCl_3$, THF and CH_2Cl_2, respectively. They proposed these phenomena might occur because of the improper solvation of the flexible linkers. The solvent molecules residing inside the cavity tended to interact with the internal surface of the cage, which gave enough time to create a new interaction with the flexible linkers. The different solvent molecules would form different geometrical conformations with the linkers, which lead to the different shapes of the products.
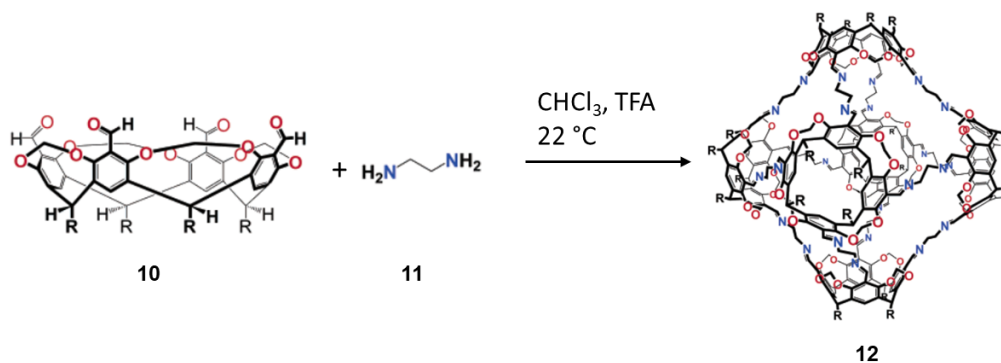
Figure 1. Synthesis of [6+12] organic cage **12**. Reproduced with permission.[40] Copyright 2006, American Chemical Society.

The Cooper group reported a series of [4+6] and [2+3] organic cage compounds synthesized through imine condensation.[41] In 2009, they synthesized three different [4+6] cages **16**, **17**, **18** (cage **18** was first reported by Gawronski and co-workers in 2008)[42] by condensation of 1,3,5-triformylbenzene **13** and 1,2-ethylenediamine **11**, 1,2-propylenediamine **14** and (R, R)-1,2-diaminocyclohexane **15**, respectively (Figure 2).[43] These three cages were obtained as crystalline solids after leaving the reaction mixtures still for 60 h. Then they used gas adsorption experiments to demonstrate the porosity of the crystalline solids. Among these first three cages, cage **18** showed interconnected permanent pore structures with a specific surface area of $SA_{BET} = 624$ m^2/g. Cage **16** was nonporous at first, but after recrystallizing in dichloromethane and o-xylene, this cage showed a porous polymorph with a specific surface area of $SA_{BET} = 533$ m^2/g.

More detailed studies were done to investigate the influence of the precursor geometry. They found if they used alkanediamine building blocks with different chain length, either the [2+3] imine cages or the [4+6] imine cages would form.[44] An odd-even effect was observed: diamines with even number of carbon atoms (1,2-ethanediamine, 1,4-butanediamine) formed preferably [4+6] cages with 1,3,5-triformylbenzene and those with odd numbers (1,3-

propanediamine, 1,5-pentanediamine) formed [2+3] cages. By computational study, the thermodynamically stabled cages and the lowest energy conformers were predicted.
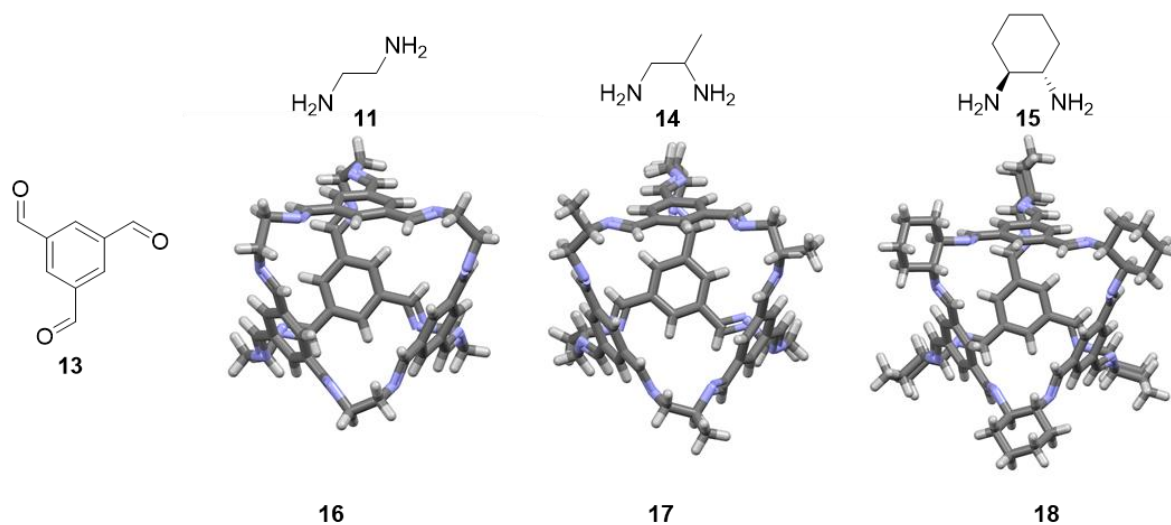
Figure 2.Synthesis of [4+6] organic cages **14**, **15**, **16**. Hydrogen atoms are omitted for clarity. Carbon and nitrogen atoms are coloured grey and blue, respectively. Reproduced with permission. [43] Copyright 2015, Springer Nature.

The Mastalerz group synthesized a series of [4+6] or [2+3] imine cages based on triptycene building blocks.[33a] The [4+6] cage **23** was obtained by reacting triaminotriptycene **19** with salicyldialdehyde **20** with a 58% yield (Figure 3).[45] The reactions using salicyldialdehydes with substituents of different bulkiness in the *para*-position to the phenolic hydroxyl group were also done and the corresponding cages were formed.[46] Among all these [4+6] imine cages, the largest specific surface area was $SA_{BET} = 2071$ m^2/g, which was achieved by cage **23**.[46-47] They also reported exo-functionalized [4+6] cage compound by imine condensation reaction of triaminotriptycene **19** with 4,6-diformayl-2-methylresorcinol,[48] and the specific surface area of this exo-cage was $SA_{BET} = 919$ m^2/g.

By changing the bite angles of the ditopic dialdehydes from 120° to 60°, a series of smaller [2+3] cages were synthesized by triamine **19** and bissalicylaldehydes which have different linkers.[49] Seven different bissalicylaldehydes were used to construct [2+3] cages, and the distance between the aldehyde groups of these seven aldehyde linkers vary from 9.3 Å to 17.8 Å. Although the NMR spectra of some cages could not be obtained because of the bad solubility, (HR)-MS, IR, elemental analysis and single crystal structures proved the formation of these cages. [49b]

Two salicylaldehyde units could be linked by rigid phenyl linker (**21** in Figure 3) or flexible linker (**25** in Figure 3), therefore, the influence of the molecular rigidity of building blocks on

the formation of organic cage compounds have been investigated. The syntheses and properties of [2+3] cages with rigid linker **21** and flexible linker **22** were studied (Figure 3). [49] The flexible linker **22** showed a negative effect on the cage formation compared with the rigid linker **21**. The crude product from the condensation reaction of bisaldehyde **21** and triamine **19** showed almost pure cage **24** in the NMR spectrum, but the crude product from the reaction between bisaldehyde **22** and triamine **19** showed a number of side products even though cage **25** could be detected from NMR spectrum. The isolated yield of cage **25** (10%) was lower than cage **24** (69%). Aside from the influence on the formation of the cage compounds, the rigidity of the building blocks also affected the gas sorption properties. The BET surface area of the flexible cage **25** ($SA_{BET} = 30$ m^2/g) was lower than that of the rigid cage **24** ($SA_{BET} = 744$ m^2/g).
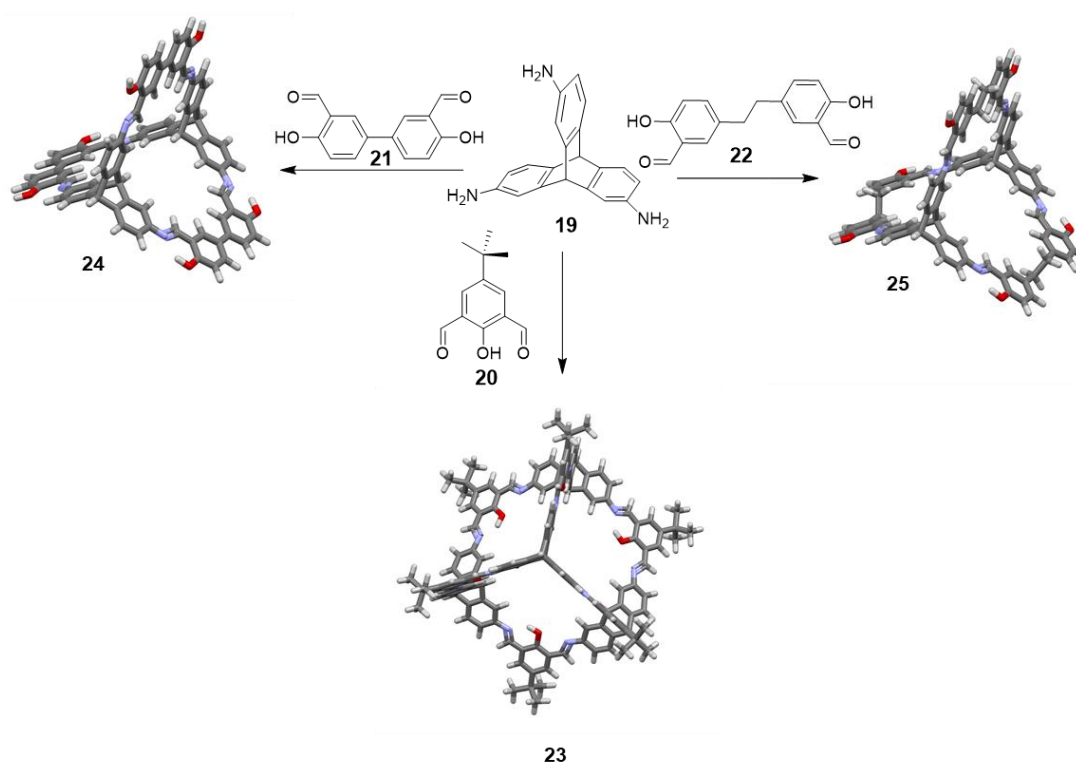
Figure **3**. Synthesis of [4+6] cage **23** and [2+3] cage **24** and **25** starting from triamino triptycene **19**.[45, 49]

1.2.2.2 Cages formed by boronic ester condensations

The condensations reaction between boronic acids and diols has been widely used to synthesize organic cage compounds.[10, 50] The Mastalerz group reported a boronic ester cage **26** by a 48-fold condensation of triptycene precursor **24** and triboronic acid **25** (Figure 4).[51] From the single crystal structure, the cavity of cage **26** was very large. The distance between the bridgehead atoms of two opposite triptycene units was 2.9-3.1 nm. This cage exhibited a high specific surface area of $SA_{BET} = 3758$ m^2/g, which is the highest specific surface area value

obtained by organic cage compounds so far. With a similar triptycene precursor **24'** (hexyl chains were introduced into the bridgehead positions instead of the ethyl group on the aromatic ring) and triboronic acid **25**, the other boronic ester cage **27** was successfully synthesized (Figure 4).[52] By vapour diffusion of *n*-hexane into a solution of cage **27** in chloroform, suitable single crystals were obtained for X-ray analysis and an interlocked catenane formed by two cages **27** was found in the crystalline state (Figure 4). The catenane **27** also showed a high specific surface area (SA_{BET} = 1540 m^2/g). In 2018, the Mastalerz group reported a series of [4+6] boronic ester cages obtained through the reaction between tribrominated hexaol triptycene and three diboronic acid building blocks with different degree of fluoride substitution.[53] The nonfluorinated cage showed a specific surface area of SA_{BET} = 511 m^2/g and a relatively high selectivity of ethane over ethylene.
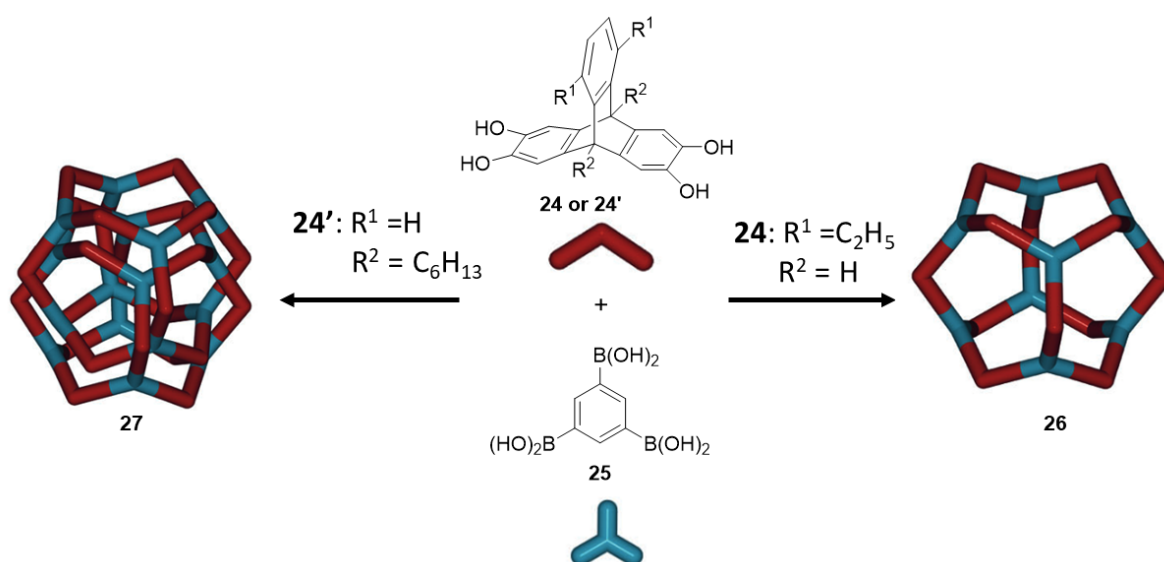
Figure **4**. Synthesis of the [12+8] boronic ester cage **26** and catenane **27**. Reproduced with permission.[51, 52] Copyright 2014, John Wiley and Sons.

The Beuerle group reported the shape-selective formation of the trigonal bipyramidal, tetrahedral and cubic TBTQ-based cages by changing the bite angle of the diboronic acid counterpart from *ortho* to *meta* or *para*, respectively (**29**, **30**, **31** in Figure 5).[54] Generally, wider angles correspond to more building blocks per cage. In addition, competitive building blocks would result in either narcissistic or social self-sorting. If the angles of the acid derivative mixtures are 60° and 120° or 60° and 180°, the narcissistic self-sorting products were formed. However, if the angles are 120° and 180°, the social self-sorting product was found.

Some other types of dynamic covalent reactions are also used in cage synthesis, but the number of examples is much smaller than the imine condensation and the boronic acid condensation.[50]

For example, the alkene metathesis and the alkyne metathesis were used in the formation of shape-persistent molecular cages.[55] Disulfide formation[56] and orthoester exchange[57] have also been used in few cases.
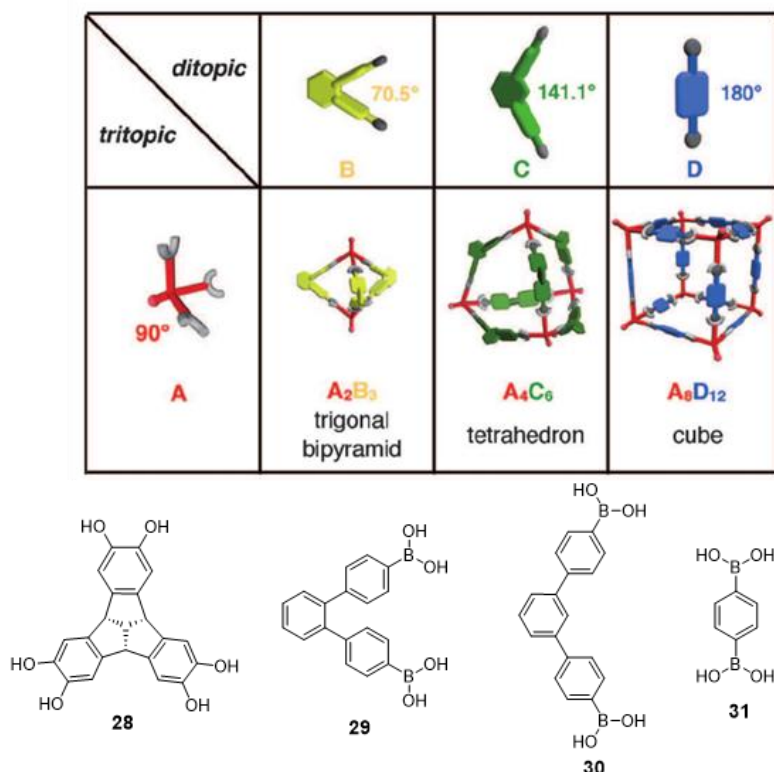
Figure 5. Shape-selective synthesis of molecular cage compounds from tritopic units **28** and ditopic linkers **29**, **30** and **31** with different angular disposition based on the directional bonding approach. Reproduced with permission. [54] Copyright 2015, John Wiley and Sons.

1.3   Functionalization of organic cages

The organic cage compounds can be functionalized endohedral[58] or exohedral[59] selectively, and the function groups can be introduced by two strategies, 1) synthesizing the cage directly from precursors with functional groups, and 2) post-synthetic modification of a pre-synthesized cage.[50] By these two methods, several functional groups have been introduced into organic cage compounds.[4]

Chiral cages have been synthesized by serval groups via using chiral precursors.[50, 60] The Mastalerz group reported the chiral self-sorting of [2+3] imine cages formed by a salicyaldehyde and two chiral trisamino TBTQs in 2017.[61] Both narcissistic self-sorting and social self-sorting were observed in this system. In most of the solvents they scanned this reaction, the narcissistic self-sorting product was the favoured one compare to the social self-

sorting product, and the ratio of two narcissistic self-sorting products were between 86: 14 (in 1,4-dioxane) and 63: 37 (in ethanol). But in ethyl acetate, the formation of social self-sorting product was enhanced by the its lower solubility. A Van't Hoff plot was obtained by recording NMR spectra in THF-d_8 at different temperatures, which revealed the formation of naricissistic self-sorting products were entropy favored while the social self-sorting product was enthalpy favored.
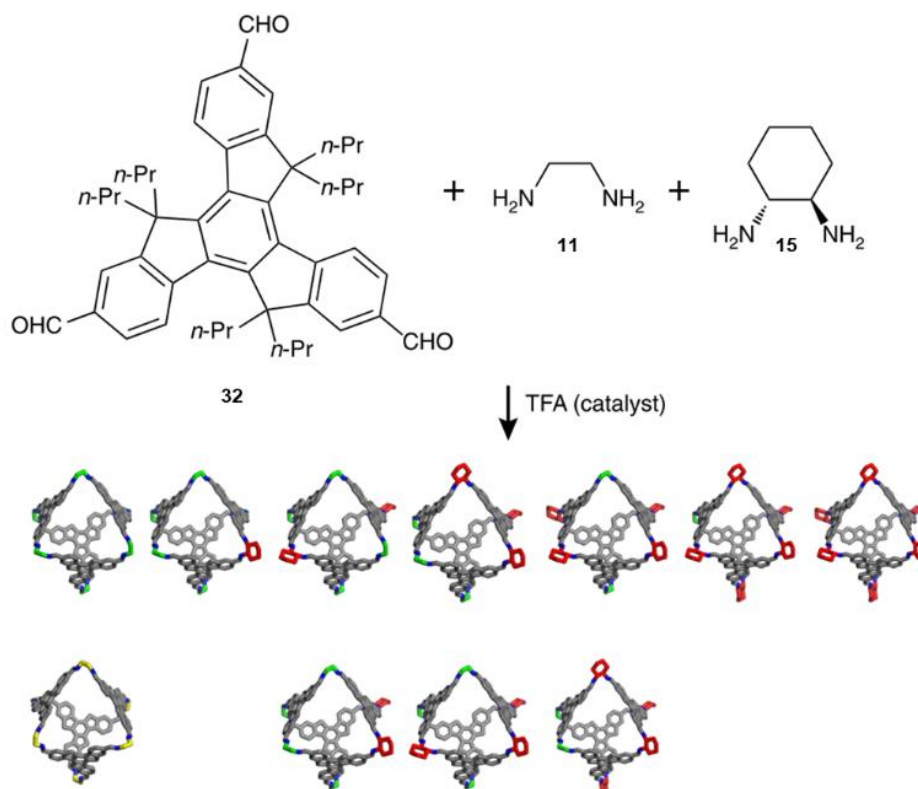
Figure 6. Reaction of two different diamines **11** and **15** with trialdehyde **32** leads to a mixture of molecular octahedra. The ethyl and cyclohexyl groups on the octahedral are shown in green and red, respectively. Reproduced with permission. [62a] Copyright 2018, Creative Commons.

Cao and co-workers also reported several chiral cages.[62] In 2016, they used a 2D chiral truxene trialdehyde and ethylene diamine to construct the 3D chiral polyhedrons. Two enantiomers were obtained in a 1:1 ratio either in the crystal state or in the solution (proved by crystal structures, HPLC and circular dichroism). By this strategy, they successfully transferred the chirality from 2D to 3D structures.[62a] Later, they studied amplification of chirality in self-assembling systems (sergeants-and-soldiers effect) through a series of octahedrons constructed by truxene trialdehyde **32** , ethylene diamine **11** and chiral (*R, R*)-diaminocyclohexane **15** (two

amine precursors in the ratio of 1:1, Figure 6).[63] Through chiral HPLC they separated six different octahedrons containing both types of diamine linkers, and found that all octahedrons containing one or more chiral linkers exhibited the same CD spectrum as the octahedron containing pure chiral linkers, indicating that one chiral linker suffices to control the conformation of all achiral linkers in an octahedron. They also introduced chiral fluorescent tetraphenylethylene precursors into a molecular cube and successfully achieved a series of cubic cages with chirality and fluorescence, which may provide a new method for synthesizing chiral sensors and luminescent materials.[64]
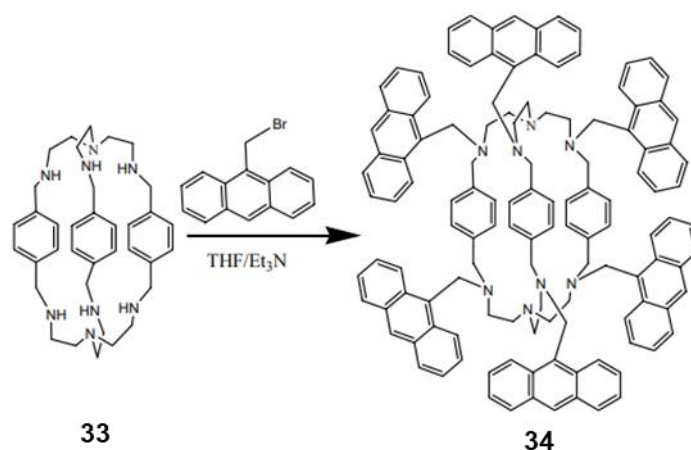
Scheme 3.Synthesis of hexannthryl octaaminocryptand **34**. Reproduced with permission.[66] Copyright 2006, American Chemical Society.

Post-synthetic modifications have been used to introduce functional groups into materials such as MOFs and COFs.[65] Until now, only a few of examples have been reported about the post-synthetic modifications on the organic cage compounds. By this strategy, some cage compounds which are difficult to synthesize directly by precursors can be synthesized. In 2006, Ghosh *et.al* gave an example of a post-synthetic modification of an organic cage compound (Scheme 3).[66] They functionalized the secondary nitrogen atoms of amine cage **33** using anthryl groups with a yield of 60%.

The Mastalerz group reported the post-synthetic modification of cage **23** through a Williamson etherification (Scheme 4), which allowed to "fine-tune" the pore structure of the product in the solid state.[67] After the reactions, the phenolic protons of cage **23** were substituted by five different groups (methyl, propyl, allyl, benzyl and 4-nitrobenzyl), giving cages **40**-**44** with the yields between 63% and 81% (except the cage **44** with the yield of 12%). Cages **40**-**44** were also synthesized by imine condensation directly from triamine **19** and salicylaldehydes **35**-**39**,

but the yields were much lower because the corresponding cage products were not the main products of a DCC library.
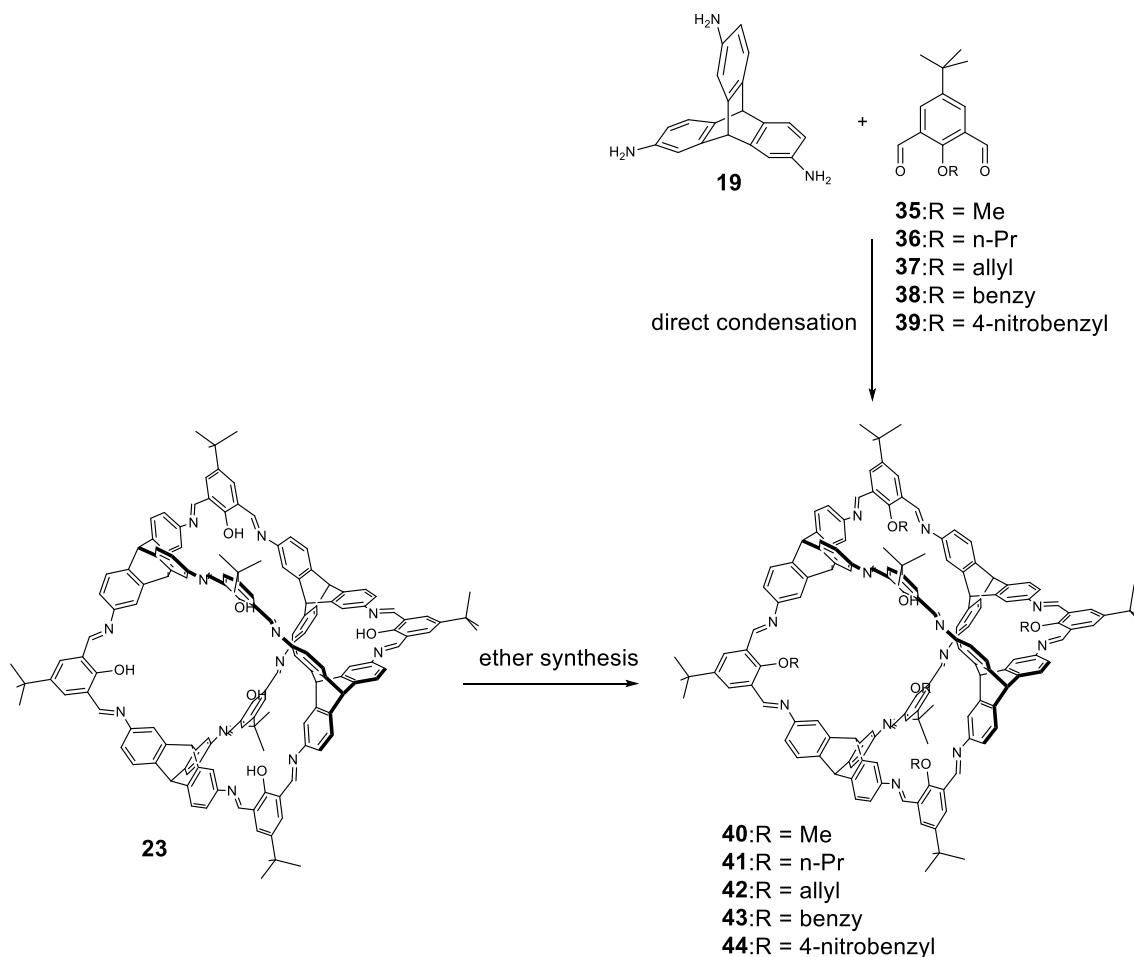
Scheme 4. Synthesis of cages **40**-**44** from cage **23**.[67]

The Cooper group also used acid halides to react with the amine [4+6] cage and formed a range of dodecanamide organic cages.[68] The Mukherjee group reported a new synthetic protocol which based on the multicomponent reaction of a formaldehyde, a secondary amine and a terminal alkyne catalyzed by copper(I).[69] By using this reaction, they modified an organic amine cage with phenyl-, xylyl- and naphthyl-acetylene groups. These new cages were fluorescent and could be used as chemosensors for the detection of nitroaromatics. Moore and co-workers utilized post-synthetic modifications (the bromination or the hydrogenation) on an aryleneethynylene-based cage and synthesized two new cages in high yields (the brominated one: 40%, the hydrogenated one: 90%).[70] These modifications characteristically affected the crystal packing motifs and gas adsorption capacities, which showed a relationship between shape-persistence and porosity. The cage without modification showed a specific surface area

of $SA_{BET} = 509$ m^2/g, while the hydrogenated cage, which had the more flexible linkers, had a specific surface area of $SA_{BET} = 0$ m^2/g.

1.4 Porous molecules and porous organic cage compounds

Porous materials have attracted scientific and industrial interest because of their broad applicability.[71] The research in porous materials is mostly focused on extended solids like zeolites,[72] metal-organic frameworks (MOFs)[73] and covalent organic frameworks (COFs).[74] These materials exhibit high specific surface area[75] and applications in many fields such as molecular separation,[76] catalysis,[77] and environmental science.[78]

Apart from these polymeric solids, some discrete molecules, which can form porous structures, also have been reported.[79] Compared with porous networks, porous molecules have potential benefits in 1) solubility, which gives processing advantages such as making thin porous films after solution casting,[80] 2) synthetic diversification,[81] and 3) mobility,[81] because the molecular crystals are connected with noncovalent interactions, which make them more flexible than porous network.

The porosities of these porous molecules mainly depend on their packing motifs, which can generate pores between neighbouring molecules (the extrinsic pores).[82] Because the extrinsic pores are only resulted from the crystal packing, the elegant designs of the molecules are quite important.[83] But in most cases, these studies only generated specific structures, which made it difficult to introduce functional groups because sometimes even a small change of the molecules can result in different packing motifs.[84] Only a few examples have been reported that the packing motifs of the porous molecules kept the same even the functional groups were different,[85] which made it possible to use the functional groups to adjust the diameters and chemical environment of the extrinsic pores.[84]

The Davis group reported a series of porous molecules, what they called "nanoporous sterioidal ureas (NPSUs)", based on cholic acid **45** (Figure 7).[86] In 2005, they synthesized three steroidal ureas (**46** in Figure 7, $R^1 = CF_3$, NHPh and OBu^t) and found that these three molecules had the same packing motif in the crystalline state. Molecules could form one-dimensional channels with different diameters (from 11.6 Å to 14.3 Å). [86a] Later they expanded the NPSUs family by synthesizing different monomers **47** (Figure 7).[86b] In this case they kept R^1 unchanged while R^2 was replaced with different aromatic moieties (for instance, $R^2 = CH_2CH_2$naphthyl, CH_2CH_2pyrenyl). According to the crystal structures, the aromatic groups covered the pore

walls which resulted in a hydrophobic environment of the channels. The different size of the aromatic groups could adjust the diameters of the channels from 5.5 Å to 7.6 Å.
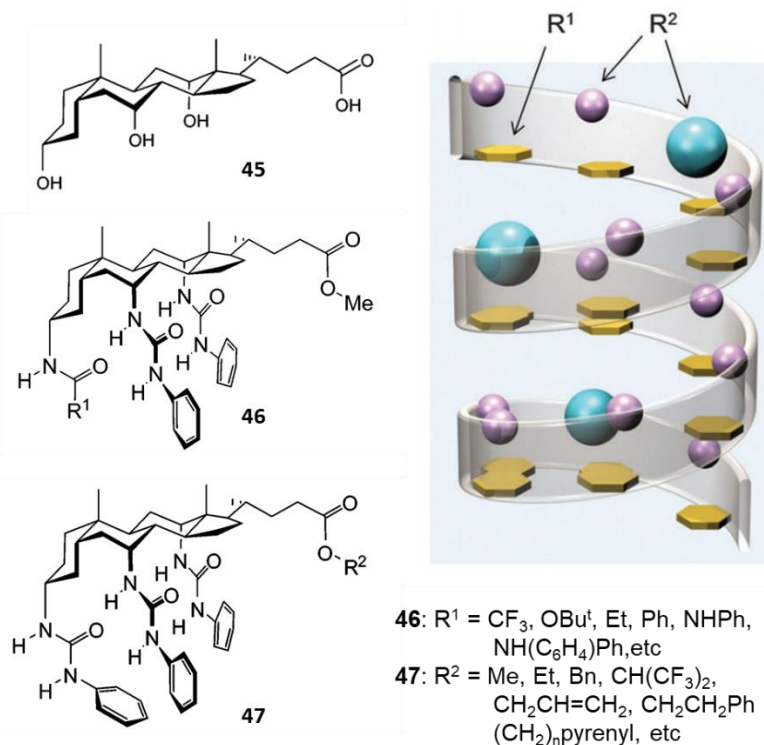
Figure 7. Left: formulae of cholic acid **45** and general structure of NPSU monomers **46** and **47**. Right: schematic depiction of channels in crystals, showing the helical arrangements of R^1 and R^2. Reproduced with permission[86c] Copyright 2011, John Wiley and Sons.

As R^1 and R^2 seemed not to affect the packing motifs of the molecules, and the unit cell parameters of these cholic acid based molecules were similar, Davis and co-workers created the porous "organic alloys"[87] by co-crystallizing different molecules from this NPSUs family.[86c] By this method, they could 1) obtain co-crystals with different functional groups inside the channels, and 2) introduced steroidal ureas with some large functional groups such as the perylenediimide, into this NPSU packing system. Until now, more than thirty NPSU crystal structures have been reported and the diameters of the channels varied from 0 to 14.3 Å.[86d, e] This indicated that by changing the functional groups R^1 and R^2, they could easily control the size, the shape and the chemical environment of the pores in crystalline states without damaging the pores of the crystals.

Porous organic cage compounds are another kind of porous molecules, because the porosity comes from both extrinsic pores and intrinsic cavities.[88] Sometimes cage compounds exhibit porosities in the amorphous states.[88, 89] In 2009, the Cooper group demonstrated permanent porosity of [4+6] cage **18** (Figure 2) by gas sorption experiments.[43] This field has developed

quite fast after that. The Mastalerz group synthesized a series of porous imine and boronic ester cages based on triptycene building blocks.[33] The highest specific surface area of an organic cage compound (SA_{BET} = 3758 m^2/g) was obtained by the boronic ester cage **26** (Figure 4) reported by this group in 2014,[51] and this specific surface area is comparable to many porous networks.

β polymorph
porous to H_2 but not N_2

α polymorph
non-porous to H_2 and N_2

γ polymorph
porous to H_2 and N_2
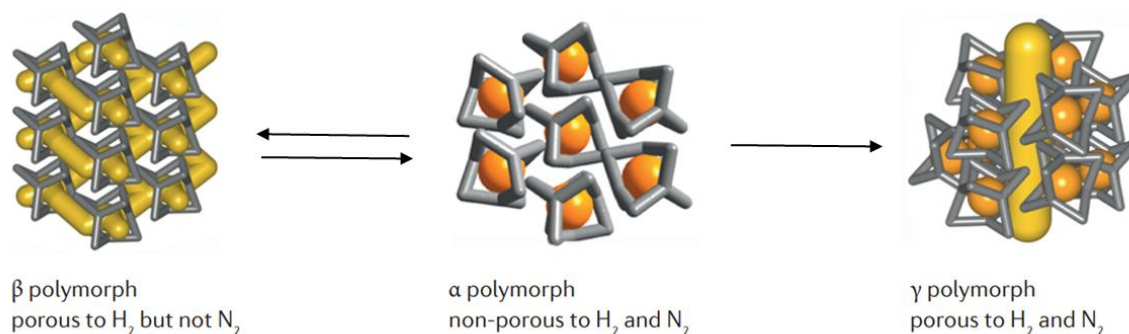
Figure 8. Cage **16** can be induced to pack in different polymorphs with different gas selectivity.[90] Reproduced with permission,[88] Copyright 2016, Springer Nature.

One of the advantages of porous cage materials is that they can "switch" the porosity "on and off" by changing the polymorphism of the organic cage compounds. [4] An example was done by the Cooper group.[90] They discovered that cage **16** (structure in Figure 2) could form three different polymorphs from different solvents (Figure 8). The polymorph α was nonporous while the polymorphs β and γ were porous. The polymorph α could be transformed into β by exposing the solid to dichloromethane vapour and the transformations of these two polymorphs were reversible (exposing β into ethyl acetate vapour to obtain α). The polymorph γ was obtained by recrystallizing cage **16** in o-xylene.[43] By gas sorption experiments, they found the polymorph γ was porous to both nitrogen and hydrogen at 77 K. The polymorph β exhibited high selectivity because it showed nonporous to nitrogen at 77 K, but it adsorbed significant amounts of hydrogen (5.9 mmol/g).

The organic cages also can generate an "organic alloy" by co-crystallizing two or more different cage compounds together.[88, 91] Cages **16**, **18** (structures showed in Figure 2) and **48** were used to produce the binary or ternary crystals (Figure 9).[92] These three cages have similar symmetry and the only difference is the vertices of the cages (see in Figure 9). Cage **18** and **48**, which are both locked in the *R* configuration, were added into cage **16** solution, as it showed in Figure 9, the chirality of racemic cage **16** (always in *S* enantiomer) was resolved by co-crystallization with **18** and **48**. By changing the ratio of **18-R**: **48-R**, a range of ternary co-crystals were obtained and studied. The unit cell dimensions decreased linearly with the

proportion of cage **48-R**,[93] which made it possible to "fine-tune" the surface areas by changing the molecular composition. The gas sorption experiments proved that with different ratio of **18-R** : **48-R**, the apparent Brunauer-Emmett-Teller (BET) surface areas of the ternary co-crystals ranged from 373 to 670 m^2/g.
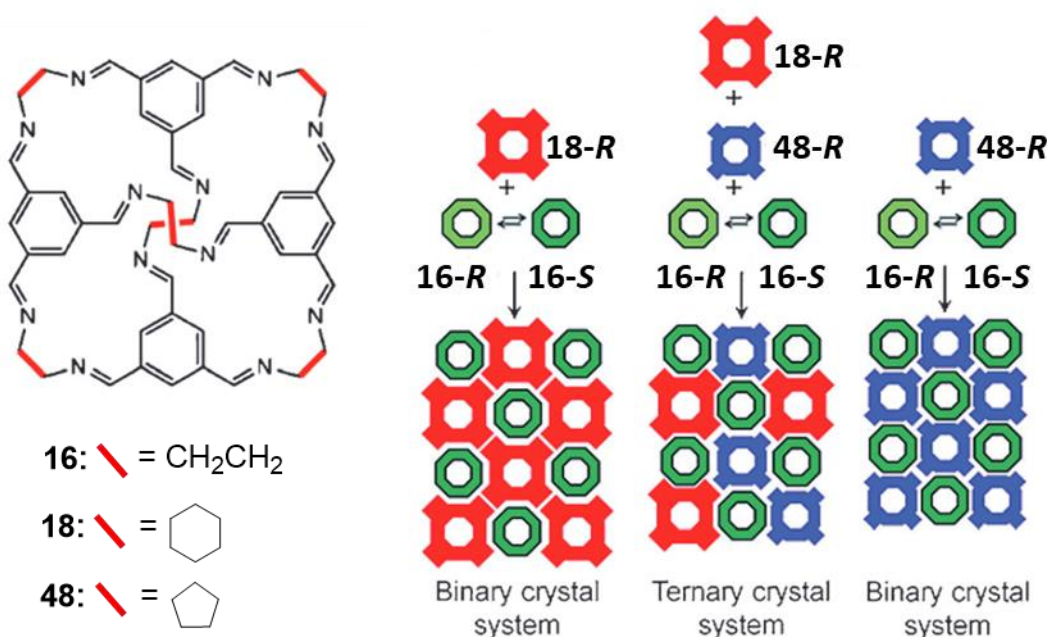
Figure 9. The formation of a ternary cage co-crystal using cage **16**, **18** and **48**. Left: Chemical structure of cage **16**, **18** and **48**. Right: the chirality of 16 is resolved by co-crystallization with **18-R** and **48-R**. Reproduced with permission,[92] Copyright 2012, John Willey and Sons.

1.5 Applications of organic cage compounds

Up until now, a number of organic cage compounds have been successfully synthesized,[10] and their potential applications in several fields such as molecule recognition and separation,[94] gas storage,[95] and stabilizing reactive species[96] have been investigated.

The storage of natural gas and selective adsorption between gases like CO_2/CH_4, CO_2/N_2, H_2/N_2 are important in the industrial and the environmental fields.[97] A quadrangular prismatic tricyclooxacalixarene cage based on tetraphenylethylene (TPE) showed a good CO_2 uptake capacity of 12.5 wt% (273 K, 1 bar) and a high selectivity for CO_2 over N_2 adsorption of 80 (Henry selectivity, 273 K, 1bar) with a specific surface area of $SA_{BET} = 432$ m^2/g.[98] The Mastalerz group reported a porous molecular cube in 2014.[95b] This molecular cube showed a high specific surface area of $SA_{BET} = 1014$ m^2/g as well as a high uptake of CO_2 (18.2 wt%, 273 K, 1 bar).

Soluble organic cages are also suitable for molecular recognition and separation.[94] Cage **18** (structure shown in Figure 9) was used to separate the mesitylene from its isomer 4-ethyltoluene.[99] This cage also showed great potential in the separation of rare gases.[100] By break-through experiments, it could successfully separate Kr, Xe and Rn from air at ppm concentrations.[100]
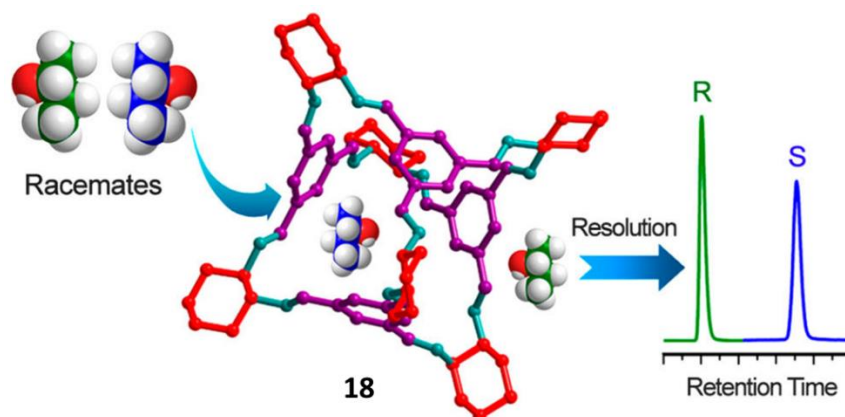
Figure 10. Selective separation of racements using cage **18-R**. Reproduced with permission,[94c] Copyright 2015, American Chemical Society.

In 2015, the Yuan group reported the separations of a large number of optical isomers by using chiral cage **18-R** as the stationary phase for gas chromatography (GC, Figure 10).[94c] They diluted **18-R** with polysiloxane to produce the stationary phase of GC, and different classes of racemates including chiral alcohols, diols, esters, organic acid, *etc*. were resolved. They compared the column coated with **18-R** with two commercially available columns Chirasil-L-Val and β-DEX 120 and found that the **18-R** column could separate the chiral compounds more effectively. This **18-R** coated column exhibited good repeatability and thermal stability (stable at least to 260 °C for 6 hours), which is important for a commercial column. After subjecting more than 500 injections, the column showed almost no changes in retention time, selectivity and recognition ability.

The tetraphenylethylene (TPE) based cages showed the ability to detect TNT.[101] For instance, the Zheng group reported a TPE self-inclusion cage in 2018, which exhibited a high selectivity of TNT.[102] The crystal structure showed one self-inclusion cage could accommodate two TNT molecules, and the interactions between the nitro oxygen of the TNT molecule and the pyridyl ring play a key role in TNT inclusion rather than donor-acceptor or π-π interactions.

Porous liquids are "the liquids have permanent, well-defined, empty pores capable of molecular recognition when exposed to other species." [103] Several efforts have been done to decrease the

melting point of organic cages in order to obtained porous liquids.[104] For instance, James and co-workers decreased the melting point of the [4+6] imine cages from higher than 300 °C to 50 °C by attaching long alkyl chains.[104b] However, the liquid product was not porous anymore because the long alkyl chains might block the voids formed by the cage compound.
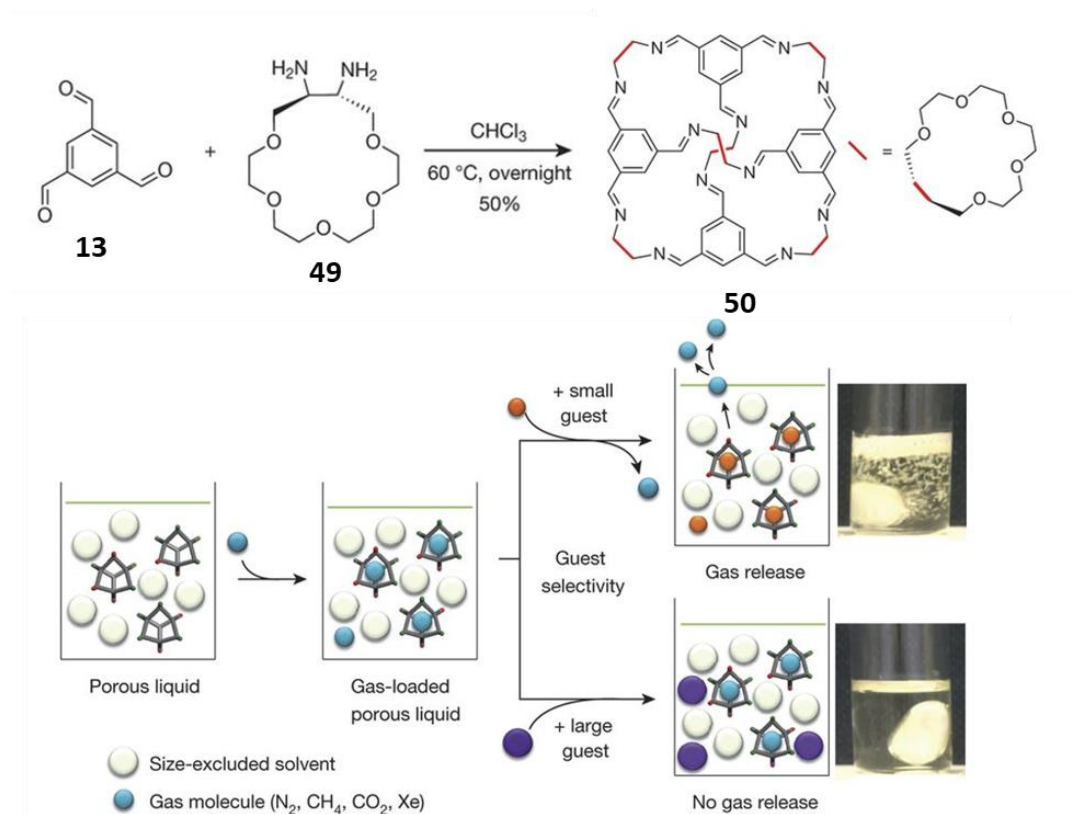
Figure 11. Top: synthesis of the crown-ether cage **50**. bottom: the gas-release behaviour of porous liquids. Reproduced with permission,[105] Copyright 2015, Springer Nature.

In 2015, the James group reported a porous liquid, which was prepared by attaching crown ethers instead of long alkyl chains to the [4+6] imine cage (Figure 11).[105] The cage **50** itself was not a liquid and had a melting point of 180 °C, but if this rigid organic cage was dissolved in 15-crown-5 with the ratio of cage **50**: solvent = 1:12, a porous liquid was obtained. The 15-crown-5 molecules could maintain the flowing property of the porous liquid, and they were too big to enter the cavities of the cages, which made sure that the pores generated by the cages were not blocked. This porous liquid improved the solubility of methane, nitrogen, carbon dioxide and xenon compared with pure liquid 15-crown-5. For the porous liquid which was saturated with gas, if another solvent molecule, which was small enough to enter the cavity of the cage (e.g. chloroform), was added, bubbles were observed immediately because the gas was released from the liquid (Figure 11). However, if the solvent molecule was too big to enter the cavity, such as the 1-*t*-butyl-3,5-dimethylbenzene, no bubble could be observed.

2 Objectives

The aim of the thesis was to introduce functional groups into triptycene based [2+3] imine cages (Scheme 5), and to investigate whether these functional groups will affect the properties of the cages (stability, porosity, selectivity, *etc*.).
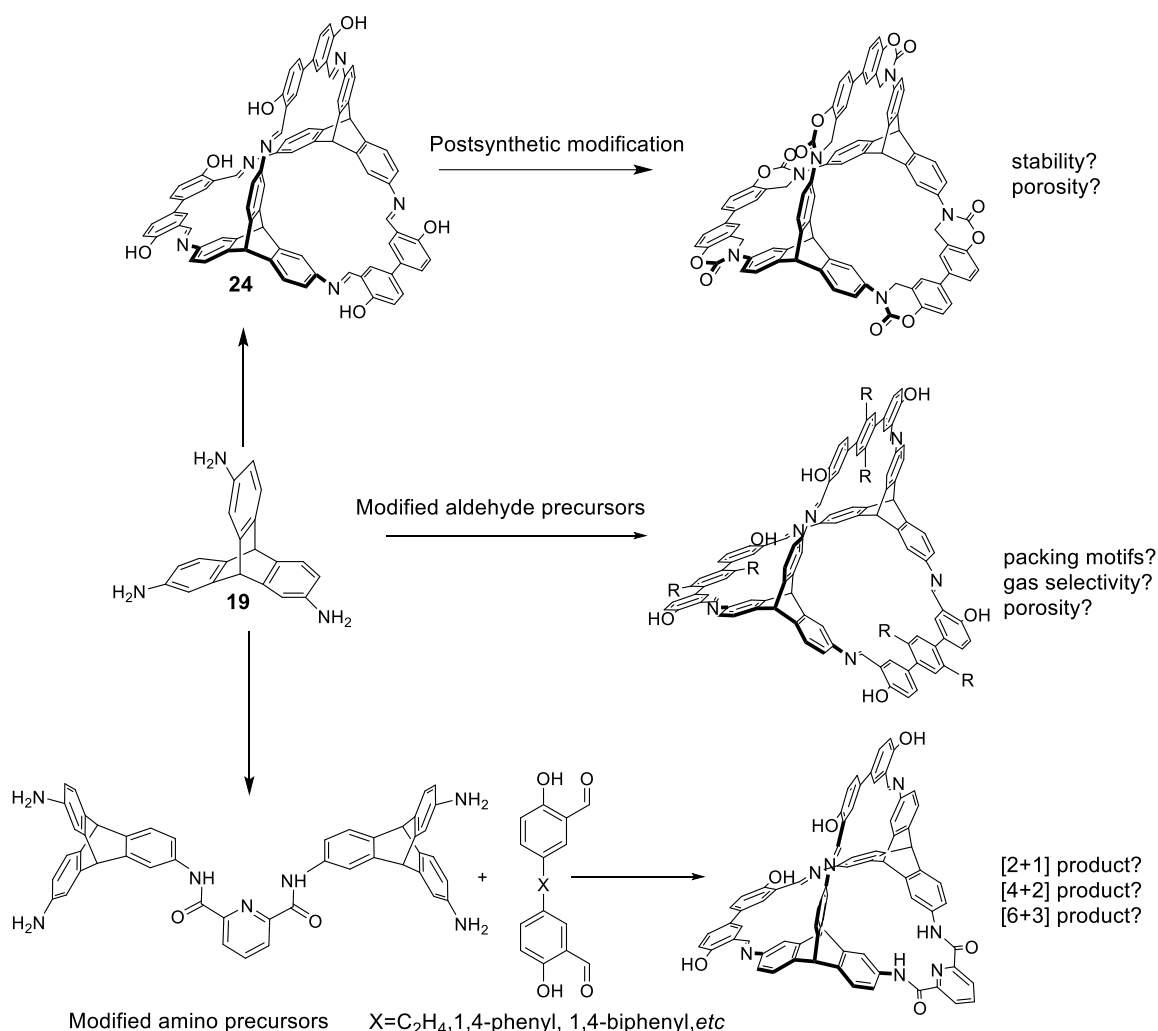
Scheme 5. Modification of the triptycene based [2+3] imine cages.

A series of [2+3] imine cages with different length of aldehyde building blocks have been synthesized by Dr M. Schneider from the Mastalerz group,[49b] but the influence of the side-chain on the building blocks have not been investigated. Therefore, several terphenyl bisalicylaldehyde precursors with different side-chains were designed, which made it possible to study the influence of the side chains on the porosity and selectivity of the organic cage compounds as well as the effect on the packing motifs of the cages in the crystalline state.

Another pyridine modified amine was also designed (Scheme 5), which provided access to several new "three-component" organic cage compounds with different aldehydes.

Furthermore, by using the length of the aldehyde building blocks, the shapes of the formed cages were needed to investigate.

The imine bonds are susceptible to hydrolysis in an acidic or basic environment,[106] which leads to the cages constructed via imine bonds being not stable in the presence of high concentrations of acids or bases. According to literature, [107] reducing the imine bonds to amine bonds could improve the chemical stability of imine cages, but the shape persistence of the cages was lost in that case. Therefore, a new strategy to synthesize a pH stable shape persistent cage is needed.

3 Result and discussion

3.1 Soluble [2+3] terphenyl imine cage with different side-chains

A series of [2+3] imine cages formed by condensation of 2,7,14-triaminotriptycene **19** and salicyldialdehyde building blocks with different linkers ranging from biphenyl linker to tetraphenyl linker have been successfully synthesized by Dr. M. Schneider.[49b, 108] The cages with biphenyl or terphenyl linker showed relatively large specific surface areas (biphenyl: [49] $SA_{BET} = 744 \ m^2/g$, terphenyl:[49b, 108] $SA_{BET} = 626 \ m^2/g$). However, for these [2+3] imine cages, except the biphenyl one, all displayed poor solubility in common organic solvents,[49b] including DMSO and DMF, which made it difficult to characterize them and to find further applications.

In this chapter, a series of side-chain attached aldehyde building blocks were synthesized first. The new [2+3] imine cages were constructed by condensation of these new salicylaldehydes with triaminotriptycene **19**, wishing to obtain more soluble cages. Furthermore, the influence of different side-chains on the properties of the cage compounds, such as the packing motifs in the crystalline state, the porosities and the selectivity of different gases, were also investigated.

3.1.1 Synthesis of terphenyl aldehyde building blocks

52: R^1=C$_4$H$_9$, R^2= H
53: R^1 =C$_6$H$_{13}$, R^2= H
54: R^1 =C$_8$H$_{17}$, R^2= H
55: R^1 =OC$_4$H$_9$, R^2= H
56: R^1 =OC$_6$H$_{13}$, R^2= H
57: R^1 =OC$_8$H$_{17}$, R^2= H
58: R^1=O(CH$_2$)$_3$CH=CH$_2$, R^2= H
59: R^1 =C$_4$F$_9$, R^2= H
60: R^1 =OCH$_2$CH$_2$OCH$_3$, R^2= H
61: R^1 =O(CH$_2$CH$_2$O)$_3$CH$_3$, R^2= H
62: R^1 =H, R^2= t-Bu
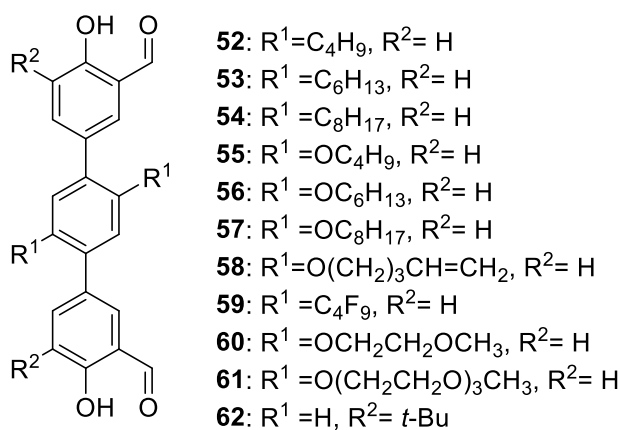
Scheme 6. Chemical structure of compound **52-62**.

Ten terphenyl aldehydes with different side-chains, which can be classified in five groups (Scheme 6), alkyl chains (**52-54**, **62**), oxyalkyl (oxyalkylene) chains (**55-58**), perfluorobutyl chain (**59**), and ether chains (**61**, **62**), are described in this chapter.

The syntheses of aldehydes **52-54** are shown in Scheme 7. The alkyl chain modified benzenes **67-69** were synthesized from the corresponding Grignard reagents (alkyl-magnesium bromide **64-66**) and 1,4-dichlorobenzene **63** via Kumada alkylation.[109] Compounds **67-69** were brominated by using two equivalents of bromine at room temperature to obtain the dibromo derivatives **70-72**.[110] The brominated products **70-72** were purified by recrystallization and the yields were higher than 60% in all cases. The boronic ester **74** was synthesized according to literature through Miyaura borylation reaction[111] from bromosalicylaldehyde **73** and

bis(pinacolato)diboron (B_2pin_2).[112] After recrystallization from petroleum ether, **74** was obtained as colourless solid with a yield of 88%. The final aldehydes **52-54** were synthesized through Suzuki-Miyaura reaction[113] of dibromo derivatives **70-72** with boronic ester **74**, catalysed by 10% of $Pd_2(dba)_3$. The final products were obtained as colourless solids after purification by column chromatography with yields of 40% or higher.
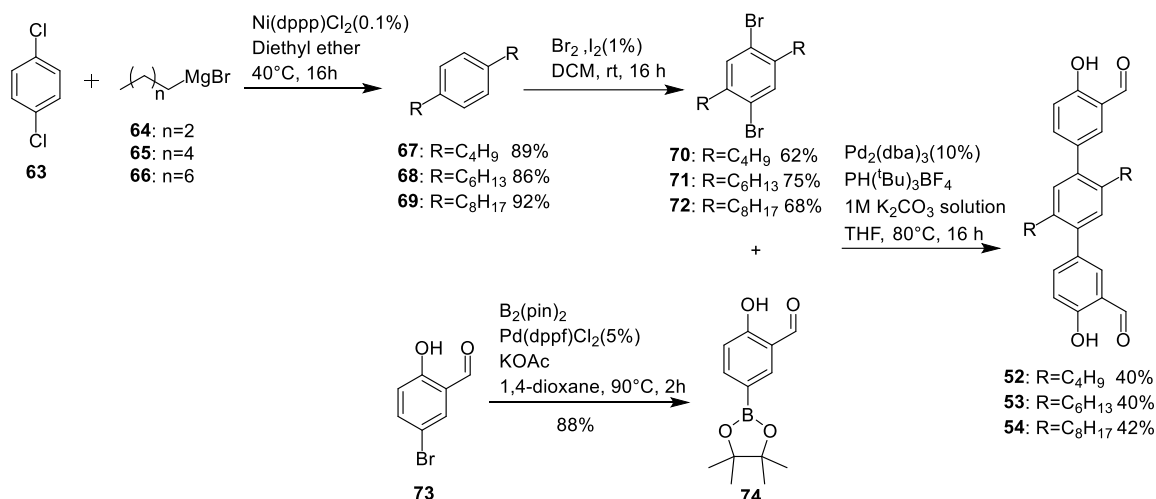
Scheme 7. Synthesis of compounds **52-54**. [110b-113]
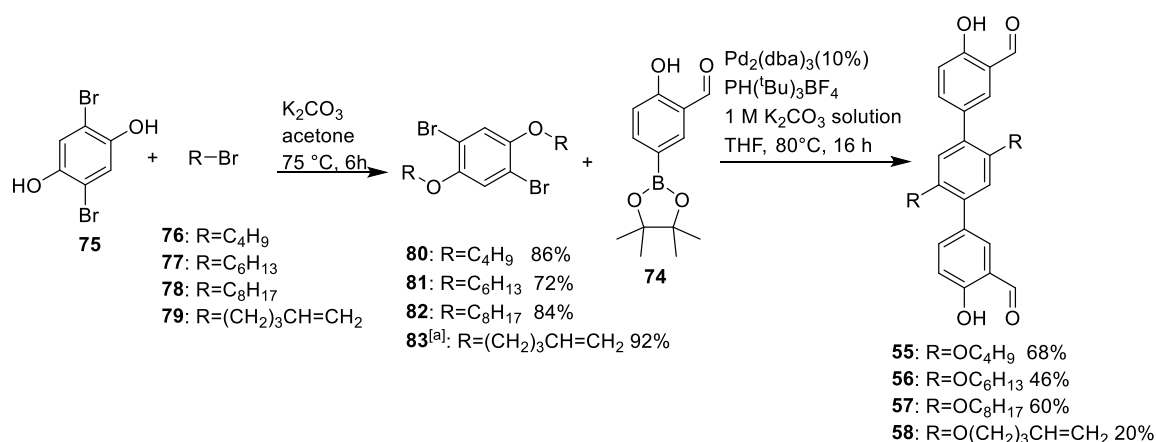
Scheme 8. Synthesis of compounds **55-58**.[113-114] [a]:in DMF, K_3PO_4.

The syntheses of compounds **55-58** are shown in Scheme 8. Compounds **80-83** were synthesized from dibromobenzenediol **75** and corresponding bromoalkanes **76-79** via Williamson ether synthesis.[114] Dibromo derivatives **80, 81** and **82** were purified by recrystallization in ethanol as colorless solids. The compound **83** (with oxypentene chains) was purified by column chromatography. The final aldehydes **55-58** were also synthesized by Suzuki-Miyaura reaction[113] of boronic ester **80** with dibromo derivatives **86-89** (Scheme 8) with 10% of $Pd_2(dba)_3$ as the catalyst. Compounds **55-57** were obtained as yellow solids after

purification by column chromatography. The low yield of **58** was because during this Suzuki-Miyaura reaction, a double-bond shifted product was obtained, which will be discussed later.
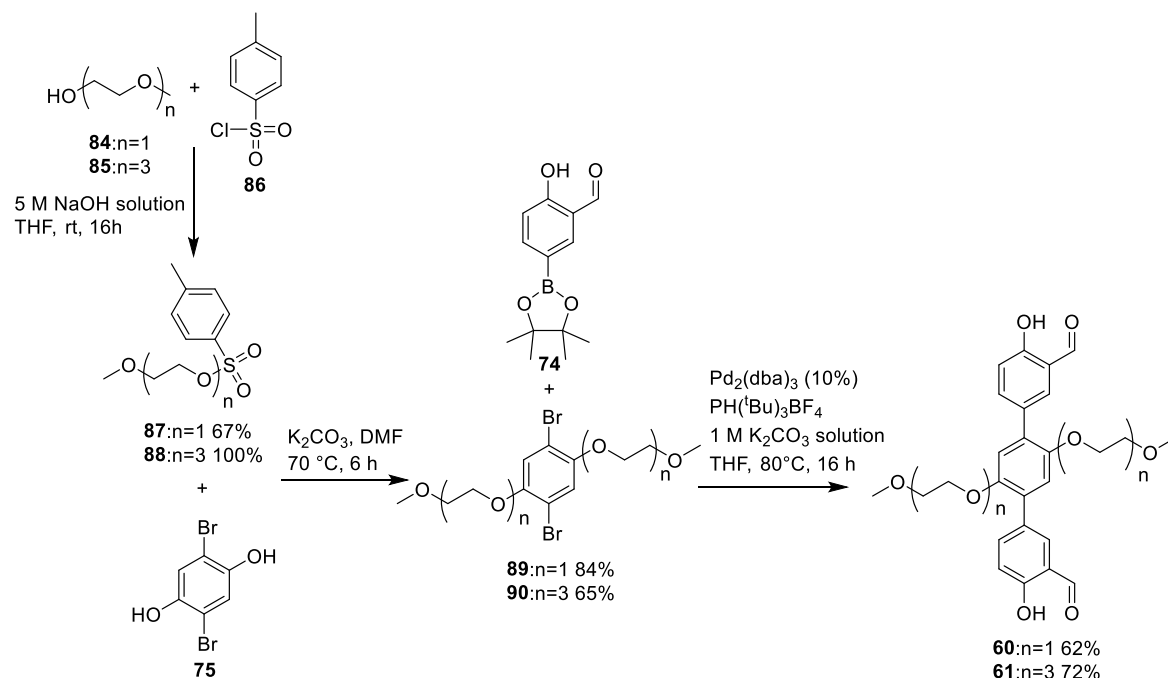
Scheme 9. Synthesis of compounds **60** and **61**.[113-115]

The syntheses of dialdehydes **60** and **61** are shown in Scheme 9. Dibromobenezenes **89** and **90** were synthesized from tosylates **87**, **88** and dibromobenzenediol **75** (Scheme 9) by Williamson ether synthesis.[115] Compound **89** (with shorter ether chains) was obtained as colourless solid after recrystallization from ethanol at 0 °C.[115a] Compound **90** (with longer ether chains) was recrystallized from ethanol using a liquid nitrogen bath and the colourless solid obtained from the recrystallization would soon become colourless liquid at room temperature.[115b] The aldehydes **60** and **61** were synthesized from the dibromo derivatives **89**/**90** and boronic ester **74** by Suzuki-Miyaura reaction.[113] Pure compounds **60** and **61** were obtained after column chromatography as yellow solids with the yields being higher than 60%.

1,4-bisperfluorobutyl benzene **92** was synthesized from diiodobenzene **91** and iodoperfluorobutane, using copper powder as the catalyst (Scheme 10).[116] Compound **92** was obtained as colourless liquid and used for next step without further purification. Then 1,4-bisperfluorobutane benzene **92** was brominated by *N*-bromosuccinimide (NBS) in a mixture of sulphuric acid and trifluoroacetic acid (3: 10) and the dibromo derivative **93** was obtained as a colourless solid after recrystallization.[116] The aldehyde **59** was synthesized from dibromo

derivative **93** and boronic ester **74** by Suzuki-Miyaura reaction, and obtained as a white solid with a yield of 30% after column chromatography.[113]
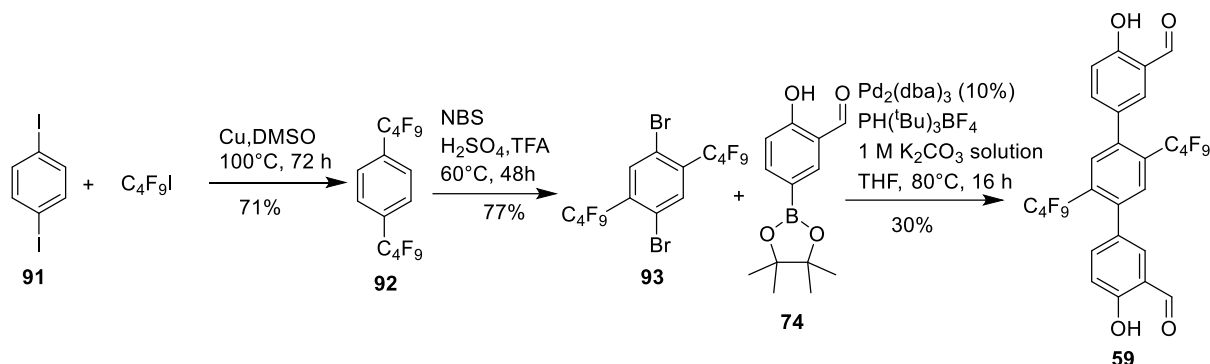
Scheme 10. Synthesis of compounds **59**.[116]
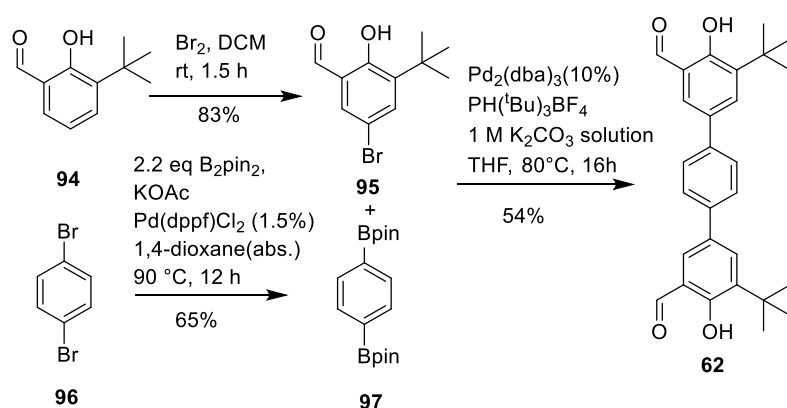
Scheme 11. Synthesis of compound **62**.[117-118]

Besides the terphenyl aldehydes whose side chains are located at the *para*-position of the middle benzene ring, another aldehyde **62** which has two *t*-butyl groups at the *ortho*-position of the phenol unit was also synthesized (Scheme 11). The bromo derivative **95** was obtained by bromination of **94** with bromine at room temperature.[117] Pure compound **95** was obtained as a yellow solid after recrystallization from ethanol with a yield of 83%. The boronic ester **97** was synthesized by Miyaura borylation reaction[111] from dibromobenzen **96** and B_2pin_2.[118] Dialdehyde **62** was synthesized by Suzuki-Miyaura coupling[113] from bromo derivative **95** and boronic ester **97** as a yellow solid with a yield of 54%. All these aldehyde building blocks were characterized by ^{1}H NMR, ^{13}C NMR, ESI-MS, elemental analysis and IR.
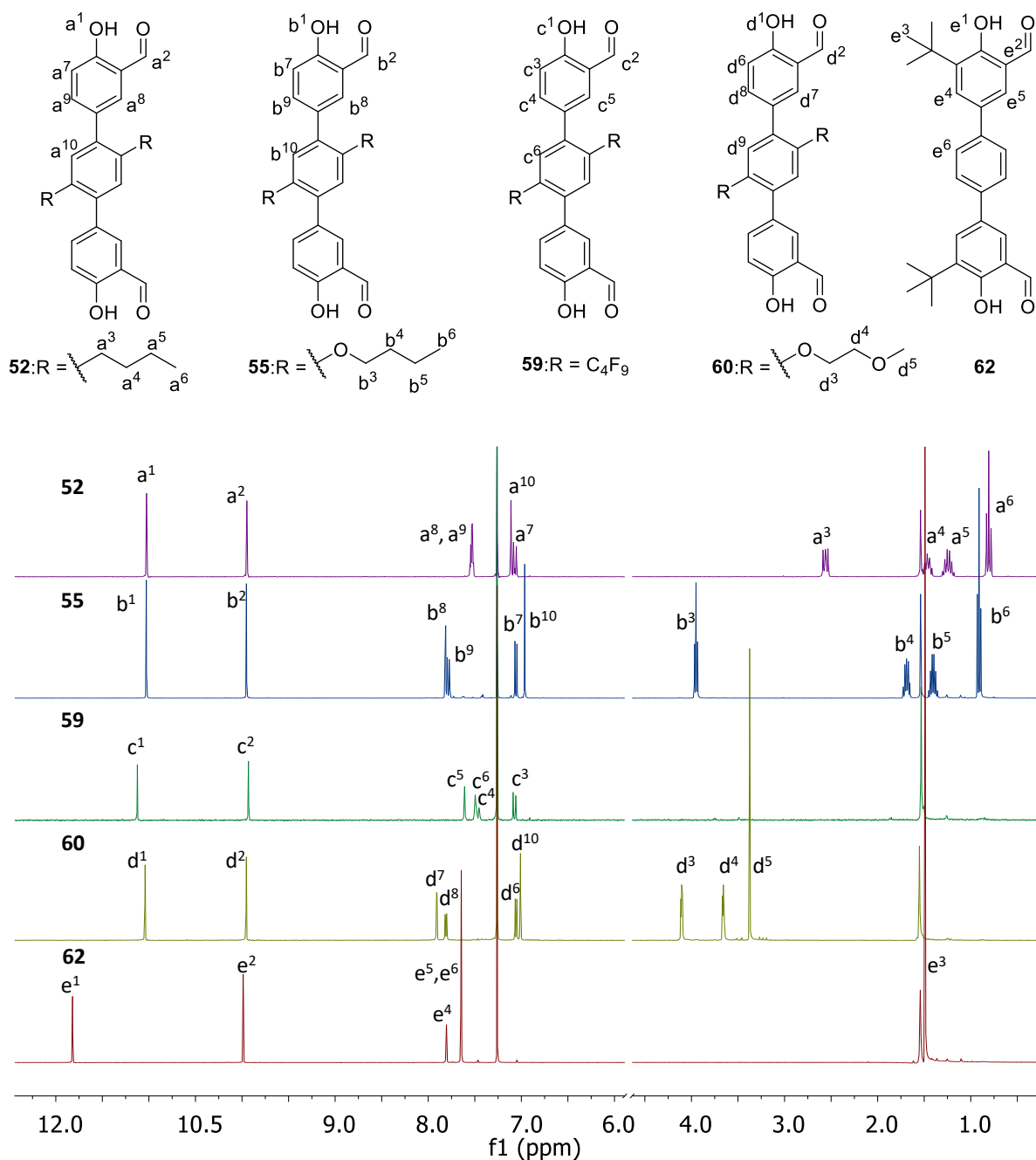
Figure 12. ^{1}H NMR spectra of compounds **52, 55, 59, 60** and **62** (from top to bottom, CDCl$_3$, 500 MHz)

The structures and ^{1}H NMR spectra of aldehydes **52, 55, 59, 60** and **62** are shown in Figure 12. These five compounds were chosen as examples to compare because they bear different side chains but with a similar length. From the ^{1}H NMR spectra of **52, 55, 59** and **60** (Figure 12), the peaks of -OH proton, -CHO proton and aromatic protons are similar, but the peaks for the side chains protons are different. For instance, the triplet signal for H^{b3} of **55** ($\delta = 3.9$ ppm) shifts to low field compared with **52** (H^{a3}, $\delta = 2.5$ ppm). The reason is that the electronegativity of oxygen atom in oxybutyl chain is higher than carbon atom in butyl chain, which decreases

the electron density around the proton. Compound **59** (with perfluorobutyl chains) shows no peaks in the side chain area of the ^{1}H NMR spectrum, but the ^{19}F NMR spectrum presents four group of signals. For compound **60** (with ether chains), two groups of -CH$_2$- protons H^{d3}, H^{d4} are observed at $\delta = 4.1$ and 3.8 ppm and one singlet for -CH$_3$ proton H^{d5} at $\delta = 3.3$ ppm, which fits the chemical structure of the ether chains. Compound **62** shows a bigger difference as the positon of side chain is different. The -OH singlet shifts more to the low field ($\delta = 11.8$ ppm) compared with all other aldehydes ($\delta = 11.0$ ppm) and the singlet for *t*-Bu group protons is found at $\delta = 1.5$ ppm.

It needs to be mentioned that during the synthesis of compound **58** (with oxypentene chains), a double bonds-shift product **58'** was obtained in the final step. From the ^{1}H NMR (Figure 13), it can be seen that compared with unshifted compound **58**, the signal of the pentene side chain protons has changed: the peak for –CH= proton H$^{a'}$ ($\delta = 5.7$ ppm) and =CH$_2$ proton H$^{b'}$ ($\delta = 5.0$ ppm) of the terminal double bond disappear, instead, a new multiplet ($\delta = 5.47$ ppm) for the proton H^a of the internal double bond appears. According to literature, this may because the Pd catalyst used for the Suzuki-Miyaura reaction also can catalyze a double bond shift.[119] A possible mechanism of this reaction is shown in Scheme 12. The palladium(II) ion coordinates onto the double bond, followed by an oxidative addition of one α-hydrogen on palladium. The Pd(IV) coordinates with the vinyl anion, and the reductive elimination gives the thermodynamically more stable secondary double bond.

Scheme 12. Possible mechanism of Pd (II) catalysed double bond shift.[120]

Table 1. Different condition influence on double bond shifting

Entry	Amount of catalyst (%)	Concentration (compound 83)	Reaction time	Yield (58+58') (%)^a	Ratio of 58:58'^{a}
1	10	0.1237 mol/mL	1 d	70	1:10
2	10	0.1237 mol/mL	4 d	88	1:10
3	5	0.1237 mol/mL	1 d	71	1:0.23
4	1	0.1237 mol/mL	1 d	60	1:0.22
5	5	0.2474 mol/mL	1 d	63	1:0.38
6	5	0.0619 mol/mL	1 d	64	1:0.08

a: the yield and ratio of products are calculated by the ^{1}H NMR spectra
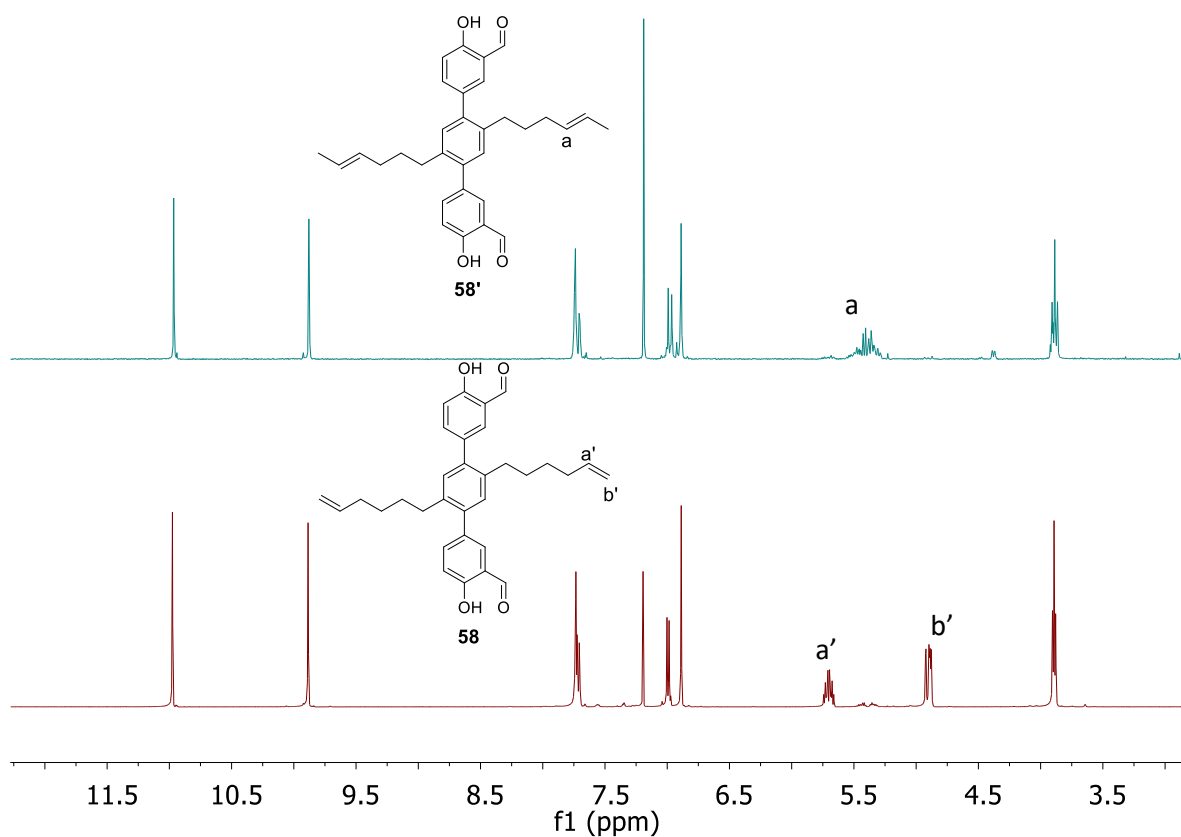
Figure 13. ^{1}H NMR of top: compound **58'** and bottom: compound **58** (CDCl$_3$, 300 MHz)

Furthermore, the effect of reaction time, catalyst amount and concentration on the yield and isomer selectivity of the products were investigated (Table 1). When increasing the reaction time from 16 h to 4 days (entry 1 and 2, Table 1), the yield is increased to 80% with 90% shifted product **58'**. For a better comparison, the reaction time of the following reactions was set to 1 day. Decreasing the catalyst amount from 10% to 5% reduced the ratio of shifted product **58'** to 10% (entry 3, Table 1), but a further decrease to 1% of catalyst did not have a significant influence on the ratio of double bond shift, but lowered the yield to 63% (entry 4, Table 1). For the concentration test, the catalyst amount was set to 5%. Doubling concentration of the starting materials leads to 15% shifted product (entry 5, Table 1) and half the concentration led to 7% shifted product (entry 6, Table 1). From these result, the amount of catalyst and concentration of reactant have influence on the shift of the double bond, and decreasing the amount of catalyst and concentration can prevent the formation of shift-product. All the yields and ratio of unshifted product **58**: shifted product **58'** were calculated by ^{1}H NMR spectra.

26
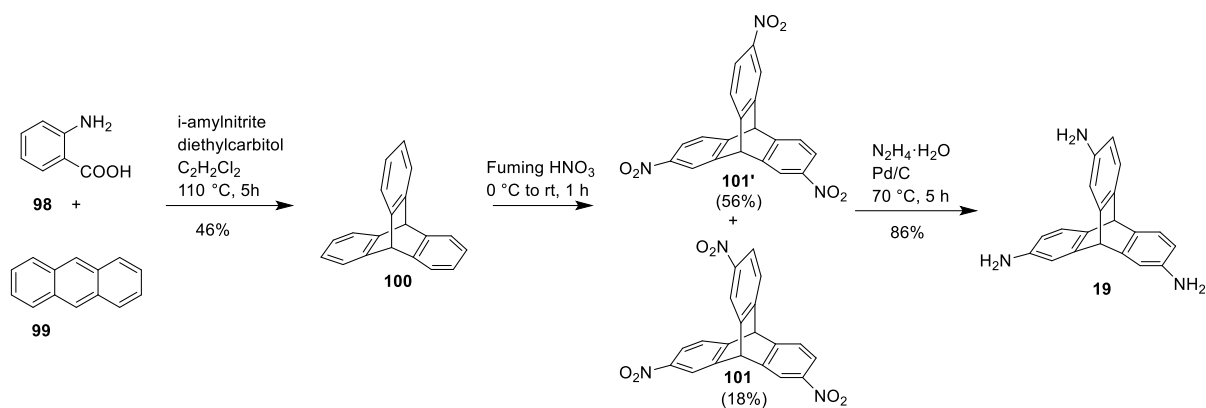
Scheme 13. Synthesis of 2,7,14-triaminotriptycene **19**.[120-122]

The synthesis of the 2,7,14-triaminotriptycene **19** (Scheme 13) starts with a Diels-Alder reaction between anthracene **99** and anthranilic acid **98**, yielding unsubstituted triptycene **100** with a yield of 46%.[120] The trinitrotriptycene was prepared according to literature,[121] by using fuming HNO_3 in acetic acid for one hour. 2,7,14-trinitrotriptycene **101** and its isomer, 2,6,14-trinitrotriptycene **102'** could be isolated by column chromatography with a yield of 18% and 56%, respectively. The triaminotriptycene **19** was obtained by reacting **101** with hydrazine hydrate, catalysed by Raney-Nickel[122] or Pd/C. The triaminotriptycene **19** should be kept in the freezer because it easily decomposes at room temperature (colour change from white to pink then to brown).

3.1.2 Synthesis of [2+3] terphenyl imine cages with different side chains
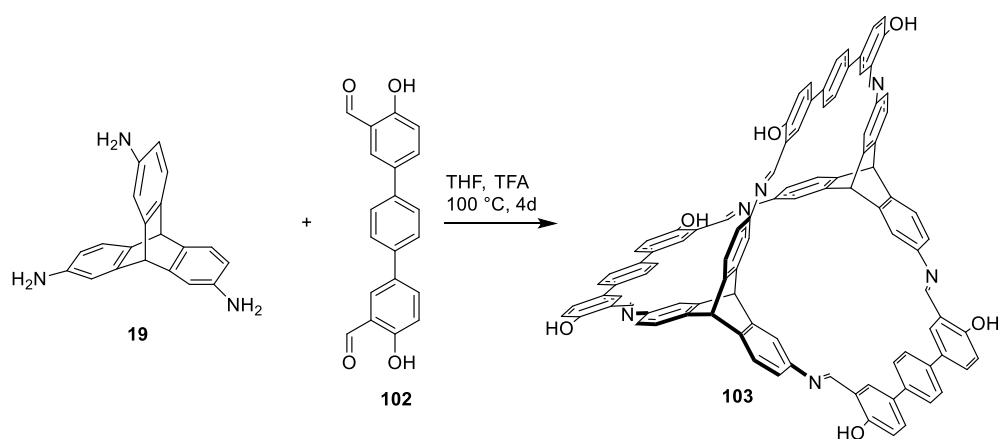
Scheme 14. Synthesis of cage compound **103**.[49b]

The [2+3] terphenyl imine cage **103** was synthesized by condensing triaminotriptycene **19** and terphenylsalicyaldehyde **102** in THF at 100 °C for 4 days (Scheme 14).[49b] The pure product **103** was obtained with a yield of 11% (purified by recrystallization from DMF/methanol). The

yield is lower than the bisphenyl imine cage **24**,[49] and because of the poor solubility in organic solvents, no NMR spectrum of **103** could be measured.
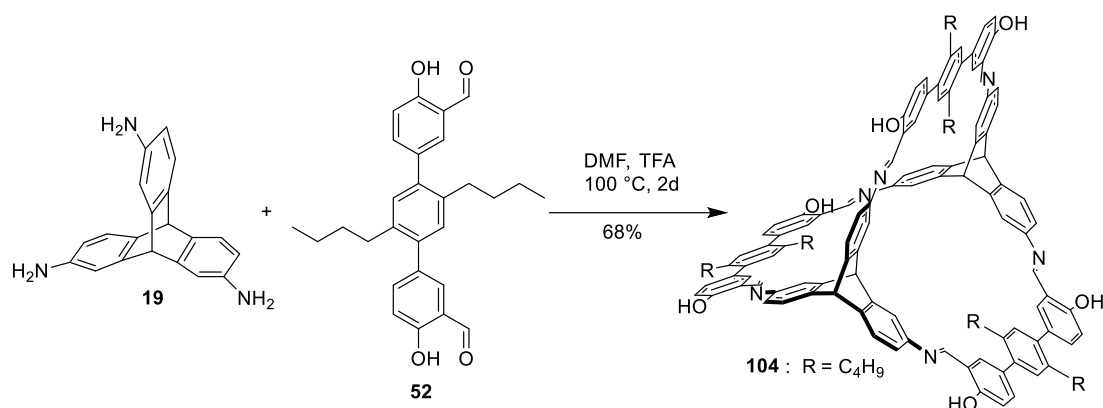
Scheme 15. Synthesis of cage **100**.

Aldehyde **52** (with butyl chains) was used to react with triaminotriptycene **19** in order to investigate whether the corresponding [2+3] imine cage **104** would form or not (Scheme 15). The same reaction conditions as **103** were taken (THF, 100 °C, 4 d, catalysed by TFA) at first. During the reaction, a lot of orange precipitate appeared. The MS spectra of the reaction mixture proved the formation of the [2+3] cage **104**, but because of the poor solubility of the precipitate in organic solvents such as DMF, DMSO and THF, it was difficult to further characterize the compound. In order to improve the reaction conditions, other solvents such as DMF, toluene, chloroform and ethyl acetate were used for this reaction. Only in DMF the reaction mixture remained transparent during the reaction time. After the reaction, the reaction mixture was concentrated and added into methanol. An orange precipitate appeared and this precipitate could be dissolved in DMF and THF, which allowed further characterization. After washing with methanol, the pure compound **104** could be obtained in a yield of 68%.

For the other aldehydes, the same reaction conditions were used and the corresponding cages were obtained (Scheme 16, Table 2). One exception was compound **111** (with perfluorobutyl chains). A precipitate appeared when the reaction was done in DMF. If the reaction was done in THF, however, the reaction mixture stayed transparent. So this reaction was carried out in abs. THF and compound **111** was obtained as a yellow powder with a yield of 67%. The other exception was compound **112** (with shorter ether chains). The reaction mixture remained transparent at 100 °C, but when the temperature was lower than 70 °C, an orange precipitate appeared. This precipitate (desired product proved by ^{1}H NMR) can be dissolved again after heating to 100 °C. The yields of all cages are shown in Table 2. The same reaction condition

(DMF, 100 °C, 2 days) was also used to synthesized cage **103** (without side-chain), but the experimental phenomenon was as same as the reaction in THF, and the yield was not improved. All cages with side-chains dissolved well in THF or DMF at room temperature except cage **112**, which was only dissolve in hot DMF or DMSO.

52 : R^1 = C$_4$H$_9$, R^2 = H
53 : R^1 = C$_6$H$_{13}$, R^2 = H
54 : R^1 = C$_8$H$_{17}$, R^2 = H
55: R^1 = OC$_4$H$_9$, R^2 = H
56: R^1 = OC$_6$H$_{13}$, R^2 = H
57: R^1 = OC$_8$H$_{17}$, R^2 = H
58: R^1 = O(CH$_2$)$_3$CH=CH$_2$, R^2 = H
59: R^1 = C$_4$F$_9$, R^2 = H
60: R^1 = O(CH$_2$)$_2$OCH$_3$, R^2 = H
61: R^1 = O(C$_2$H$_4$O)$_3$CH$_3$, R^2 = H
62: R^1 =H, R^2 = t-Bu

104 : R^1 = C$_4$H$_9$, R^2 = H 68%
105 : R^1 = C$_6$H$_{13}$, R^2 = H 78%
106 : R^1 = C$_8$H$_{17}$, R^2 = H 67%
107 : R^1 = OC$_4$H$_9$, R^2 = H 65%
108 : R^1 = OC$_6$H$_{13}$, R^2 = H 66%
109 : R^1 = OC$_8$H$_{17}$, R^2 = H 67%
110 : R^1 = O(CH$_2$)$_3$CH=CH$_2$, R^2 = H 77%
111 : R^1 = C$_4$F$_9$, R^2 = H 67%
112 : R^1 = O(CH$_2$)$_2$OCH$_3$, R^2 = H 73%
113 : R^1 = O(C$_2$H$_4$O)$_3$CH$_3$, R^2 = H 52%
114 : R^1 =H, R^2 = t-Bu 78%

Scheme 16. Synthesis of cage **104-114**.

Table 2. Summary of reaction condtions and characteristic analytical data of Cage **103-114**.

	Reaction condition		Yield	MS	^{1}H NMR [ppm](THF-d$_8$)	
	Solvent	time	%	(m/z)	-CH=N-	Bridgehead-H
103[a]	THF	4d	11	1445.49	n.d	n.d
104	DMF	2d	68	1782.92	9.15	5.71, 5.63
105	DMF	2d	78	1951.32	9.04	5.60, 5.51
106	DMF	2d	67	2119.76	9.03	5.60, 5.51
107	DMF	2d	65	1878.84	9.21	5.71, 5.68
108	DMF	2d	66	2046.30	9.21	5.71. 5.67
109	DMF	2d	67	2215.70	9.10	5.60. 5.57
110	DMF	2d	77	1950.05	9.25	5.28,5. 21
111	THF	2d	67	2755.26	9.15	5.72, 5.57
112	DMF	2d	73	1889.76	9.30[b]	5.83[b]
113	DMF	2d	52	2420.39	9.24	5.73, 5.70
114	DMF	2d	78	1781.87	9.30	5.73

a: From Ref [49b]. b: Measured in DMSO-d$_6$, 100 ℃
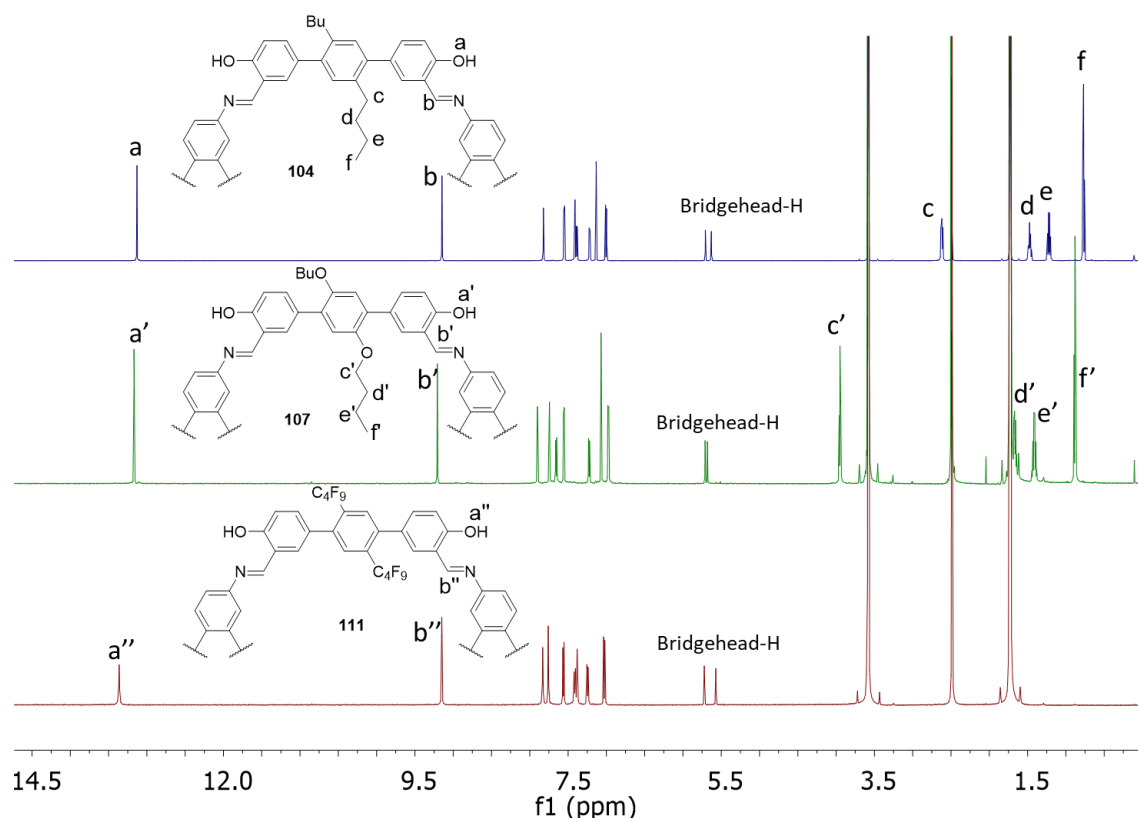
Figure 14. ^{1}H NMR spectra of compound **104**, **107**, and **111** (from top to bottom, THF-d$_8$, 500 MHz).

Cages **104**, **107**, and **101** are taken as example to compare the ^{1}H NMR spectra (Figure 14, Table 2). Cage **104** (with butyl chains) shows the singlet of imine proton H^b at $\delta = 9.15$ ppm, which indicates the condensation of amino groups and aldehyde groups succeeded. Seven peaks appear in the aromatic region, which fit for the structure of cage **104** (four inequivalent aromatic protons from terphenyl part and three inequivalent aromatic protons from the triptycene part). Two bridgehead protons appear at $\delta = 5.71$, 5.63 ppm. Cage **104** shows four peaks in side-chain region: triplet of proton H^c at $\delta = 2.6$ ppm, quintet of proton H^d at $\delta = 1.47$ ppm, double of triplet of proton H^e at $\delta = 1.22$ ppm and triplet of H^f at $\delta = 0.77$ ppm, which chemical shifts and splitting pattern fit well with the butyl side chain. Cage **107** (with oxybutyl chains) shows a singlet of the imine proton H$^{b'}$ at $\delta = 9.21$ ppm and seven peaks in the aromatic region, which is similar to cage **104**. **107** also shows four groups of peaks in the side-chain region: triplet of proton H$^{c'}$ at $\delta = 3.95$ ppm, quintet of proton H$^{d'}$ at $\delta = 1.67$ ppm, double of triplet of proton H$^{e'}$ at $\delta = 1.41$ ppm and triplet of proton H$^{f'}$ at $\delta = 0.88$ ppm. Cage **111** (with perfluorobutyl chains) shows the proton of imine bond H$^{b''}$ at $\delta = 9.15$ ppm and seven groups of peaks in the aromatic region. Four different peaks can be observed from ^{19}F NMR, which fit for the structure of perfluorobutyl chains.

30
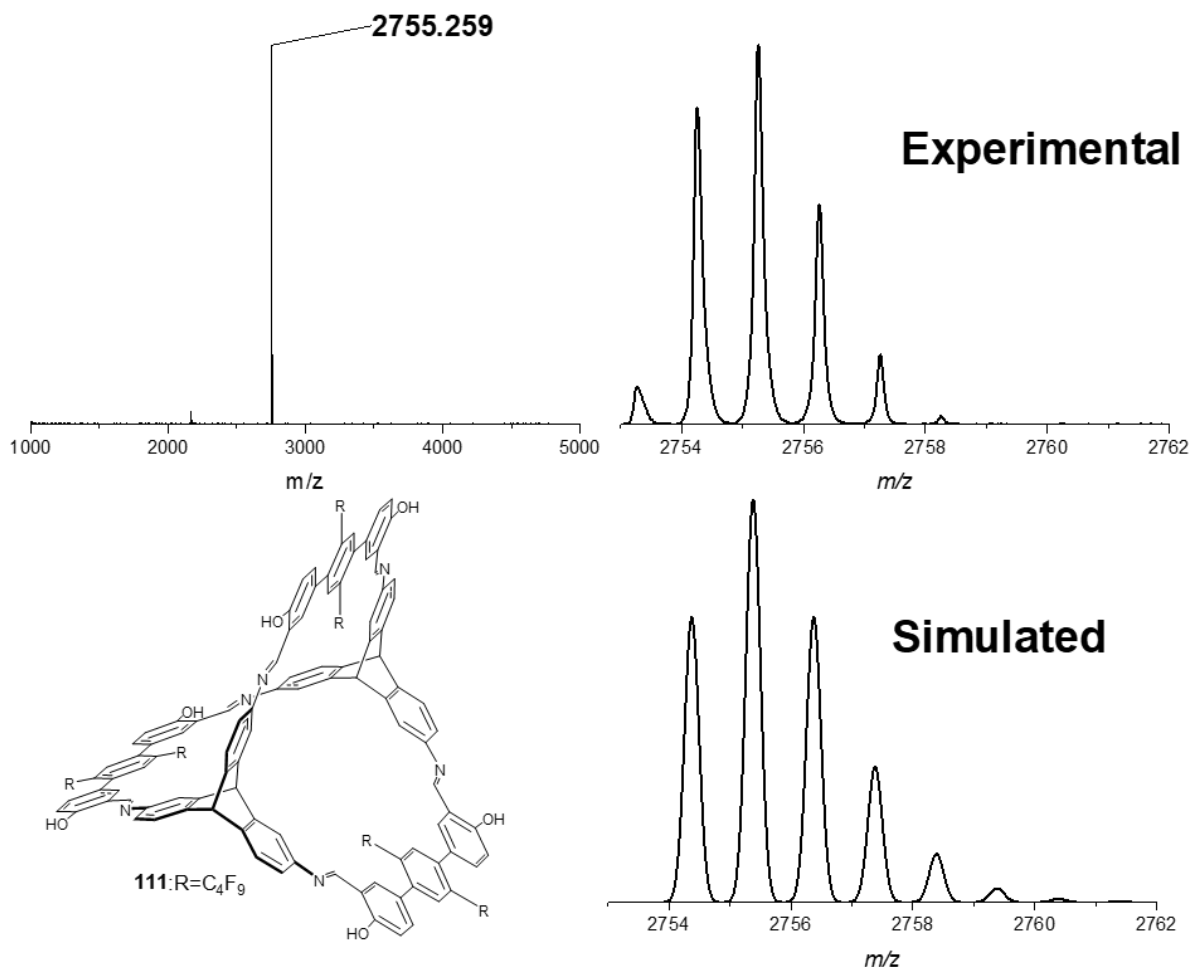
Figure 15. Mass spectra of cage **111** (MALDI-TOF, matrix: DCTB)

Besides NMR spectra, MS spectra are also an important proof for cages' formation. From the MALDI-TOF-MS spectra, only [2+3] cages were observed (Table 2). The MS spectrum of cage **111** (with perfluorobutyl chains) is depicted as an example in Figure 15. The peak shown in Figure 15 fits for the molecule weight of cage **104** ([M+H]$^+$: *m/z* calcd. for ($C_{124}H_{59}O_6N_6F_{54}^+$): 2755.79, found:2755.259). The simulated distribution also fits with the experimental result. Table 2 shows the MS and the important ^{1}H NMR data for all cages with side-chains.

3.1.3 Crystal structure of terphenyl cages

Via different methods like vapour diffusion, slow evaporation or slow cooling, several crystalline materials were obtained (crystal of cage **106** and **111** are shown in Figure 16). However, the disorder of side chains and a lot of disordered solvent molecule inside the crystal made it difficult to determine the structures. Among cage compounds **104**-**114**, the crystal structures of five cages (**105**, **106**, **110**, **111**, **112**) were determined by the X-ray diffraction measurement. It needs to be mentioned that most of the side chains cannot be localized in the crystal structure, so what will be discussed next is mainly based on the skeleton of the cage. Solvent

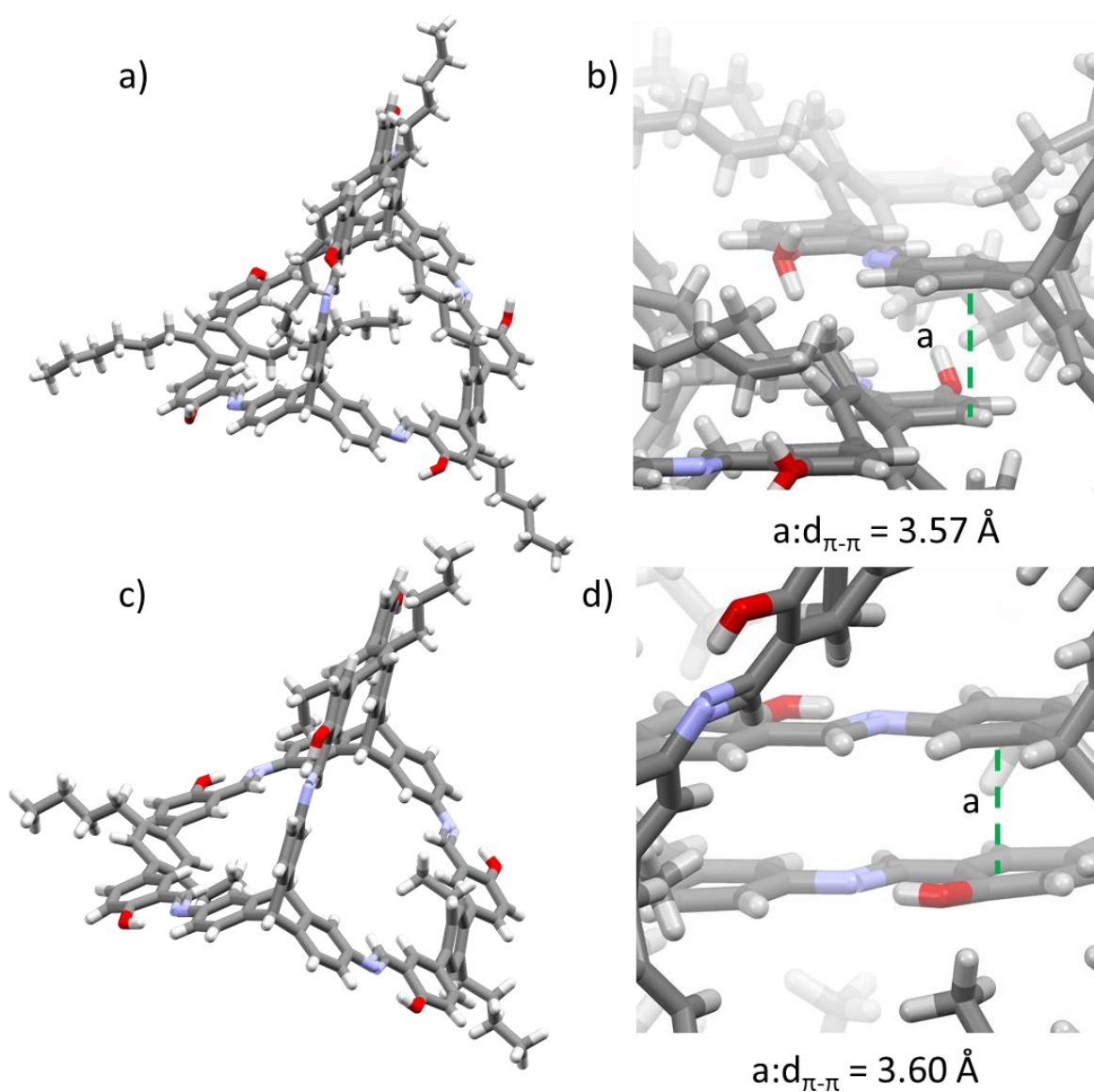**Figure 16**.Photo of crystal of (a) cage **106** and (b) cage **111**.

molecules are disordered in the large void, and it is necessary to use the SQUEEZE routine in PLATON during refinement. The critical information about the crystal structure is presented in Table 3. These five crystal structures can be divided into two types. One with $P6_3$ space group (cage **105**, **106**, **110**, and **112**) and the other one with R3c space group (cage **111**).

Table 3. Overview of selected crystallographic parameters.

Entry	solvent	Crystal system	Space group	Z	Unit cell parameter
105	THF/methanol	hexagonal	$P6_3/m$	2	$a = b = 19.6363$ Å, $c = 27.033$ Å, $V = 9026$ Å^3
106	THF/methanol	hexagonal	$P6_3$	2	$a = b = 19.697$ Å, $c = 26.904$ Å, $V = 9040$ Å^3
110	THF	hexagonal	$P6_3/m$	2	$a = b = 20.0491$Å, $c = 23.410$ Å, $V = 8149.2$ Å^3
111	THF/methanol	trigonal	R3c	6	$a = b = 19.0156$ Å, $c = 64.026$ Å, $V = 20049.6$ Å3
112	DMF	hexagonal	$P6_3/m$	2	$a = b = 19.2235$ Å, $c = 26.6855$ Å, $V = 8540.3$ Å3

Figure 17. a) crystal structure of **105** (with hexyl chains) shown as stick model. b) π-π stacking between two cage **105** molecules. c) crystal structure of **106** (with octyl chains) shown as stick model. d) π-π stacking between two cage **106** molecules

Compound **105** and **106** are cages with alkyl chains (hexyl chains and octyl chains). They were both crystallized by slowly diffusing methanol into a solution of **105**/**106** in THF at room temperature. Cage **105** (Figure 17 a, b) crystallizes in the hexagonal space group P6_3/m, $a = b$ = 19.6363 Å, c = 27.033 Å, V = 9026.9 Å^3. The distance between two interior bridgehead-H of triptycenes is 12 Å. The crystalline packing is mainly determined by π-π stacking, with the distance $d_{\pi\text{-}\pi}$ = 3.57 Å (Figure 17b). Because of the disorder of the side chains, the interaction between side chains are not discussed, but a C-H···π interaction between side chains and

benzene rings exists. Compound **106** is isomorphous with **105** (Figure 17c, d). It crystallizes in the hexagonal space group P6$_3$, $a = b = 19.697$ Å, $c = 26.904$ Å, $V = 9040$ Å^3. The distance between interior triptycene bridgehead-H is 12 Å.

a:d$_{\pi-\pi}$ = 3.58 Å

a:d$_{\pi-\pi}$ = 3.58 Å
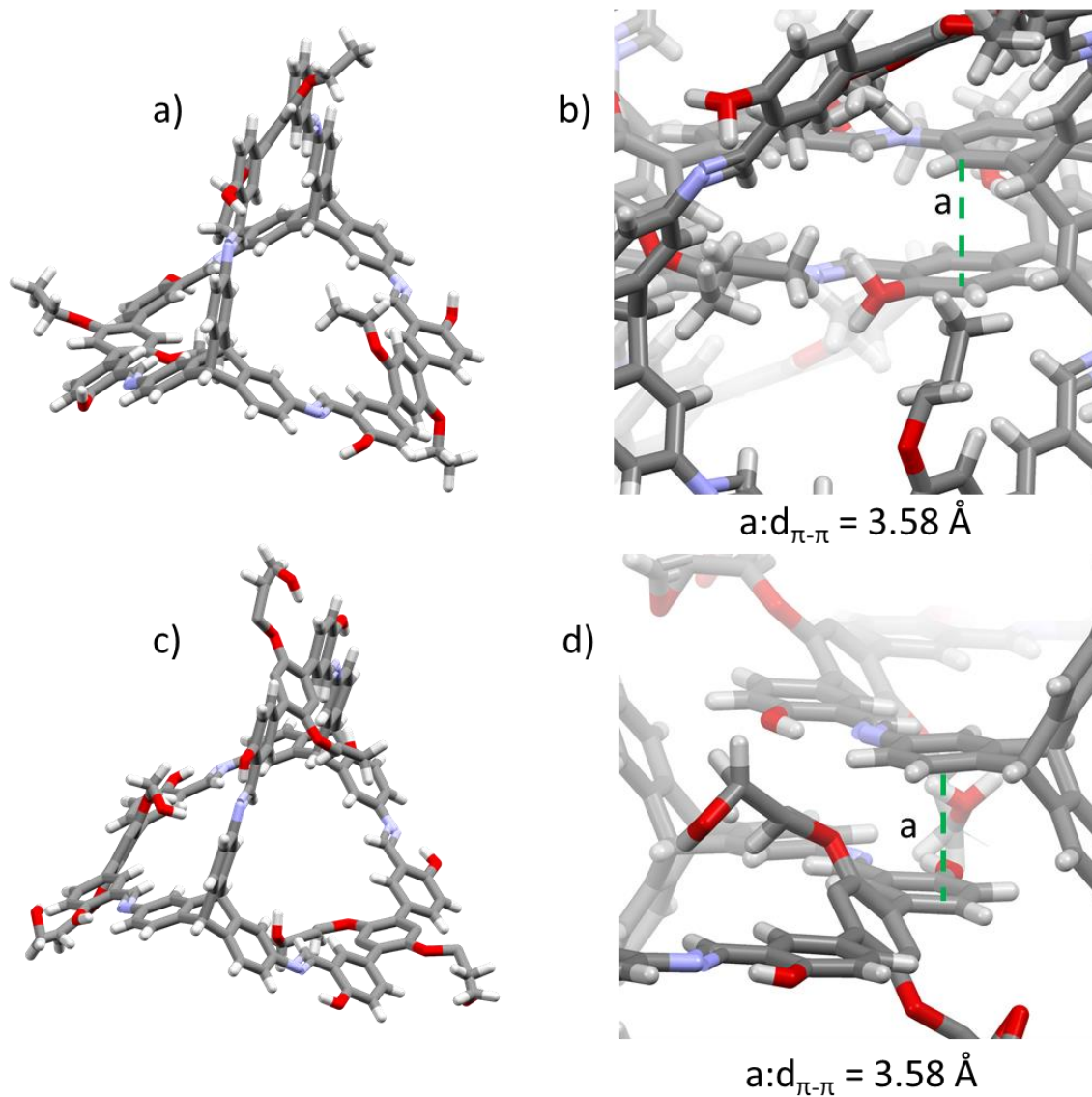
Figure 18. a) crystal structure of **110** (with oxypentene chains) shown as stick model. b) π-π stacking between two cage **110** molecules. c) crystal structure of **112** (with shorter ether chains) shown as stick model. d) π-π stacking between two cage **112** molecules

Compound **110** is the cage with oxypentene chains. The crystals were obtained by slow evaporation of a solution of **110** in THF-d$_8$ in a NMR tube. From the crystal structure, **110** crystallizes in the hexagonal space group P6$_3$/m, $a = b = 20.0491$ Å, $c = 23.410$ Å, $V = 8149.2$ Å^3 (Figure 18a, b). Crystals of cage **112** (with shorter ether chains) were obtained by slowly cooling of a solution of **112** in DMF from 100 °C to 75 °C. Cage **112** crystallizes in the

hexagonal space group P6$_3$/m, $a = b = 19.2235$ Å, $c = 26.6855$ Å, $V = 8540.3$ Å^3 (Figure 18c, d). **110** and **112** have oxygen atoms in the side-chains, but their packing motifs are similar to **105** and **106**. The main driving force of packing is the π-π stacking interaction between aromatic rings, which can be seen in Figure 18b, d.

105:d$_1$ = 22.87 Å   **106**:d$_2$ = 22.75 Å

110:d$_3$ = 23.65 Å   **112**:d$_4$ = 22.43 Å
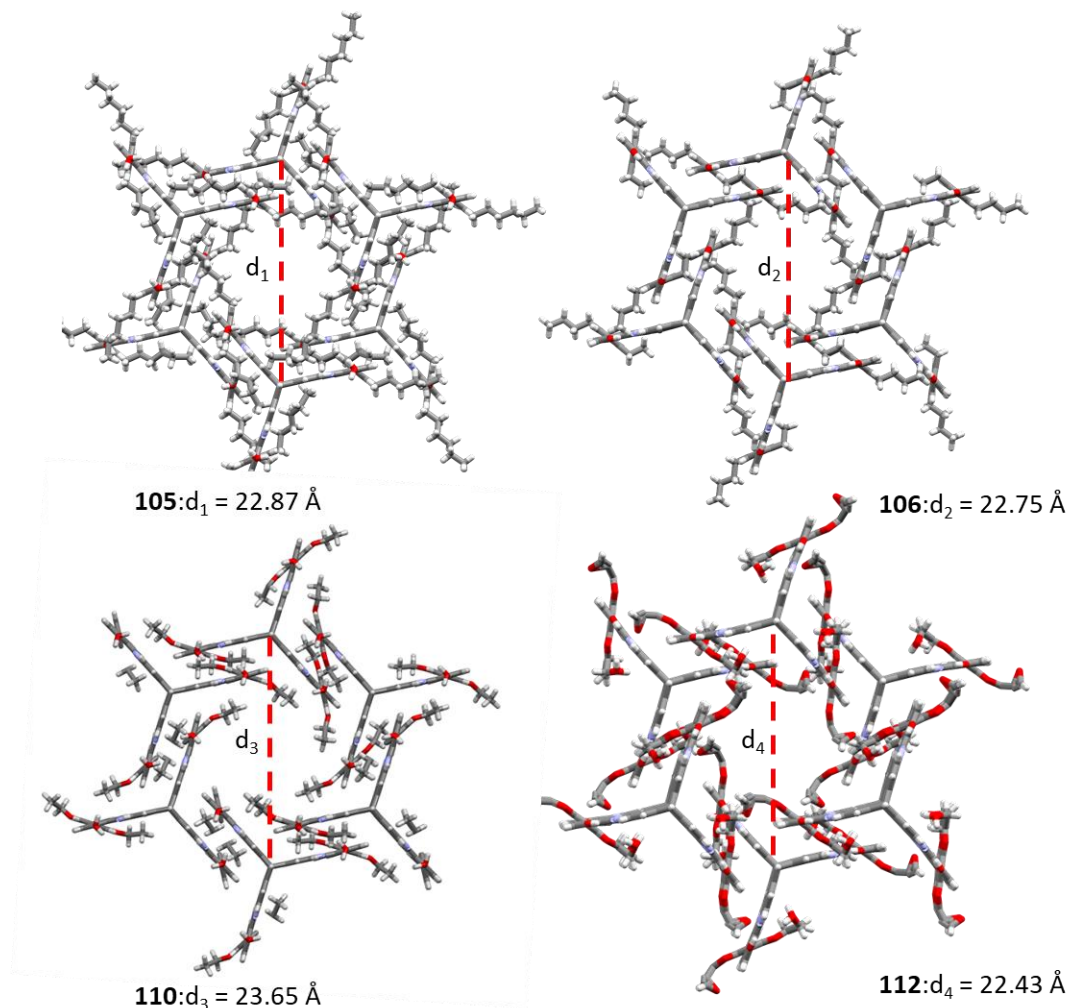
Figure 19. The macrocycle-like structure formed by six molecules of cage **105** (hexyl chains), **106** (octyl chains), **110** (oxypentene chains) and **112** (shorter ether chains)

From Table 3 and Figure 17, 18, it can be seen that although cage **105**, **106**, **110** and **112** have different side-chains, the unit cell parameters and the packing motifs are quite similar. Six cage molecules can be recognized as a group which forms a "macrocycle" structure (Figure 19), and further forms a hexagonal channel along the *c*-axis. The distances between two opposite cage molecules of the "macrocycle" are shown in Figure 19 and it can be figured out the size of the channels are similar. For cage **104** (with butyl chains), although the crystal structure was not obtained, the Powder XRD result (Figure 20) indicates that the packing motif of cage **104**

should be similar to cage **106** (with octyl chain) because the experimental data of cage **104** is similar to the calculated data from the crystal structure of cage **106**. For these five cages (**104**, **105**, **106**, **110**, **112**), different side-chains don't show influence on the packing motifs and the unit cell parameters.
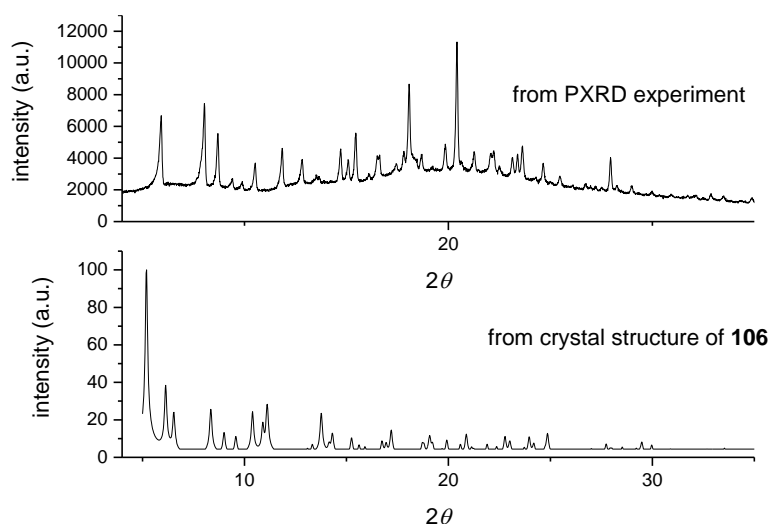

Figure 20. Top: PXRD experimental data of cage **104** (with butyl chains), bottom: calculated result from the crystal structure of cage **106** (with octyl chains)

Cage **111**, the terphenyl cage with perfluorobutyl chains, has another type of crystal structure. The crystals of **111** were obtained by methanol slowly diffusing into a solution of **107** in THF at room temperature. **111** crystallizes in the trigonal space group R3c, $a = b = 19.0156$ Å, $c = 64.026$ Å, $V = 20049.6$ Å^3 (Table 3). The distance between the two interior bridgehead-protons is 11 Å. As is depicted in Figure 21, the two triptycene parts are not aligned with each other. Instead, they are rotated by 30 degrees to each other (Figure 21c). As all hydrogen atoms have been replaced by fluorine atoms in the side-chains, no obvious C-H···π interactions are found in crystal packing. From Figure 21, **111** packs in some kind of "window-to-skeleton" mode and no π···π interaction are observed either. However, intermolecular halogen bonds can be found in this crystal between the fluorine atoms.[123]

The halogen bond is an electrostatically driven and noncovalent interaction, which has broad applications[123] in molecular self-assembly,[123b] crystal engineering[123c] and drug design.[123d] The polarizability of the halogen atom is the key to halogen bond.[123b] Therefore, the strength of halogen bonds typically decrease in order of I > Br > Cl > F.[123b] Two types of preferential angular geometries are identified as type 1 and type 2 contacts (Scheme 17).[124] Type 1 contact is symmetrical with $\theta_1 = \theta_2$, whereas type 2 contact is characterized by $\theta_1 \approx 150°$ to $180°$, $\theta_2 \approx 90°$ to $120°$. Furthermore, a triangular structure involving three halogen···halogen contacts,

X-3 synthon, has been identified as a common building block for various supramolecular structures.
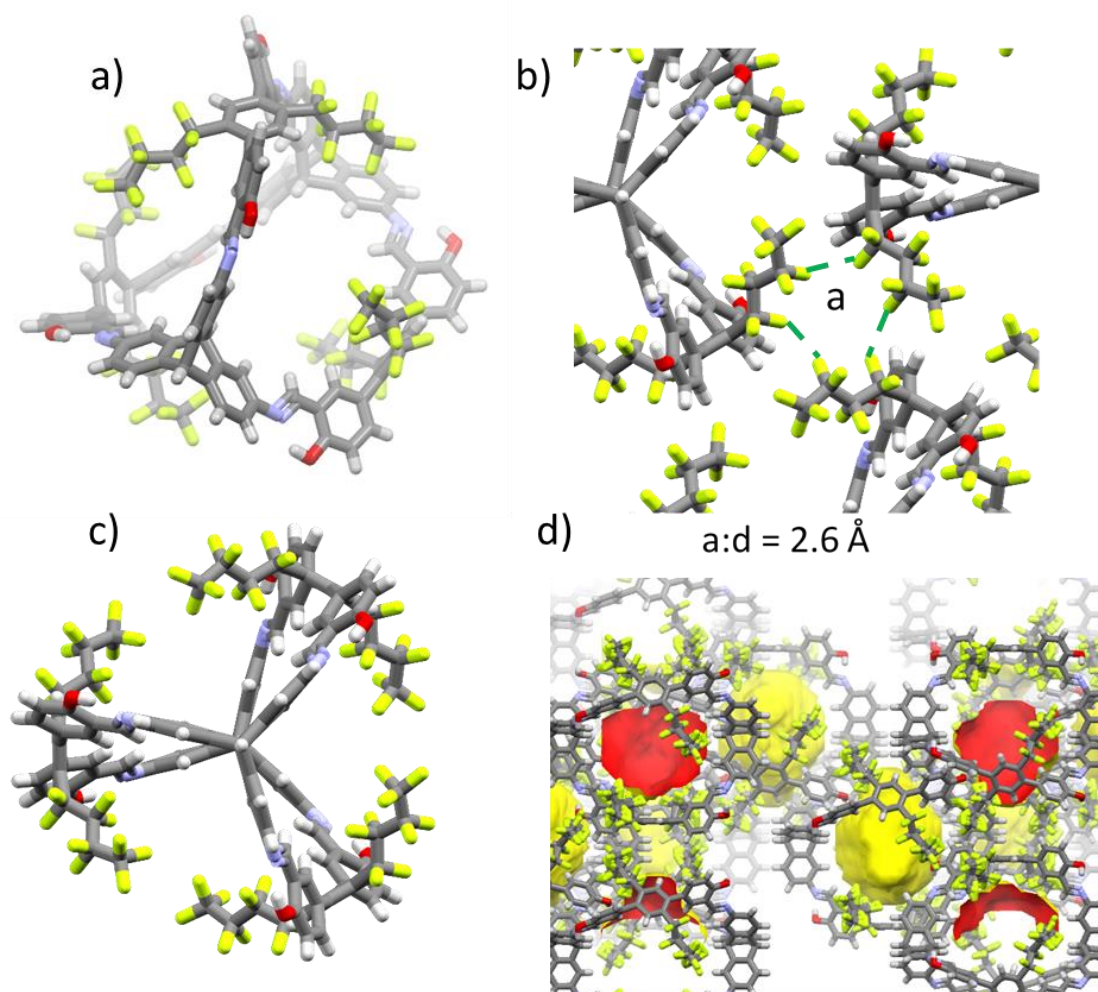
Figure 21. Single crystal structure of cage **111** a) crystal structure of **111** shown as stick model. b) F-F interaction between cage molecules c) single molecular shown from top side d) solvent accessible pores calculated for a probe with radius 1.82 Å.
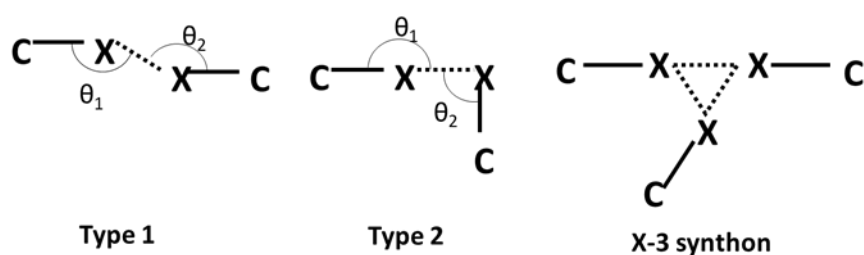
Scheme 17. Different kinds of halogen bonds.[124]

A few theories have been proposed to explain halogen bonding, among them the σ-hole theory is the most successful one.[123b] In this theory σ-holes are defined as regions of positive
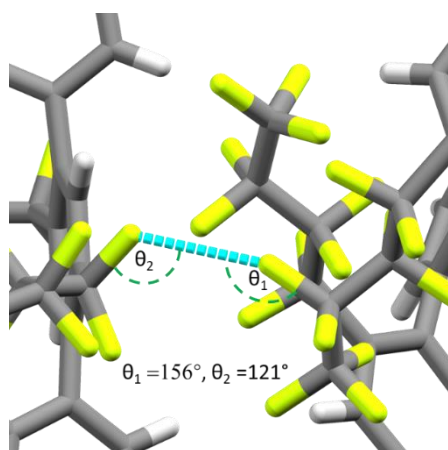
Figure 22. F-F bonds in cage **111**.

electrostatic potential on the outsides of halogen atoms, located at the extension of the halogen atom's covalent bonds. Three factors are used to determine whether σ-holes are present or not and determines their magnitudes. 1) the polarizability of halogen atom, 2) the electronegativity, and 3) the electron-withdrawing power. So the positivity of the σ-hole increases in order of F<Cl<Br<I.

The halogen interaction in compound **111** belongs to type 2, with $\theta_1 = 156°$ and $\theta_2 = 121°$ (Figure 22). The distance of this interaction is 2.6 Å. Meanwhile, every three molecules have formed a triangular structure by F···F contacts (Figure 21b), and the distance between different fluoride atom is 2.6 Å, which may be the main force for the formation of the trigonal space group. However, as the packing mode is quite dense compared with other terphenyl cages, no connected void is observed in this crystal structure. The voids large enough for the radius of the probe (1.82 Å) are the cavities inside the cages (Figure 21d).

3.1.4 Theory of determining the surface of porous materials

Adsorption happens when a solid surface is exposed to a gas or liquid: it is defined as the "enrichment of material or increase in the density of the fluid in the vicinity of an interface."[125] In this section, only the adsorption occurring between gas and solid surface will be discussed.

Table 4. Several important definitions about determining surface area from IUPAC.[127]

Term	Definition
Adsorption	Enrichment of one or more components in the vicinity of an interface
Adsorbate	Substance in the adsorbed state
Adsorbent	Solid material on which adsorption occurs
Physisorption	Adsorption without chemical bonding
Surface area	Extent of the surface assessed by a given method under stated conditions
Specific surface area	Surface area of unit mass of powder, as assessed under stated conditions
Micropore	Pore of internal width < 2 nm
Mesopore	Pore of internal width between 2 and 50 nm
Macropore	Pore of internal width > 50 nm

Adsorption measurements are important techniques which are widely used in many academic and industrial fields, and gas adsorption has become one of the most widely used measurements

for determining the surface area and pore sizes distribution of porous materials.[126] Some important definitions which will be used in discussion are listed in Table 4. These definitions are congruent with the International Union of Pure and Applied Chemistry (IUPAC).[127]

For a gas adsorbed on a particular solid at a given temperature, the equation between the amount of gas n^a adsorbed by unit mass of solid m^s and the relative pressure p at known temperature T can be written as:[125]

$$n^a/m^s = f(p/p^0)T \tag{1}$$

Where p^0 is the saturation pressure of the adsorptive. f is the function between relative pressure and the amount of gas adsorbed by unit mass of solid.

Equations (4) represents the adsorption isotherm which is usually presented in graphical form. By investigating many gas-solid adsorption systems, the adsorption isotherms show several characteristic shapes.[127] These shapes will provide useful information about the pore structure of the adsorbent. Most adsorption isotherms can be divided into six groups according to IUPAC classification (Figure 23).[123]
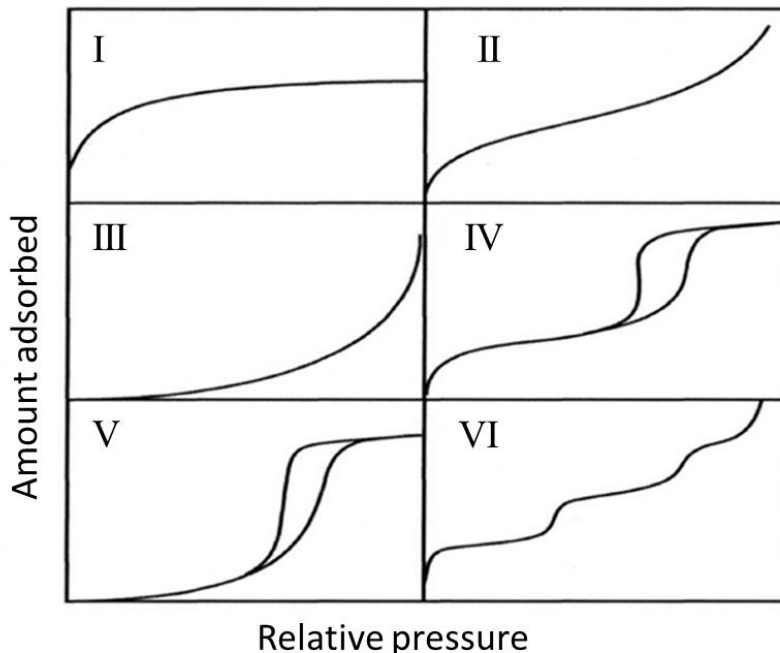
Figure 23.Classification of vapour adsorption isotherms combining proposals from IUPAC. [125] Reproduced with permission.[128] Copyright 2012, open access Creative Commons Attribution License

The Type I isotherm is concave to the X-axis (p/p_0), which is characteristic for microporous materials (Figure 23).[129] It can be seen as a rise of the curve due to the filling of the micropores

at low relative pressures, and ends in a saturation at higher relative pressures. The limitation of adsorption is dependent on the available micropore volume. The Type II is typical for non-porous or macroporous materials. This isotherm is concave to the X axis at first, then a turning point appears and the curve finally becomes convex to the X axis. The turning point means the monolayer sorption is complete and the multilayer sorption begins. Type III isotherm is convex to the X axis and no turning point appears, which indicates the weak interactions between the adsorbent and adsorbate. Type IV is quite similar to the Type II isotherm, but a plateau can be observed at high relative pressure. This isotherm is typical for mesoporous adsorbents. A Type V isotherm indicates the weak adsorbent-adsorbate interactions on a microporous or mesoporous solid. Type VI isotherm, which is also called stepwise isotherm, is quite rare and is obtained on one uniform, non-porous surface.

3.1.5   The Langmuir Theory and Brunauer-Emmett-Teller (BET)Theory

The Langmuir theory is based on the idea of monolayer adsorption on homogeneous surfaces,[130] and the assumptions of this theory include 1) all adsorption sites are equivalent, 2) each site can adsorpt only one molecule ,3) there are no interactions between adsorbate molecules and 4) the adsorption sites are independent of each other.

It needs to be mentioned that the original Langmuir model is only for monolayer adsorption and is of limited use, but it is the start for the BET treatment and other more refined physisorption isotherm equations.[131] The original derivation of the Langmuir equation is a kinetic one.[124] The adsorbent surface can be regarded as an array of N^s independent sites for adsorption gas molecules. The fraction of N^s sites occupied by N^a molecules is $\theta = \frac{N^a}{N^S}$.

From the kinetic theory of gases,[132] the pressure p and the fraction of unoccupied sites $(1-\theta)$ determine the rate of adsorption. And the fraction of occupied sites θ and activation energy E determine the rate of desorption. When the adsorption reaches the equilibrium, which means the progress reaches a point that the rates of adsorption and desorption are same. The net rate of adsorption is zero:

$$\frac{dN^a}{dt} = \alpha p(1 - \theta) - \beta\theta e^{(-\frac{E}{RT})} = 0 \tag{2}$$

Where α and β are the characteristic constants for the given gas-solid system.

In the assumptions of the Langmuir theory, there is on interaction between the adsorbed molecules, so the adsorption energy E is a constant. By rearrangement and simplification, equation (2) could be written like this:

$$\theta = \frac{bp}{1+bp} \tag{3}$$

where b is the adsorption coefficient, which is defined as:

$$b = K\, e^{\left(\frac{E}{RT}\right)} \tag{4}$$

where K is the ratio of the adsorption and desorption coefficients.

In the 1930s, research indicated that the physical adsorption of gas is not a monomolecular surface coverage if the relative pressure is high enough.[125] In 1938, Emmett and Brunauer found the turning point the Type II isotherm (Figure 23) was the point that the monolayer adsorption completed.[132] Brunauer and co-workers proposed the BET theory, which extended the Langmuir theory to a multilayer adsorption. According to the BET theory, the adsorbed molecules in one layer can be regarded as the ideal layer to adsorb molecules as the next layer (Figure 24). At any pressure below the saturation pressure p_0, fractions of the surface are covered by 0, 1, 2, …, i layers of adsorbed molecules. The BET theory is based on the following assumptions: [132]

1) Gas molecules only interact with adjacent layers;

2) The Langmuir theory can be applied to each layer
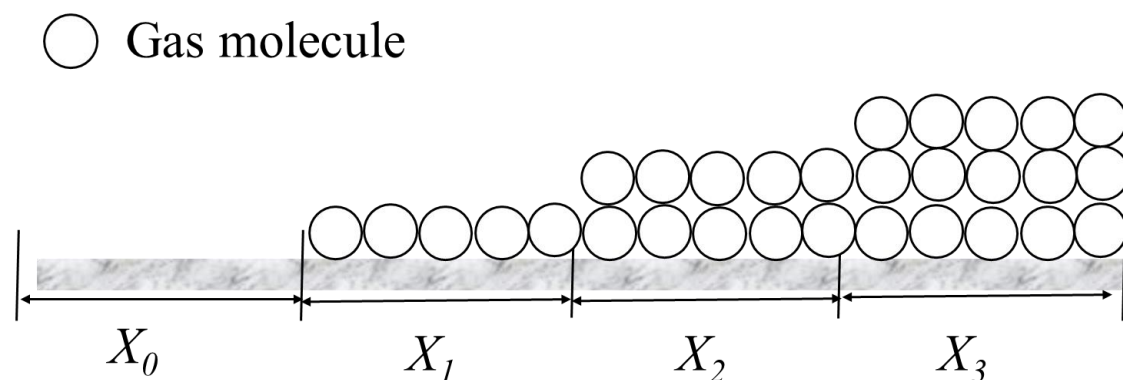
Figure 24. Schematic model of BET theory.

If it is assumed as a pressure p, the adsorption and desorption progress reaches the equilibrium, the fractions of uncovered and covered surface, θ_0 and θ_1 remain constant. So the rate of adsorption of the bare surface and the desorption of first layer are equal:

$$a_1 p \theta_0 = b_1 \theta_1 e^{(-\frac{E_1}{RT})} \tag{5}$$

Where a_1 and b_1 are the constant for adsorption and desorption of the first layer, and E_1 is the value of the energy of adsorption in the first layer. If equation (5) is extended to layer i, the adsorption of layer i-1 and the desorption of layer i could be written as:

$$a_i \mathrm{p} \theta_{i-1} = b_i \theta_i e^{(-\frac{E_i}{RT})} \tag{6}$$

The sum of the fractions of surface equals unity:

$$\theta_0 + \theta_1 + \cdots + \theta_i + \cdots = 1 \tag{7}$$

The total adsorbed amount n could be written as:

$$n = n_m [1\theta_1 + 2\theta_2 + \cdots + i\theta_i + \cdots] \tag{8}$$

Where n is the total amount gas adsorbed at pressure p, n_m is the occupied amount of monolayer

According to the assumptions, the Langmuir model could be applied to each layer, so each layer has a different group of a_i, b_i and E_i, for the layers higher than the second layer, the energy of adsorption E_i is equal to the liquefaction energy, E_L,

Let

$$g = \frac{b_i}{a_i} \tag{9}$$

As b_i and a_i are constant of adsorption and desorption of layer i, g is also a constant. So for θ_0, equation (8) can be written as

$$\theta_0 = y\theta_0 \tag{10}$$

Where

$$y = \frac{a_1}{b_1} p e^{(\frac{E_1}{RT})}$$

And θ_i can be written as:

$$\theta_i = x\theta_{i-1} = x^{i-1}\theta_1 = yx^{i-1}\theta_0 \tag{11}$$

Where

$$x = \frac{p}{g} e^{\left(\frac{E_L}{RT}\right)} \tag{12}$$

If we define a constant C:

$$C = \frac{y}{x} = \frac{a_1}{b_1} g e^{\left(\frac{E_1 - E_L}{RT}\right)} \tag{13}$$

Then

$$\theta_i = C x^i \theta_0 \tag{14}$$

So equation (8) can be written as:

$$\frac{n}{n_m} = \sum_{i=1}^{\infty} i\theta^i = C \sum_{i=1}^{\infty} i x^i \theta_0 \tag{15}$$

Because

$$\sum_{i=1}^{\infty} i x^i = \frac{x}{(1-x)^2} \tag{16}$$

So equation (15) can be written as:

$$\frac{n}{n_m} = \frac{Cx}{(1-x)(1-x+Cx)} \tag{17}$$

If at the saturation pressure p_0, and the adsorbed layer is assumed to be of infinite thickness, $x = \frac{p}{p_0}$, so that:

$$\frac{n}{n_m} = \frac{C\left(\frac{p}{p_0}\right)}{\left(1-\left(\frac{p}{p_0}\right)\right)\left(1-\left(\frac{p}{p_0}\right)+C\left(\frac{p}{p_0}\right)\right)} \tag{18}$$

Which could be written in the linear form:

$$\frac{p}{n(p_0-p)} = \frac{1}{n_m C} + \frac{C-1}{n_m C} \cdot \frac{p}{p_0} \tag{19}$$

3.1.6 The Gas-sorption properties of terphenyl imine cage with side chains

Gas sorption experiments of cages **104** (with butyl chains), **105** (with hexyl chains), **106** (with octyl chains), **111** (with perfluorobutyl chains) and **112** (with shorter ether chains) were performed because enough crystalline materials of these five cages were collected. The crystalline materials were needed were prepared from THF (**104**, **105**, **106**, **111**) or DMF (**112**).

After carefully removing the crystals from the growing solutions, the solvent was exchanged by methanol then pentane or liquid ethane. From the PXRD results (Figure 25), cages **105**, **106** (still show some peaks) and **112** lost their crystallinity but cage **104** and **111** were still crystalline materials after pre-activation at 40 °C. TGA measurements of these five cages were also done to make sure the cage would not decompose at high temperature. From Figure 26, it can be seen that all cages are stable under 350 °C. The thermal stabilities of cage **104** (decomposed at 450 °C) and **112** (decomposed at 500 °C) are comparable to cage **103** (terphenyl cage without side chain, decomposed at 450 °C).[49b] The most unstable one among these five cages is cage **106** (with octyl chains), which began to decompose at 350 °C.
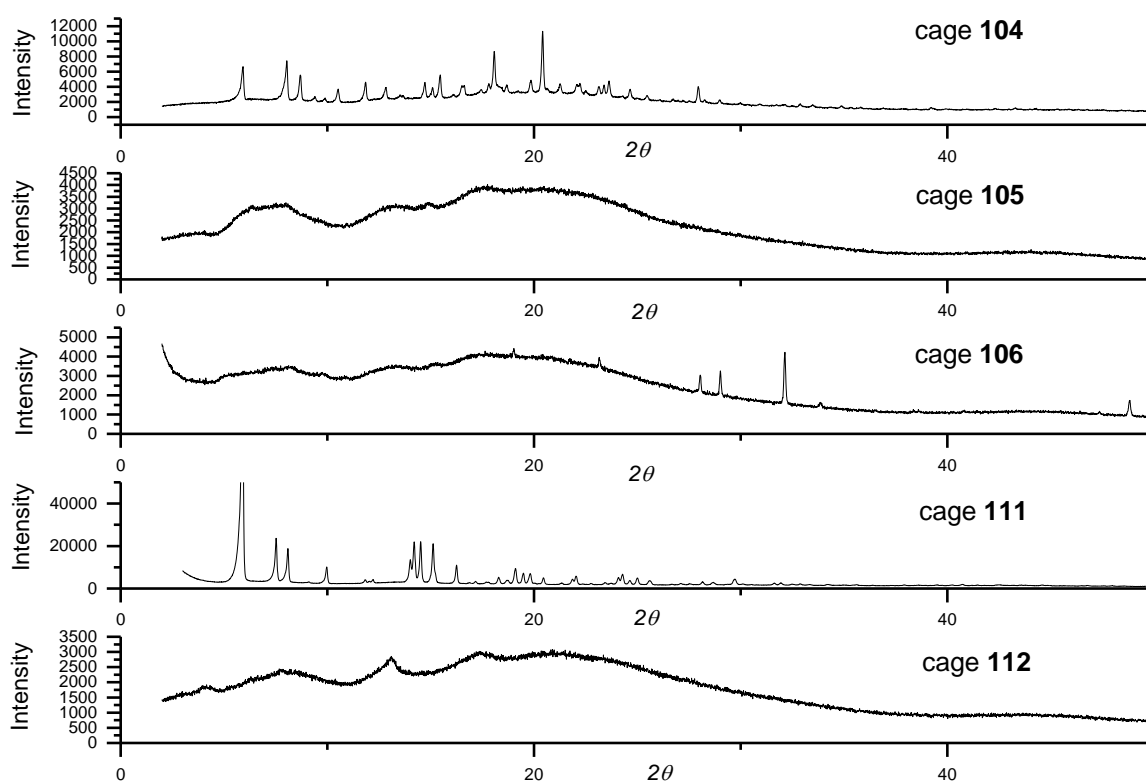
Figure 25 From top to bottom: PXRD of cage **104** (with butyl chain), **105** (with hexyl chain), **106** (with octyl chain), **111** (with perfluorobutyl chain) and **112** (with shorter ether chain).

The gas sorption experiment (N_2, 77 K) results reveal that all of these cages are not porous except cage **111** (Table 5, Figure 27). These results are opposite to the crystal structures. For alkyl cages **104**, as explained in **3.2.3** (page 35), six single molecules pack like a hexagon macrocycle and these macrocycles form channels inside the material. However, as the cages contain side chains which fail to be determined by the crystal structures, these side chains may lie inside the channels and transform the pore type from through pores to closed pores.
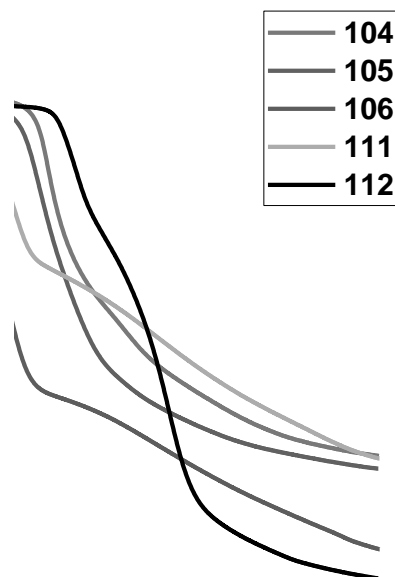
Figure 26 TGA curves of cage **104** (with butyl chain, red), **105** (with hexyl chain, blue), **106** (with octyl chain, purple), **111** (with perfluorobutyl chain, green) and **112** (with shorter ether chain, black).

Table 5. Specific surface areas[a] of cage compounds **104**, **105**, **106**, **111**, **112**

	Phase [b]	SA_{BET} (m^2/g)
104 (with butyl chain)	crystalline	28
105 (with hexyl chain)	amorphous	15
106 (with octyl chain)	amorphous	15
111 (with perfluorobutyl chain)	crystalline	588
112 (with shorter ether chain)	amorphous	4

a: measured by N_2 at 77 K. b: determined by PXRD experiment.

What is difficult to explain is the result of cage **111** (with perfluorobutyl chain). According to the crystal structure, **111** only contains closed pores, but from the gas sorption experiment (Table 5, N_2, 77K), **111** shows porosity with ta specific surface area of $SA_{BET} = 588$ m^2/g. The isotherm can be classified as Type I isotherm (Figure 27a), which indicates this material contains micropores. The NL-DFT calculation yields a pore size of 0.8 nm for the material (Figure 27b). A possible explanation is that the packing motif of the crystal used for gas sorption is different from the one used for XRD measurement, so a PXRD measurement was done to compare with the simulated one from the crystal structure. From Figure 28, it can be seen that the peaks are quite similar, suggesting the packing motifs of these two crystal are the same. The second explanation for this is that maybe the perfluorobutyl chains are flexible

enough for that the gas molecules to pass through the side chains and access to the void inside the cage.
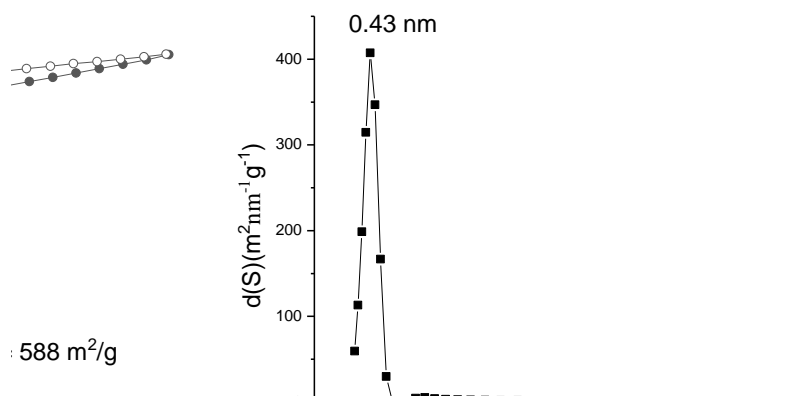
Figure 27.a): Nitrogen sorption at 77 K for cage **111** (with perfluorobutyl chain).Filled symbol: adsorption, open symbols: desorption b):NL-DFT pore size distribution
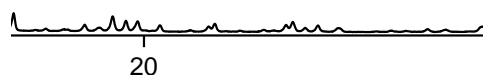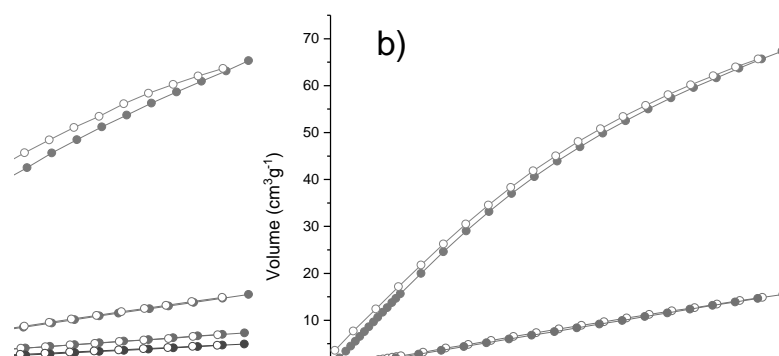

Figure 28 PXRD of cage **111**(with perfluorobutyl chain). top: the data from PXRD experiment. bottom: data calculated from crystal structure.

As cage **111** is the only sample that possesses a specific surface area of 588 m^2/g, the adsorption of other gases was further investigated (Figure 29). However, compared with other porous cages, the uptakes of H$_2$, CO$_2$ and methane were not high (Table 6). The uptake of hydrogen at 77 K was 4.9 mmol/g (0.99 wt%, 1 bar), which is lower than CC5-*R* (8.5 mmol/g,

1.71 wt%),[133] and an imine cube (7.3 mmol/g, 1.43 wt%) synthesized by the Mastalerz group.[95b] The uptake of CO_2 was 2.72 mmol/g (11.96 wt%, 1 bar) and for CH_4 it was 0.65 mmol/g (1.03 wt%, 1 bar). The uptake of CO_2 is comparable to some other imine cages, for instance, CC5-*R* (3.1 mmol/g, 13.6 wt%) synthesized by the Cooper group,[133] and the [2+3] imine cage **24** (2.7 mmol/g, 11.9 wt%) synthesized by the Mastalerz group,[49] but lower than the imine cube (4.1 mmol/g, 18.2 wt%). The Henry selectivity of CO_2/CH_4 is 5.6, which is higher than cage **24** (4.0),[49] but lower than the imine cube (7.7)[95b].

Figure 29. Other gas sorption isotherms of **111** (with perfluorobutyl chain). a) at 273 K. b) at 263 K. CO_2: red, CH_4: purple, N_2: green and H_2: blue.

Table 6. Comparison of gas sorption data of cage **111** (with perfluorobutyl chain) with other cage compounds published previously

Entry	Phase	SA_{BET}[a]	Uptake in mmol/g (wt%, 1bar)			Selectivity		Ref.
		(m^2/g)	H_2 (77 K)	CO_2 (273 K)	CH_4 (273 K)	CO_2/CH_4	CO_2/N_2	
111	crystalline	588	4.9 (0.99)	2.7 (11.96)	0.65 (1.03)	5.6	11.7	
24	crystalline	744	n. d	2.7 (11.9)[b]	0.7 (1.12)[b]	4.0	n. d	49
CC5-*R*	crystalline	1333	8.5 (1.71)	3.1 (13.6)	n. d	n. d	n. d	133
Imine cube	amorphous	1014	7.3 (1.43)	4.1 (18.2)	1.3 (2.04)	7.7	34	95b

a: SA = specific surface area, N_2, 77 K. b: measured at 298 K

A lot of attention has been paid to Greenhouse gases because of their ability to affect Earth's climate. [134] Except CO_2, which is the biggest problem in this area, there are still some other potential global warming gases.[134] For example, chlorofluorocarbons and fluorocarbons are commonly used as refrigerants, propellants, or in the electronics industry. [135] Among all the greenhouse gases, SF_6 has the highest global warming potential (GWP, "a measure of how much heat a greenhouse gas traps in the atmosphere up to a specific time horizon")[136] value of 22800 over a 100-year time horizon (CO_2, according to the definition, has a GWP value of 1 regardless of the time period used). Furthermore, this figure further increases almost 50% for a 100-year timescale because of the stability and high lifetime of SF_6 (SF_6: 3200 years, CO_2: 30-95 years).[135] Meanwhile, the emission levels of SF_6 rise continuously with an annual increase rate of 5 to 10% due to the increase of industrial use (as a dielectric medium),[137] including the electrical equipment sector, semiconductor manufacturing and magnesium production. For instance, the emission of SF_6 in China in 1990 was 45 t, but it is predicted to reach 4270 t by 2020.[137] So the capture and separation of SF_6 or other perfluorocarbons are of great interest. According to literature, zeolites and MOFs have been investigated for the selective adsorption of SF_6.[138] However, there is only one paper using organic cage compounds.[139]
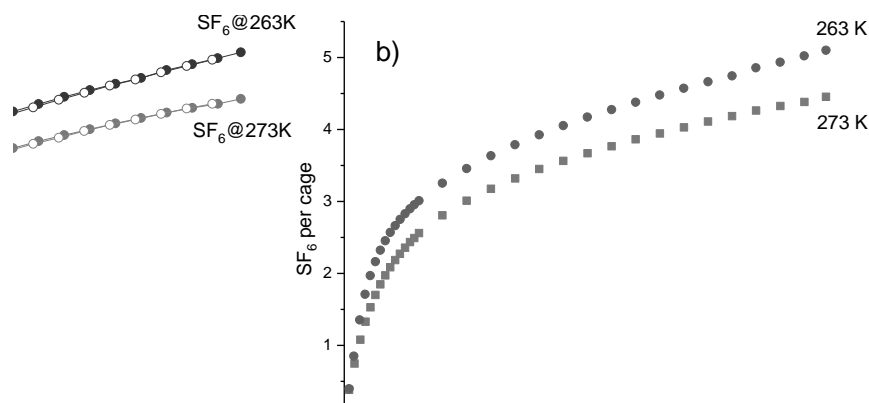
Figure 30. a) SF_6 sorption of cage **111** (with perfluorobutyl chain) at 263 K and 273 K. b) The uptake expressed in terms of the number of SF_6 molecules per cage molecule at 263 K and 273 K.

Cage **111** shows a high affinity for SF_6, and a type I isotherm (Figure 30a) is produced from the gas sorption experiment. The saturation uptake of SF_6 is 1.61 mmol/g at 273 K and 1.8 mmol/g at 263 K, which corresponds to four (273 K) or five (263 K) SF_6 molecules per cage **111** molecule (Figure 30b). The crystal structure of cage **111** shows the distance between two triptycene bridgehead-H is 11 Å. The kinetic diameter of SF_6 is 5.13 Å.[139] So according to

calculation, if four small spheres are put into a larger sphere which diameter is 11 Å, the longest dimeter of these small spheres is 5.07 Å, which fit for the kinetic diameter of SF$_6$ (assume the void of **111** and SF$_6$ molecule as spheres).

This uptake of SF$_6$ is lower than the [4+6] CC3α cage (2.3 mmol/g)[139] and Mg-MOF-74 (highest, 6.42 mmol/g), but can be comparable to frameworks like UiO-66-Zr (1.5 mmol, 293 K),[140] CAU-17 (1.61 mmol, 273 K)[141] and MIL-100 (1.45 mmol, 283 K).[142] SF$_6$ isotherm for cage **111** suggests a potential application for SF$_6$ separation from nitrogen, and therefore a nitrogen isotherm was also measured at 273 K which made it possible to predict the selectivity based on the ideal adsorbed solution theory.

3.1.7 Ideal adsorbed solution theory (IAST) selectivity

The ideal adsorbed solution theory was proposed by Prausnitz and co-workers in 1965.[143] This theory has been widely used to study the adsorption equilibria of gas mixtures, but it only need the isotherms of the pure gases.[144]

IAST is based on three assumptions: 1) the surface is the same for all gases, 2) the gases have no interaction to each other, and 3) the gas mixture behaves as an ideal solution.[143]

The spreading pressure can be calculated according to Gibbs isotherm:[145]

$$\frac{\pi A}{RT} = \int_0^{p_i^0} \frac{n_i}{P_i} \, dP_i \tag{20}$$

π is the spreading pressure, P_i is the partial pressure, n_i is the amount of adsorbed component i at pressure, p. A is the surface area of the adsorbent, and R is the ideal gas constant. P_i can be calculated as:

$$P_i = y_i P = x_i p_i^0(\pi) \tag{21}$$

Where $p_i^0(\pi)$ is the partial pressure of component i at given temperature and spreading pressure π. x_i is the mole fraction of component i in the mixture At equilibrium, each component has the same spreading pressure:

$$\pi_i = \pi_j \quad i \neq j \tag{22}$$

The total amount adsorbed of the mixture, n_t, can be calculate from:

$$\frac{1}{n_t} = \sum_{i=1}^{N} \frac{x_i}{n_i^0} \tag{23}$$

Where N is the total species of the gas mixture, n_i^0 is the amount of component i adsorbed at the same temperature and pressure when there is no other components. The actual loading of component i is:

$$n_i = x_i n_t \tag{24}$$

So according to IAST, the selectivity for component A relative to component B is defined as

$$S_{A/B} = \frac{x_A/x_B}{y_A/y_B} \tag{25}$$

Where x_A and x_B are the loading of components A and B in the adsorbed phase, y_A and y_B are the partial pressure of component A and B.

As the selectivity of IAST is calculated from the single-component system, a proper model must be carefully chosen for the single-component isotherm. In this chapter, for the CO_2 and SF_6 isotherms were used the Tóth model, while for the CH_4 and N_2 adsorption isotherms were used the single site Langmuir-Freundlich model.
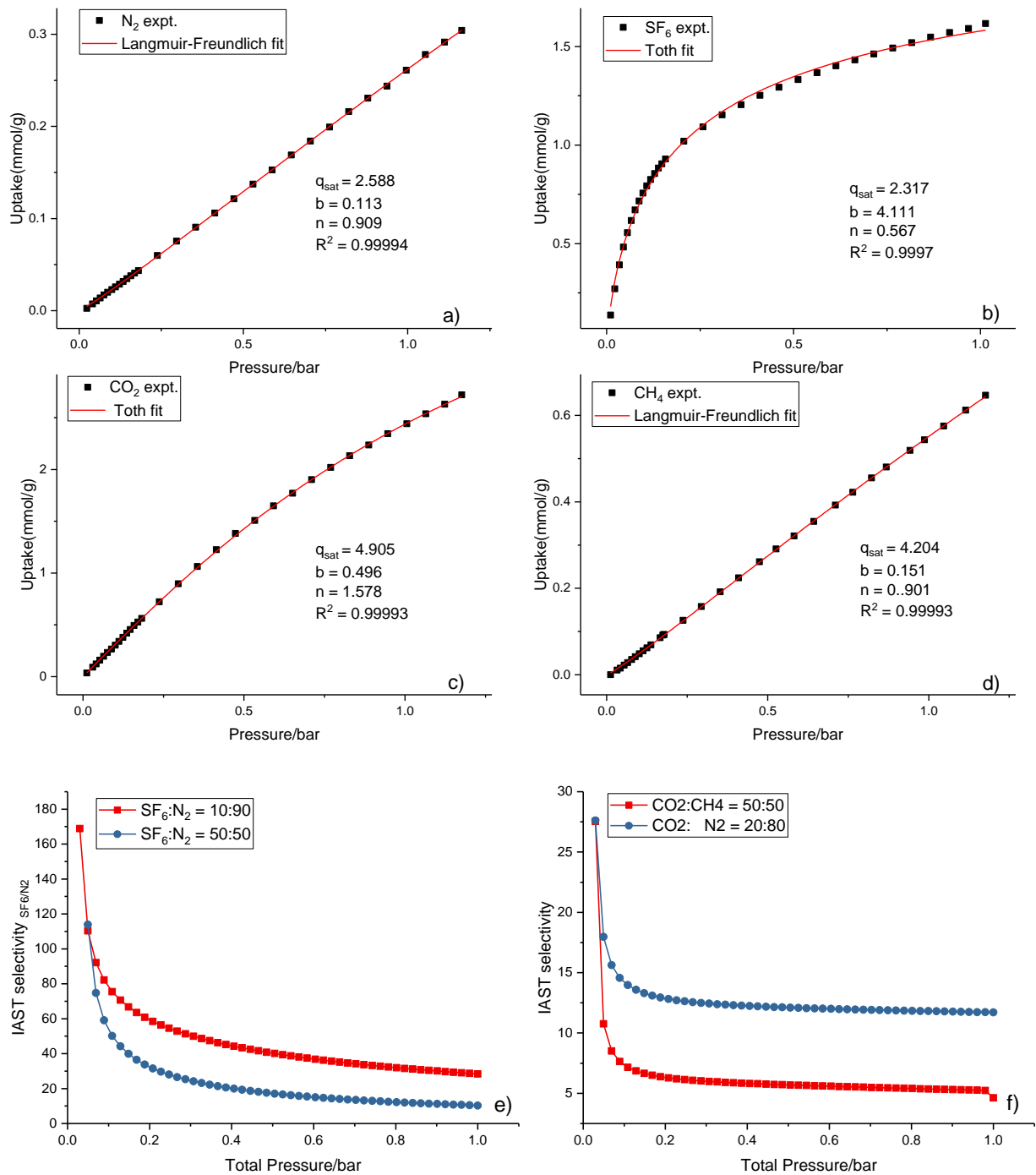
Langmuir-Freundlich equation:[146]

$$q = \frac{q_{sat} \times b \times p^{1/n}}{1 + b \times p^{1/n}} \tag{26}$$

where p is the pressure of the gas at equilibrium, q is the adsorbed amount per mass of adsorbent, q_{sat} is the saturation adsorbed amount of the site, and b is the affinity coefficient of the site, and n is the deviation from the ideal surface.

The Tóth equation is:[147]

$$q = \frac{q_{sat} \times b^{1/n} \times p}{(1 + b \times p^n)^{1/n}} \tag{27}$$

Figure 31. The IAST selectivity was derived using experimental, single-component isotherms of a) N_2, b) SF_6, c) CO_2, d) CH_4 at 273 K. The IAST selectivity of e) SF_6 over N_2 of cage **111** at SF_6:N_2 ratios of 50:50 and 10:90 and f) CO_2 over N_2 at CO_2: N_2 ratio of 20:80 and CO_2 over CH_4 at CO_2:CH_4 ratio of 50:50 at 273 K.

For cage **111**, the Henry selectivity was $S_{CO2/CH4} = 5.6$, $S_{CO2/N2} = 11.78$, $S_{SF6/N2} = 107$. The IAST selectivities of SF_6/N_2, CO_2/N_2 and CO_2/CH_4 were calculated in order to study the behaviour of mixture adsorption (Figure 31). Based on the industrial application,[148] the compositions of these two-gas mixtures used were: SF_6:N_2 = 10%:90% and 50%:50%, CO_2:CH_4 = 50%:50% and CO_2: N_2= 20%:80%, From Figure 31 and Table 7, the IAST selectivity of SF_6/N_2 of cage

111 was 28 at 1 bar, 273 K, which is similar to some frameworks and zeolites (Mg-MOF-74:[138] 20, at 1bar, 298 K, Ca-A-zeolite:[141] 28, at 1bar, 298 K, MIL-100:[142] 24, at 1bar, 298 K, CAU-17:[149] 31, at 1 bar, 273 K), but lower than Cooper's CC3α cage (178, 1 bar, 273 K)[139], Zeolite-13X (44, 1 bar, 298 K),[150] Uio-66-Zr (74, 1 bar, 298 K).[140] But from the IAST curve of SF_6/N_2, the selectivity increases at lower pressure, for instance, at 0.1 bar, the IAST selectivity of SF_6/N_2 (10:90) would become 78. The selectivity decreases if the percentage of SF_6 is increased to 50%, but the curves of IAST selectivity are of similar shape, which inferrs that cage **111** has better selectivity on SF_6/N_2 at lower pressure. The IAST selectivity of CO_2/N_2 is 11 (1 bar, 273 K, 20: 80), and CO_2/CH_4 is 5 (1 bar, 273 K, 50:50). Although from Figure 31, the selectivity for all these group of mixtures becomes higher at the lower pressure, they still exhibit some differences. For SF_6/N_2, it slowly increases from 1 bar to 0.3 bar, but from 0.3 to 0.1 bar, the selectivity increases sharply. For CO_2/CH_4 and CO_2/N_2, the selectivity stays more or less constant from 1 bar to 0.2 bar, and shows a sharp increase when the pressure is lower than 0.1 bar, which is no longer the effective range of IAST selectivity. So comparing IAST selectivity and Henry selectivity, the Henry selectivity is almost the same as the IAST selectivity for CO_2/N_2 and CO_2/CH_4, but for SF_6/N_2, it differs a lot. This may be because of the adsorbed amount of SF_6 increases more quickly in low pressure area than for CO_2, which is consistent with the gas sorption isotherms of these two gases at 273K (Figure 29, Figure 30).

Table 7. Comparison of gas sorption data of cage **111** with selected literature known materials which showed adsorption of SF_6.

Entry	SA$_{BET}$ (m^2/g)^a	Uptake in mmol/g (273 K, 1bar)	IAST selectivity SF$_6$/N$_2$ (10:90)	Ref.
111	588	1.61	28(1 bar, 273 K)	
			78(0.1 bar, 273 K)	
CC3α	624	2.3	178 (1 bar,273 K)	139
			150(0.1 bar, 273 K)	
Zeolite-13X	n.d.	n.d.	44 (1 bar,298 K)	150
Mg-MOF-74	1640	6.42 (298 K)	20 (1 bar,298 K)	138
Zn-MOF-74	992	3.3 (298 K)	46 (1 bar,298 K)	138
UiO-66-Zr	1290	1.5 (293 K)	74 (1 bar,298 K)	140

Ca-A-zeolite	n.d.	n.d.	28 (1 bar,298 K)	141
			Molecule sieve	
CAU-17	530	1.61 (273 K)	31 (1 bar, 273 K)	149
MIL-100	1772	1.45 (283 K)	24 (1 bar,298 K)	142

a: SA = specific surface area, N_2, 77 K

3.1.8　Conclusion

A series of terphenyl disalicylaldehydes with different side-chains were designed and synthesized. These aldehydes were used as precursors for the synthesis of ten new [2+3] terphenyl imine cages. All these cages show good solubility in DMF or THF compared with [2+3] terphenyl cage **103** (without side-chain). Five crystal structures of cages are obtained, and cage **104** (hexyl chains), **105** (octyl chains), **110** (oxypentene chains) and **112** (shorter ether chains) show similar unit cell parameters and packing motifs. According to nitrogen sorption data, cage **111** (perfluorobutyl chains) has a specific surface area $SA_{BET} = 588$ m^2/g, while the other cages exhibit no porosity in the crystalline or amorphous phase. Cage **111** also presents a good Henry selectivity of SF_6/N_2 $S_{SF6/N2} = 107$, and an IAST selectivity of SF_6/N_2 (10:90, 273 K) $S_{SF6/N2} = 28$, which gives cage **111** potential application in gas separations.

## 3.2 Synthesis and characterization of "three-component" cages

In Chapter **3.1**, a series of new imine cages were synthesized by introducing side-chains into the aldehyde building blocks. In this chapter, a new amine building block is synthesized by linking two triaminotriptycenes with a pyridine via amide bonds. This new amine building block can react with aldehydes to give new cages linked by imine bonds. As the amine building block has contained amide bonds already, the new synthesized cage contains two different linking bonds.

Meanwhile, there are some literature reports that the angle of the building blocks can determine the shape of the resulting cage.[54] In this chapter, the new amine building block is reacted with aldehydes with different length (by changing linkers), to see if the length of the aldehyde building block will affect the shapes of the formed cages.

3.2.1 Synthesis of tetraamine and dialdehyde building blocks
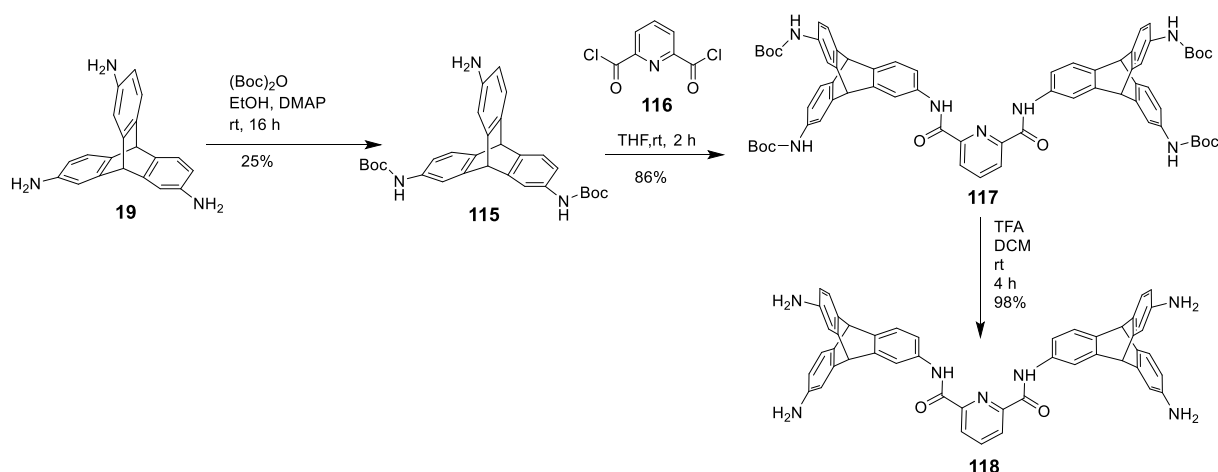
**Scheme 18.** Synthesis route of compound **114**. [151-153]
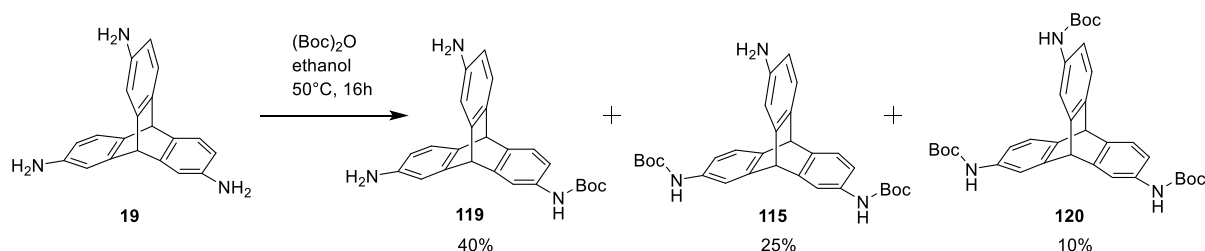
Scheme 19. Synthesis of compound **115**, **119** and **120**.[151]

The final product tetraamine **114** is obtained after three steps from triamine **19** (Scheme 18). *Tert*-butyloxycarbonyl (Boc) was used to prectect the amine group of triamine triptycene **19** first (Scheme 19), [151] in this reaction, three different products (one-fold **1119**, two-fold **115**

and three-fold **120,** Scheme 19) were obtained and isolated by column chromatography. The ^{1}H NMR spectra of these three compounds are presented in Figure 32. Protons H^a, $H^{a'}$ and $H^{a''}$ of the amines protected by Boc group show signlet at $\delta = 9.1$ ppm. Protons $H^{h'}$ and $H^{h''}$ of the free amines groups show singlet at $\delta = 4.8$ ppm. Three-fold **120** doesn't show the singlet at $\delta = 4.8$ ppm, and the ratio of the protected amine proton H^a and the bridgehead-H is 3:2, which indicates that three amine groups are all protected by Boc groups. For two-fold product **115**, the ratio of protons $H^{a'}$(-NH-): $H^{h'}$(-NH$_2$): bridgehead-H = 1:1:1, indicating two amine groups are protected by Boc groups. For one-fold product **119**, the ratio of protons $H^{a''}$(-NH-): $H^{h''}$(-NH$_2$): bridgehead-H = 1:4:2, which suggests only one amine group was protected by Boc group.
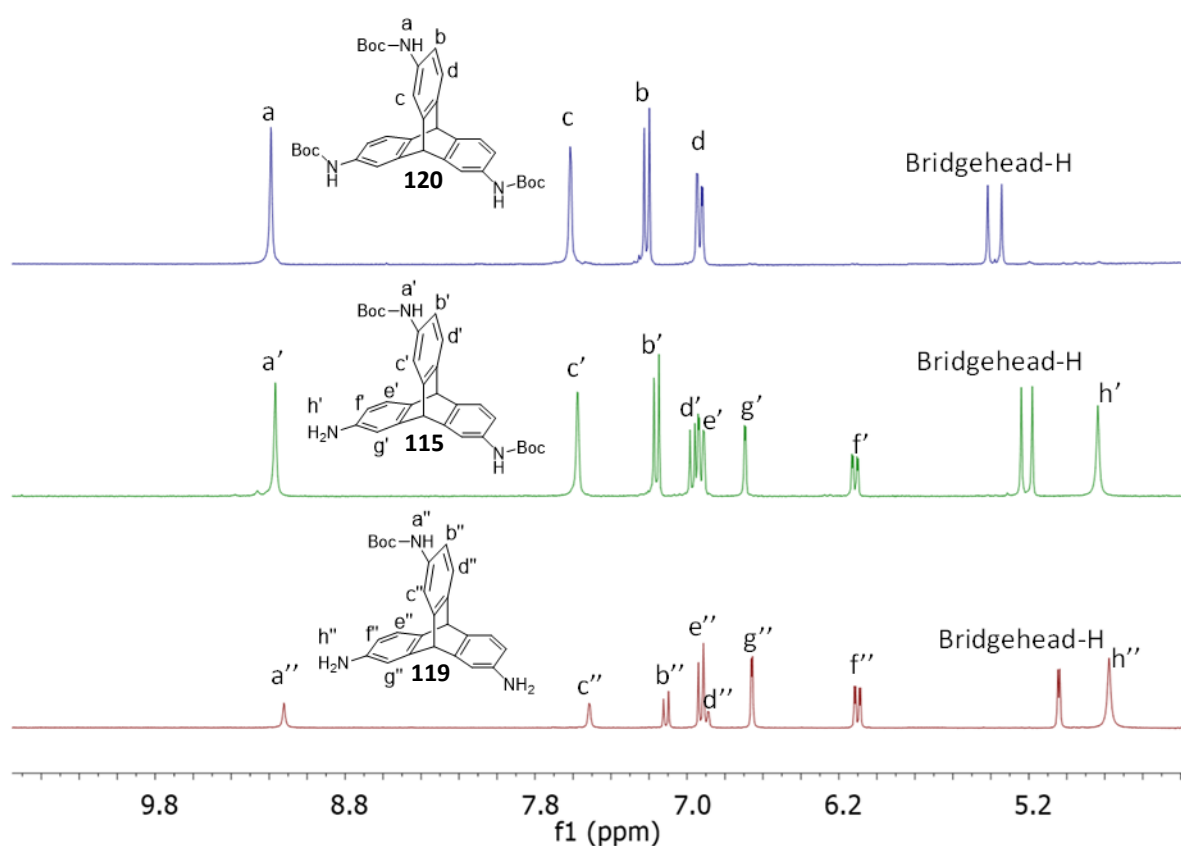
Figure 32.^{1}H NMR spectra of compound **115,119** and **120** (DMSO-d$_6$, 300 MHz)

Compound **117** is synthesized[j] with pyridine dicarbonyl dichloride **116** and two-fold triptycene **115** (Scheme 18).[152] The reaction was done in THF at room temperature and ratio of two starting materials (**115:116**) is 2:1.2, giving the yield of 86% after washing with water. The Boc protecting groups were deprotected in 10% TFA in DCM,[149] giving the final product **118** as a colourless powder with a yield of 98%.

The ^{1}H NMR spectrum of **118** is shown in Figure 33. The singlet H^k at $\delta = 4.73$ ppm is the -NH$_2$ protons while the singlet H^a at $\delta = 10.78$ ppm is the –NH- proton which is linked to the

triptycene and pyridine. The ratio $H^k:H^a = 4:1$, which fits for the structure of **118** (four amino groups and two amide groups). Two bridgehead proton H^j and $H^{j'}$ ($\delta = 5.13$ and $\delta = 5.06$ ppm) are shown in the ^{1}H NMR spectrum. Eight different peaks appears in the aromatic region, which can be assigned to two protons in pyridine (H^b, H^c) and six protons in aromatic part of triptycene (H^d, H^e, H^f, H^g, H^h, H^i). The MS of compound **118** is found at $m/z = 729.267$ (Calculated: 729.84), which also proves the formation of **118**.
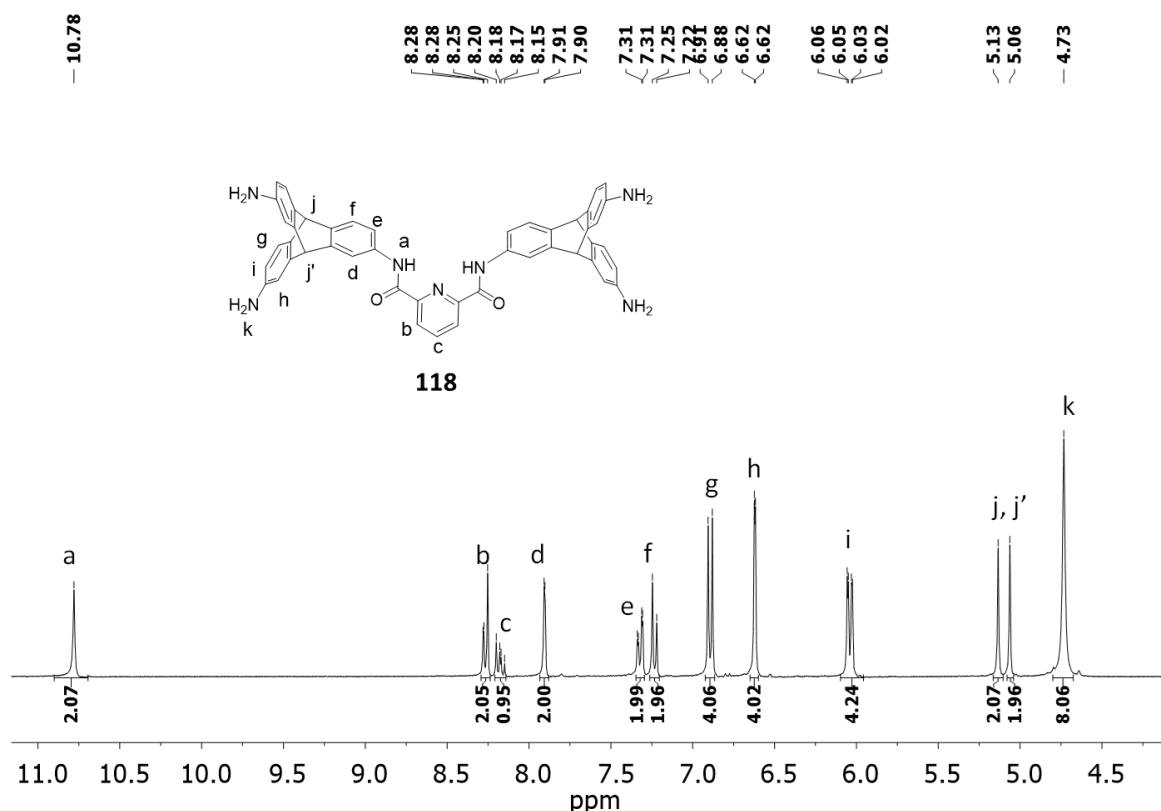

Figure 33. ^{1}H NMR spectrum of compound **118** (DMSO-d$_6$, 500 MHz).

A single crystal of **118** was obtained by diffusing methanol into a solution of **118** in THF. **118** crystallizes in the monoclinic, space group C2/c, $a = 23.5123$Å, $b = 18.7580$Å, $c = 22.9427$ Å, $V = 9473.7$ Å^3. **118** shows a tweezer-like shape in the crystal with an angle of 108 °C (Figure 34). The driving forces of packing are mainly $\pi\cdots\pi$ interaction (between triptycene groups) with the distance of 2.65 Å (Figure 34), and hydrogen bonds (-NH$\cdots$N, between two amino groups from adjacent **118** molecules, Figure 34).

a: $d_{\pi-\pi}$ = 2.65 Å, b: $d_{H\text{-}bond}$ = 2.06 Å
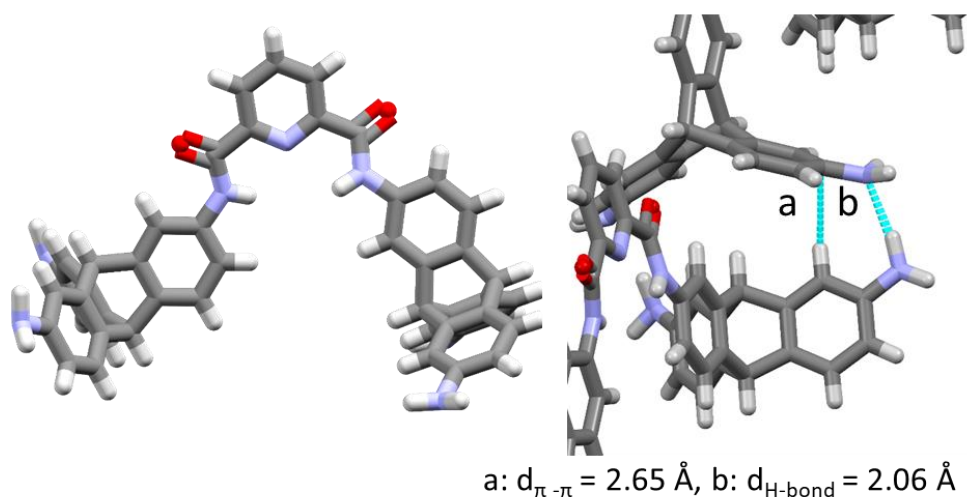
Figure 34. Crystal structure and interaction in packing motif of **118**.

| **20**	**121**	**21**	**22**	**102**	**122**
5.05 Å	9.3 Å	9.6 Å	12.0 Å	13.7 Å	17.8 Å
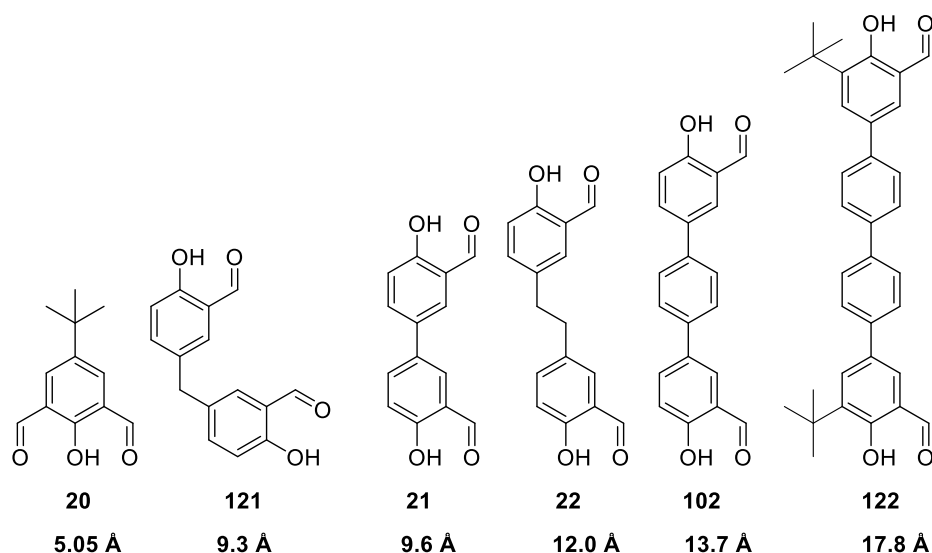
Scheme 20.Chemical structures of disalicylaldehydes and their length between O···O of two aldehyde groups (calculated by MM2 model).

Dr. M. Schneider from the Mastalerz group used several disalicylaldehydes with different length to reacted with triamine **19** and synthesized a series of [4+6] or [2+3] imine cages.[49] Similar aldehyde building blocks (Scheme 20) were chosen to react with the tetraamine **118** to investigate if new imine cages can be obtained. The distance between the aldehyde groups (O···O distance) ranges from 5.05 Å to 17.8 Å (calculated by MM2 model, Scheme 20). which makes it possible to study whether the length of aldehydes affect the formation of cages. Aldehyde **20** is commercial available. The synthesis of **121**, **21**, **22**, **102** were done according to the Ph.D. thesis of Dr. M. Schneider.[49b]
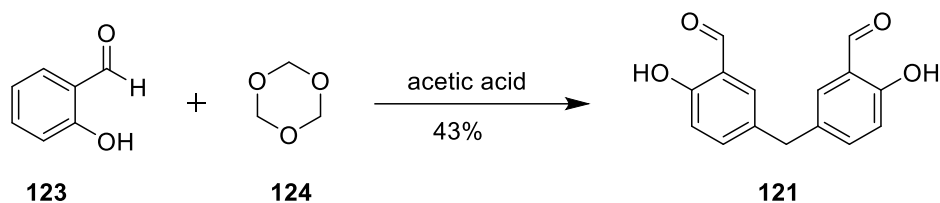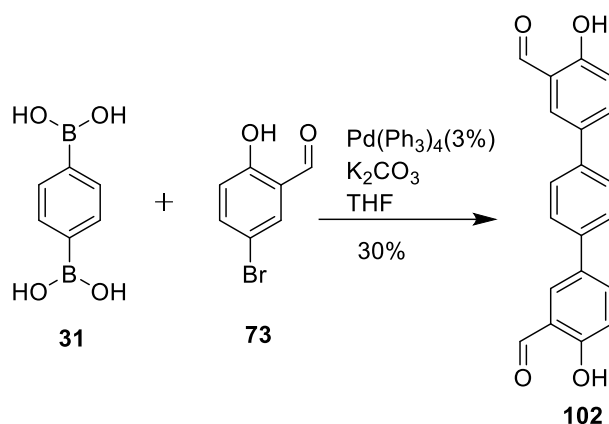
Scheme 21. Synthesis of compound **121**.[153]

Bisaldehyde **117** was synthesized from salicylaldehyde **119** and trioxane **120** with a yield of 43% after recrystallization from acetone (Scheme 21).[153] Because the methylene bridge which links the two benzene rings is not planar, the two aldehyde groups have a bond angle of 113.5° while the other bissalicylaldehydes are 180°.
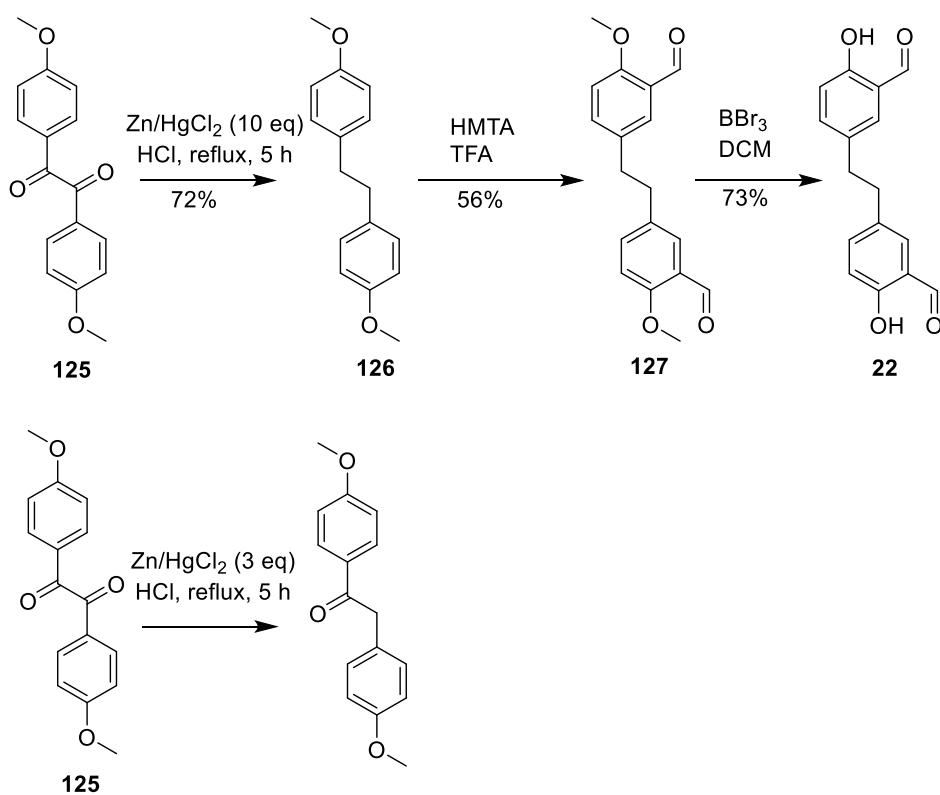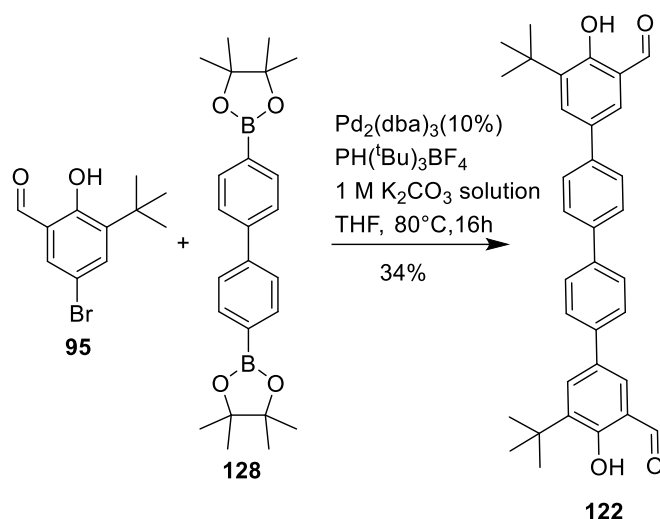

Scheme 22. Synthesis of compound **22**.[49b]

Bissalicylaldehyde **22** was synthesized in three steps from dimethoxybenzil **125** (Scheme 22). Clemmensen reduction[154] was used as the first step to reduce the ketone **125** to the methylene compound **126** with a yield of 72%.[49b] The amount of zinc was more than ten equivalents of **125** because if not enough zinc was used, the mono-reduced product would be obtained (Scheme 22). The following step was the formylation of **126** to **127**, and the pure compound could be purified by column chromatography.[49b] The final product was obtained through cleaving the methyl ether by boron tribromide.[49b]

Scheme 23. Synthesis of compound **102**.[49b]

Aldehyde **102** was synthesized by Suzuki-Miyaura reaction (Scheme 23).[114] Benzene diboronic acid **31** and bromide salicylaldehyde **73** were reacted in a by Pd(Ph3)4 catalyzed reaction to obtain aldehyde **102** with a yield of 30%.[49b] Similar terphenyl aldehydes modified with alkyl chains **53** are also used in further reactions (see in **3.1.1**, page 22).

Scheme 24. Synthesis of compound **122**.

Bissalicylaldehyde **122** was synthesized by Suzuki-Miyaura reaction.[114] The reaction was conducted with *t*-Bu salicylaldehyde **95** and diboronic ester **128** (Scheme 24). **122** was purified by column chromatography and obtained as light yellow powder with a yield of 34%.

3.2.2 Reaction of amine 118 and aldehyde 20
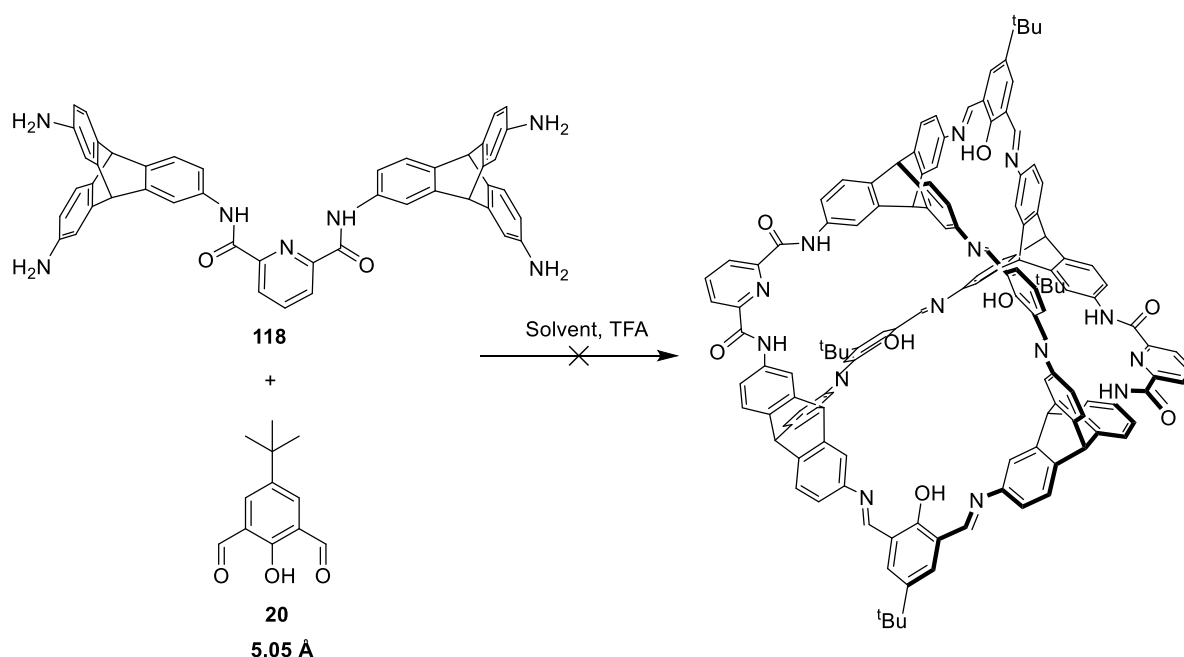
**Scheme 25**.Reaction of compounds **118** and **20**.

t-Bu salicylaldehyde **20** has been used to react with triamine **19** and successfully produced the [4+6] imine cage.[45] The reaction was performed in THF at room temperature for seven days. In this chapter, **20** is used to react with tetraamine **118** to see if they can form an [4+2] cage (Scheme 25). This reaction was performed under different conditions (Table 8), such as different solvents (THF, DMF, ethyl acetate), different temperatures (room temperature or heated) or different amount of catalyst TFA (Table 8). The starting materials dissolved well in THF and DMF at the beginning of the reaction, however, orange solids appeared after half an hour in all cases. These orange solids could not be dissolved in organic solvents (DMF, DMSO, chloroform, ethanol, *etc*.) anymore, which made it a problem to monitor the reaction by NMR.

The MALDI-TOF MS spectrum taken from the reaction in DMF at 90 °C (reaction mixture, entry 5, Table 8) shows a lot of peaks (Figure 35). Firstly, no peak fits for the desired cage compound (*m/z* =2140.48). But there are some [n· amines + m· aldehydes] by-products in the reaction mixture: the peak *m/z* = 1482 can be assigned as one amine **118** condensed with four aldehydes **20**, while the peak *m/z* = 2553 fits for three **118** molecules reacted with two aldehydes **20**. However, there are still many peaks, including two strong peaks *m/z* = 2799 and *m/z* = 3418, which cannot be assigned to the [n· amines + m· aldehydes] form. The reactions in THF and ethyl acetate showed similar results. The MS results showed that amine **118** reacted

with aldehyde **20** and formed [n· amines + m· aldehydes] products, but no highly-ordered cage compounds were formed.
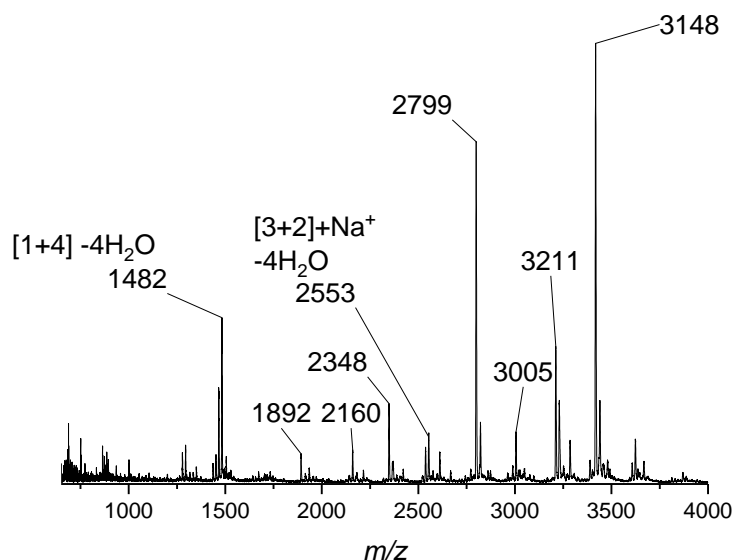

Figure 35. MS spectrum of the reaction of **118** and **20** (reacted in DMF at 90 °C, MALDI-TOF, matrix: DCTB).

Table 8. A small reaction condition screening for the reaction of **118** and **20**.

| entry	solvent	temperature	time	Result
1	THF(4% TFA)	RT	5d	[1+4] by-product
2	THF (4% TFA)	80˚C	3d	[1+4] by-product
3	THF (without TFA)	RT	5d	no [n· amines + m· aldehydes] by-product observed
4	THF (8% TFA)	RT	5d	[1+4] by-product
5	DMF(4% TFA)	90˚C	3d	[1+4], [3+2] by-product
6	EA (4% TFA)	RT	5d	no [n· amines + m· aldehydes] by-product observed
7	EA (4% TFA)	70˚C	3d	[1+4] by-product

3.2.3 Reaction of amine 118 and aldehyde 21
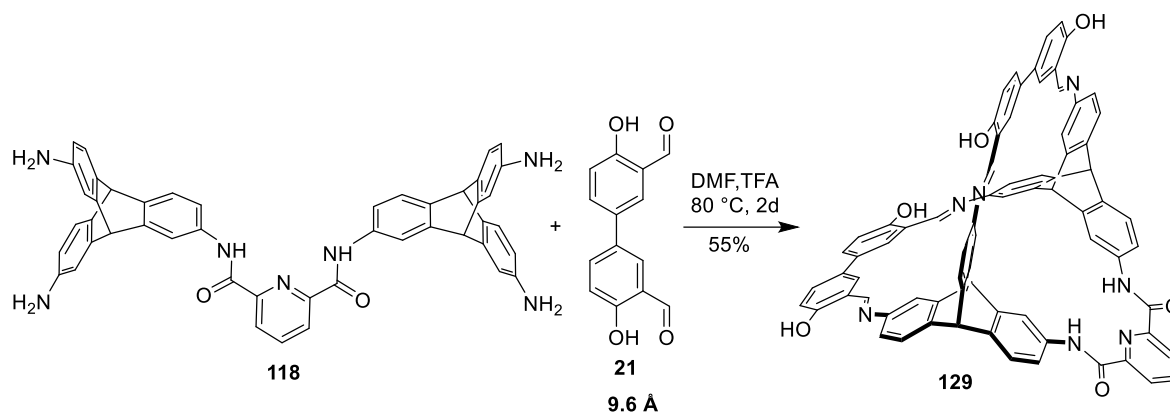
Scheme 26.Synthesis of compound **129**.

The reaction of **118** and bissalicylaldehyde **21** was carried out in THF at 90 °C, using the same reaction conditions used to synthesize [2+3] imine cage **24** (Scheme 26).[49] In this case the solubility of the product improved compared with the reaction between **118** and **20**, although a small amount of orange precipitate still appeared during the reaction. After removing the precipitate by filtration, the product was obtained by adding water to the filtrate with a yield of 30%. In order to improve the yield, the same reaction was done in DMF. During the reaction, the mixture remained transparent. The product was obtained by dropping the concentrated reaction solution into methanol, and the yield of this reaction increased from 30% to 55%.
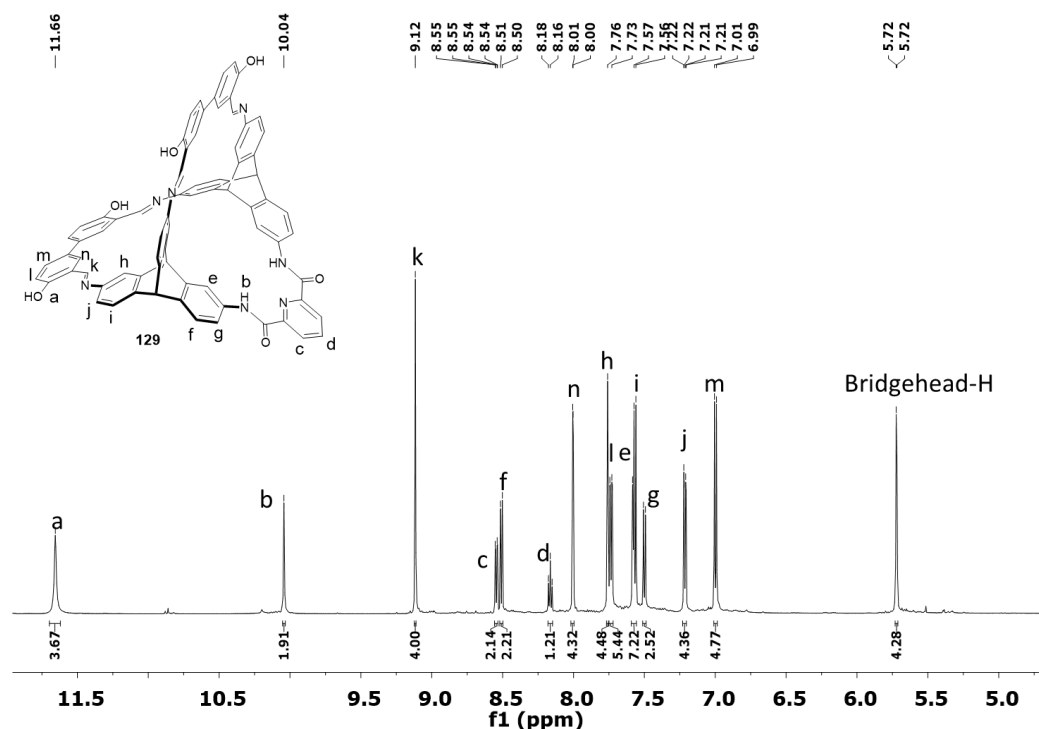
Figure 36.^{1}H NMR spectrum of compound **129** (THF-d$_8$, 500 MHz).

62

The ^{1}H NMR spectrum is shown in Figure 36, and the characteristic peaks exhibited in this spectrum are the singlet of H^a at δ = 11.66 ppm (–OH proton), singlet H^b at δ = 10.04 ppm (–NH- proton) and singlet H^k at δ = 9.12 ppm (imine proton). Two singlets at δ = 5.72 ppm correspond to the bridgehead protons of triptycene. The ratio of H^a: H^b:H^k is 2:1:2, which indicates two equivalents of **21** react with one equivalent of **118**. MALDI-MS was done to confirm the structure of the product. In the MS spectrum (Figure 37), only the [2+1] product (*m/z* = 1142.401, calculated result [M+H]$^+$ = 1142.24) can be observed.
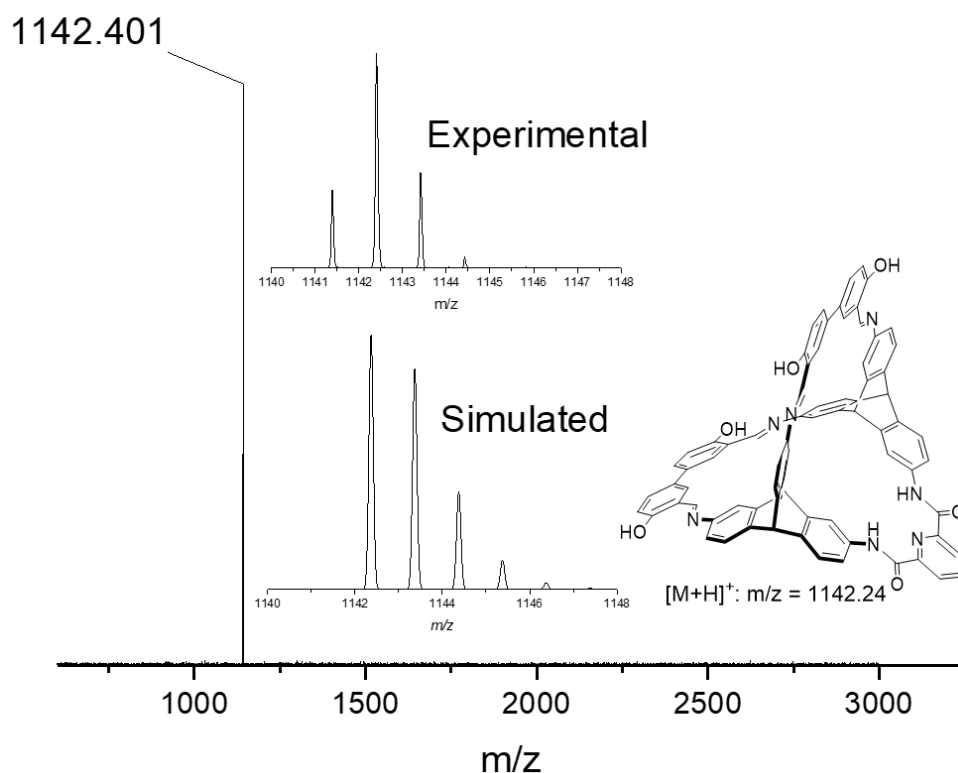
Figure 37. MALDI-TOF MS spectrum of cage **129**.

Diffusion-ordered spectroscopy (DOSY) is a powerful tool to calculate the size of the cage. DOSY can separate the NMR signals of different species according to their different diffusion coefficient.[155] The diffusion coefficient D of the cage compounds can be determined by the DOSY-NMR, which can be used to calculate the solvodynamic radius r_s of the cages at a temperature T according to the Stokes-Einstein equation:[156]

$$D = \frac{k_B T}{c\pi\eta r_s} \tag{28}$$

Where D is diffusion coefficient (m^2·s^{-1})

k_B is Boltzmann constant ($1.3806485 \times 10^{-23}$ ·m^2·kg ·s^{-2} ·K^{-1})

T is absolute temperature (K)

η is viscosity of medium (kg· m^{-1}·s^{-1})

r_s is solvodynamic radius of analyte (m)

c is size factor

As c could be defined as:[157]

$$c = \frac{6}{1 + 0.695 \left(\frac{r_{solv}}{r_s}\right)^{2.234}} \tag{29}$$

Where r_{solve} is the hydrodynamic radius of the solvent used for DOSY-NMR (m)

D can be written as:

$$D = \frac{k_B T}{\left(\frac{6}{1 + 0.695 \left(\frac{r_{solv}}{r_s}\right)^{2.234}}\right) \pi \eta r_s} \tag{30}$$

So if the diffusion coefficient D is obtained by DOSY NMR, it is easy to calculate the hydrodynamic radius of the molecule.

According to the DOSY-NMR spectrum of cage **129** (Figure 38), three groups of signals can be found in the spectrum which were assigned as DMSO, water and cage **129**. The solvodynamic radius r_{solv} of DMSO at 298K is 0.263 nm, η is 1.99×10^{-3} kg·m^{-1}·s^{-1} according to literature,[158] the diffusion coefficient D of cage **129** measured from this spectrum is 1.12×10^{-10} m^2/s. So according to the equation (30), r_s of cage **129** is 0.82 nm, which fits the MM2 model of [2+1] cage **129** (Figure 38)
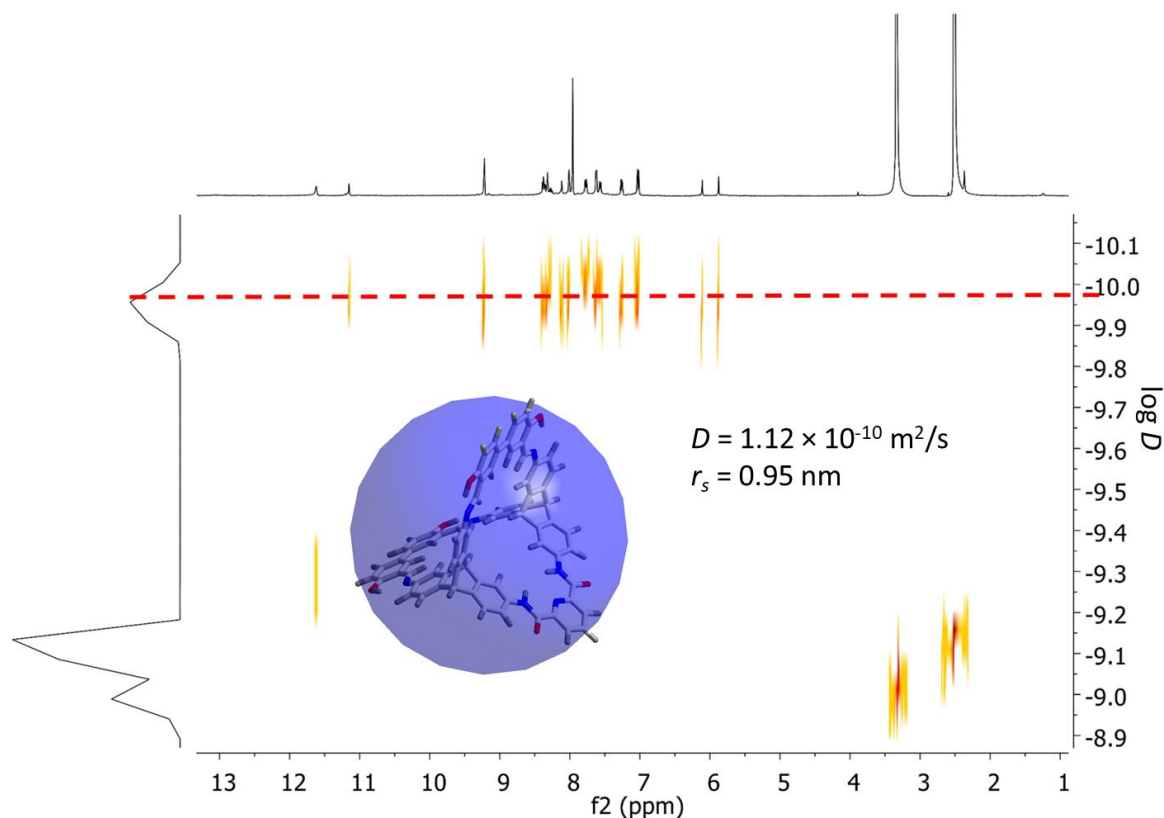
Figure 38. DOSY NMR of cage **129** (DMSO-d$_6$, 400 MHz). The inset shows the sticks representation of the MM2 model of cage **129** with a sphere with the size of the calculated solvodynamic radius in its center

3.2.4 Reactions of amine 118 and other aldehydes

The reactions of amine **118** with aldehydes **121**, **22** or **102** (Scheme 27) were done in DMF with TFA as catalyst, heated to 80 °C for two days, using the same conditions used for synthesizing the [2+1] cage **129**. The observations made during these three reactions are similar so they are discussed together. The starting materials dissolved well in DMF at the beginning of the reaction, but a lot of orange precipitate appeared after one hour. The precipitate could not dissolve in organic solvents such as DMF, DMSO and THF, which made it difficult to monitor these reactions by NMR.

MALDI-MS measurements were done with the precipitates and filtrates of these three reactions. The filtrates of the reactions show no peaks of $m/z > 650$. The MS of the precipitates show peaks which fit the cage compounds (Figure 39). The reaction of amine **118** with aldehyde **121** (with methylene linker) shows peaks at $m/z = 1170.41$ and 1192.39 in the MS spectrum, which fit for the molecular weight of the [2+1] cage (two aldehydes + one amine, [M+H]$^+$, calculated: $m/z = 1170.39$, [M+Na]$^+$ calculated: $m/z = 1192.28$. Scheme 27, Figure 39a) The reaction of amine **118** with aldehyde **22** (with ethylene linker) shows peaks at $m/z = 1196.69$ and 1218.68

in the MS spectrum, which also fit for the molecular weight of [2+1] cage ([M]$^+$ calculated: m/z = 1196.41, [M+Na]$^+$ calculated: *m/z* = 1219.04, Scheme 27, Figure 39b). The reaction between amine **118** and aldehyde **102** (with phenyl linker) shows a peak at *m/z* = 2589.05, which fits for the molecular weight of the [4+2] cage ([M+H]$^+$ calculated: *m/z* = 2588.85, Scheme 27, Figure 39c). Although these insoluble solids are difficult to purity further, the results of the MS measurements give a hint that the length of the aldehyde building block has an influence on the size of the cages.
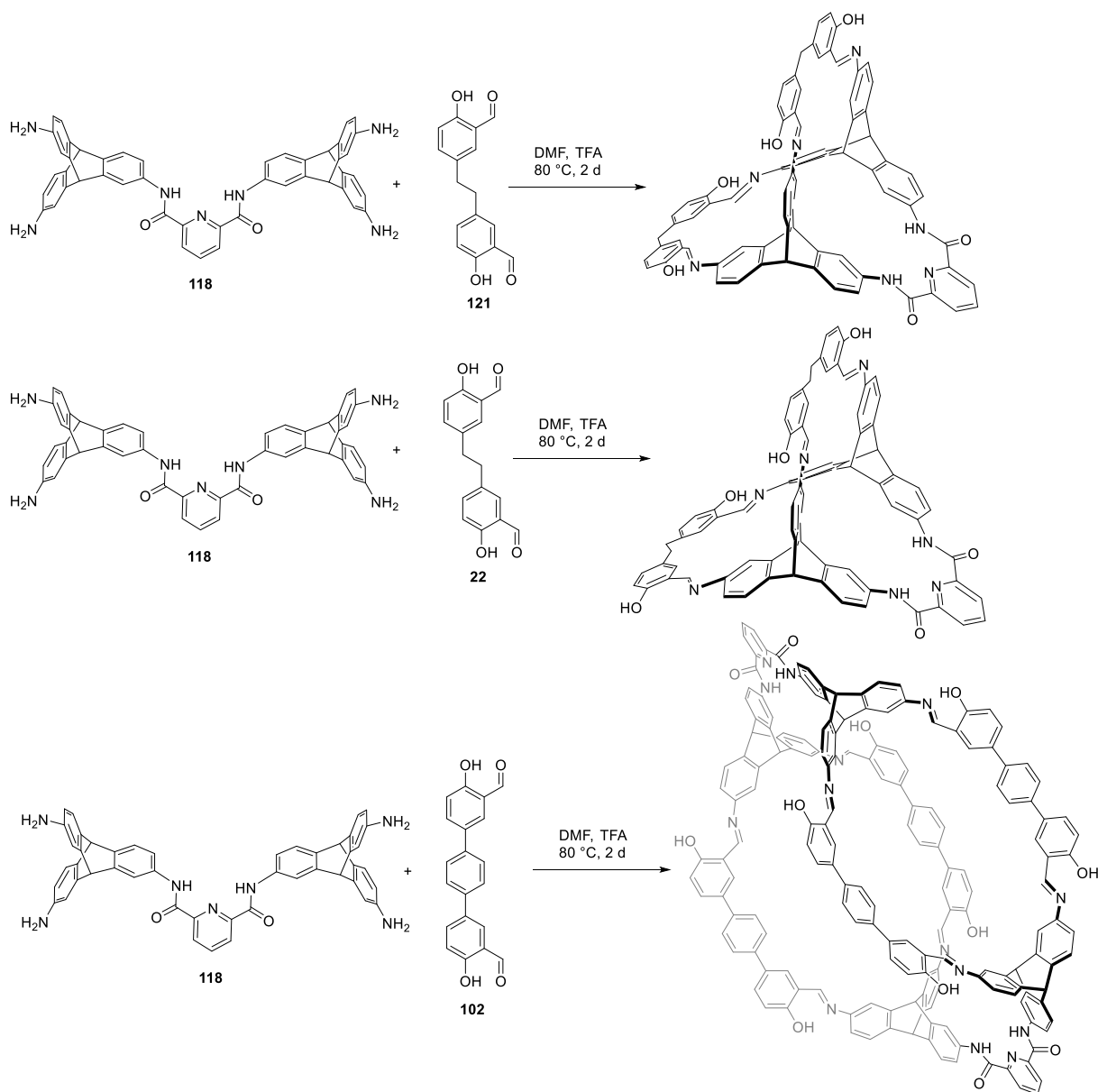
Scheme 27. Reactions between amine **118** and aldehydes **121**, **22** or **102**.
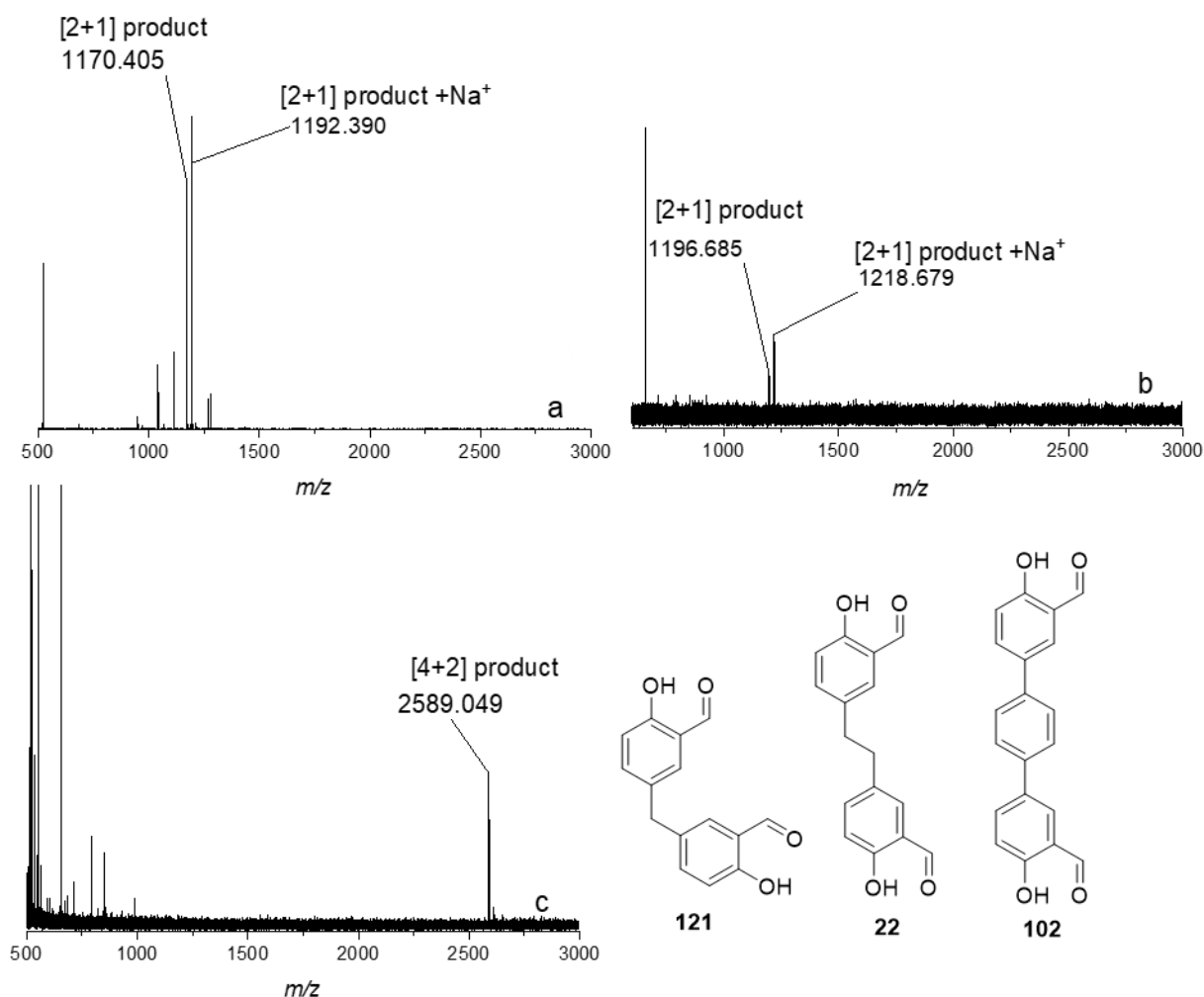
Figure 39. MS spectra of compound **118** reacted with a) compound **121**, b) compound **22**, c) compound **102** in DMF (MALDI-TOF, matrix: DCTB).

In order to improve the solubility of the product, aldehyde **53** (phenyl linker with hexyl chains) was chosen to react with amine **118** (Scheme 28). The precipitate appearing in this reaction has better solubility than the precipitate formed in the reaction with aldehyde **102**.

The MS spectrum (Figure 40) of the precipitate shows peaks at m/z = 1631.08, 3263.19 and 4894.73, which fit for the molecular weight of a [2+1] cage ([M]$^+$ calculated: m/z = 1630.8), a [4+2] cage ([M+H]$^+$ calculated: m/z = 3262.61) and a [6+3] cage ([M+H]$^+$ calculated: m/z = 4894.41), respectively.

An NMR spectrum was measured in THF-d$_8$ (Figure 40). However, the peaks in this ^{1}H NMR spectrum are too broad to see the splitting. Some characteristic peaks can be observed in this NMR spectrum. The –OH proton shows a peak at δ = 13.01 ppm, the –NH– shows a peak at δ = 10.08 ppm and the proton of the imine bond shows a peak at δ = 8.69 ppm. The bridgehead protons show peaks at δ = 5.52 and 5.48 ppm.
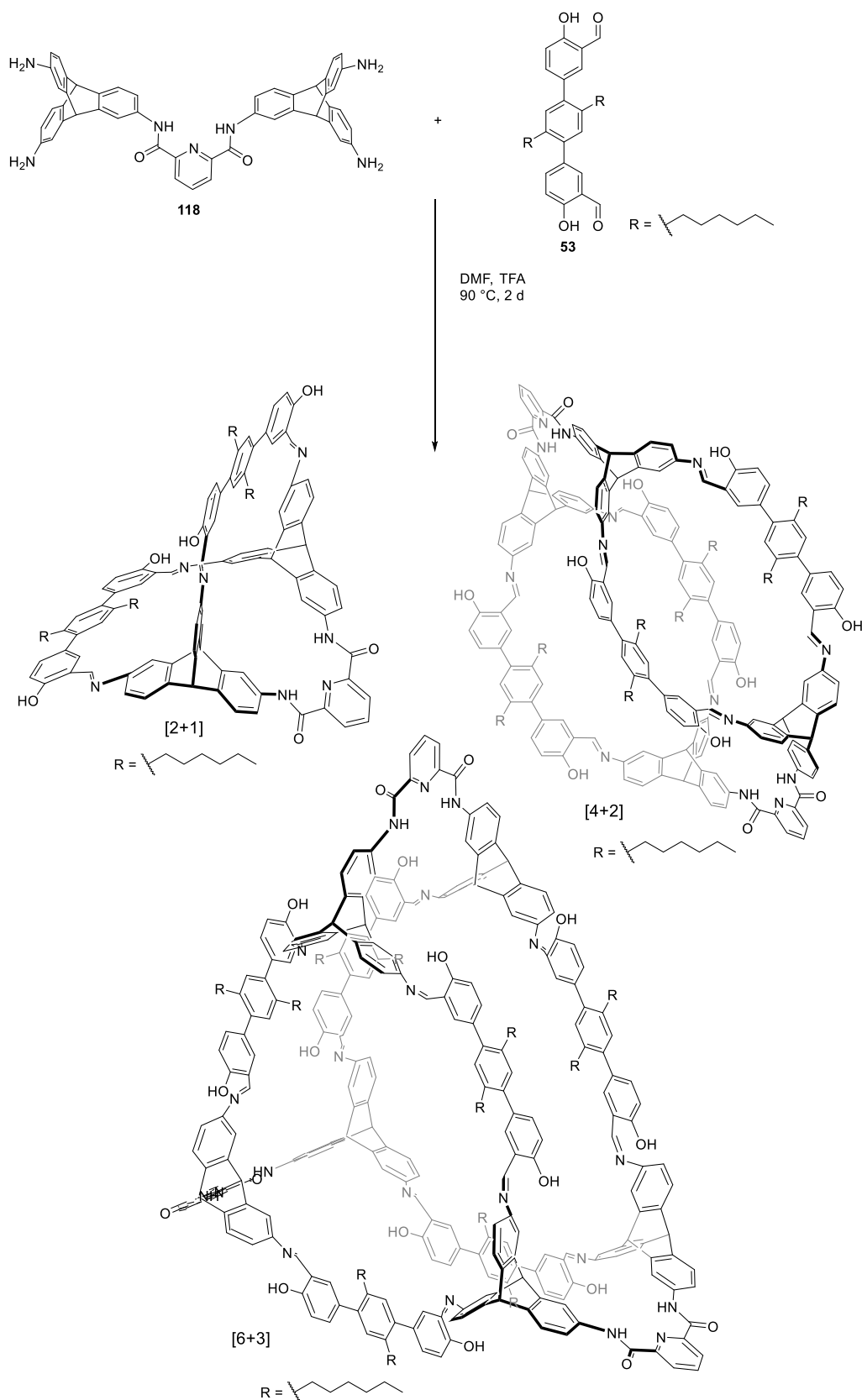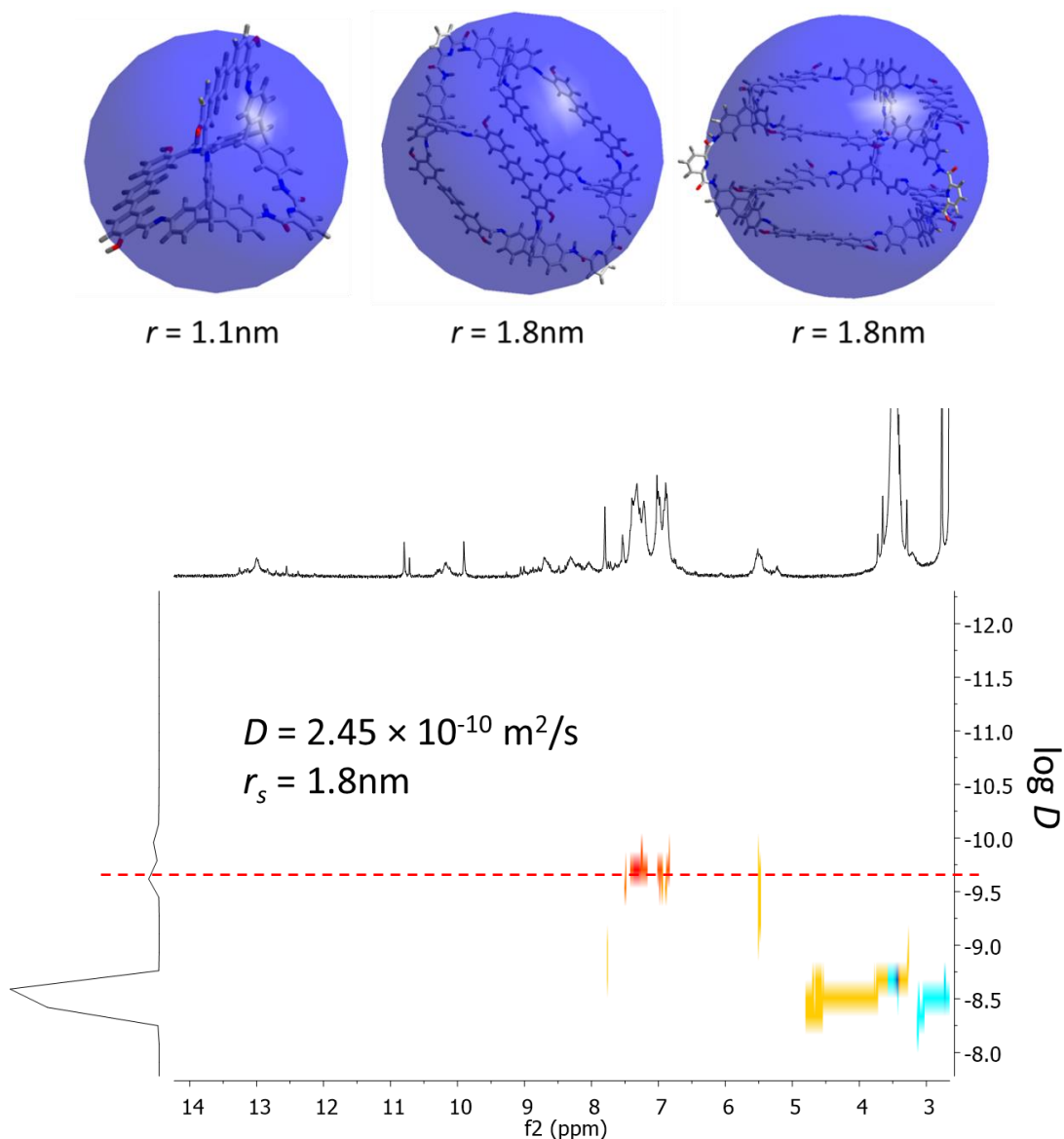
Scheme 28. Reaction between amine **118** and aldehyde **53** (with hexyl chains)

DOSY NMR was done to measure the size of the cage. Although three different products can be observed in the MS spectrum, only one signal is observed on DOSY NMR spectrum, except for the solvent. According to the DOSY NMR spectrum (Figure 41), The solvodynamic radius r_{solv} of THF at 298K is 0.263 nm, η is 0.48 $\times 10^{-3}$ kg·m^{-1}·s^{-1},[158] the diffusion coefficient D of product measured from this spectrum is 2.45 $\times 10^{-10}$ m^2/s. According to the equation (30), the r_s of the product is 1.8 nm. This radius fits for both the [4+2] cage (the distance between two pyridines is 3.5 nm) and the [6+3] cage (the distance between the pyridine and the opposite terphenyl linker is 2.9 nm) based on their MM2 models (Figure 41). The MM2 model of the [2+1] cage shows the distance between the pyridine and opposite terphenyl linker is 15 nm (Figure 41), which not fits for the r_s calculated from DOSY NMR. This may be because the amount of the [2+1] cage is too small to be observed in the DOSY NMR spectrum.
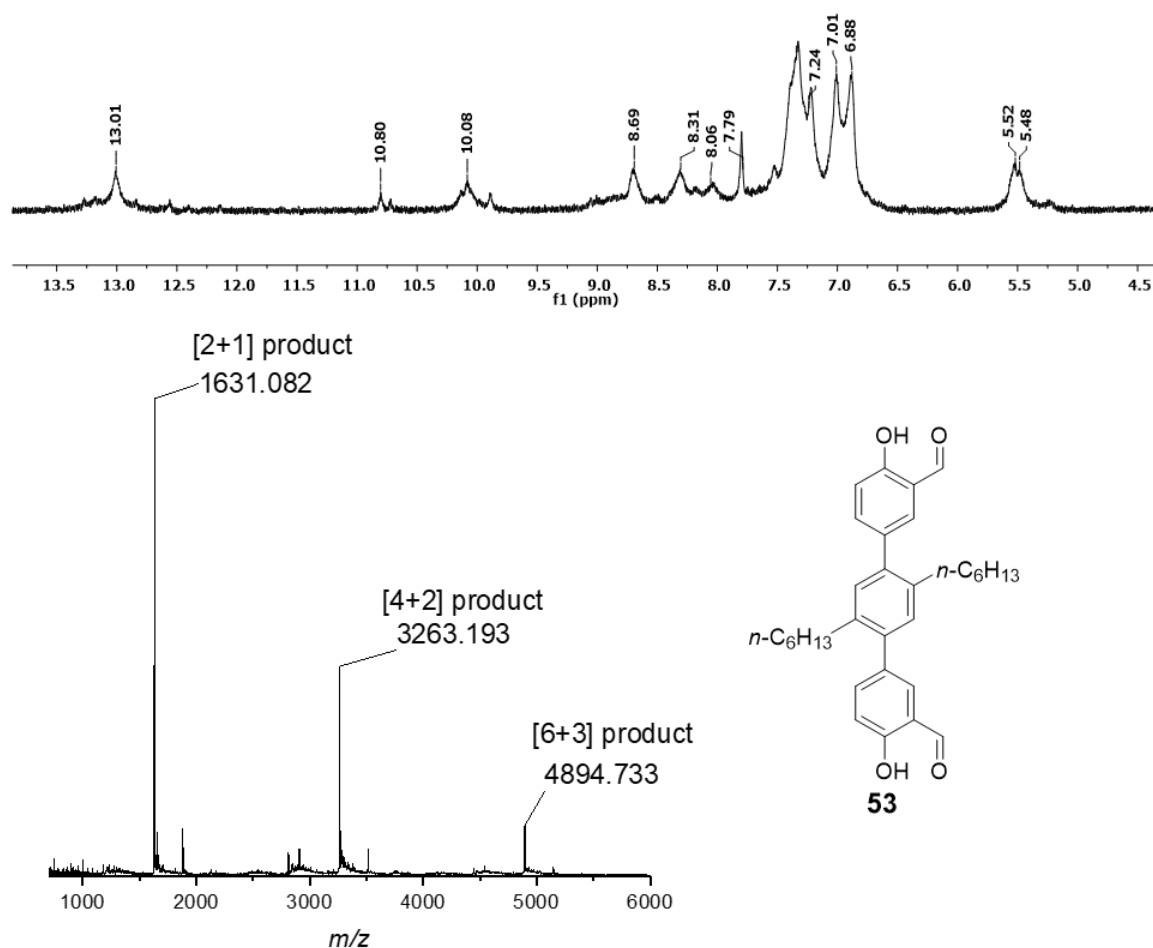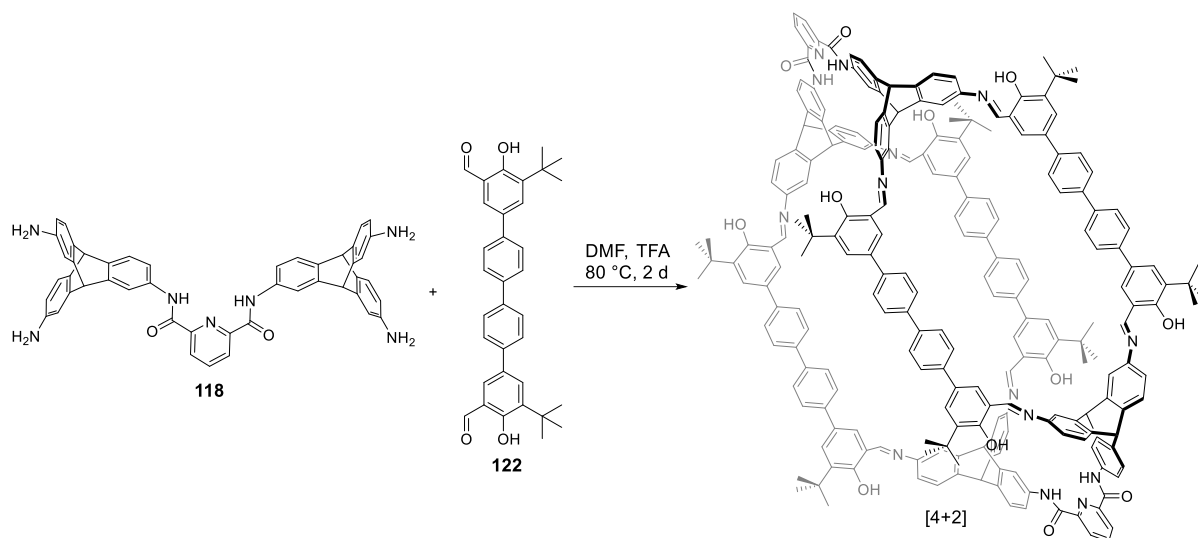

Figure 40. top: ^{1}H NMR spectrum of the crude product from the reaction of **118** with **53** (THF-d$_8$, 500 MHz). bottom: MS spectrum of the crude product (MALDI-TOF, matrix: DCTB).

$$D = 2.45 \times 10^{-10} \text{ m}^2/\text{s}$$
$$r_s = 1.8\text{nm}$$

Figure 41. Top: The MM2 models of the [2+1] product, the [4+2] product and the [6+3] product from the reaction between amine **118** and aldehyde **53**. The radii of the sphere in the centre are 1.1 nm, 1.8 nm and 1.8 nm, respectively. Down: DOSY NMR of reaction between amine **118** and aldehyde **53** (THF-d$_8$, 400 MHz)

Size exclusion chromatography (SEC) was used in an attempt to separate these three cages because their molecular weights differed a lot. Unfortunately, after the SEC column (DMF as mobile phase), no product could be observed in the ^{1}H NMR spectra and MALDI-MS spectra. One possible explanation is that these imine cages decompose on the SEC column. Several crystallization methods were tried in an attempt to purify or enrich one cage, but no crystalline material was formed during these attempts.

70

Scheme 29. Reaction between amine **118** and aldehyde **112**.
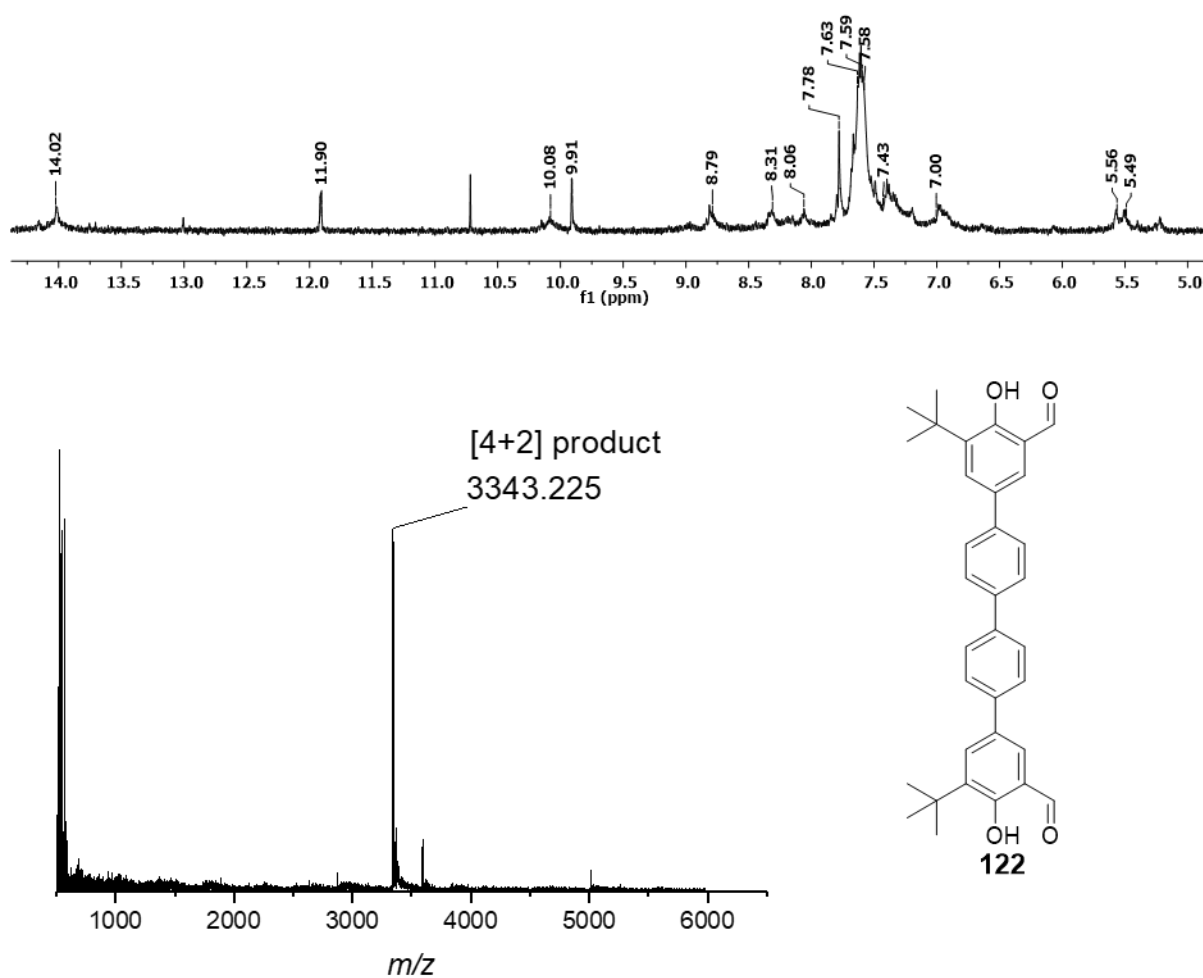
Figure 42.) ¹H NMR spectrum of the crude product from the reaction of **118** with **122** (THF-d8, 500 MHz). b) MS spectrum of the crude product (MALDI-TOF, matrix: DCTB).

The reaction of amine **118** with the longest aldehyde **122** (with biphenyl linker) was performed in DMF at 80 °C for two days (Scheme 29). The experimental observations were similar to the reaction with **53** (phenyl linker with hexyl chains), but the solubility of the product was worse. The MALDI-MS spectrum shows a peak at *m/z* = 3343.225, which fits for the [4+2] product ([M+H]$^+$ calculated: *m/z* = 3343.14, Scheme 29, Figure 42). The ^{1}H NMR spectrum is shown in Figure 42. From the ^{1}H NMR spectrum, the proton of imine bond can be observed as a singlet at δ = 8.79 ppm, and bridgehead protons of triptycene are found at δ = 5.56 and 5.49 ppm. Impurities can also be observed in the ^{1}H NMR spectrum. SEC column chromatography was also tried to purified the product, but like in the reaction with aldehyde **53**, this imine cage also decomposed on the column. Recrystallization was also attempted, but no crystalline material formed.

3.2.5 Conclusion

In this chapter, a new amine building block **118** was synthesized in three steps from triamino triptycene **19** and a new [2+1] cage **129** was synthesized formed amine **118** and bisphenyl aldehyde **21**.This new amine building block was used to react with eight disalicylaldehydes, in order to investigate whether the length of the aldehydes has an influence on the formation of the cage compounds. According to the crystal structure of compound **118**, the distance between the two triptycenes is 13 Å. For aldehyde building blocks shorter than this distance (**21**, **22**, **121**), the [2+1] product is preferred as the starting materials easily form this kind of pre-organized structures. For the aldehyde building blocks with the equal distance **102**, the [4+2] product is preferred according to the MS spectrum. For aldehyde **53**, the [2+1] product, the [4+2] product and the [6+3] product were formed. For the aldehyde building block with longer length (**122**), the [2+1] product cannot be formed during the reaction, instead, the [4+2] product was formed. For amine **118**, the length of aldehyde building blocks is important for the formation of the cage compound (Scheme 30).
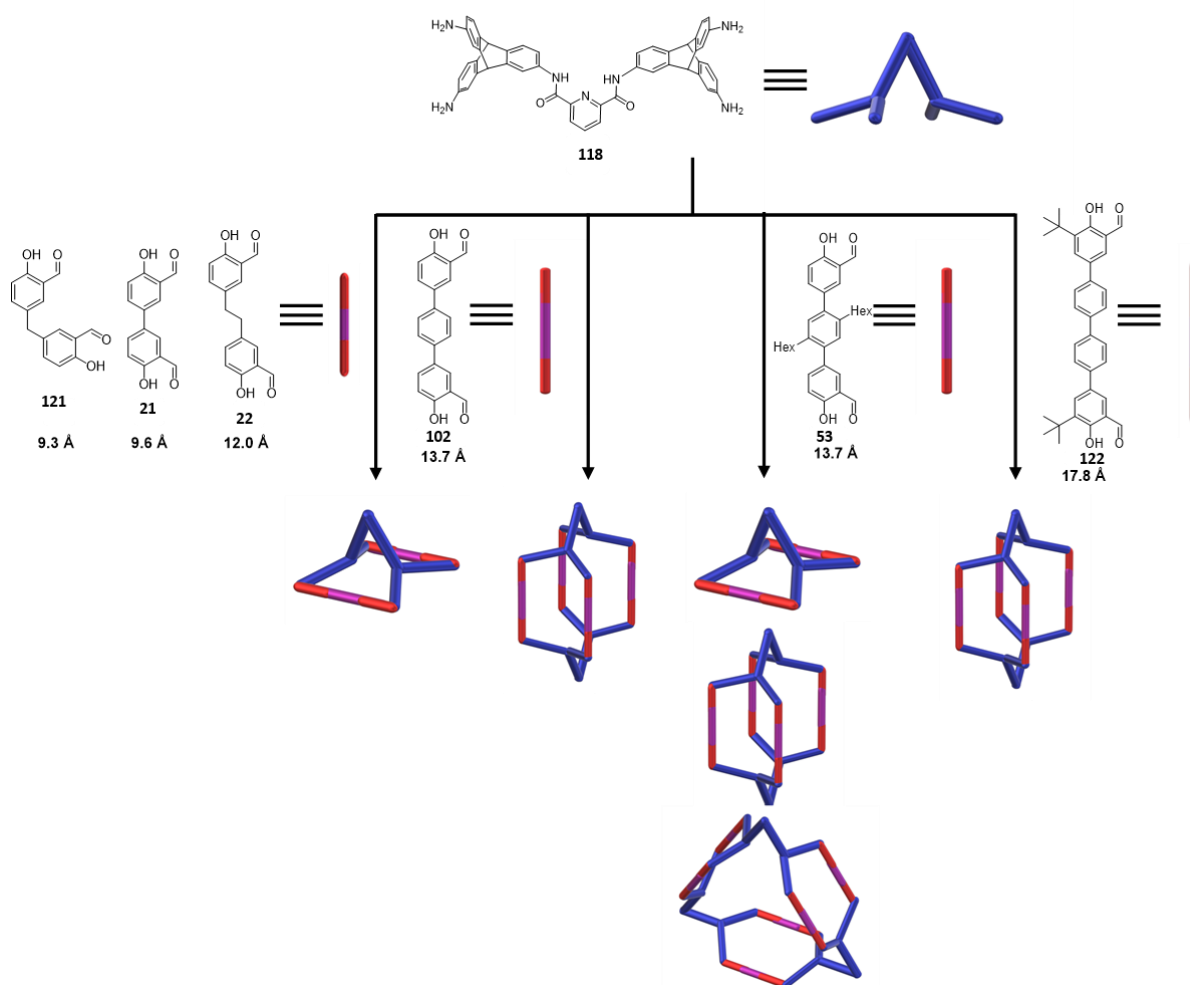
Scheme 30. Conclsion of amine **118** reacted with aldehydes with different length.

3.3 Transforming a chemically labile [2+3] imine cage into a robust carbamate cage

Dynamic covalent chemistry (DCC) is applied to synthesize shape-persistent organic cages because the high yield and self-correcting effects.[4, 35] However, the reversible reaction of DCC is also a double-edged sword in material science. For instance, the imine bonds, which are commonly used to construct organic cages, are susceptible to hydrolysis in the presence of water, especially in acidic or basic environment.[106] The cages formed by imine bonds, like the [4+6] cage from the Cooper group, are easily cleaved in highly acidic or basic solutions.[107] Because of their instability, wider applications of the cages have been limited. For example, the cage compounds have shown potential applications in gas separation and purification,[88] but in the industrial field, the exhaust gases are often mixed with water vapour.[159]

A common way to stabilize the imine bonds is to reduce them to amine bonds,[67] but the reduction often results in a loss of the shape persistency of the cage compounds, which leads to the loss of the porosity of the material.[67, 107] Until now, only few examples of shape-persistent organic cages with high pH stability have been reported. [107, 160] Therefore a new method to produce pH-stable cage compounds is needed.
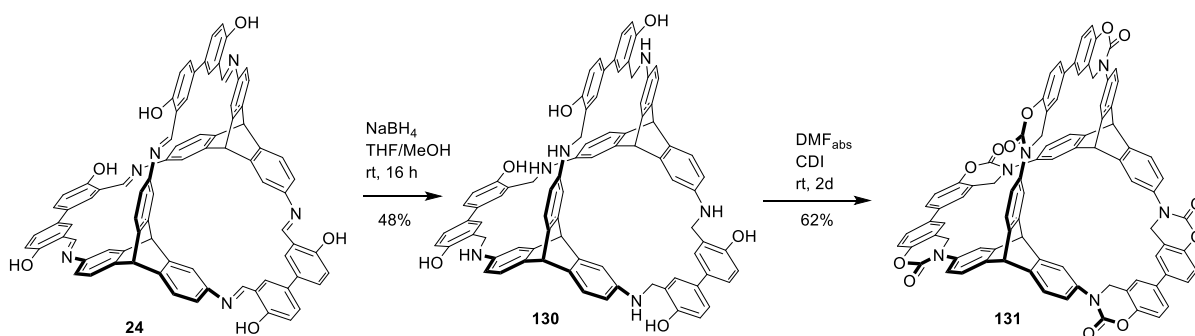
3.3.1 Synthesis of a [2+3] carbamate cage
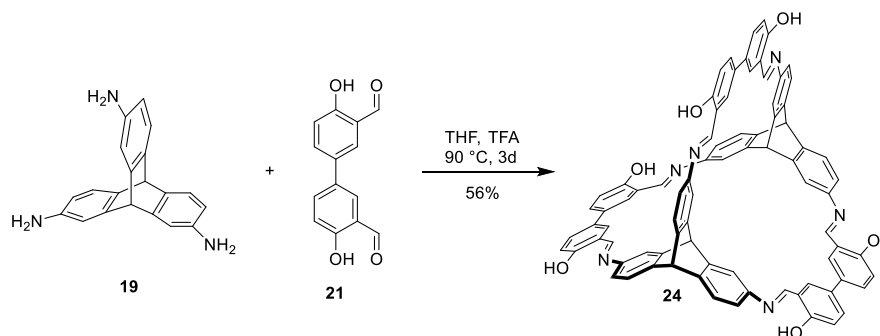
Scheme 31. Synthesis of [2+3] imine cage **24**.[49]

The [2+3] imine cage **24** was synthesized by a six-fold condensation of triaminotriptycene **19** and bissalicylaldehyde **21** according to literature,[49] in THF with a catalytic amount of TFA at 90 °C with a yield of 56% (Scheme 31).

The [2+3] imine cage **24** was reduced with NaBH$_4$ in methanol to obtain the amine cage **130**. Although the reduced amine cage **130** could be observed by ^{1}H NMR spectrum, the yield of this reaction was only 10%, which was much lower than the similar reduction for other imine cages.[67],[107] This may be because the poor solubility of cage **24** in methanol prevents the

progress of the reaction. In order to improve the solubility, the reaction was performed in a THF/methanol mixture (THF: methanol = 1:1). After extracting with ethyl acetate, amine cage **130** was obtained in a 54% yield. Subsequent treatment with *N, N'*-carbonylbisimidazole (CDI) in DMF at room temperature gave the carbamate cage **131** in 62% yield as a colourless solid (Scheme 32) after column chromatography. Both cages were characterized by ¹H NMR, ¹³C NMR, MALDI-MS, elemental analysis and IR.


Scheme 32. Synthesis of carbamate cage **131**.

The ¹H NMR spectra show big differences among cage **24**, **130** and **131**. For instance, imine cage **24** shows characteristic peaks of the protons of imine bonds (e in Figure 43) at $\delta = 9.27$ ppm and the protons of –OH group (H^a in Figure 43) at $\delta = 12.7$ ppm. For reduced amine cage **130**, the amine protons give a broad pseudo-triplet peak (H$^{f'}$ in Figure 43) by coupling with the methylene protons (H$^{e'}$ in Figure 43) at $\delta = 5.4$ ppm, indicating the success of the reduction. The –OH proton (H$^{a'}$ in Figure 43) shows a large up-field shift compared with the imine cage **24**, which appears at $\delta = 9.4$ ppm. For carbamate cage **131**, the –OH and –NH– peaks both disappear in the spectrum. What can be seen in the spectrum are six peaks in the aromatic region, two bridgehead proton peaks ($\delta = 5.5$ and 5.8 ppm) and a singlet for the methylene group ($\delta = 4.9$ ppm, H$^{d''}$ in Figure 43). The most characteristic peaks are the two peaks of the triptycene bridgehead protons at $\delta = 5.5$ and 5.8 ppm (Figure 43), and the peak of the carbonyl C-nucleus of the formed carbamate unit at $\delta = 150.9$ ppm in the ¹³C NMR spectrum. The IR spectra also prove the formation of these two cages (Figure 44). The spectrum of cage **130** shows a broad stretching band at $\tilde{v} = 3341$ cm^{-1}, which can be assigned to the –NH- and –OH-groups.[162] The IR spectrum of cage **131** (Figure 44) shows the characteristic stretching band of the carbamate CO ($\tilde{v} = 1729$ cm^{-1}).[161] The MALDI-MS spectra also give the fitting results for the cages (cage **130**: calculated :1229.45, found *m/z* =1229.495, cage **131**: calculated: 1385.41, found *m/z* =1385.367).
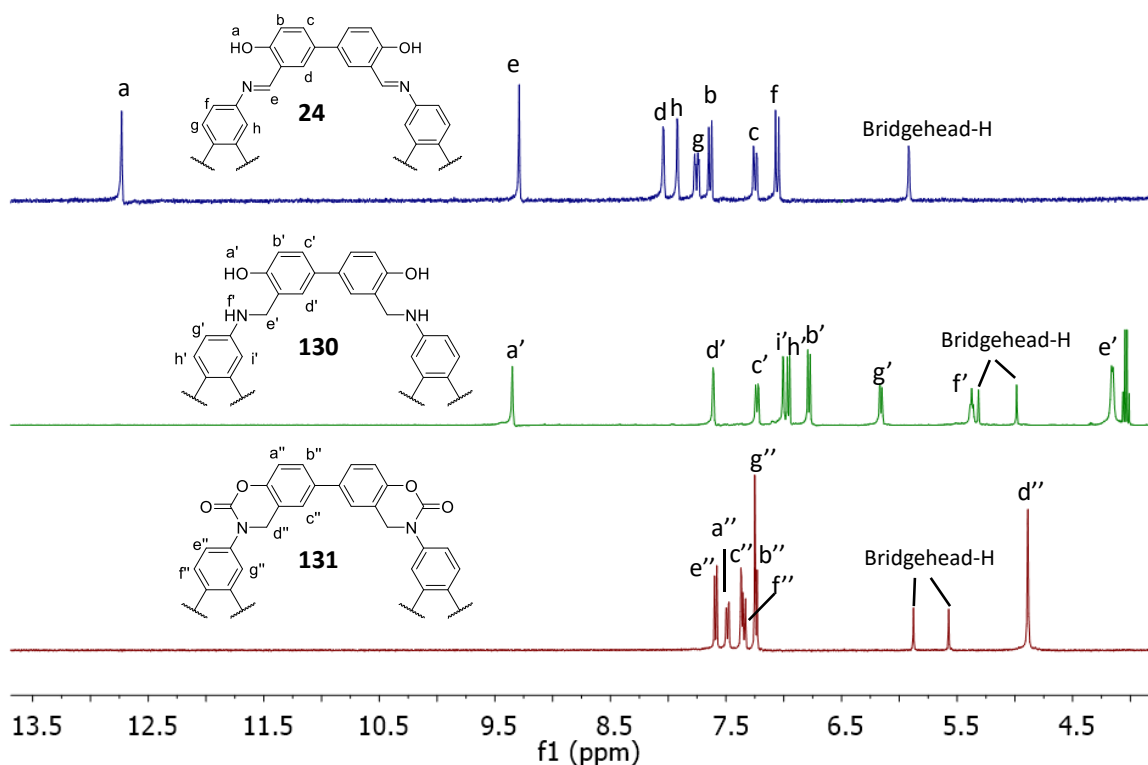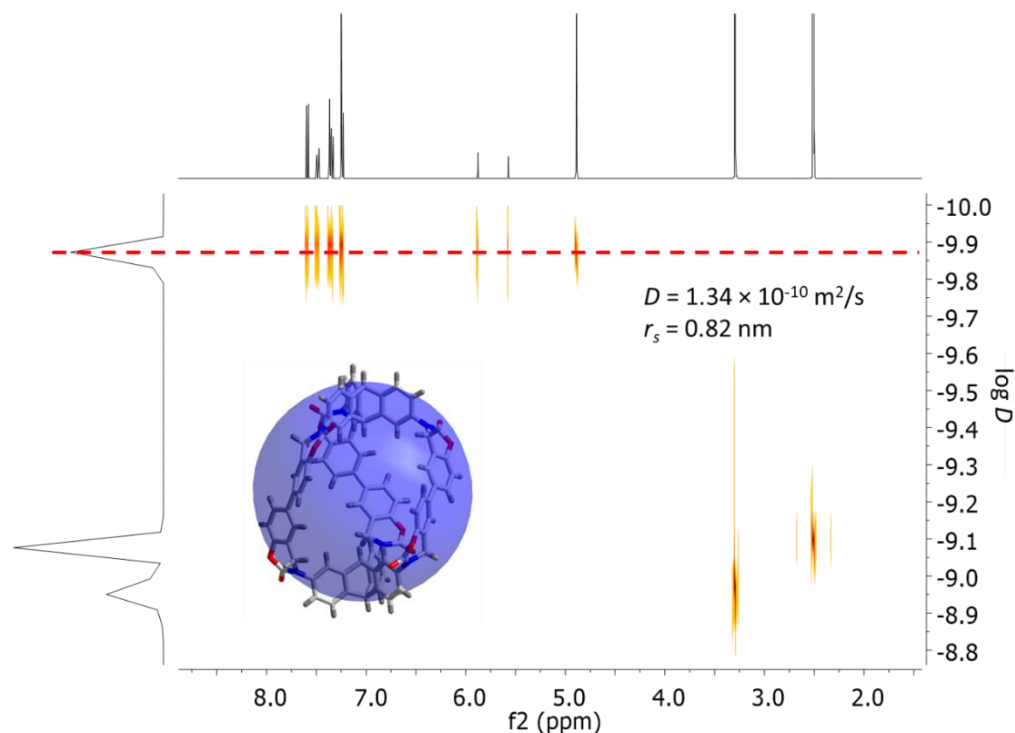
Figure 43. ^{1}H NMR spectra (DMSO-d$_6$, 500 MHz) of imine cage **24** (top), amine cage **130** (middle) and carbamate cage **131** (bottom).
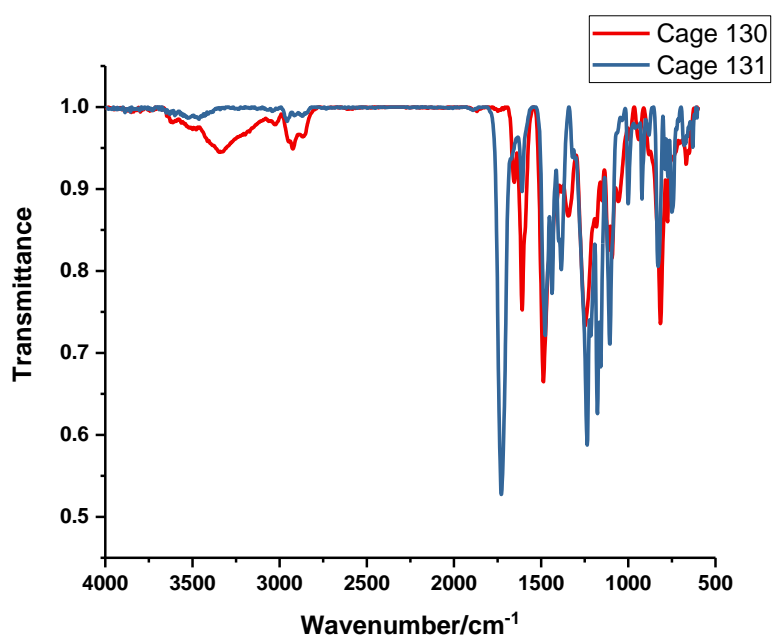

Figure 44. IR spectra of cage **130** and cage **131**. **130** and **131** are shown in red line and blue line, respectively.

Figure 45. DOSY NMR of cage **131** (DMSO-d$_6$, 400 MHz). The inset shows the sticks representation of the MM2 model of cage **131** with a sphere with the size of the calculated solvodynamic radius in its center

According to the DOSY-NMR of cage **131** (Figure 45), three groups of signals can be found in the spectrum, which are assigned as DMSO, water and cage **131**. The solvodynamic radius r_{solv} of DMSO at 298K is 0.263 nm, η is 1.99×10^{-3} kg·m^{-1}·s^{-1} according to literature,[162] the diffusion coefficient D of cage **131** measured from this spectrum is 1.34×10^{-10} m^2/s. So according to the equation (30), r_s of cage **131** is 0.82 nm, which fits the MM2 model of cage **131** (Figure 45), where the distance between the two inter bridgehead hydrogen atoms is 0.86 nm.

3.3.2 Crystal structure of the carbamate cage

a: $d_{CH-\pi}$ =2.6 Å
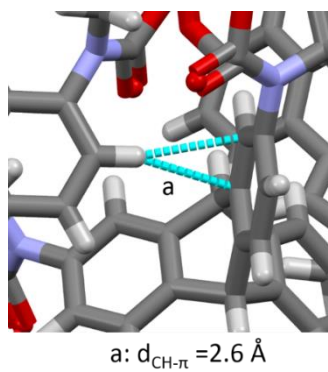
Figure 46. CH-π interaction in Cage **131**.

For the amine cage **130**, although several methods have been tried to grow single crystals, only amorphous materials were obtained. For the carbamate cage **131**, single crystals were obtained in two ways: 1) mixing a DMSO solution of **131** into acetone (polymorph α, Figure 47a) or diffusing methanol into a solution of **131** in DMF (polymorph β, Figure 47b). Both polymorphs crystallize in the triclinic space group P-1. However, polymorph β, which contains two molecules in the asymmetric unit, has a larger unit cell (V =

9758 Å^3) than polymorph α (V = 4204 Å^3), with only one molecule in the asymmetric unit. The distance between the inner triptycene bridgehead hydrogen atoms (8.5 Å) is substantially larger than for the [2+3]-imine cage **24** (7.8 Å),[49a] and the size measured from the crystal structure fits with the one calculated by DOSY-NMR (r_s = 0.82 nm, see in Figure 45). However, because of the rotation of the biphenyl linker, instead of π–π and CH-π interaction like for cage **24**,[49a] in both polymorphs, the cages are packing mainly *via* the CH-π interactions (d$_{CH-\pi}$ =2.6 Å, Figure 46).
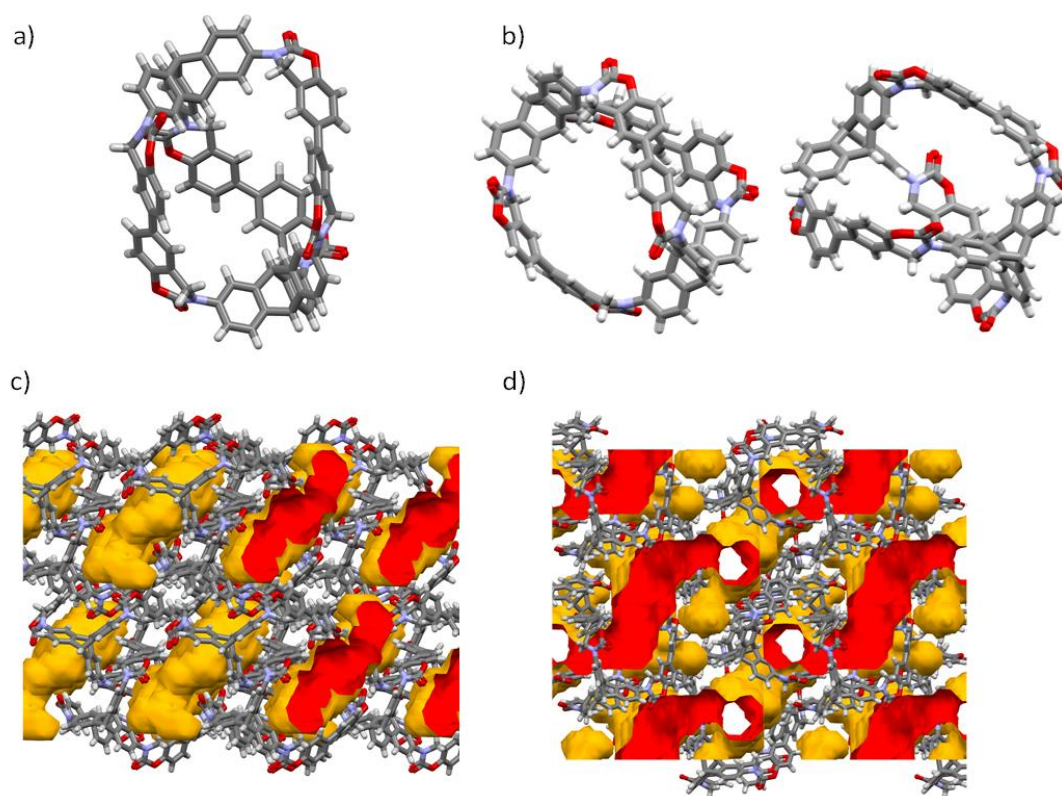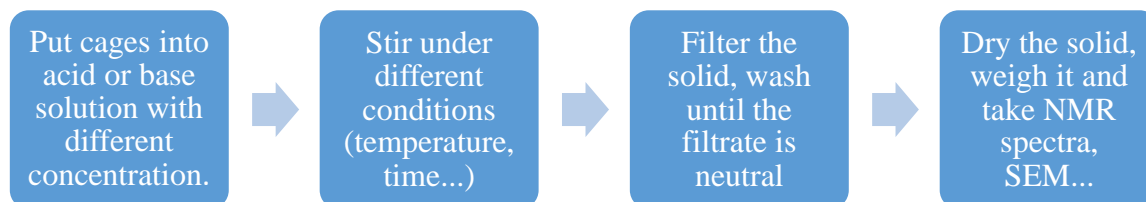

Figure 47. Single crystal structure of cage **131**. a) molecular structure of polymorph α. b) molecular structure of polymorph β. pore system of c) polymorph α and d) polymorph β, for a probe of radius 1.82 Å.

What is more interesting is that these two polymorphs show different pore systems (Figure 47c, d). Polymorph β (from DMF/methanol) has a three-dimensional pore system as well as some 'dead-ends' which cannot connect with other pores (Figure 47d). For polymorph α (from DMSO/acetone), only isolated pores which are surrounded by cage molecules can be found (Figure 47c). The cages packs in a "window-to-arene" fashion,[164] which results in the cavities of cages not being connecting with each other. In polymorph β, although the cages also pack in a "window-to-arene" fashion, two molecules being in the asymmetric unit result in a more loose packing pattern for polymorph α. The calculated pore volume for polymorph β is 29%

of the cell volume for a probe with a radius of 1.82 Å, which is smaller than for the [2+3] imine cage **24** (72%).[49] These two kinds of polymorph suggest cage **131** is potentially porous, but the type of polymorphs is really important.

3.3.3   pH stability of the carbamate cage.

To investigate the stability of cage **131** in different pH environments, some analytical methods need to be used to prove that the cage compound does not decompose. According to literature,[109] NMR spectroscopy, Powder X-Ray Diffraction (PXRD), Electron microscopy, *etc.* are often used as proof of the stability of cages in different chemical or physical environments. The experiments of cage **131**'s stability at different pH were done in the following way (Scheme 33): a certain amount of cage **131** (see in Table 9) was weighed and stirred with 1 mL HCl or NaOH solution (with different concentrations) for 8 h to 5 days. After the treatment, the solid was filtered and washed until pH of 7 was reached. ^{1}H NMR experiments were carried out to see if cage **131** was decomposed or not. The same experiments were done with imine cage **24** for comparison. The treatment at higher temperature was done in the same way. Besides HCl and NaOH, the stability in TFA and nitric acid were investigated by a similar procedure.

Put cages into acid or base solution with different concentration.	Stir under different conditions (temperature, time...)	Filter the solid, wash until the filtrate is neutral	Dry the solid, weigh it and take NMR spectra, SEM...

Scheme 33.Experimental procedure for the pH stability of cage **131** and cage **24**.

First, diluted HCl (1 M, pH= 0) was tested at room temperature (entry 3 and 5 in Table 9). Neither after 16 h nor after 5 days any decomposition was observed: the carbamate cage **57** was nearly fully recovered, concluding that the material is stable at pH = 0. Even when this mixture was heated to 100 °C (entry 4, Table 9), no structural change was detected in the corresponding ^{1}H NMR spectrum (Figure 48). The next test was the stability in concentrated HCl (10 M, see in entry 1, Table 9). The ^{1}H NMR spectra showed that the carbamate cage is stable at pH = -1 at room temperature. The carbamate cage **131** started to decompose only when heated to 100 °C (entry 2, Table 9 and Figure 48). For the basic conditions, the carbamate cage **131** is stable in 1 M NaOH (pH = 14) at room temperature, even for a longer time (entry 7 and 9, Table 9, Figure 49). The compound does not decompose in 1 M NaOH at 100 °C (entry 8,

Table 9). Only in concentrated NaOH (10 M), the compound degrades at room temperature (entry 6, Table 9). Besides HCl, some other acids were used in these experiments. In concentrated trifluoroacetic acid compound **131** is stable, whereas in concentrated nitric acid, which is an oxidizing acid, it starts to decompose (entry 10 and 11, Table 9).

Table 9. The weight change of cage **131** after the treatments under acidic or basic conditions.

Entry	Treatment	Weight (before) (mg)	Weight (after) (mg)	Weight loss (%)
1	10 M HCl (16 h)	3.3	3.1	6.1
2	10 M HCl (8 h, 100 °C)	3.4	2.7	20.7
3	1 M HCl (16 h)	2.7	2.5	7.4
4	1 M HCl (16 h, 100 °C)	3.1	2.9	6.4
5	1 M HCl (5 d)	3.7	3.5	5.4
6	10 M NaOH (16 h)	4.2	0.6	85.7
7	1 M NaOH (16 h)	1.9	1.8	5.2
8	1 M NaOH (16 h, 100 °C)	2.9	2.8	3.5
9	1 M NaOH (5 d)	3.2	3.1	3.1
10	trifluoroacetic acid (16 h)	4.5	4	11
11	16 M HNO_3 (16 h)	5.3	4.5	15
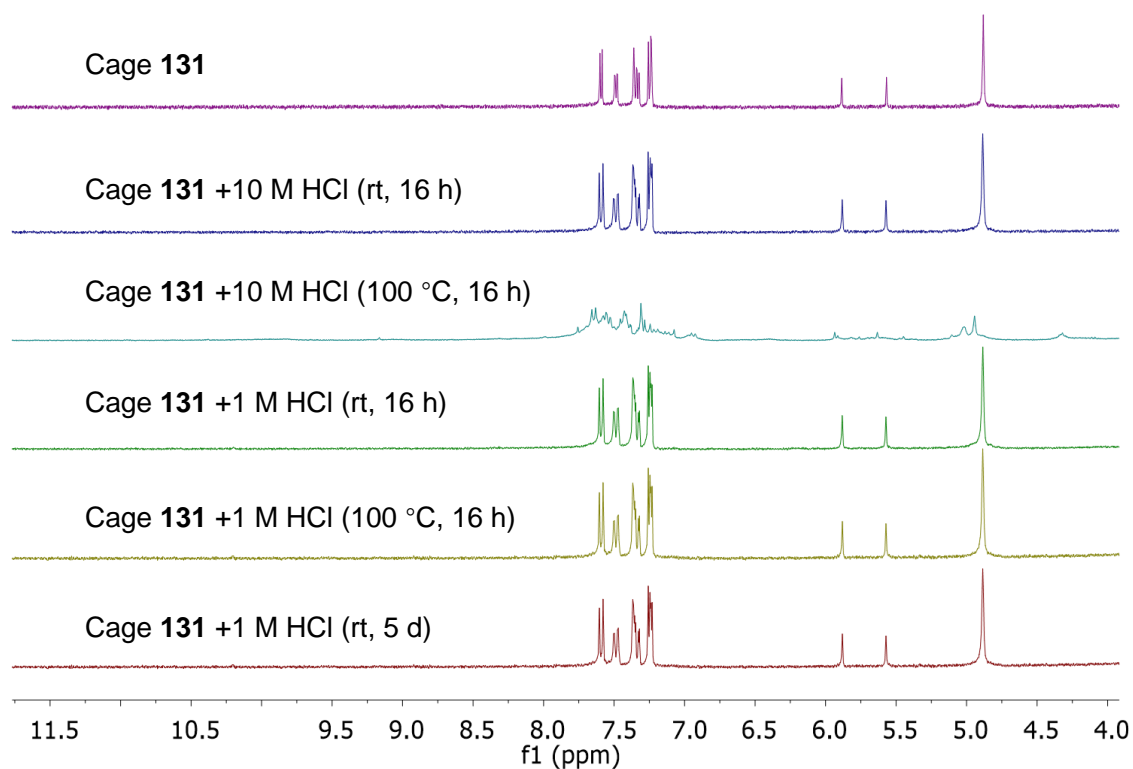
Figure 48. Comparison of the ^{1}H NMR spectra of cage **131** after treatment under acidic conditions (300 MHz, DMSO-d_6).
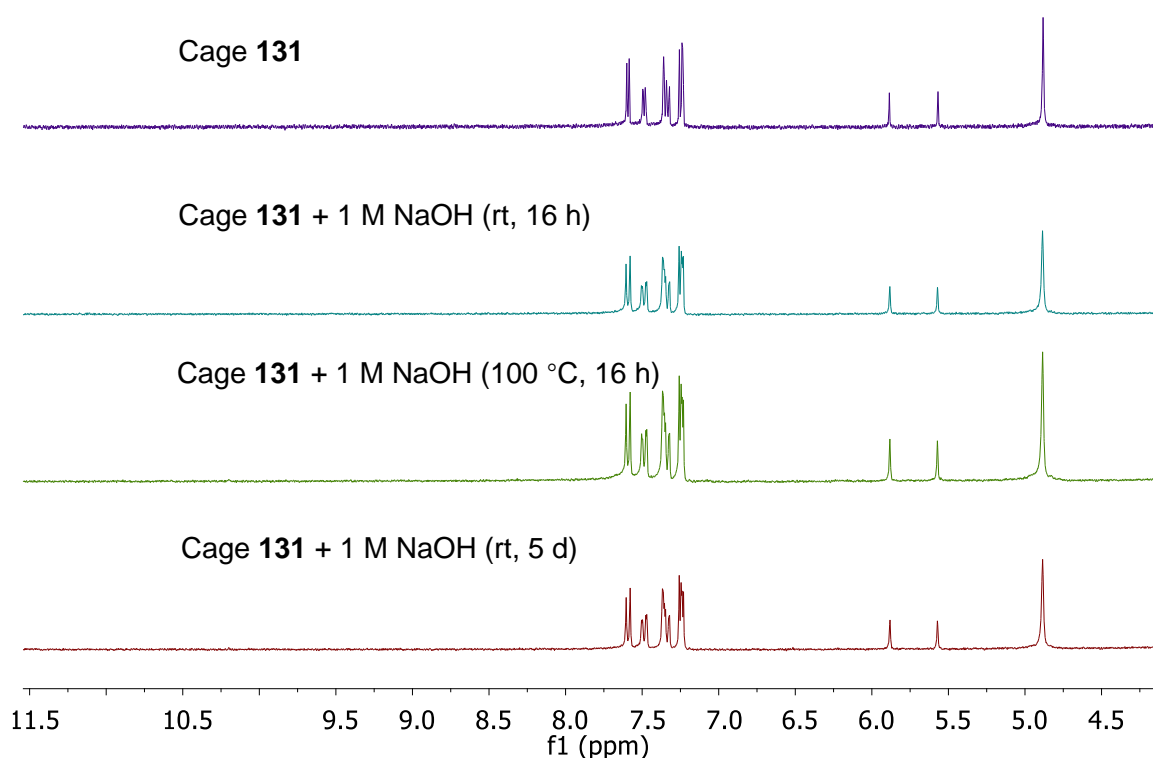
Figure 49. Comparison of the ^{1}H NMR spectra of cage **131** after treatment under basic conditions (300 MHz, DMSO-d_6).

To investigate if the chemical stability is improved through the post-synthetic modification, the same stability tests were done with imine cage **24** (Table 10). In contrast to the high acidity stability of the carbamate cage **131**, the imine cage **24** started decomposing at pH = 4 (0.001 M HCl, rt, 16 h, Figure 50). Although the largest fraction was still intact, the characteristic signals of the bissalicylaldehyde **21** could be found in the ^{1}H NMR spectrum of the remaining solid at δ = 10.32 and 10.81 ppm (Figure 50). In basic conditions, cage **24** began to decompose at pH = 10 (0.001 M, rt, 16 h), shown by the two peaks for the aldehyde precursor appearing in the ^{1}H NMR spectra (Figure 51).

A large weight loss after treatment in 1M HCl solution was observed (entry 1, Table 10), and the ^{1}H NMR proved the remaining solid was the bissalicylaldehyde **21** (Figure 50). The other part which dissolved in the acidic solution was also characterized and it turned out to be the triaminotriptycene **19**, whose –NH$_2$ proton signal was shifted to lower field and became a broad peak. (Figure 52). Comparing the performance of imine cage **24** with carbamate cage **131**, introducing the carbamate group to the imine cage can significantly enhance the chemical stability from pH 4 to 10 to pH -1 to 14.

**Table 10**. The weight loss of cage **24** after treatments under acidic or basic conditions

Entry	Treatment	Weight (before) (mg)	Weight (after)(mg)	Weight loss(%)
1	1 M HCl (16 h)	5.9	2	66.1
2	0.1 M HCl(16 h)	4.4	3.5	20.4
3	0.01 M HCl (16 h)	4.2	3.8	9.5
4	0.001 M HCl (16 h)	5.2	4.9	5.7
5	0.0001 M HCl (16 h)	3.4	3.3	2.9
6	0.0001 M HCl (16 h,100 °C)	3.4	3.0	13.3
7	0.00001 M HCl (16 h)	3.8	3.6	5.2
8	0.00001 M HCl (16 h,100 °C)	3.6	3.3	8.3
9	1 M NaOH (16h)	5	0	100
10	0.1 M NaOH (16h)	3.6	2.7	25
11	0.01 M NaOH (16h)	4.6	4.1	10.8
12	0.001 M NaOH(16h)	3.4	3.2	5.8
13	0.0001 M NaOH (16 h)	3.8	3.7	2.6
14	0.0001 M NaOH (16 h,100 °C)	2.9	2.7	6.9
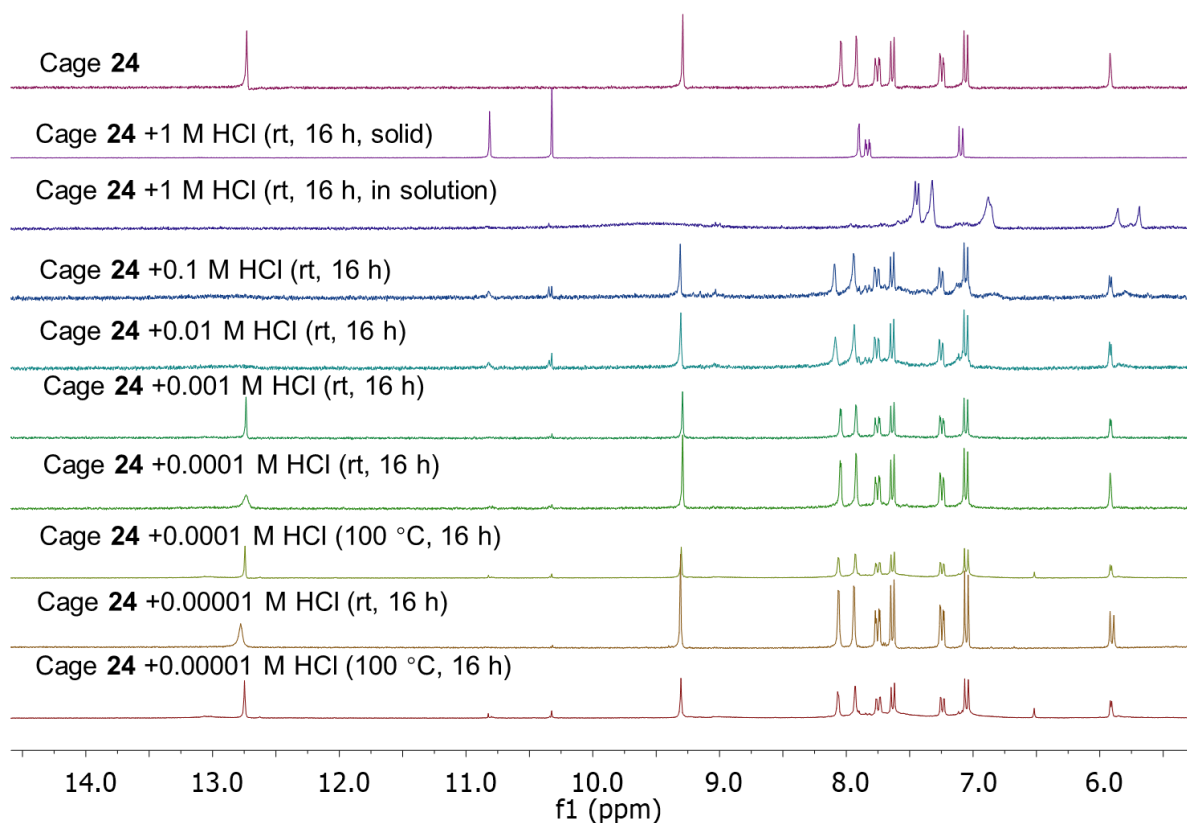
Figure 50. Comparison of the ^{1}H NMR spectra of cage **24** after treatment under acidic conditions (300 MHz, DMSO-d$_6$).
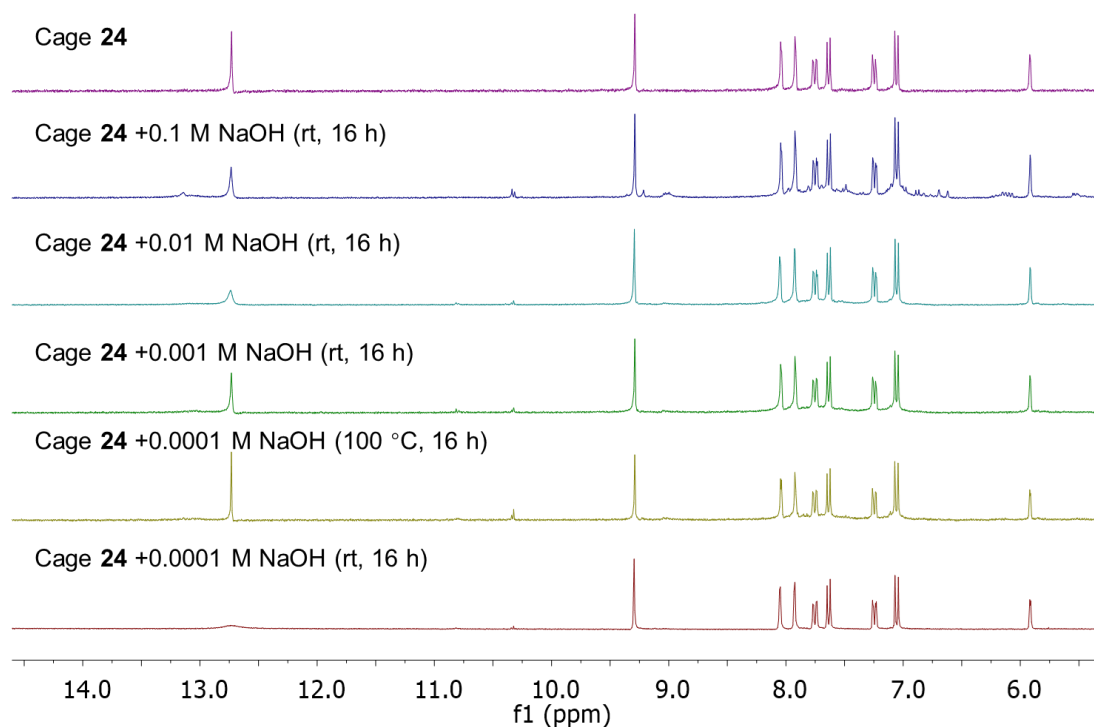
**Figure 51**. Comparison of the ^{1}H NMR spectra of cage **24** after treatment under basic conditions (300 MHz, DMSO-d$_6$).
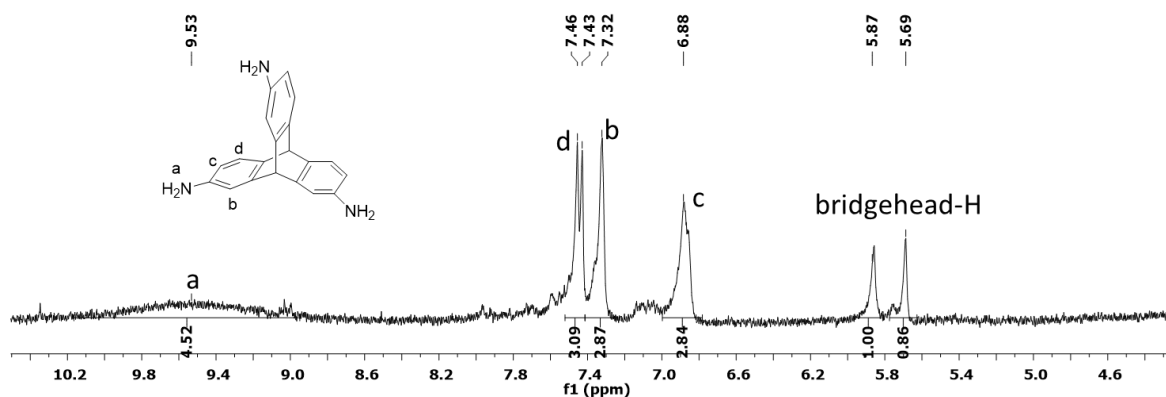
Figure 52. ^{1}H NMR spectrum of the compound dissolved in HCl solution after cage **24** was treated in 1 M HCl (300 MHz, DMSO-d$_6$).

Several pH-stable organic cages have been reported. For instance, the porphyrin box synthesized by the Kim group was stable in solution from pH = 4.8 to 13,[160a] but the [2+3] imine cage **24** shows a comparable stability from pH = 4 to 11. The pyrogallol-based imine cages synthesized by Banerjee and co-workers showed a stability from pH = 1 to 14.[160b] The conversion of enol imines to β-keto enamines increased the stability, which conferred remarkable robustness to the cages towards water, acids and bases. The Cooper group reported a pH-stable shape persistent cage in 2014.[107] The imine bonds of cage **18** (structure in Figure 9) were reduced to amine bonds, then the diamine vertices were 'tied' with acetone.[107] The

83

aminal cage obtained by this strategy showed a stability in solutions between pH =1.7 to 12.3 at room temperature. Cage **131** is stable in concentrated hydrochloric acid (pH = -1) at room temperature, and also stable in 1 M aqueous NaOH solution (pH = 14) at room temperature, which is better than the pyrogallol-based imine cages[160b] and the aminal cage.[107]

Scanning Electron Microscopy (SEM) is also used to test whether or not the morphology of the compound is changed in an acidic or basic environment. In this case, SEM images are taken before and after the treatment (cage **131** immersed into HCl and NaOH solution for 16 h). From the SEM images (Figure 53), cage **131** forms rod-like microcrystals with different length. After treatments with acid or base, the morphology of the material does not change at all, which gives another proof of the stability of cage **131**. The gas sorption experiments performed before and after the pH treatment will be discussed later.
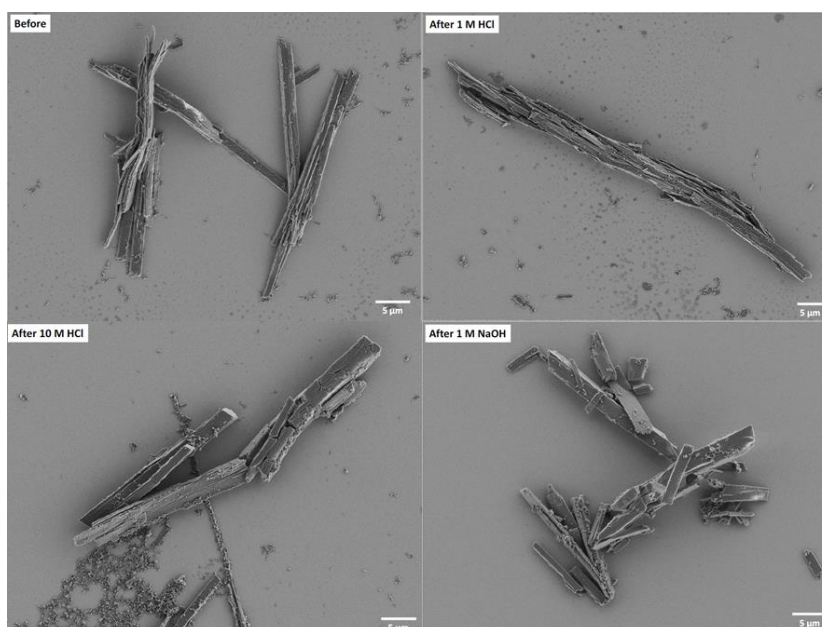

Figure 53. SEM images of cage **131** before and after treatment with HCl and NaOH.

3.3.4   Gas sorption properties of the carbamate cage

As was discussed in **3.3.2**, the crystal structure of cage **131** indicates that this cage is potentially porous. For this reason, gas sorption experiments of amine cage **130** and carbamate cage **131** were performed. For cage **130**, the specific surface area (Brunauer-Emmett-Teller model) is SA_{BET} =12 m^2/g (N_2, 77K, Figure 55b). Compared with the original [2+3] imine cage **24**,[49a] cage **130**, whose imine bonds are reduced to amine bonds, has a more flexible structure, which results in the loss of shape persistence. Although the crystal structure of cage **130** was not obtained, similar phenomena has been observed in literature.[107]

For cage **131**, the first sample of microcrystalline material used for gas sorption was obtained from DMSO/methanol. Thermogravimetric analysis (TGA) was carried out in order to determine the activation temperature (Figure 54). The TGA curve (nitrogen atmosphere) presents a small weight loss under 100 °C, which may be the solvent molecules residing inside the cage compound. Then cage **131** remains stable until 400 °C, and a larger weight loss happens at 400 to 500 °C.
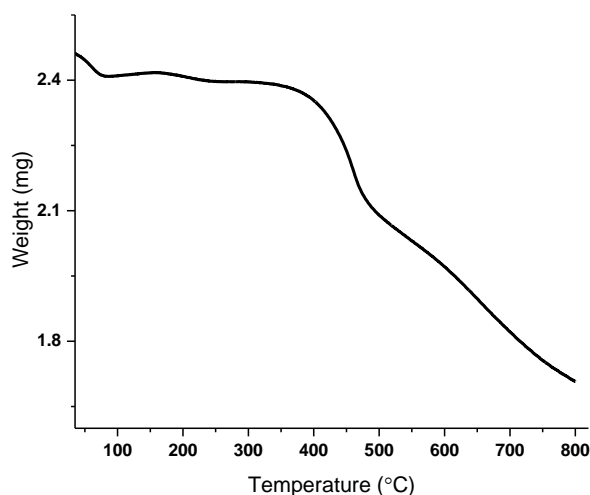

Figure 54.TGA curve of cage **131**.

According to the TGA curve, no decomposition of cage **131** occurs until 400 °C. So cage **131** was activated at 200 °C for 3 h before measuring gas sorption. At 77 K using N_2, cage **131** adsorbed 130 cm^3/g nitrogen, and the specific surface area is $SA_{BET} = 105$ m^2/g (BET model, Figure 55a).

The second sample was prepared by dissolving the carbamate cage **131** in DMSO at 100 °C. The clear solution was dropped into cold water to crash out the compound. The colourless solid was activated at 200 °C in vacuum for 16 h. However, the nitrogen sorption isotherm was very similar to the first sample, only with a slight increase of nitrogen uptake and the specific surface area ($SA_{BET} = 113$ m^2/g, Figure 55a), but it can be treated as the same level.

The third sample was obtained in a similar way to the second sample, but the colourless solid was crashed out from DMF/methanol. The precipitate was treated by solvent exchange (from DMF/methanol to methanol then to *n*-pentane), then activated at room temperature for 16 h. The gas sorption experiment showed the third sample owns the lowest uptake of nitrogen and smallest specific surface area among these three samples. The specific surface area is $SA_{BET} = 50$ m^2/g (Figure 55a) and the uptake of nitrogen at 77 K is 53 cm^3/g.
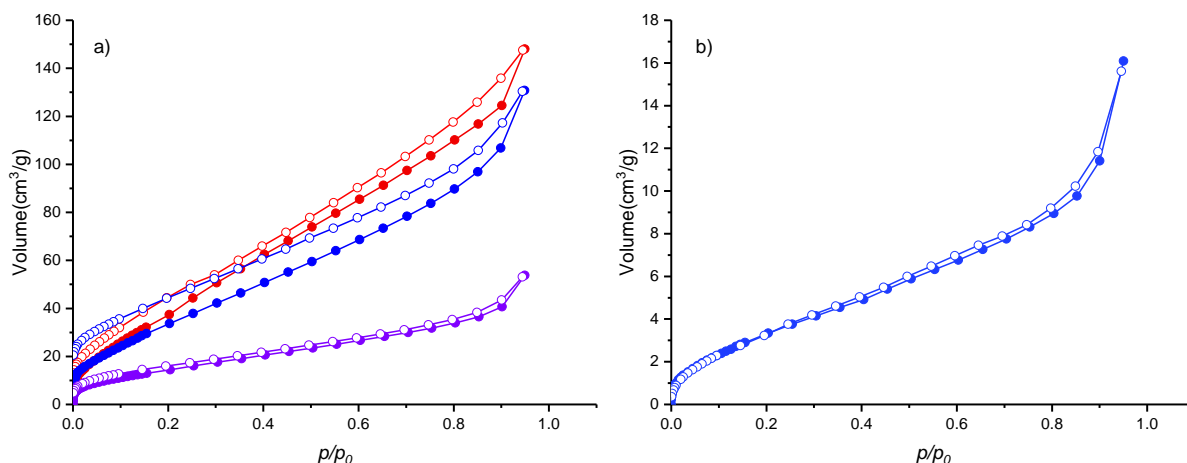
Figure 55. N_2 sorption isotherms of a) cage **131**, the sample got from DMSO/methanol, DMSO/water and DMF/methanol was shown in red, blue and purple, respectively at 77 K. b) cage **130** at 77 K.

Although the surface area and uptake of nitrogen show some differences, the shapes of these three isotherms are quite similar. They can all be classified as a mixture of type I and type IV isotherms (Figure 55).[155a] According to the two kinds of polymorphs from the crystal structure (see in **3.3.2**), the porous and nonporous polymorph may both exist in these three samples, and the nonporous one preponderates. The other possible reason is that during the activation progress, the porous polymorph transfers to the nonporous one. The specific surface area of cage **131** (from all three samples) is lower than the [2+3] imine cage **24** ($SA_{BET} = 744$ m^2/g),[49] but much higher than the corresponding flexible amine cage **130** ($SA_{BET} = 12$ m^2/g). This also suggests that after adding the carbamate group, the cage keeps the shape persistency to some degree.

In **3.2.3**, the stability of cage **131** in acidic and basic environment was proven by ^{1}H NMR and SEM. In order to test if acid affects the surface area, a gas sorption experiment of the cage **131** after treatment with 10 M HCl at room temperature for 16 h was carried out (Figure 56). The sample was treated by solvent exchange (from water to acetone to *n*-pentane), then activated at room temperature for 16 h. The specific surface area is $SA_{BET} = 194$ m^2/g (N_2, 77 K), which represents a slight increase compared to
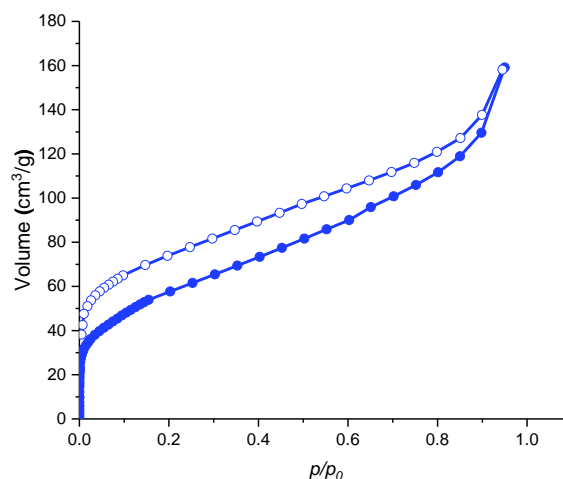
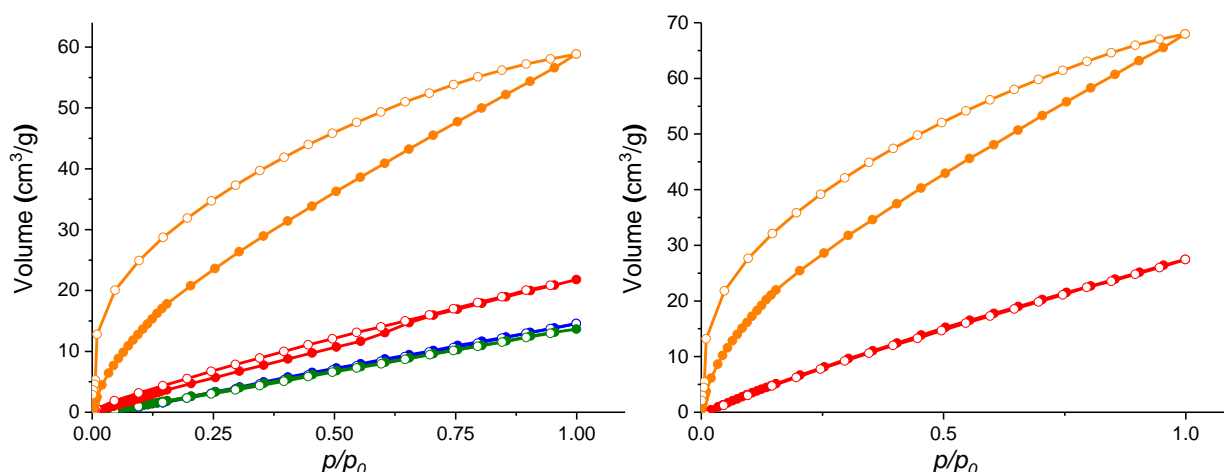**Figure 56.** N_2 sorption isotherm of cage **131** after treatment of 10 M HCl at 77 K.

before (SA_{BET} = 113 m^2/g), but is still in the same order of magnitude, showing that the treatment by acid does not affect the properties of the material.

Besides N_2 at 77 K, the adsorption of some other gases was also investigated. Figure 55 illustrates that despite the small specific surface area of cage **131** measured by N_2 at 77 K, this cage shows some interesting properties with other gases. For example, it adsorbs relatively large amounts of CO_2 at 273 K, 1 bar (58 cm^3/g, 11.5 wt%). Similar phenomena have been observed for the flexible [2+3] imine cage **25**,[49] whose surface area is only SA_{BET} =30 m^2/g (BET model, Table 11), but has a higher uptake of CO_2 at 298 K, 1 bar (74 cm^3/g, 14.5 wt%, Table 11) than the rigid [2+3] imine cage **24** (11.9 wt%, Table 11).[49] This may because the diffusion of gas molecules is kinetically hindered at 77 K. Compared with Cooper's pH stable aminal cage FT-RCC3 (Table 11), cage **131** shows smaller specific surface area, but higher CO_2 uptake (39 cm^3/g, 7.6 wt%).[107]

By comparison with other organic cages (Table 11), the CO_2 uptake of cage **131** is quite similar to the imine cage **24** (11.9 wt%)[49] and [2+3]-*rac* imine cage (10.9 wt%) from the Mastalerz group,[61] but still lower than for the imine cube (18.2 wt%) from the Mastalerz group,[95b] the CC1-*R* (14.5 wt%) cage and CC5-*R* cage (13.6 wt%) from the Cooper group.[43] Apart from CO_2, cage **131** also adsorbs 21.8 cm^3/g (1.6 wt%) CH_4 at 273 K, 1 bar and 97.2 cm^3/g (0.87 wt%) H_2 at 77 K, 1 bar. The Henry selectivity is $S_{CO2/N2}$ = 13.9 for CO_2 over N_2 and $S_{CO2/CH4}$ = 7.6 for CO_2 over CH_4. The selectivity of CO_2/CH_4 can compare with the imine cube (7.7),[95b] but is worse than for the [4+6] cage **23** (10).[47]

Figure 57. Gas sorption isotherm of cage **131** left: CO_2, CH_4, N_2, H_2 at 273 K and right CO_2 and CH_4 at 263 K. The CO_2, CH_4, N_2 and H_2 are showed in orange, red, blue and green, respectively.

Table 11. Comparison of gas sorption data for cage compound **131** with those imine cages published previously[a]

| Entry	Phase	SA_{BET}	Uptake in mmol/g(wt%, 1bar)			Selectivity	Ref.
		(m^2/g)	H_2(77 K)	CO_2(273 K)	CH_4(273 K)	CO_2/CH_4	
Cage 131	amorphous	113	4.3(0.88)	2.6 (11.6)	0.97 (1.6)	7.6	
Cage 24	crystalline	744	n.d	2.7(11.9)[b]	0.7 (1.12)[b]	4.0[b]	[49]
Cage 25	crystalline	30	n.d.	3.3 (14.5)	0.34 (0.5)[b]	n.d.	[49]
Cage 23	crystalline	2071	5.6 (1.13)	2.7(11.9)	0.7 (1.12)	10	[47]
Imine cube	crystalline	1014	7.3 (1.43)	4.1(18.2)	1.3 (2.04)	7.7	[95b]
[2+3]-*rac*	crystalline	211	4.7 (0.95)	2.5 (10.9)	1.0 (1.62)	4.6	[61]
AT-RCC3	crystalline	67		1.77 (7.6)[b]			[107]
FT-RCC3	crystalline	377	4.3 (0.88)	1.75 (7.6)			[107]

a:SA =specific surface area. b: Measured at 298 K.

3.3.5 Conclusion

A new carbamate cage **131** has been synthesized base on [2+3] imine cage **24** in a two-step approach. The imine bonds were reduced to amine bonds first, then react with *N*, *N*'-carbonyldiimidazole to give the carbamate cage **131**. This cage shows stability in 1 M hydrochloric acid, even after heating to 100 °C and also in concentrated hydrochloric acid (10 M) at room temperature. The cage is also stable in 1 M NaOH solution. The surface area measured by N_2 sorption at 77 K is $SA_{BET} = 113$ m^2/g, and it could take up significant amounts of CO_2 (11.5 wt%) at 273 K, 1 bar. The strategy for synthesizing this carbamate cage can be applied to other imine cages[49] formed from salicylaldehyde building blocks to increase their chemical stability.

4 Summary

In this thesis, several new cage compounds have been synthesized by both post-synthetic modification and the modification of building blocks. A series of new [2+3] imine cage compounds were synthesized from triaminotriptycene **19** and side chain modified terphenyl bisalicylaldehydes (Scheme 34). All these cages possess good solubility in DMF or THF compared with the [2+3] terphenyl cage without side-chains. For five of the cages crystal structure were obtained and according to gas sorption experiments, the cage with perfluorobutyl chains shows a specific surface area of $SA_{BET} = 588$ m^2/g. This cage also exhibits a good Henry selectivity of SF$_6$/N$_2$ $S_{SF_6/N_2} = 107$, and an IAST selectivity of SF$_6$/N$_2$ (10:90, 273 K) $S_{SF_6/N_2} = 28$, which gives the cage potential applications in gas separation.

Besides modifying the aldehyde building blocks, a new amine building block which contains four amine functional groups was synthesized in three steps from triamino triptycene (Scheme 34). This new amine building block was used to reacted with eight disalicylaldehydes with different lengths. A [2+1] cage was formed when a bisphenyl salicyl aldehyde was used. For the terphenyl aldehydes, the amine precursor can form not only the [2+1] cage, but also the [4+2] and the [6+3] cages. For the tetraphenyl aldehyde, a [4+2] cage is formed instead of the [2+1] cage. These results suggest that the length of the precursor has an influence on the size of the formed cage compounds.
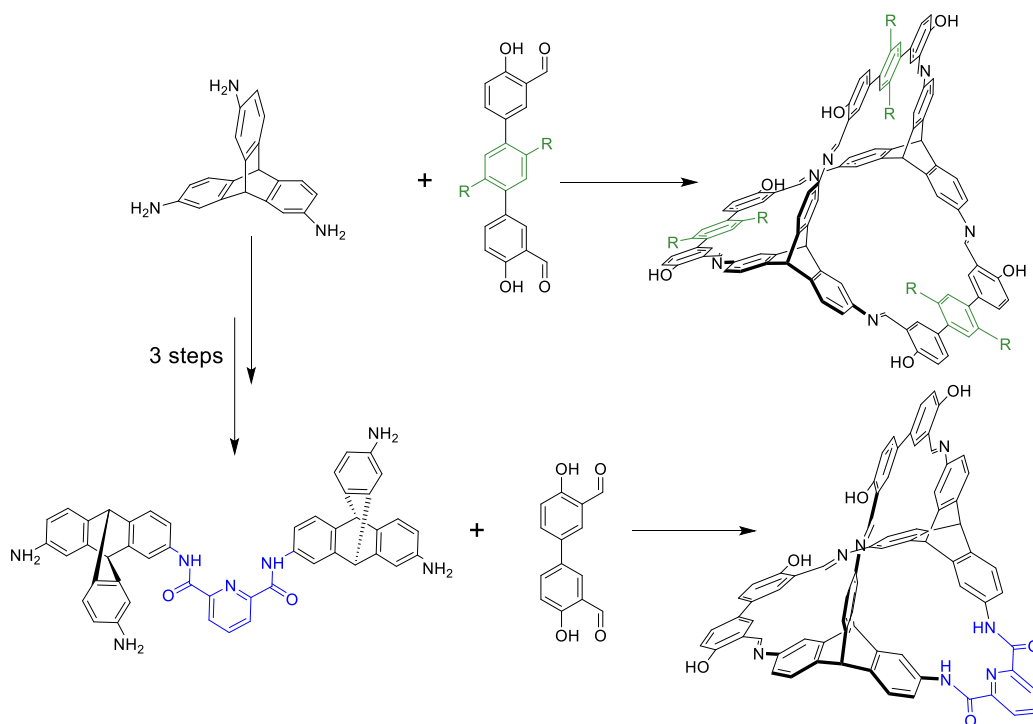
Scheme 34.Synthesis of new cages by modifying amine or aldehyde building blocks.

A carbamate cage was synthesized based on a [2+3] imine cage in a two-step approach: the imine bonds were first reduced to amine bonds, then reacted with *N, N'*-carbonyldiimidazole to give the carbamate cage (Scheme 35). Single crystal structures show the carbamate cage forms two polymorphs depending on the solvents used for crystallization. The gas adsorption experiments show that the specific surface area of the carbamate cage is $SA_{BET} = 113$ m^2/g. This new carbamate cage exhibits better stability in both acidic and basic environment (pH = -1 to 14) compared with the imine cage. The stability is confirmed by ^{1}H NMR spectra, SEM images and gas sorption experiments. This strategy provides a new way to synthesize chemically stable cage compounds which can be used for further functionalization.
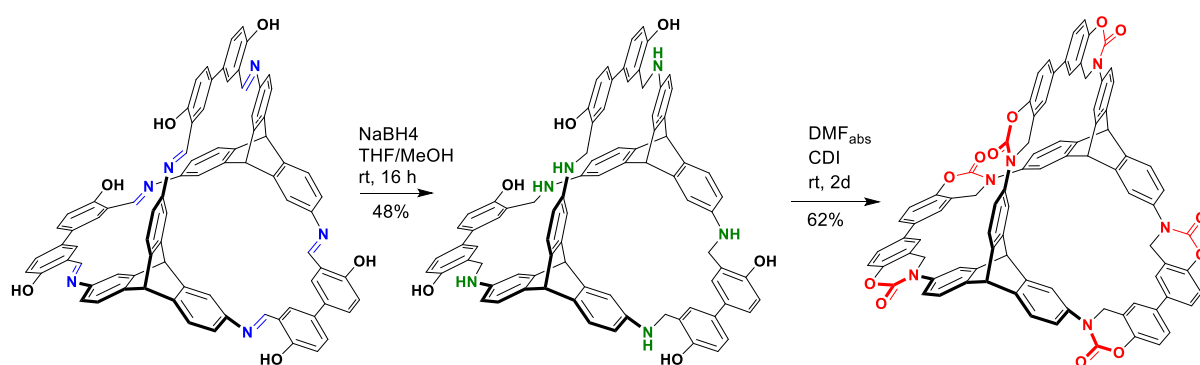
Scheme 35.Synthesis of the carbamate cage by post-synthetic modification.

5 Experimental Section

5.1 General Remarks

Flash column chromatography was performed on silica gel from Macherey-Nagel&Co.KG (particle sizes:0.04-0.063 mm) using petroleum ether, ethyl acetate, chloroform, dichloromethane, toluene, methanol or their mixtures as eluents. For Thin Layer Chromatography (TLC) gel 60 F254 plates form Merck were used and examined under UV-light irradiation (254 nm and 365 nm). Size Exclusion Chromatography (SEC) was performed on BioBeads SX1 from BioRad Laboratories, Inc. and DMF was used as solvent. Melting points (not correct) were measured by Buchi Melting Point B-545. Nuclear Magnetic Resonance Spectroscopy (NMR) ^{1}H, ^{13}C, ^{19}F, 2D coupling experiments were performed in CDCl$_3$, DMSO-d$_6$, THF-d$_8$ using a Bruker Avance III 300, Bruker Avance DRX 300, Bruker Avance III 400, Bruker Avance III 500, Bruker Avance III 600. Chemical shifts were reported in parts per million (ppm) relative to the traces of CHCl$_3$ (δ_H = 7.26 ppm, δ_C = 77.2 ppm), DMSO-d$_5$ (δ_H = 2.50 ppm, δ_C = 39.5 ppm), THF-d$_7$ (δ_H = 3.58, 1.72 ppm, δ_C = 67.2, 25.3 ppm) in the corresponding fully deuterated solvent. Mass Spectrometry (MS) were performed on a Fourier Transform Ion Cyclotron Resonance (FT-ICR) mass spectrometer ApexQe hybrid 9.4 T (Bruker Daltonik GmbH, Bremen, Germany) equipped with a 9.4 T superconducting magnet and interfaced to an Apollo II MTP Dual ESI/MALDI source for DART, EST and MADIL experiments. MADIL-TOF MS experiments were carried out on a Bruker AutoFlex Speed time of flight with trans-2-[3-(4-tert-butylphenyl)-2-methyl-2-propenylidene] malononitrile (DCTB) as matrix. Electrospray ionization (ESI) mass spectra were recorded on a Finnigan LCQ quadrupole ion trap. Infrared spectroscopy (IR) were performed on a Fourier transform spectrophotometer equipped with ATR crystal. The signal was described as: strong (s), medium (m), weak (w) and broad (br). Thermal Gravimetric Analysis (TGA) were measured on a Mettler-Toledo TGA/DSC1 instrument with a TGA/DSC-Sensor 1100 equipped with a MX1 balance (Mettler-Toledo) and a GC100 gas control box for nitrogen supply. TGA samples were measured in 70 HL Al2O3 crucibles. Powder X-ray Diffractometry (PXRD) was performed with a STOE STADI 611KLS/N 61263 with Ge (111)-monochromated copper radiation (λ(CuKα) = 1.54060 Å). The diffractograms were obtained with a Stoe linear PSD Detector, measured in a glass capillary (Ø = 0.5 mm) as sample container. X-ray crystal structure analysis was accomplished on a Quazar Bruker APEX I (λMoKα= 0.71073 Å), Bruker APEX II (λMoKα = 0.71073 Å) or a Stoe Stadivari (λCuKα = 1.54186 Å) diffractometer. Scanning

Electron Microscopy (SEM) micrographs in Figure 53 were acquired using an Ultra 55 field emission scanning electron microscope (Carl Zeiss Microscopy, Germany). Imaging was performed with a working distance of 3.0 mm and a landing energy of 1.2 keV and an aperture of 10 μm. Gas sorption Experiments: The surface areas and porosities were characterized by nitrogen adsorption and desorption analysis at 77.35 K with an autosorb computer controlled surface analyser (AUTOSORB-iQ2, Quantachrome). The Brunauer-Emmett-Teller (BET) surface areas were calculated assuming a cross sectional area of 0.162 nm^2 for the nitrogen molecules in the pressure range $p/p_0 = 0.01\text{-}0.1$. The quenched solid-density functional theory (NL-DFT model) and isotherm data were used to calculate the pore size distribution. Measurements of N_2, H_2, CH_4, and CO_2 at 273 K were carried out using a simple Dewar vacuum flask with an ice/water mixture. A temperature of 263 K was applied by using a frozen mixture of water/EtOH (80: 20, v/v) and for measurements between 298 K and 363 K a Lauda C6 CS thermostat was used, which was equipped with a Fryka KT 12-52 cryostat for the measurements at 298 K and 313 K. The temperatures were frequently monitored by a VWR TD 131 digital thermometer.

5.2 Chemicals

Chemicals	Purities	Source
Acetic acid	n.d.	VWR
Acetone	≥ 99.5%	Honeywell
Acetonitrile	≥ 99.9%	Sigma-Aldrich
Anisil	≥99%	Fluka
Anthracene	97%	Sigma-Aldrich
Anthranilic acid	98%	Acros Organics
Benzene-1,4-diboronic acid	95%	Sigma-Aldrich
Bromine	reagent grade	Sigma-Aldrich
5-Bromopent-1-ene	n.d.	Fluorochem
1-Bromobutene	≥98%	Merck
1-Bromohexane	≥98%	Merck
1-Bromooctane	≥98%	Merck
Carbonyldiimidazole	97%	Sigma-Aldrich
Chloroform-d	99.8%	Sigma-Aldrich
Dichloromethane	n.d.	VMR
Dichloroethane	99%	Honeywell
Diethyl ether	99.80%	Sigma-Aldrich
Diethylene glycol diethyl ether	>98%	Acros Organics
Di-t-butyl-dicarbonate	>98%	Sigma-Aldrich
DMSO-d_6	99.9%	Sigma-Aldrich
1,4-Dibromobenzene	98%	Aldrich
1,4-Dichlorobenzene	≥99%	Aldrich
1,4-diiodobenzene	99%	Aldrich
1,4-dioxane	>99%	Aldrich
2,5-dibromohydroquinone	>98%	TCI
4,4' – dibromobiphenyl	98%	Aldrich
4,4'-Dihydroxybiphenyl	99.50%	ACROS
Ethanol	96%	Sigma Aldrich
Ethyl acetate	≥99.5%	Honeywell
Hexamethylenetetraamine	99%	Gruessing
Hexylmagnesiumbromide	n.d.	Aldrich
Hydrazine monohydrate	98%	Merck
Hydrochloric acid	36.5%-38%	Sigma-Aldrich
Iodine	99.80%	Fluka
Isopentyl nitrite	>95%	TCI
l, 5-bromosalicylaldehyde	n.d.	Alfa-Aesar
Maleic anhydride	>99%	Merck
Methanol	>99.8	Honerwell
2-methoxyethanol	>98%	TCI
4-methylbenzenesulfonyl chloride	>98%	Sigma-Aldrich

N,N-Dimethylformamide	≥99.8%	Sigma-Aldrich
N-bromosuccinimide	99%	Sigma-Aldrich
Nitric acid(fuming, 90%)		Acros Organics
Nonafluoro-1-iodobutane	98%	Aldrich
Nonafluoro-1-iodobutane	98%	Aldrich
n-Pentane	98%	Sigma-Aldrich
Petroleum ether (40-60 °C)	n.d.	Honeywell
4-(*N, N*-dimethylamino) pyridine	n.d.	Merck
Octylmagnesiumbromide	n.d.	Aldrich
Palladium on act. Charcoal (5% Pd basis)	n.d.	Degussa
Pd(dppf)Cl$_2$	99%	Carbolution
Pd(PPh$_3$)$_4$	99%	Aldrich
Pd$_2$(dba)$_3$	99%	Carbolution
Potassium acetate	> 99%	Sigma-Aldrich
Potassium carbonate	99%	Gruessing
Potassium fluoride	99%	Gruessing
Potassium hydroxide	99.90%	Sigma-Aldrich
Pyridine carbonyl dichloride	97%	Aldrich
Sodium boronhydride		Merck
Sodium hydroxide	>98%	Honeywell
Sodium sulfate	>99%	Bernd Kraft
Sodium thiosulfate	99%	Gruessing
Tetrahydrofurane	≥99.9	Honerwell
Toluene	≥99.7%	Sigma-Aldrich
Triethylene glycol monomethyl ether	>98%	TCI
Trifluoroacetic acid	99%	abcr
Trioxane	>99%	Aldrich
Tri-*tert*-butylphosphonium Tetrafluoroborate	97%	Sigma-Aldrich
Zinc dust	99.90%	Gruessing

5.3 Synthesis

5.3.1 Compounds of Chapter 3.1

5.3.1.1 Synthesis of 1,4-dibutylbenzene (67):[163]
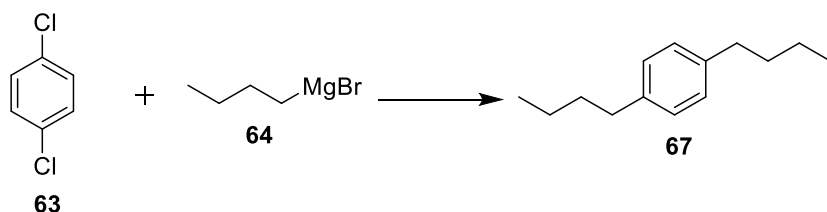
1,4-Dichlorobenzene **63** (2.0 g, 13.6 mmol) and Ni(dppp)Cl$_2$ (10 mg, 0.018 mmol) were stirred in anhydrous diethyl ether (20 mL) at 0 °C. Butylmagnesiumbromide **64** (17 mL, 2 mol/L, in diethyl ether) was added dropwise under Ar, then the reaction mixture was refluxed for 16 h. After cooling to room temperature, the reaction was quenched by adding water (10 mL) and 2 mol/L HCl (50 mL). The aqueous layer was extracted with diethyl ether (3 × 10 mL). The combined organic layers were washed with water and dried over Na$_2$SO$_4$. The solvent was removed under reduced pressure, to give the product as a colourless oil with the yield of 89% (2.29 g, 12.1 mmol).

^{1}H NMR (300 MHz, CDCl$_3$) δ = 7.09 (s, 4H), 2.58 (t, J = 7.3 Hz, 4H), 1.68 – 1.50 (m, 4H), 1.36 (dq, J = 14.3, 7.2 Hz, 4H), 0.92 (t, J = 7.3 Hz, 6H) ppm.

Analytical data are in accordance with those previously reported.[163]

5.3.1.2 Synthesis of 1,4-dihexylbenzene (68):[164]
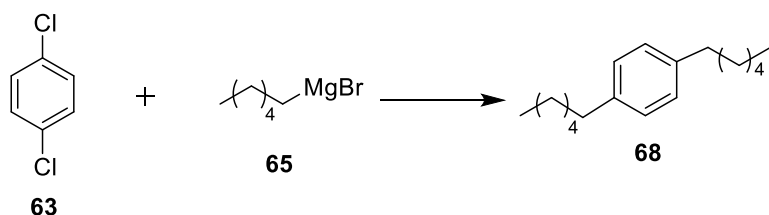
1,4-Dichlorobenzene **63** (2.0 g, 13.6 mmol), Ni(dppp)Cl$_2$ (10 mg, 0.018 mmol) were stirred in anhydrous diethyl ether (20 mL) at 0 °C. Hexylmagnesiumbromide **65** (17 mL, 2 mol/L, in diethyl ether) was added dropwise under Ar, then the reaction mixture was refluxed for 16 h. After cooling to room temperature, the reaction was quenched by adding water (10 mL) and 2 mol/L HCl (50 mL). The aqueous layer was extracted with diethyl ether (3 × 10 mL). The combined organic layers were washed with water and dried over Na$_2$SO$_4$. The solvent was

removed under reduced pressure, to give the product as a colourless oil with the yield of 86% (2.8 g, 11.7 mmol).

^{1}H NMR (300 MHz, CDCl$_3$) δ = 7.09 (s, 4H), 2.57 (t, J = 6.7 Hz, 4H), 1.59 (dd, J = 14.9, 7.2 Hz, 4H), 1.43 – 1.18 (m, 12H), 0.89 (t, J = 6.7 Hz, 6H) ppm.

Analytical data are in accordance with those previously reported. [164]

5.3.1.3 Synthesis of 1,4-dioctylbenzene (69):[165]
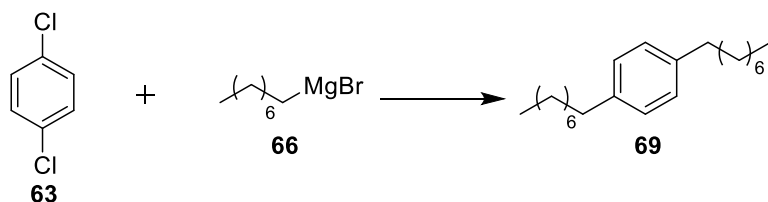
1,4-Dichlorobenzene **63** (2.0 g, 13.6 mmol), Ni(dppp)Cl$_2$ (10 mg, 0.018 mmol) were stirred in anhydrous diethyl ether (20 mL) at 0 °C. Octylmagnesiumbromide **66** (17 mL, 2 mol/L, in diethyl ether) was added dropwise under Ar, then the reaction mixture was refluxed for 16 h. After cooling to room temperature, the reaction was quenched by adding water (10 mL) and 2 mol/L HCl (50 mL). The aqueous layer was extracted with diethyl ether (3 × 10 mL). The combined organic layers were washed with water and dried over Na$_2$SO$_4$. The solvent was removed under reduced pressure, to give the product as a colourless oil with the yield of 92% (3.7 g, 12.51 mmol).

^{1}H NMR (300 MHz, CDCl$_3$): δ =7.01 (s, 4H), 2.52 (t, J = 6.7 Hz, 4H), 1.52 (m, 4H), 1.23 (m, 20H), 0.81 (t, J = 6.7 Hz, 6H).

Analytical data are in accordance with those previously reported.[165]

### 5.3.1.4 Synthesis of 1,4-dibromo-2,5-dibutylbenzene (70):[163]
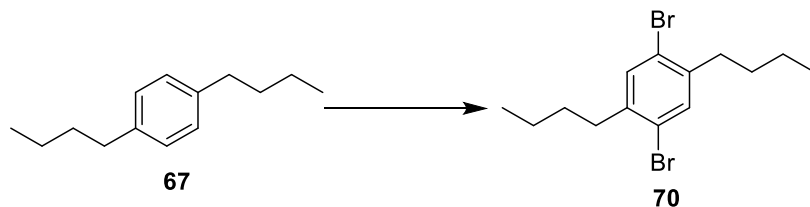
1,4-dibutylbenzene **67** (1.9 g, 9.9 mmol) was mixed with iodine (10 mg) in DCM (10 mL) at 0 °C. The bromine (4.0 g, 24.9 mmol) was dissolved in DCM (10 mL) and added dropwise over a period of 30 min, and the mixture was stirred at room temperature for 16 h. KOH solution (15 mL, 10%) was added to the mixture and stirred until the colour changed from brown to

light yellow (may need heating to 40 °C). The DCM layer was washed with $Na_2S_2O_3$ (1 M, 20 mL) and water (3 × 10 mL). The light yellow solution was dried over Na_2SO_4, and the solvent was removed under reduced pressure to obtain the crude product. The product was purified by recrystallization from ethanol at 0 °C, to give the product as colourless srystals, which melted upon warming to room temperature in a 62% yield (2.1 g, 6.1 mmol).

^{1}H NMR (300 MHz, CDCl$_3$) δ = 7.35 (s, 2H), 2.65 (t, J = 7.3 Hz, 4H), 1.62 – 1.52 (m, 4H), 1.40 (dq, J = 14.3, 7.2 Hz, 4H), 0.95 (t, J = 7.3 Hz, 6H).

Analytical data are in accordance with those previously reported.[163]

5.3.1.5 Synthesis of 1,4-dibromo-2,5-dihexylbenzene (71):[166]
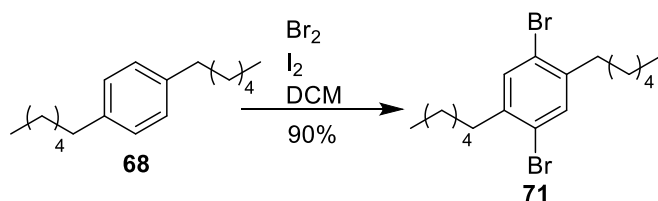
1,4-dihexylbenzene **68** (1.2 g, 4.69 mmol) was mixed with iodine (10 mg) in DCM (10 mL) at 0 °C. The bromine (1.65 g, 10.31 mmol) was dissolved in DCM (10 mL) and added dropwise over a period of 30 min, and the mixture was stirred at room temperature for 16 h. KOH solution (15 mL, 10%) was added to the mixture and stirred until the colour changed from brown to light yellow (may need heating to 40 °C). The DCM layer was washed with $Na_2S_2O_3$ (1 M, 20 mL) and water (3 × 10 mL). The light yellow solution was dried over Na_2SO_4, and the solvent was removed under reduced pressure to obtain the crude product. The product was purified by recrystallization from ethanol at 0 °C, to give the product as colourless crystals, which melted upon warming to room temperature in a 75% yield (1.4 g, 3.5 mmol).

^{1}H NMR (300 MHz, CDCl$_3$) δ = 7.28 (s, 2H), 2.56 (m, 4H), 1.50 (m, 4H), 1.21 – 1.27 (m, 12H), 0.82 (m, 6H) ppm.

Analytical data are in accordance with those previously reported.[166]

5.3.1.6 Synthesis of 1,4-dibromo-2,5-dioctylbenzene (72):[167]
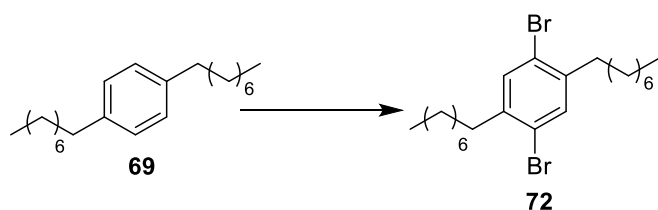
1,4-dihexylbenzene **69** (1.42 g, 4.69 mmol) was mixed with iodine (10 mg) in DCM (10 mL) at 0 °C. The bromine (1.65 g, 10.31 mmol) was dissolved in DCM (10 mL) and added dropwise over a period of 30 min, and the mixture was stirred at room temperature for 16 h. KOH solution (15 mL, 10%) was added to the mixture and stirred until the colour changed from brown to light yellow (may need heating to 40 °C). The DCM layer was washed with $Na_2S_2O_3$ (1 M, 20 mL) and water (3 × 10 mL). The light yellow solution was dried over Na_2SO_4, and the solvent was removed under reduced pressure to obtain the crude product. The product was purified by recrystallization from ethanol at 0 °C, to give the product as colourless crystals, which melted upon warming to room temperature in a 68% yield (1.46 g, 3.19 mmol).

^{1}H NMR (300 MHz, CDCl$_3$,) δ = 7.28 (s, 2H), 2.59 (m, 4H), 1.50 (m, 4H), 1.21 − 1.27 (m, 20H), 0.88 (m, 6H) ppm.

Analytical data are in accordance with those previously reported.[167]

5.3.1.7 Synthesis of 3-Carbonyl-4-hydroxyphenylvoronic acid pinacol ester (74):[113]
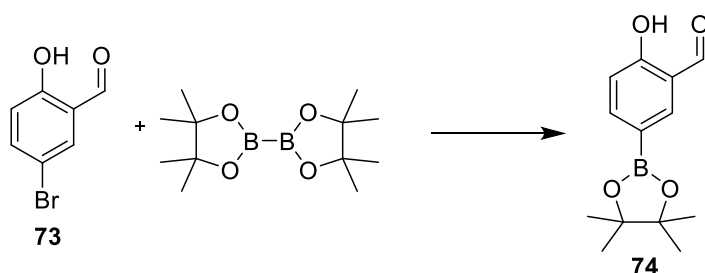
In a screw cap vessel, l, 5-bromosalicylaldehyde **73** (2.77 g, 13.78 mmol), bis(pinacolato)diboron (3.85 g, 15.16 mmol) and KOAc (4.06 g, 41.34 mmol,) were suspended in dry 1,4-dioxane (55 mL) and Pd(dppf)Cl$_2$ (302 mg, 0.41 mmol) was added under Ar. After stirring for 2 hours at 90°C, the reaction mixture was cooled to room temperature, and filtered through a pad of Celite using additional diethyl ether (200 mL). The ether phase was washed with H_2O and brine, dried over Na_2SO_4 and the solvent removed under vacuum to give the crude product as a brown residue. Purification via flash column chromatography on silica gel (petroleum ether/EtOAc 10:1 + 1% HOAc, Rf = 0.6) and recrystallization from hot petroleum ether yielded **74** as colourless crystals (1.74 g, 7.01 mmol, 88%).

M.p.: 108 °C [Lit.: 108 °C].[113]

^{1}H NMR (300 MHz, DMSO-d$_6$): δ = 11.09 (s, 1H), 10.27 (s, 1H), 8.01 (s,1H), 7.77 (d, 1H), 7.01 (d, 1H), 1.29 (s, 12H) ppm.

Analytical data are in accordance with those previously reported.[113]

5.3.1.8 Synthesis of 2',5'-dibutyl-4,4''-dihydroxy-[1,1':4',1''-terphenyl]-3,3''-dicarbaldehyde (52):
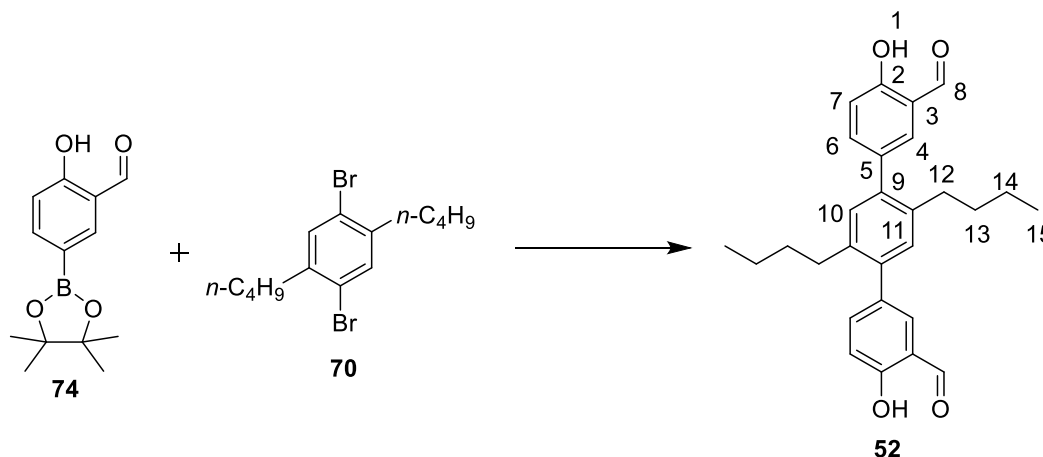
Benzaldehyde **74** (500 mg, 2.01 mmol), 1,4-dibromo-2,5-dibutoxybenzene **70** (280 mg, 0.8 mmol), and [(t-Bu)$_3$PH]BF$_4$ (46.6 mg, 0.16 mmol) were suspended in THF (10 mL) and K$_2$CO$_3$ solution (2 mol/L, 5 mL) in a screw cap vessel. The suspension was stirred under Ar for 20 min, and Pd$_2$(dba)$_3$ (73 mg, 0.08 mmol) was added to the mixture. The suspension was heated to 90 °C for 16 h. After cooling to room temperature, the suspension was poured into water (20 mL), and extracted by CH$_2$Cl$_2$ (3 × 20 mL). The combined organic layers were washed with water (3 × 10 mL), and dried over Na$_2$SO$_4$. The solvent was removed under reduced pressure and the crude product was purified by column chromatography (silica gel, EA:PE = 1:2, $R_{f=}$ 0.7) to get pure product as a colorless solid with a yield of 40% (158 mg, 0.32 mmol).

M.p.: 166 °C.

^{1}H NMR (300 MHz, CDCl$_3$) δ = 11.03 (s, 2H, -OH), 9.95 (s, 2H, 8-H), 7.67-7.39 (m, 4H), 7.11 (s, 2H, 10-H), 7.07 (d, J = 9.1 Hz, 2H, 7-H), 2.66 – 2.45 (m, 4H, 12-H), 1.52 – 1.36 (m, 4H, 13-H), 1.24 (dq, J = 14.4, 7.3 Hz, 4H, 14-H), 0.81 (t, J = 7.3 Hz, 6H, 15-H) ppm.

^{13}C NMR (100 MHz, CDCl$_3$) δ =196.56 (C-8), 160.61 (C-2), 139.26 (C-11), 138.00 (C-6), 137.89 (C-9), 133.91 (C-4), 133.61 (C-5), 131.04 (C-10), 120.31 (C-3), 117.41 (C-7), 33.62 (C-12), 32.31 (C-13), 22.57 (C-14), 13.83 (C-15) ppm.

IR(ATR): $\tilde{v}$ = 2956 (m), 2920 (m), 2858 (m), 1653 (s), 1585 (s), 1508 (w), 1470 (s), 1367 (m), 1336 (m), 1285 (s), 1252 (s), 1220 (s), 1180 (s), 1161 (s), 1129 (m), 962 (w), 904 (s), 838 (s), 813 (s), 766 (s), 742 (s), 722 (s), 699 (s), 654 (s), 633 (s), 588 (s) cm^{-1}.

MS(ESI): [M-H]⁻: *m/z* calcd. For ($C_{28}H_{29}O_4^-$): 429.54, found 429.2069.

Elemental Analysis (%): ($C_{28}H_{30}O_4$) Calcd. C 78.11, H 7.02, found C 78.14, H 7.04.

5.3.1.9 Synthesis of 2',5'-dihexyl-4,4''-dihydroxy-[1,1':4',1''-terphenyl]-3,3''-dicarbaldehyde (53):
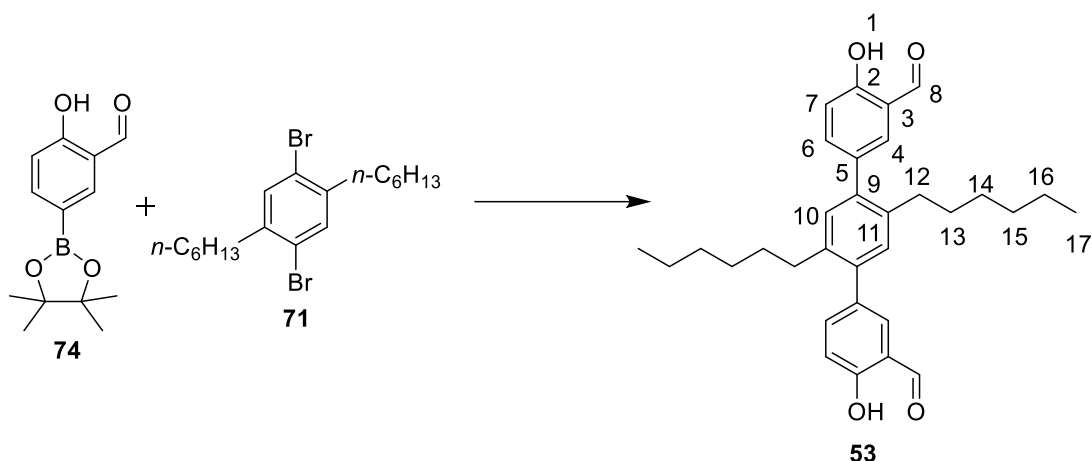
Benzaldehyde **74** (310 mg, 1.25 mmol), 1,4-dibromo-2,5-dihexylbenzene **71** (202 mg, 0.5 mmol), and [(*t*-Bu)₃PH]BF₄ (14.5 mg 0.05 mmol) were suspended into THF (5 mL) and K₂CO₃ solution (2 mol/L, 5 mL) in a screw cap vessel. The suspension was stirred under Ar for 20 min, and Pd₂(dba)₃ (45 mg, 0.05 mmol) was added to the mixture. The suspension was heated to 90 °C for 16 h. After cooling to room temperature, the suspension was poured into water (20 mL), and extracted by CH₂Cl₂ (3 × 20 mL). The combined organic layers were washed with water (3 × 10 mL), and dried over Na₂SO₄. The solvent was removed under reduced pressure and the crude product was purified by column chromatography (silica gel, EA:PE = 1:2, $R_{f=}$ 0.7) to get pure product as a colorless solid with a yield of 40% (98 mg, 0.2 mmol).

M.p.: 142 °C.

¹H NMR (300 MHz, CDCl₃): δ =10.95 (s, 2H, -OH), 9.87 (s, 2H-CHO), 7.45 (m, 4H), 7.04 (s, 2H, 4-H), 7.00 (d, 2H, *J* = 9 Hz, 10-H), 2.48 (t, 4H, *J* = 6, 12 Hz, 12-H), 1.42 – 1.45 (m, 4H, 13-H), 1.18 – 1.05 (m, 12H, 14,15,16-H), 0.8 – 0.75 (m, 6H, 17-H) ppm.

¹³C NMR (125 MHz, CDCl₃) δ = 196.90 (C-8), 160.89 (C-2), 139.53 (C-11), 138.31 (C-6), 138.26 (C-9), 134.23 (C-4), 133.89(C-5), 131.32 (C-10), 120.58 (C-3), 117.71 (C-7), 32.92 (C-12), 31.78 (C-13), 31.70 (C-14), 29.47 (C-15), 22.79 (C-16), 14.32 (C-17) ppm.

IR (ATR): $\tilde{v}$ = 3049 (w), 2953(m), 2921 (m),2852 (m),1649 (s),1586 (m), 1476 (s), 1387 (w), 1342 (w), 1316 (w), 1274 (s),1224 (s),1167 (s),1126 (s), 899 (w), 839 (m), 730 (s),668 (w),634 (w) cm^{-1}

MS (ESI): [M-H]$^-$: m/z calcd. For (C$_{32}$H$_{37}$O$_4^-$): 485.65, found 485.2703.

Elemental Analysis (%): (C$_{32}$H$_{38}$O$_4$) Calcd. C 78.98, H 7.87 found C 79.01, H 7.94.

5.3.1.10 Synthesis of 4,4''-dihydroxy-2',5'-dioctyl-[1,1':4',1''-terphenyl]-3,3''-dicarbaldehyde (54):
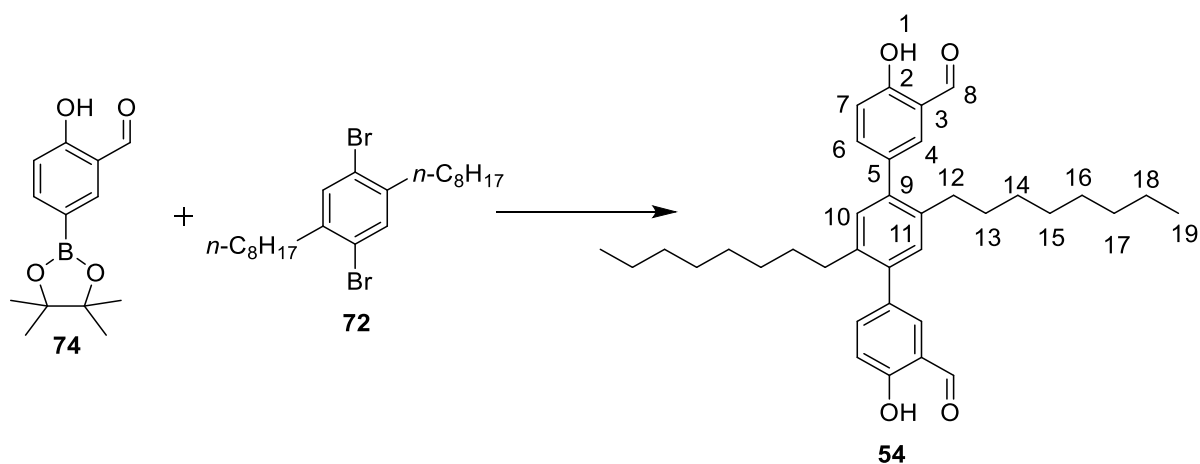
Benzaldehyde **74** (310 mg, 1.25 mmol), 1,4-dibromo-2,5-dioctylbenzene **72** (230 mg, 0.5 mmol), and [(t-Bu)$_3$PH]BF$_4$ (14.5 mg, 0.05 mmol) were suspended into THF (5 mL) and KF solution (2 mol/L, 3 mL) in a screw cap vessel. Pd$_2$(dba)$_3$ (45 mg, 0.05 mmol) was added to the solution under Ar. The suspension was heated to 90 °C for 16 h. After cooling to room temperature, the suspension was poured into water (20 mL), and extracted by CH$_2$Cl$_2$ (3 × 20 mL). The combined organic layers were washed with water (3 × 10 mL), and dried over Na$_2$SO$_4$. The solvent was removed under reduced pressure and the crude product was purified by column chromatography (silica gel, EA:PE = 1:2, R_f = 0.65) to get pure product as a colorless solid with a yield of 42% (110 mg, 0.21 mmol).

M.p.: 85 °C.

^{1}H NMR (300 MHz, CDCl$_3$): δ =10.96 (s, 2H, -OH), 9.87 (s, 2H, -CHO), 7.45 (m, 4H), 7.04 (s, 2H, 4-H), 7.00 (d, 2H, J = 9 Hz, 10-H), 2.48 (t, 4H, J = 6, 12 Hz, 12-H), 1.42 – 1.45 (m, 4H, 13-H), 1.18 – 1.05 (m, 20H, 14,15,16,17,18-H), 0.8 – 0.75 (m, 6H, 19-H) ppm

^{13}C NMR (125 MHz, CDCl$_3$) δ = 196.54 (C-8), 160.61 (C-2), 139.25 (C-11), 137.99 (C-6), 137.95 (C-9), 133.91 (C-4), 133.61 (C-5), 131.02 (C-10), 120.31 (C-3), 117.41 (C-7), 32.62

(C-12), 31.79 (C-13), 31.40 (C-14), 29.48 (C-15), 29.24 (C-16), 29.12 (C-17), 22.61 (C-18), 14.06 (C-19) ppm.

IR (ATR): $\tilde{v}$ =2960 (s), 2922 (s), 2582 (s), 1655 (s), 1587 (s), 1507 (s), 1471 (m), 1455 (s), 1410(m), 1387 (m), 1367 (s), 1311 (s)1284 (s), 1219 (s),1164 (s), 1129 (w), 908 (m), 843 (s), 794 (s), 767 (s), 740 (s) ,711 (s), 662 (s),641 (s), cm^{-1}

MS (ESI): [M-H]$^-$: m/z calcd. For ($C_{36}H_{45}O_4^-$): 541.34, found 541.3325.

Elemental Analysis (%): ($C_{36}H_{46}O_4$) Calcd. C 79.67, H8.54, found C 79.84, H 8.77.

5.3.1.11 Synthesis of 1,4-dibromo-2,5-dibutoxybenzene (80):[115a]
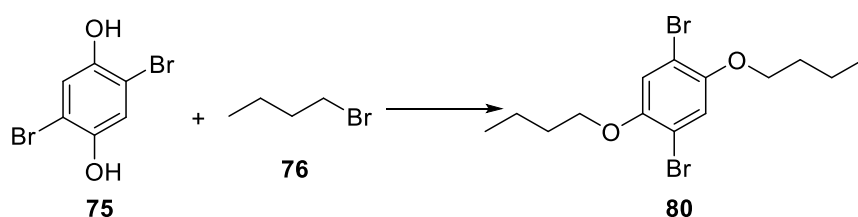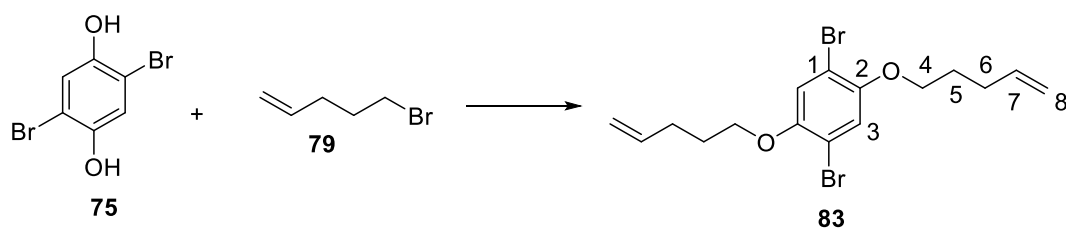

2,5-dibromohydroquinone **75** (0.5 g, 1.86 mmol) and 1-bromobutane **76** (0.74 g, 5.41 mmol) were dissolved in acetone (15 mL). K_2CO_3 (1.2 g, 8.6 mmol) was added to the reaction mixture, and resulting mixture was heated at 75 °C for 6 h. After cooling to room temperature, the solvent was removed under reduced pressure. Ethyl acetate (20 mL) and water (20 mL) were added to the remaining solid. The aqueous phase was extracted with ethyl acetate (3 × 10 mL) and the combined organic phase was dried over Na_2SO_4. The solvent was removed under reduced pressure to get the crude product as brown solid. The pure product was recrystallized from ethanol and obtained as a colourless solid a yield of 86% (0.64 g, 1.59 mmol).

M.p.: 71 °C [Lit.: 76-77 °C].[115a]

^{1}H NMR (300 MHz, CDCl$_3$) δ = 7.09 (s, 1H), 3.96 (t, J = 6.4 Hz, 2H), 1.89 – 1.69 (m, 2H), 1.52 (dq, J = 14.5, 7.3 Hz, 2H), 0.98 (t, J = 7.4 Hz, 3H).

Analytical data are in accordance with those previously reported.[115a]

5.3.1.12 Synthesis of 1,4-dibromo-2,5-bis(hexyloxy)benzene (81):[168]
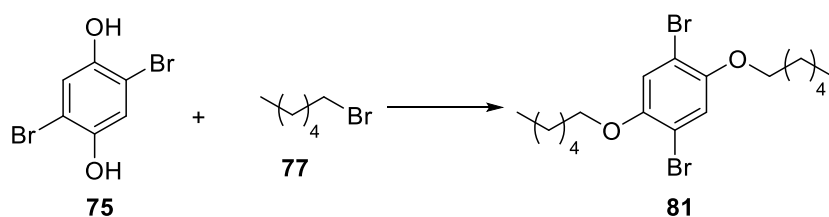
2,5-dibromohydroquinone **75** (0.5 g, 1.86 mmol) and 1-bromohexane **77** (0.89 g, 5.41 mmol) were dissolved in acetone (15 mL). K_2CO_3 (1.2 g, 8.6 mmol) was added to the reaction mixture, and resulting mixture was heated at 75 °C for 6 h. After cooling to room temperature, the solvent was removed under reduced pressure. Ethyl acetate (20 mL) and water (20 mL) were added to the remaining solid. The aqueous phase was extracted with ethyl acetate (3 × 10 mL) and the combined organic phase was dried over Na_2SO_4. The solvent was removed under reduced pressure to get the crude product as brown solid. The pure product was recrystallized from ethanol and obtained as a colourless solid a yield of 72% (0.58 g, 1.34 mmol).

M.p.: 54 °C [Lit.: 51.3-53.1 ℃].[168]

^{1}H NMR (300 MHz, $CDCl_3$) δ = 7.08 (s, 1H), 3.95 (t, J = 6.5 Hz, 2H), 1.99 – 1.65 (m, 2H), 1.49 (dd, J = 12.4, 5.2 Hz, 3H), 1.34 (td, J = 6.9, 3.4 Hz, 4H), 0.91 (t, J = 7.0 Hz, 3H) ppm.

Analytical data are in accordance with those previously reported.[169]

5.3.1.13 Synthesis of 1,4-dibromo-2,5-bis(octyloxy)benzene (82):[168]
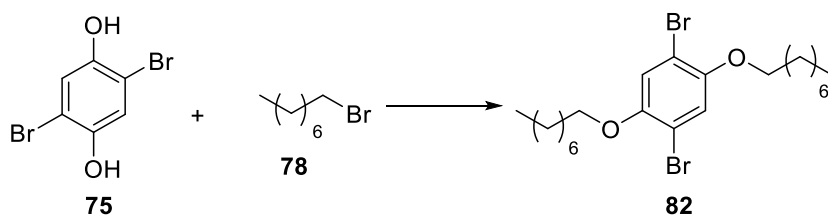
2,5-dibromohydroquinone **75** (0.5 g, 1.86 mmol) and 1-bromooctane **82** (1.04 g, 5.41 mmol) were dissolved in acetone (15 mL). K_2CO_3 (1.2 g, 8.6 mmol) was added to the reaction mixture, and resulting mixture was heated at 75 °C for 6 h. After cooling to room temperature, the solvent was removed under reduced pressure. Ethyl acetate (20 mL) and water (20 mL) were added to the remaining solid. The aqueous phase was extracted with ethyl acetate (3 × 10 mL) and the combined organic phase was dried over Na_2SO_4. The solvent was removed under reduced pressure to get the crude product as brown solid. The pure product was recrystallized from ethanol and obtained as a colourless solid a yield of 84% (0.76 g, 1.56 mmol).

M.p.: 64.7 °C [Lit.: 64-66 ℃].[168]

^{1}H NMR (300 MHz, $CDCl_3$) δ = 7.11 (s, 1H), 3.97 (t, J = 6.5 Hz, 2H), 2.05 – 1.68 (m, 2H), 1.66 – 1.43 (m, 2H), 1.32 (m, 8H), 0.92 (t, J = 6.8 Hz, 3H).

Analytical data are in accordance with those previously reported.[168]

5.3.1.14 Synthesis of 1,4-Dibromo-2,5-bis(pent-4-en-1-oxy) benzene (83):


2,5-Dibromohydroquichone **75** (2 g, 7.47 mmol) and 5-Bromopent-1-ene **79** (3.02 g, 2,64 mL, 20.3 mmol) were dissolved in DMF (40 ml). The solution was heated to 80 °C and K_3PO_4 (7.938 g, 37.4 mmol) was added, then the resulting mixture was stirred at 80 °C for 16 h. After cooling to room termperature, 40 mL water was added to the mixture and extracted with DCM (3 × 15 mL). The combined organic layers were dried over Na_2SO_4 and the solvent was removed under reduced pressure. The product was purified with short flash column chromatography (silica gel, DCM, $R_f = 0.9$) to give the product as a yellow oily liquid with a yield of 92% (2.78 g, 6.87 mmol)

^{1}H NMR (300 MHz, CDCl$_3$) $\delta = 7.09$ (s, 2H, 3-H), 5.86 (ddt, $J = 16.9, 10.1, 6.6$ Hz, 2H, 7-H), 5.13 – 4.96 (m, 4H, 4-H), 3.97 (t, $J = 6.3$ Hz, 4H, 8-H), 2.28 (dd, $J = 14.1, 7.3$ Hz, 4H, 5-H), 1.91 (dq, $J = 13.4, 6.5$ Hz, 4H, 6-H) ppm.

^{13}C NMR (101 MHz, CDCl3) $\delta = 150.55$ (C-2), 137.64 (C-7), 118.49(C-3), 115.42(C-8), 111.16 (C-1), 69.38 (C-4), 30.02 (C-5), 28.30 (C-6) ppm

IR (ATR): $\tilde{v} = 3077$ (m), 2943 (m), 2874 (m), 1741 (m), 1641 (m), 1491 (s), 1463 (s), 1391 (m), 1360 (s), 1268, (w), 1209 (s), 1062 (s), 1011 (s), 913 (s), 851 (s), 815 (s), 748 (s), 638 (s) cm^{-1}

Elemental Analysis (%): ($C_{26}H_{20}O_2Br_2$) Calcd. C 47.55, H 4.99, found C 47.83, H 5.03.

5.3.1.15 Synthesis of 2',5'-bis(butyloxy)-4,4''-dihydroxy-[1,1':4',1''-terphenyl]-3,3''-dicarbaldehyde (55):
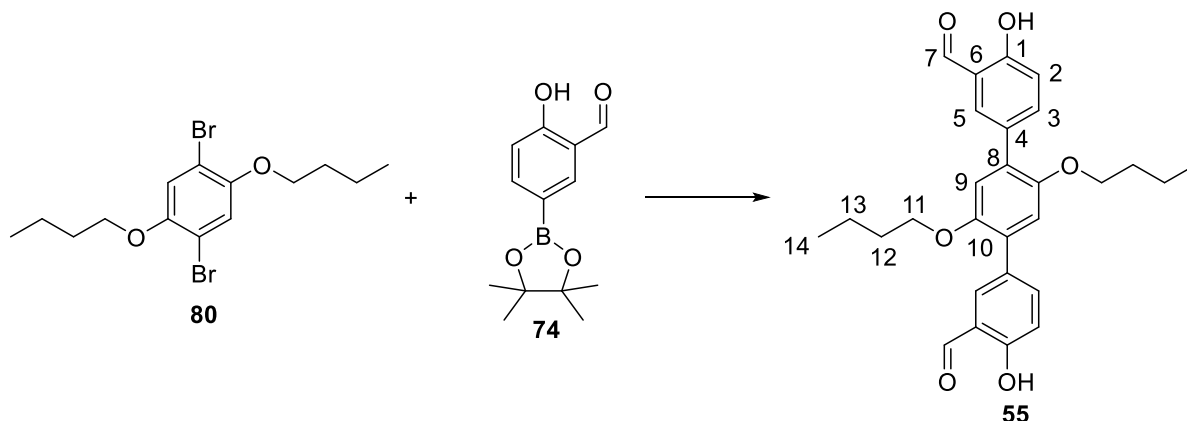
1,4-dibromo-2,5-bis(butyloxy)benzene **80** (350 mg, 0.86 mmol), benzaldehyde **74** (537 mg, 2.16 mmol), and [(*t*-Bu)$_3$PH]BF$_4$) (49.9 mg, 0.16 mmol) were suspended in THF (10 mL) and K$_2$CO$_3$ solution (2 mol/L, 4 mL) in a screw cap vessel. Pd$_2$(dba)$_3$ (78.75 mg, 0.08 mmol) was added to the reaction mixture under Ar, and the resulting mixture was heated to 90 °C for 16 h. After cooling to room temperature, the suspension was poured into water (20 mL) and extracted with CH$_2$Cl$_2$ (3 × 10 mL). The combined organic layers were washed with water (3 × 10 mL), and dried over Na$_2$SO$_4$. The solvent was removed under reduced pressure and the crude product was purified by column chromatography (silica gel, DCM:PE = 1:1, R_f = 0.65) to the get pure product as a yellow solid with a yield of 68% (275 mg, 0.58 mmol).

M.p.: 158 °C.

^{1}H NMR (300 MHz, CDCl$_3$) δ = 11.03 (s, 2H, -OH), 9.95 (s, 2H, 7-H), 7.82 (d, J = 1.9 Hz, 2H, 5-H), 7.78 (dd, J = 8.5, 2.3 Hz, 2H, 3-H), 7.06 (d, J = 8.5 Hz, 2H, 2-H), 6.96 (s, 2H, 9-H), 3.95 (t, J = 6.4 Hz, 4H, 11-H), 1.83 – 1.59 (m, 4H, 12-H), 1.40 (dq, J = 14.4, 7.3 Hz, 4H, 13-H), 0.91 (t, J = 7.4 Hz, 6H, 14-H) ppm.

^{13}C NMR (100 MHz, CDCl$_3$) δ = 196.64 (C-7), 160.72 (C-1), 150.30 (C-10), 138.27 (C-3), 134.49 (C-5), 130.11 (C-8), 129.01 (C-4), 120.36 (C-6), 117.25 (C-2), 115.50 (C-9), 69.29 (C-11), 31.43 (C-12), 19.32 (C-13), 13.75 (C-14) ppm.

IR (ATR): $\tilde{\nu}$ = 2969 (w), 2940 (w), 2855 (w), 1659 (s), 1591 (m), 1516 (m), 1468 (s), 1420 (s), 1390 (m), 1372 (s), 1338 (s), 1293 (s), 1271, (s), 1250 (m), 1227 (s), 1206 (s), 1165 (s), 1128 (s), 1051 (s), 1014 (m), 924 (m), 890 (m), 857 (m), 839 (m), 819 (m), 773 (s), 738 (s), 710 (s), 680 (s), 641 (m), 576 (m) cm^{-1}.

MS (ESI): [M-H]$^-$: m/z calcd. For ($C_{28}H_{29}O_6^-$): 461.54, found 461.2351.

Elemental Analysis (%): ($C_{28}H_{30}O_6$) Calcd. C 72.71, H 6.54, found C 72.20, H 6.44.

5.3.1.16 Synthesis of 2',5'-bis(hexyloxy)-4,4''-dihydroxy-[1,1':4',1''-terphenyl]-3,3''-dicarbaldehyde (56):
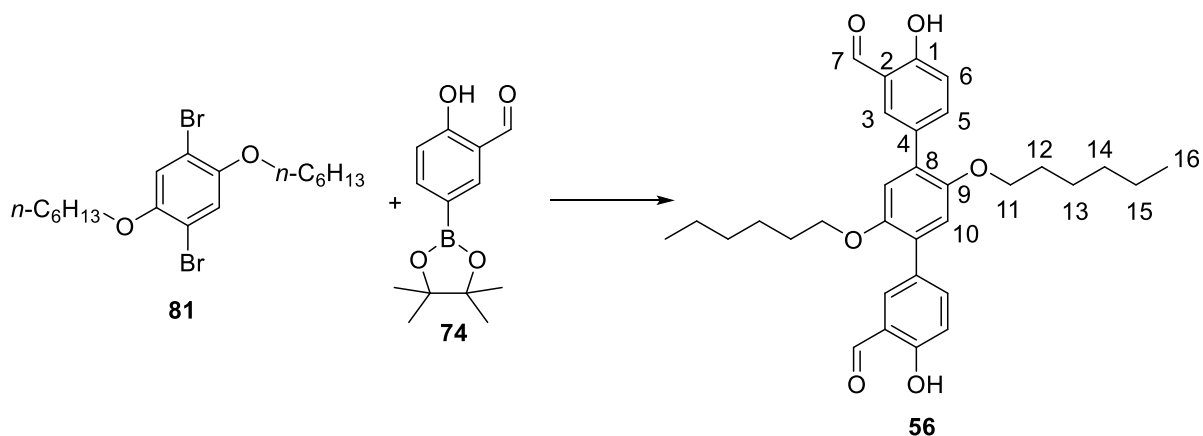
1,4-dibromo-2,5-bis(hexyloxy)benzene **81** (200 mg, 0.49 mmol), benzaldehyde **74** (286 mg, 1.15 mmol), and [(t-Bu)$_3$PH]BF$_4$ (33.4 mg, 0.11 mmol) were suspended in THF (10 mL) and K$_2$CO$_3$ solution (2 mol/L, 4 mL) in a screw cap vessel. Pd$_2$(dba)$_3$ (55 mg, 0.049 mmol) was added to the reaction mixture under Ar, and the resulting mixture was heated to 90 °C for 16 h. After cooling to room temperature, the suspension was poured into water (20 mL) and extracted with CH$_2$Cl$_2$ (3 × 10 mL). The combined organic layers were washed with water (3 × 10 mL), and dried over Na$_2$SO$_4$. The solvent was removed under reduced pressure and the crude product was purified by column chromatography (silica gel, DCM:PE = 1:1, R_f = 0.65) to the get pure product as a yellow solid with a yield of 46 % (120 mg, 0.23 mmol).

M.p.: 129 °C.

^{1}H NMR (400 MHz, CDCl$_3$) δ = 11.03 (s, 2H, -OH), 9.95 (s, 2H, 7-H), 7.81 (d, J = 2.1 Hz, 2H, 3-H), 7.78 (dd, J = 8.6, 2.2 Hz, 2H,5-H), 7.05 (d, J = 8.6 Hz, 2H, 6-H), 6.96 (s, 2H, 10-H), 3.94 (t, J = 6.4 Hz, 4H, 11-H), 1.69 (dq, J = 12.8, 6.5 Hz, 4H, 12-H), 1.46 – 1.32 (m, 4H, 13-H), 1.36 – 1.11 (m, 8H, 14,15-H), 0.86 (t, J = 6.9 Hz, 6H, 16-H) ppm.

^{13}C NMR (100 MHz, CDCl$_3$) δ = 196.62 (C-7), 160.73 (C-1), 150.30 (C-9), 138.09 (C-5), 134.50 (C-3), 130.12 (C-8), 129.03 (C-4), 120.35 (C-2), 117.24 (C-6), 115.52 (C-10), 69.65 (C-11), 31.44 (C-12), 29.33 (C-13), 25.84 (C-14), 22.58 (C-15), 13.96 (C-16) ppm.

IR (ATR): $\tilde{v}$ = 3056 (s), 2932 (m), 2868(m), 1662 (s), 1593(w), 1513(m), 1475 (s), 1417 (s), 1389 (m),)1271(s),1207(s),1163(s),1126 (s), 1056 (s), 1031 (s), 996 (m), 919 (m), 896 (m), 855 (m), 822 (m),771 (m),718 (s), 643 (m), cm^{-1}

MS (ESI): [M-H]$^-$: m/z calcd. For (C$_{32}$H$_{38}$O$_6^-$): 517.65, found 517.2596.

Elemental Analysis (%): (C$_{32}$H$_{38}$O$_6$) Calcd. C 74.11, H 7.39, found C 74.32, H 7.38.

5.3.1.17 Synthesis of 2',5'-bis(octyloxy)-4,4''-dihydroxy-[1,1':4',1''-terphenyl]-3,3''-dicarbaldehyde (57):
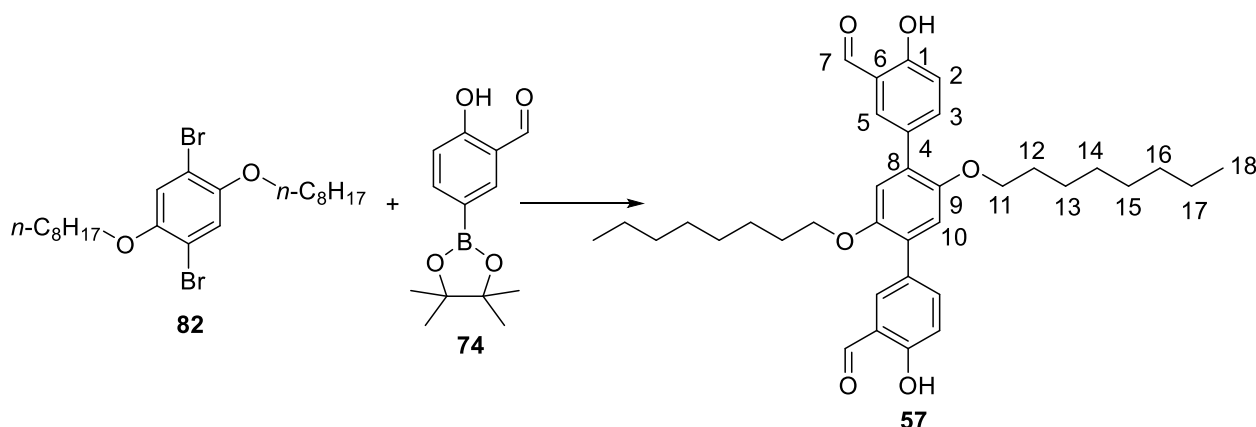
1,4-dibromo-2,5-bis(octyloxy)benzene **82** (200 mg, 0.406 mmol), benzaldehyde **74** (251 mg, 1.01 mmol), and [(*t*-Bu)$_3$PH]BF$_4$) (37.1 mg, 0.12 mmol) were suspended in THF (5 mL) and K$_2$CO$_3$ solution (2 mol/L, 2 mL) in screw cap vessel. Pd$_2$(dba)$_3$(37 mg, 0.041 mmol) was added to the reaction mixture under Ar, and the resulting mixture was heated to 90 °C for 16 h. After cooling to room temperature, the suspension was poured into water (20 mL) and extracted with CH$_2$Cl$_2$ (3 × 10 mL). The combined organic layers were washed with water (3 × 10 mL), and dried over Na$_2$SO$_4$. The solvent was removed under reduced pressure and the crude product was purified by column chromatography (silica gel, DCM:PE = 1:1, R_f = 0.6) to the get pure product as a yellow solid with a yield of 60 % (140 mg, 0.24 mmol).

M.p.: 115°C

^{1}H NMR (400 MHz, CDCl$_3$) δ = 11.03 (s, 2H, -OH), 9.95 (s, 2H, 7-H), 7.81 (d, J = 2.1 Hz, 2H, 5-H), 7.78 (dd, J = 8.6, 2.2 Hz, 2H, 3-H), 7.05 (d, J = 8.6 Hz, 2H, 2-H), 6.96 (s, 2H, 10-H), 3.94 (t, J = 6.4 Hz, 4H, 11-H), 1.75 – 1.64 (m, 4H, 12-H), 1.35 (m, 4H, 13-H), 1.26 (m, 16H, 14,15,16,17-H), 0.87 (t, J = 7.0 Hz, 6H, 18-H) ppm.

^{13}C NMR (100 MHz, CDCl$_3$) δ = 196.62 (C-7), 160.73 (C-1), 150.30 (C-9), 138.29 (C-5), 134.50 (C-3), 130.11 (C-8), 129.04 (C-4), 120.36 (C-2), 117.24 (C-6), 115.53 (C-10), 69.66 (C-11), 31.76 (C-12), 29.36 (C-13), 29.23 (C-14), 26.17 (C-15), 22.62 (C-16), 18.44 (C-17), 14.06 (C-18) ppm.

IR (ATR): $\tilde{v}$ =3060 (w), 2929 (s), 2852 (s), 1662 (s), 1624 (m), 1593 (m), 1514 (s), 1473 (s), 1416 (m), 1390 (s), 1368 (s), 1293 (s), 1271 (s), 1207 (s), 1163 (s), 1126 (s), 1057 (s), 1036 (s), 1004 (s), 919 (m), 895 (m), 855 (m), 821 (s), 771 (s), 709 (s), 680 (s), 643 (s), 579 (s) cm^{-1}.

MS (ESI): [M-H]$^-$: m/z Calcd. For (C$_{36}$H$_{45}$O$_6^-$): 573.75, found 573.3222.

Elemental Analysis (%): (C$_{36}$H$_{46}$O$_6$) Calcd. C 75.23, H 8.07, found C 75.23, H 8.07.

5.3.1.18 Synthesis of 4,4''-dihydroxy-2',5'-bis(pent-4-en-1-yloxy)-[1,1':4',1''-terphenyl]-3,3''-dicarbaldehyde (58):
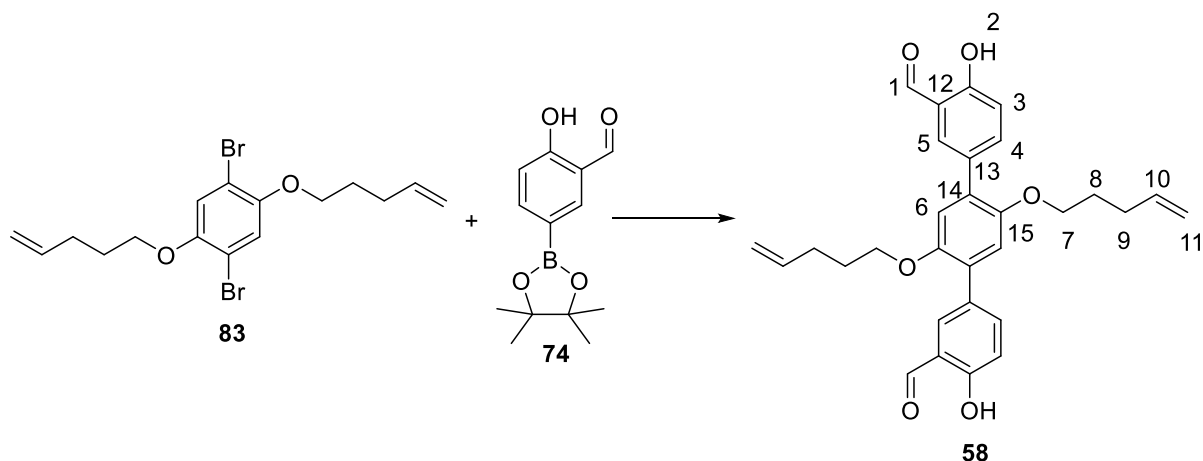
1,4-Dibromo-2,5-bis(pent-4-en-1-oxy) benzene **83** (121 mg, 0.325 mmol), benzaldehyde **74** (220 mg, 0.81 mmol) and [(t-Bu)$_3$PH]BF$_4$) (30 mg, 0.1 mmol) were suspended THF (3 mL) and K$_2$CO$_3$ solution (2 mol/L, 1 mL) in a screw cap vessel. Pd$_2$(dba)$_3$ (23 mg, 0.02 mmol) was added to the reaction mixture under Ar, and the resulting mixture was heated to 90 °C for 16 h. After cooling to room temperature, the suspension was poured into water (10 mL) and extracted with CH$_2$Cl$_2$ (3 × 10 mL). The combined organic layers were washed with water (3 × 10 mL), and dried over Na$_2$SO$_4$. The solvent was removed under reduced pressure and the crude product was purified by column chromatography (silica gel, DCM:PE = 1:1, R_f = 0.6) to the get pure product as a yellow solid with a yield of 20 % (32 mg, 0.06 mmol).

M.p.: 120 °C.

^{1}H NMR (300 MHz, CDCl$_3$) δ = 11.04 (s, 2H, 2-H), 9.96 (s, 2H, 1-H), 7.79 (t, J = 5.5 Hz, 4H, 3,5-H), 7.06 (d, J = 8.3 Hz, 2H, 6-H), 6.96 (s, 2H, 4-H), 5.77 (ddt, J = 16.9, 10.3, 6.6 Hz, 2H, 10-H), 5.02 – 4.91 (m, 4H, 11-H), 3.96 (t, J = 6.3 Hz, 4H, 7-H), 2.13 (dd, J = 14.7, 6.8 Hz, 4H, 8-H), 1.86 – 1.74 (m, 4H, 9-H) ppm.

^{13}C NMR (125 MHz, CDCl$_3$) δ = 196.67 (C-1), 160.75 (C-2), 150.19 (C-15), 138.30 (C-14), 137.58 (C-10), 134.46 (C-4), 130.04 (C-5), 129.03 (C-12), 120.35 (C-3), 117.24 (C-11), 115.39 (C-6), 68.74 (C-7), 30.20 (C-9), 28.58 (C-8) ppm.

IR (ATR): $\tilde{v}$ = 3065(w), 2967 (w), 1455 (s), 1191 (w), 1161 (w), 1021 (w), 944 (w), 858 (w), 795 (m), 737 (s), 623 (s) cm^{-1}.

MS (ESI): [M+H]$^+$: m/z calcd. For (C$_{30}$H$_{31}$O$_6^+$): 487.56, found 487.2113.

Elemental Analysis (%): (C$_{30}$H$_{30}$O$_6$) Calcd. C 74.06, H 6.22, found C 74.21, H 6.01.

5.3.1.19 Synthesis of 4,4''-dihydroxy-2',5'-bis(((E)-pent-3-en-1-yl) oxy) -[1,1':4',1''-terphenyl] -3,3''-dicarbaldehyde (58'):
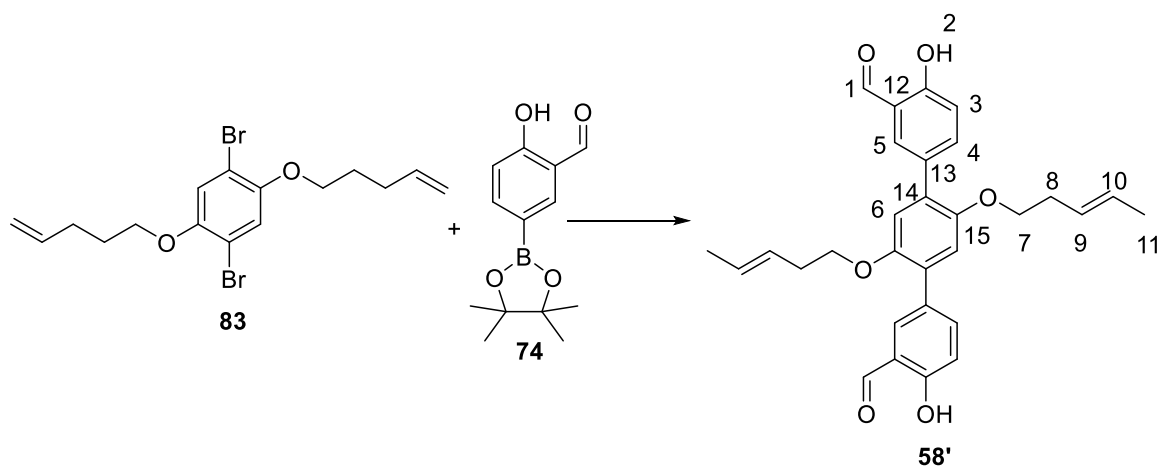
1,4-Dibromo-2,5-bis(pent-4-en-1-oxy) benzene **83** (402 mg, 0.975 mmol), benzaldehyde **74** (660 mg, 2.88 mmol) and [(t-Bu)$_3$PH]BF$_4$) (58 mg, 0.2 mmol) suspended THF (8 mL) and K$_2$CO$_3$ solution (2 mol/L, 3 mL) in a screw cap vessel. Pd$_2$(dba)$_3$ (90 mg, 0.0975 mmol) was added to the reaction mixture under Ar, and the resulting mixture was heated to 90 °C for 16 h. After cooling to room temperature, the suspension was poured into water (10 mL) and extracted with CH$_2$Cl$_2$ (3 × 10 mL). The combined organic layers were washed with water (3 × 10 mL), and dried over Na$_2$SO$_4$. The solvent was removed under reduced pressure and the crude product was purified by column chromatography (silica gel, DCM:PE = 1:1, R_f = 0.6) to the get pure product as a yellow solid with a yield of 70 % (343 mg, 0.68 mmol).

M.p.: 143 °C

^{1}H NMR (300 MHz, DMSO-d_6): δ = 10.79 (s, 2H, 2-H), 10.33 (s, 2H, 1-H), 7.92 (d, J = 2.3 Hz, 2H, 5-H), 7.78 (dd, J = 8.6, 2.4 Hz, 2H, 3-H), 7.06 (d, J = 10.0 Hz, 4H, 4,6-H), 5.46 (dd, J = 6.9, 4.0 Hz, 4H, 9,10-H), 3.99 (dd, J = 8.2, 4.6 Hz, 4H, 7-H), 2.43 – 2.26 (m, 4H, 8-H), 1.61 (d, J = 4.5 Hz, 6H, 11-H).

^{13}C NMR (101 MHz, CDCl3): δ = 196.65 (C-1), 160.75 (C-2), 150.21 (C-15), 138.37 (C-14), 134.53 (C-4), 129.98 (C-5), 129.00 (C-12), 127.74 (C-13), 126.96 (C-9), 120.36 (C-10), 117.19 (C-3), 115.55 (C-6), 69.42 (C-7), 32.70 (C-8), 18.02 (C-11).

IR (ATR): $\tilde{v}$ = 2935(w), 2852 (w), 1660 (s), 1590 (w), 15131 (m), 1473 (m), 1438 (w), 1386 (m), 1341 (w), 1268 (s), 1206 (s), 1167 (m), 1054 (m), 1029 (s), 968 (s), 922 (w), 903 (w), 872 (w), 826 (w), 806 (w), 769 (w), 747 (s), 715 (s), 683 (w), 645 (m) cm^{-1}.

MS (ESI): [M+H] $^+$: m/z calcd. For ($C_{30}H_{31}O_6^+$): 487.56, found 487.2114.

5.3.1.20 Synthesis of 2-methoxyethyl p-toluenesulfonate (87):[116a]
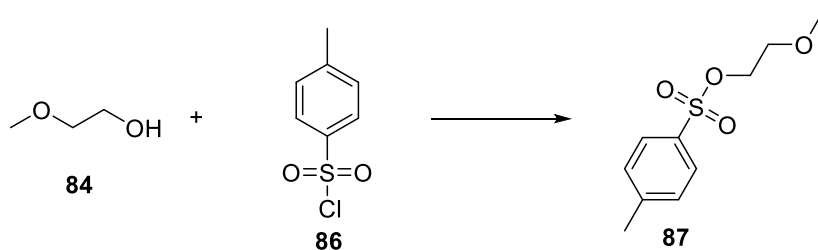
2-methoxyethanol **84** (20.8 g ,173 mmol) and NaOH (10.0 g, 250 mmol) were dissolved in water (50 mL) in a 1 L flask. *p*-toluene sulfonyl chloride **86** (36.2 g, 190 mmol) in THF (50 mL) was added to the above solution in an ice bath. The mixture was stirred at room temperature for 12 h. The resulting mixture was mixed with ice water and extracted with CH$_2$Cl$_2$ (3 × 100 mL). The combined organic layers were washed with hydrochloric acid (1 M, 2 × 250 mL) and brine followed by drying over Na$_2$SO$_4$. After the solvent was removed under reduced pressure, the product was obtained as a yellowish oil with a yield of 68 %(24.8g, 117 mmol).

^{1}H NMR (300 MHz, CDCl$_3$) δ = 7.80 (d, J = 8.3 Hz, 2H), 7.34 (d, J = 8.0 Hz, 2H), 4.21 – 4.11 (m, 2H), 3.63– 3.52 (m, 2H), 3.31 (s, 3H), 2.44 (s, 3H) ppm.

Analytical data are in accordance with those previously reported.[116a]

5.3.1.21 Synthesis of 1-(((2-(2-methoxyethoxy) ethoxy) methyl) sulfonyl)-4-methylbenzene (88):[116a]
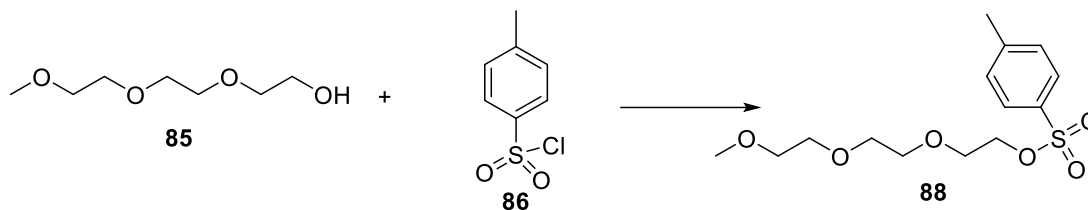
Triethylene glycol monomethyl ether **85** (8.21 g, 50 mmol), sodium hydroxide (7.00 g, 175 mmol), THF (35 mL), and water (35 mL) were placed in a three-necked flask and stirred at 0 ˚C. A THF solution (50 mL) of *p*-toluene sulfonyl chloride **86** (11.4 g, 60 mmol) was added dropwise to the mixture in 30 min. The reaction mixture was stirred at 0 ˚C for 2 h, and then at room temperature for 12 h. The reaction mixture was poured into aqueous hydrochloric acid (150 mL, 5wt%) and extracted with chloroform (3 × 30 mL). The combined organic layers were dried over NaSO$_4$. The solvent was removed under reduced pressure and the crude product was obtained as a pale brown liquid with quantitative yield (15.9, 50 mmol) and used for subsequent synthesis without purification.

^{1}H NMR (300 MHz, CDCl$_3$) δ = 7.80 (d, J = 8.3 Hz, 2H), 7.34 (d, J = 8.0 Hz, 2H), 4.19 – 4.13 (m, 2H), 3.73 – 3.65 (m, 6H), 3.65 – 3.48 (m, 2H), 3.37 (s, 3H), 2.45 (s, 3H) ppm.

Analytical data are in accordance with those previously reported.[116b]

5.3.1.22 Synthesis of 1,4-dibromo-2,5-bis(2-methoxyethoxy) benzene (89):[116a]
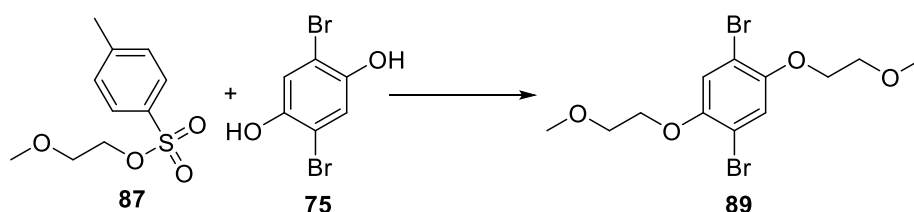
Under argon atmosphere, 2-methoxyethyl *p*-toluenesulfonate **87** (10.0 g, 43.3 mmol) in DMF (20 mL) was added dropwise to a mixture of 2,5-dibromo-1,4-benzenediol **75** (4.7 g, 17.3 mmol) and K$_2$CO$_3$ (13.5 g) in DMF (150 ml) at 0 °C. After 15 minutes the reaction mixture was heated to 80 °C for 6 h. The mixture was cooled to room temperature and quenched with water (50 mL). The organic phase was washed with water until the pH = 7 and dried over Na$_2$SO$_4$. The solvent was removed under reduced pressure and after recrystallization from ethanol, the product was obtained as a colourless solid with a yield of 84 % (5.6 g, 14.5 mmol).

M.p.: 102.7 °C.

^{1}H NMR (300 MHz, CDCl$_3$) δ = 7.15 (s, 2H), 4.21 – 3.94 (m, 4H), 3.89 – 3.63 (m, 4H), 3.47 (s, 6H) ppm.

Analytical data are in accordance with those previously reported.[116a]

### 5.3.1.23 Synthesis of 1,4-dibromo-2,5-bis((2-(2-methoxyethoxy) ethoxy) methyl) benzene (90):[116a]
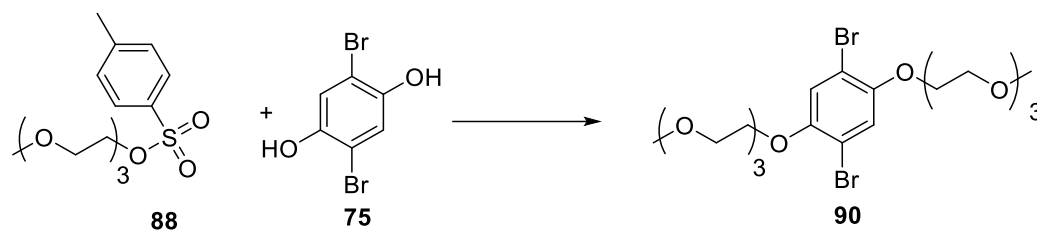
Under argon atmosphere tetraethylene glycol methyl p-tosyl ether **88** (16.6 g, 44.5 mmol) in dry DMF (20 mL) was added dropwise to a mixture of 2,5-dibromo-1,4-benzenediol **75** (5.3 g, 19.6 mmol) and K$_2$CO$_3$ (13.5 g) in dry DMF (150 ml) at 0 °C. After 15 minutes the reaction mixture was heated to 70 °C for 6 h. Water (50 mL) was added to the reaction mixture and was extracted with chloroform (3 × 40 mL). The collected organic phase was washed with water until the pH = 7 and dried over Na$_2$SO$_4$. The solvent was removed under reduced pressure and the product was obtained after recrystallization from ethanol (cooled in liquid nitrogen) as an off-white solid with a yield of 65 % (7.1 g, 12.7 mmol).

^{1}H NMR (300 MHz, CDCl$_3$) δ = 7.14 (s, 1H), 4.11 (t, J = 4.7 Hz, 2H), 3.86 (t, J = 4.8 Hz, 2H), 3.77 (m, 2H), 3.66 (m, 2H), 3.58 – 3.47 (m, 2H), 3.37 (s, 3H) ppm.

Analytical data are in accordance with those previously reported[116a].

5.3.1.24 Synthesis of 4,4''-dihydroxy-2',5'-bis(2-methoxyethoxy)-[1,1':4',1''-terphenyl]-3,3''-dicarbaldehyde (60):
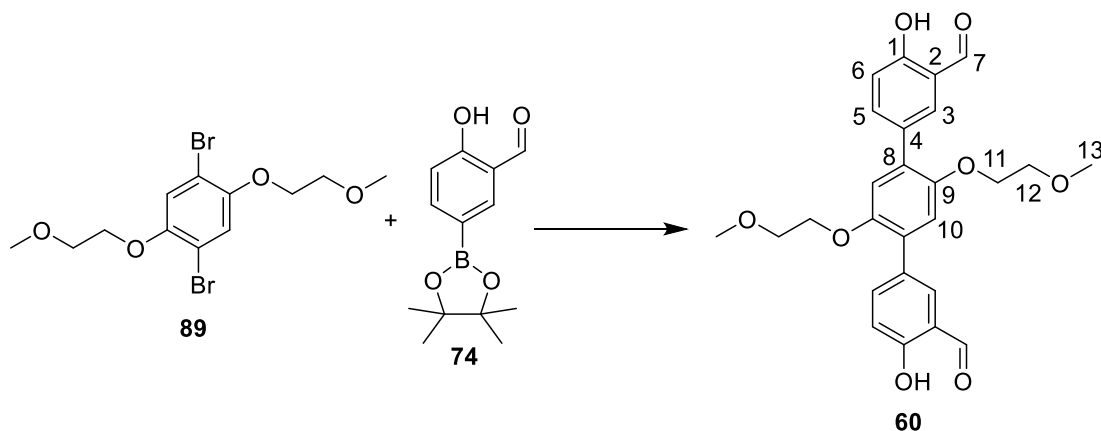
1,4-dibromo-2,5-bis(2-methoxyethoxy) benzene **89** (300 mg, 0.35 mmol), benzaldehyde **74** (221mg, 0.89 mmol), were suspended in THF (4 mL) and K_2CO_3 solution (2 mol/L, 2 mL) in a screw cap vessel. $Pd_2(dba)_3$ (143 mg, 0.15 mmol) and [(t-Bu)$_3$PH]BF$_4$) (91 mg, 0.31 mmol) $Pd_2(dba)_3$ (90 mg, 0.0975 mmol) was added to the reaction mixture under Ar, and the resulting mixture was heated to 90 °C for 16 h. After cooling to room temperature, the suspension was pouring into water (20 mL) and extracted with CH_2Cl_2 (3 × 10 mL). The combined organic layers and washed with water (3 × 10 mL), and dried over Na_2SO_4. The solvent was removed under reduced pressure and the crude product was purified by column chromatography (silica gel, DCM to DCM: MeOH = 50:1, R_f = 0.1) to give the product a yellow solid with a yield of 62% (230 mg, 0.22 mmol).

M.p.: 169 °C.

^{1}H NMR (500 MHz, CDCl$_3$) δ = 10.97 (s, 2H, -OH), 9.89 (s, 2H, 7-H), 7.84 (d, J = 2.1 Hz, 2H, 3-H), 7.74 (dd, J = 8.6, 2.1 Hz, 2H, 5-H), 6.99 (d, J = 8.6 Hz, 2H, 6-H), 6.94 (s, 2H, 10-H), 4.13 – 3.89 (m, 4H, 11-H), 3.75 – 3.49 (m, 4H, 12-H), 3.31 (s, 6H, 13-H) ppm.

^{13}C NMR (100 MHz, CDCl$_3$) δ = 196.76 (C-7), 160.79 (C-1), 150.49 (C-9), 138.14 (C-5), 134.77 (C-3), 129.68 (C-8), 129.35 (C-4), 120.43 (C-2), 117.31 (C-6), 116.24 (C-10), 71.16 (C-11), 69.30 (C-12, 59.12 (C-13) ppm.

IR(ATR): $\tilde{v}$ = 2956 (m), 2920 (s), 2858 (s), 1653 (s), 1585 (s), 1508 (w), 1470 (s), 1367 (m), 1336 (m), 1285 (s), 1252 (s), 1220 (s), 1180 (s), 1161 (s), 1130 (s), 962 (w), 904 (s), 838 (s), 813 (s), 766 (s), 742 (s), 722 (s), 699 (s), 654 (s), 633 (s), 587 (s) cm^{-1}.

MS (ESI): [M-H]$^-$: m/z calcd. For (C$_{26}$H$_{25}$O$_8^-$): 466.15, found 465.1554.

Elemental Analysis (%): (C$_{26}$H$_{26}$O$_8$·$\frac{1}{3}$H$_2$O) Calcd. C 66.09, H 5.69, found C 66.22, H 5.94.

5.3.1.25 Synthesis of 4,4''-dihydroxy-2',5'-bis(2-(2-(2-methoxyethoxy) ethoxy) ethoxy)-[1,1':4',1''-terphenyl]-3,3''-dicarbaldehyde (61):
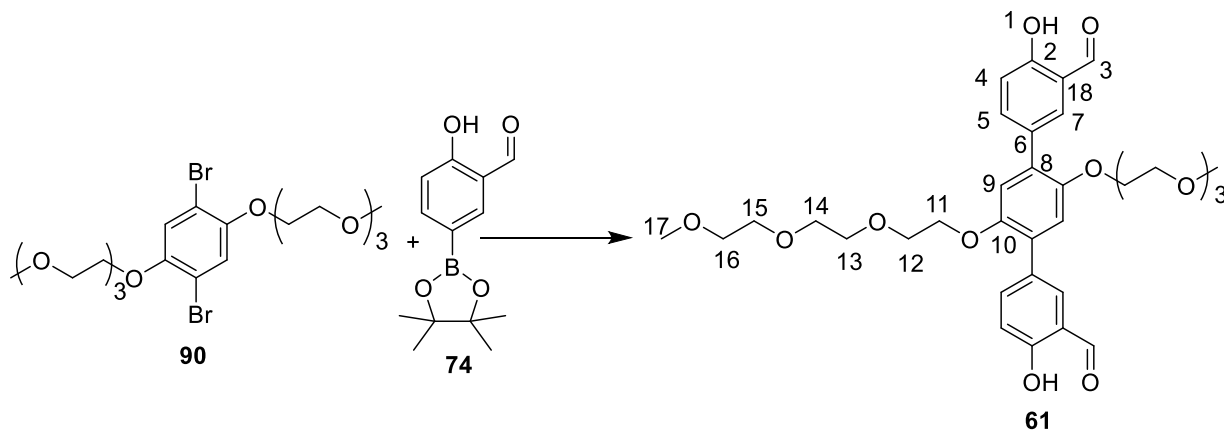
1,4-dibromo-2,5-bis((2-(2-methoxyethoxy) ethoxy) methyl) benzene **90** (200 mg, 0.35 mmol), benzaldehyde **74** (221mg, 0.89 mmol) were suspended in THF (5 mL) and K$_2$CO$_3$ solution (2 mol/L, 2 mL) in a screw cap vessel. Pd$_2$(dba)$_3$(32 mg, 0.035 mmol) and [(*t*-Bu)$_3$PH]BF$_4$ (20.71 mg, 0.07 mmol) was added to the reaction mixture under Ar, and the resulting mixture was heated to 90 °C for 16 h. After cooling to room temperature, the suspension was pouring into water (20 mL) and extracted with CH$_2$Cl$_2$ (3 × 10 mL). The combined organic layers and washed with water (3 × 10 mL), and dried over Na$_2$SO$_4$. The solvent was removed under reduced pressure and the crude product was purified by column chromatography (silica gel, DCM to DCM: MeOH = 50:1, R_f= 0.1) to give the product as yellow solid with a yield of 72% (120 mg, 0.25 mmol).

M.p.: 77.6 °C.

^{1}H NMR (400 MHz, CDCl$_3$) δ = 11.06 (s, 2H, -OH), 9.97 (s, 2H, 3-H), 7.88 (d, J = 2.2 Hz, 2H, 7-H), 7.82 (dd, J = 8.6, 2.2 Hz, 2H, 5-H), 7.05 (d, J = 8.6 Hz, 2H, 4-H), 6.99 (s, 2H, 9-H), 4.18 – 4.04 (m, 4H, 11-H), 3.83 – 3.70 (m, 4H, 12-H), 3.68 – 3.55 (m, 12H,13,14,15-H), 3.56 – 3.48 (m, 4H, 16-H), 3.34 (s, 6H, 17-H) ppm.

^{13}C NMR (100 MHz, CDCl$_3$) δ = 196.94 (C-3), 160.77 (C-2), 150.34 (C-10), 138.25 (C-5), 134.65 (C-7), 129.77 (C-6), 129.18 (C-8), 120.44 (C-18), 117.28 (C-4), 115.92 (C-9), 71.91 (C-11), 70.76 (C-12), 70.69 (C-13), 70.56 (C-14), 69.78 (C-15), 69.18 (C-16), 58.98 (C-17) ppm.

IR (ATR): $\tilde{v}$ = 2873(s), 2817 (m), 1650 (s), 1617 (s), 1594 (m), 1513 (s), 1480 (s), 1450 (s), 1401 (s), 1359 (s), 1321 (w), 1287 (s), 1267 (s), 1212 (s), 1168 (m), 1123 (s), 1053 (s), 943 (s), 892 (s), 828 (s), 800 (w), 759 (s), 713 (s), 683 (s), 642 (s), 563 (s) cm^{-1}.

MS (ESI): [M-H]$^-$: m/z calcd. For ($C_{34}H_{41}O_{12}{}^-$): 641.69, found 641.2601.

Elemental Analysis (%): ($C_{34}H_{42}O_{12}$) Calcd. C 63.54, H 6.59, found C 63.25, H 6.69.

5.3.1.26 Synthesis of 1,4-bis(perfluorobutyl)benzene (92):[117]
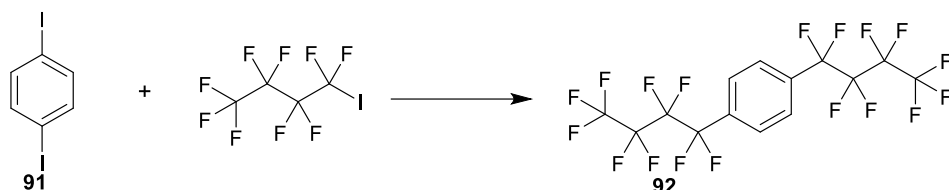
Nonafluoro-1-iodobutane (2.43 g, 7.04 mmol) was added to a mixture of 1,4-diiodobenzene **91** (1.05g, 3.2 mmol) and Cu powder (0.82 g, 12.8 mmol) in anhydrous DMSO (35 mL). The mixture was stirred for 70 h at 120 °C. After cooling to room termperature, water (20 mL) and diethyl ether (20 mL) were added to the mixture and stirred for 30 min. The mixture was filtered, and the filtrate was extracted with diethyl ether (3 × 10 mL). The combined organic layers were washed with brine (2 × 5 mL), dried over Na$_2$SO$_4$, and concentrated under reduced pressure. The resulting residue was used for the next step without further purification with a yield of 71 % (1.5 g, 5 mmol) as transparent liquid.

^{1}H NMR (500 MHz, CDCl$_3$) δ = 7.76 (s, 4H) ppm.

^{19}F NMR (471 MHz, CDCl$_3$) δ = -80.98 (s), -111.53 (s), -122.65 (s), -125.58 (s) ppm.

Analytical data are in accordance with those previously reported.[117]

5.3.1.27 Synthesis of 1,4-dibromo-2,5-bis(perfluorobutyl)benzene (93):[117]
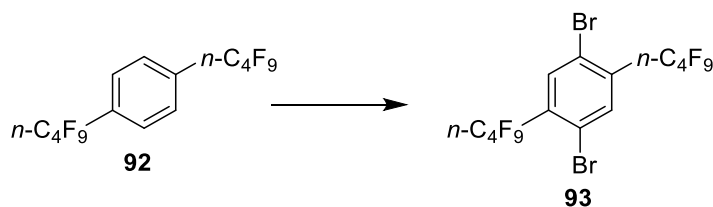
1,4-bis(perfluorobutyl)benzene **92** (13.6 g, 26.4 mmol) was added to a mixture of trifluoroacetic acid (100 mL) and concentrated sulfuric acid (30 mL). The mixture was heated to 60 °C, and *N*-bromosuccinimide (14.3 g, 79.5 mmol) was added in portions (2.39 g/h) over

6 h. The mixture was stirred for 48 h at 60 °C, then ice water (50 mL) was added to the reaction mixture and the aqueous phase was extracted with DCM (3 × 30 mL). The organic phases were combined and dried over Na_2SO_4, and concentrated *in vacuo*. The resulting residue was recrystallized from ethanol to give the product as a colourless crystal in a 77% yield (13.6 g, 20.4 mmol).

M.p.: 56 °C.

^{1}H NMR (300 MHz, $CDCl_3$) δ = 7.94 (s, 2H) ppm.

^{19}F NMR (283 MHz, $CDCl_3$) δ = -80.86, -107.86, -120.24, -125.77 ppm.

Analytical data are in accordance with those previously reported.[117]

5.3.1.28 Synthesis of 4,4''-dihydroxy-2',5'-bis(perfluorobutyl)-[1,1':4',1''-terphenyl]-3,3''-dicarbaldehyde (59):
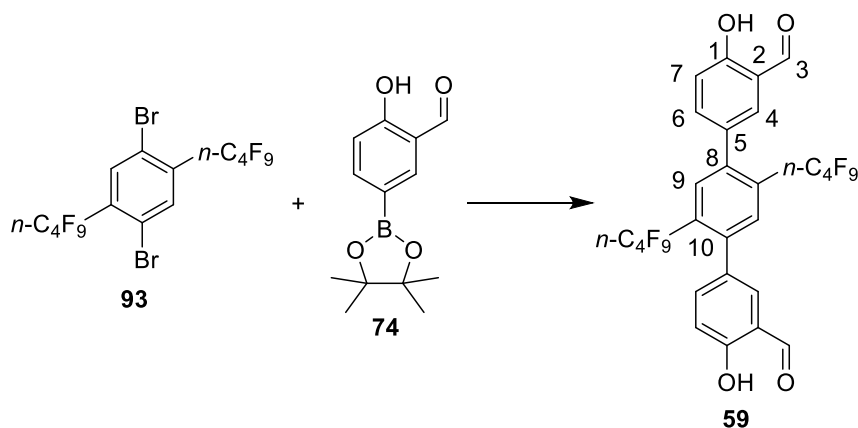
1,4-dibromo-2,5-bis(perfluorobutyl)benzene **93** (100 mg, 0.14 mmol) and benzaldehyde **74** (92.31 mg, 0.89 mmol) were suspended into THF (3 mL) and K_2CO_3 solution (2 mol/L, 1 mL) in a screw cap vessel. $Pd_2(dba)_3$ (27 mg, 0.014 mmol) and [(*t*-Bu)$_3$PH]BF$_4$ (18 mg, 0.028 mmol) were added to the reaction mixture under Ar, and the resulting mixture was heated to 90 °C for 16 h. After cooling to room temperature, the suspension was poured to water (20 mL) and extracted with CH_2Cl_2 (3 × 10 mL). The combined organic layers were washed with water (3 × 10 mL) and dried over Na_2SO_4. The solvent was removed under reduced pressure and the crude product was purified by column chromatography (silica gel, PE: DCM = 2:1, R_f = 0.7) to obtain the product as colourless solid with a yield of 30% (34 mg, 0.04 mmol).

M.p.: 216 °C.

^{1}H NMR (300 MHz, CDCl$_3$) δ = 11.12 (s, 2H, -OH), 9.93 (s, 2H, 3-H), 7.61 (s, 2H, 4-H), 7.49 (s, 2H, 9-H), 7.47 (d, J = 9.2 Hz, 2H, 6-H), 7.07 (d, J = 8.5 Hz, 2H, 7-H) ppm.

^{19}F NMR (471 MHz, CDCl3) δ = -80.95, -103.66, -120.47, -125.79 ppm.

^{13}C NMR (151 MHz, THF) δ = 194.08 (C-3), 159.72 (C-1), 139.81 (C-5), 135.37 (C-6), 131.91 (C-4), 131.82 (C-9), 128.16 (C-10), 127.86 (C-2), 118.88 (C-8), 115.10 (C-7) ppm.

IR (ATR): $\tilde{v}$ =3059 (w), 2868 (w), 1663 (s), 1593 (m), 1477 (s), 1371 (m), 1349 (s), 1285 (s), 1230 (s), 1190 (s), 1167 (s), 1130 (s), 1102 (s), 1058 (s), 1016 (s), 943 (m), 912 (m), 822 (s), 751 (s), 723 (s), 672 (s), 639 (s), 583 (s), 535 (s) cm^{-1}.

MS (ESI): [M-H]$^-$: m/z calcd. For (C$_{28}$H$_{11}$O$_4$F$_{18}$$^-$): 753.36, found 753.0383.

Elemental analysis: (C$_{28}$H$_{12}$O$_4$F$_{18}$) Calcd. C 44.58, H 1.6, found C 43.96, H 1.58.

5.3.1.29 Synthesis of 5-bromo-3-(tert-butyl)-2-hydroxybenzaldehyde (95):[118]

A solution of Br$_2$ (0.3 g, 5.6 mmol) in CH$_2$Cl$_2$ (10 mL) was added dropwise to a solution of 3-tert-butyl-2-hydroxybenzaldehyde **94** (1.0 g, 5.6 mmol) in CH$_2$Cl$_2$ (5 mL) at 0 °C in 30 min. The reaction mixture was stirred for 1 h at 0 °C. Water (20 mL) was added and the aqueous layer was separated and he organic layer was washed with Na$_2$S$_2$O$_3$ solution (3 × 10 mL) and NaHCO$_3$ solution (3 × 10 mL), then dried over NaSO$_4$. The solvent was removed under reduced pressure to obtain the product as a yellow solid with a yield of 83 % (1.2 g, 4.65 mmol).

M.p.: 60 °C [Lit.: 58-60 ºC].[118]

^{1}H NMR (300 MHz, CDCl$_3$) δ = 11.72 (s, 1H), 9.81 (s, 1H), 7.58 (d, J = 2.4 Hz, 1H), 7.52 (d, J = 2.5 Hz, 1H), 7.26 (s, 1H), 1.41 (s, 9H) ppm.

Analytical data are in accordance with those previously reported.[118]

5.3.1.30 Synthesis of 1,4-bis(4,4,5,5-tetramethyl-1,3,2-dioxaborolan-2-yl) benzene (97):[119]

1,4-Dibromobenzene **96** (1.28 g, 5 mmol), bis(pinacolato)diboron (2.66 g, 10.5 mmol), potassium acetate (1.03 g, 10.5 mmol) and 40 mL of 1,4-dioxane were placed in a 100-mL Schlenk flask under an argon atmosphere. Pd(dppf)Cl$_2$ (50 mg, 0.07 mmol) was added to the flask under Ar, and the mixture was refluxed for 16 h. After cooling to room termperature, the mixture was poured into water (100 mL), and extracted with dichloromethane (2 × 20 mL). The organic layers were dried over Na$_2$SO$_4$ and evaporated. The crude product was dissolved in dichloromethane and passed through a short pad of silica gel. After removal of the solvent, the residue was recrystallized from acetone to produce pure product as a colourless crystal with a yield of 65% (1.07 g, 3.25 mmol).

M.p.: 245 °C [Lit: 245.3 ºC].[119]

^{1}H NMR (300 MHz, CDCl$_3$) δ = 7.80 (s, 4H), 1.35 (s, 24H) ppm.

^{13}C NMR (125 MHz, CDCl3) δ = 133.89, 83.85, 24.87 ppm.

Analytical data are in accordance with those previously reported[119]

5.3.1.31 Synthesis of 5,5''-di-tert-butyl-4,4''-dihydroxy-[1,1':4',1''-terphenyl]-3,3''-dicarbaldehyde (62):

1,4-bis(4,4,5,5-tetramethyl-1,3,2-dioxaborolan-2-yl) benzene **97** (200 mg, 0.61mmol), 5-bromo-3-(tert-butyl)-2-hydroxybenzaldehyde **95** (389 mg, 1.5 mmol), [(*t*-Bu)$_3$PH]BF$_4$ (35.1 mg, 0.12 mmol) were suspended in THF (4 mL) and K$_2$CO$_3$ solution (1 mol/L, 2 mL) in a screw cap vessel. Pd$_2$(dba)$_3$ (55 mg, 0.06 mmol) was added under Ar, and the resulting mixture was heated to 90 °C for 16 h. After cooling to room temperature, the suspension was poured into water (20 mL) and extracted with CH$_2$Cl$_2$ (10 mL× 3). The combined organic layers were washed with water (3 × 10 mL) and dried over Na$_2$SO$_4$. The solvent was removed under reduced pressure and the crude product was purified by column chromatography (silica gel, DCM:PE= 1:1, R_f = 0.65) to give the product as a yellow solid with a yield of 54% (146 mg, 0.03 mmol).

M.p.: 274 °C.

^{1}H NMR (500 MHz, CDCl$_3$) δ = 11.82 (s, 2H, -OH), 9.99 (s, 2H, 7-H), 7.81 (d, J = 2.2 Hz, 2H, 5-H), 7.65 (m, 6H, 3,9-H), 1.49 (s, 18H, 11-H) ppm.

^{13}C NMR (125 MHz, CDCl$_3$) δ = 197.25 (C-7), 160.76 (C-1), 138.98 (C-6), 138.93 (C-8), 133.02 (C-5), 131.80 (C-4), 129.93 (C-3), 127.21 (C-9), 120.80 (C-7), 35.09 (C-10), 29.25 (C-11) ppm.

IR(ATR): $\tilde{v}$ = 2942 (w), 2909 (w), 2855 (w), 1642 (s), 1612 (m), 1520 (w), 1459 (m), 1436 (s), 1389 (s), 1375 (s), 1332 (s), 1293 (s), 1267 (s), 1248 (s), 1218 (m), 1196 (m), 1166 (s), 1083 (m), 1025 (w), 1005 (w), 959 (w), 930 (w), 906 (w), 882 (m), 843 (m), 784 (s), 734 (s), 708 (s), 634 (w) cm^{-1}.

MS (ESI): [M-H]$^-$: *m/z* calcd. For (C$_{30}$H$_{29}$O$_4$$^-$): 429.54, found 429.0383.
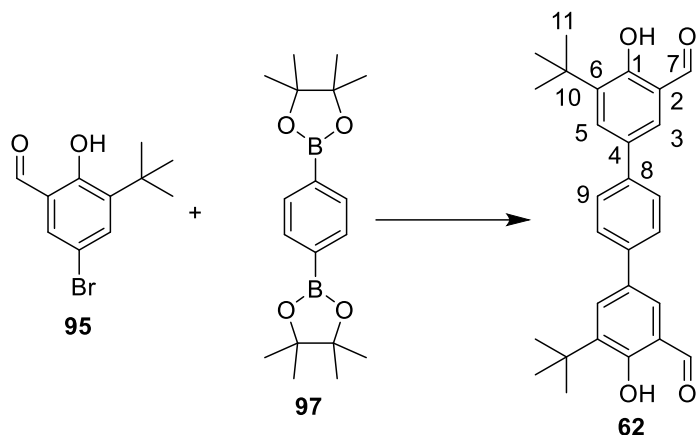
Elemental Analysis (%): ($C_{28}H_{30}O_4$) Calcd. C 78.11, H 7.02 found C 77.40, H 6.93.

5.3.1.32 Synthesis of triptycene (100):[120]
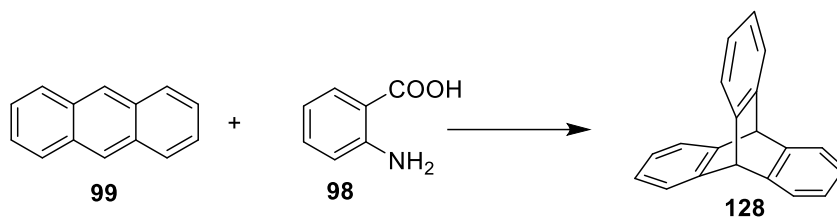
Anthracene **99** (17.8 g, 100 mmol) was dissolved in 1,2- dichloroethane (400 mL) and heated to reflux. Isopentyl nitrite (16.1 mL, 14.1 g, 120 mmol) was added in one portion. The solution of anthranilic acid **98** (15.1 g, 110 mmol) in diethylene glycol diethyl ether (150 mL) was added dropwise to the reaction mixture over approximately 1 h. The reaction mixture was heated under reflux for 2 hours, then the temperature increased to 170 °C to distill the solvent. Maleic anhydride (9.82 g, 100 mmol) was added to the residue, and the suspension was heated under reflux for another 1 h. The reaction was cooled to room temperature and poured into a mixture of methanol (500 mL), water (500 mL), and KOH (50 g) and cooled in an ice-bath. The resulting pale brown suspension was stirred for 40 min and then filtered. The solid was washed with a methanol and water mixture (4:1 V/V, 4 × 100 mL) to give the crude product as a brown solid. After subsequent recrystallizations from acetone, triptycene **100** was isolated in 52% yield (13.2 g, 52 mmol) as a colorless solid.

M.p.: 252 °C [Lit.: 253-254 °C].[120]

^{1}H NMR (300 MHz, CDCl$_3$) δ = 7.42 (m, 6H), 7.02 (m, 6H), 5.46 (s, 2H) ppm.

Analytical data are in accordance with those previously reported.[120]

**5.3.1.33   Synthesis of 2,7,14-Trinitrotriptycene (101):[122]**
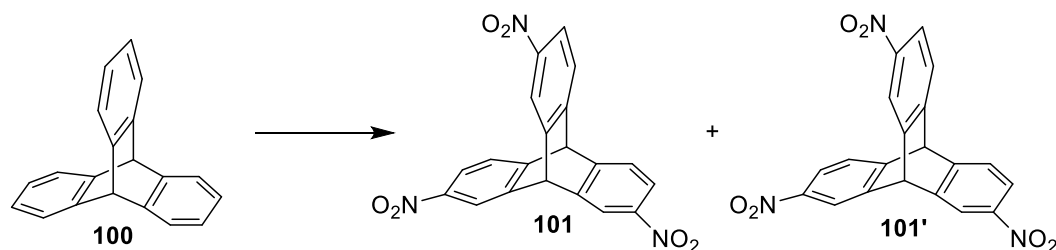
Triptycene **100** (14 g, 55 mmol) was stirred in acetic acid (80 mL) in an ice bath. Fuming HNO$_3$ (70 mL) was dropped into the mixture in 1 min. The mixture was stirred in an ice bath for 1 h and then poured onto ice water (1000 mL). The yellow precipitate was filterd, washed with

acetic acid and water (1 L), then dried in air. The crude product was separated by column chromatography (silica gel, ethyl acetate /petroleum ether, 1:4) afford a white solid with a yield of 15% (3.29 g, 8.25 mmol). The isomer **101'** was obtained as a yellow solid with a yield of 56% (12.28 g, 30.8 mmol)

101'

M.p.: 180 °C [Lit.: 178-180 °C].[122]

^{1}H NMR (300 MHz, CDCl$_3$): δ = 5.80 (s, 1H, bridgehead), 5.84 (s, 1H, bridgehead), 7.62 (m, 3H), 8.05 (m, 3H), 8.34 (m, 3H) ppm.

101

M.p.: 348 °C [Lit.: > 300 °C].[122]

^{1}H NMR (300 MHz, CDCl$_3$): δ = 5.82 (s, 1H, bridgehead), 5.84 (s, 1H, bridgehead), 7.62 (d, J = 8.2 Hz, 3H), 8.05 (dd, J = 8.2, 2.2 Hz, 3H), 8.34 (d, J = 2.2 Hz, 3H) ppm.

Analytical data are in accordance with those previously reported.[122]

5.3.1.34 Synthesis of 2,7,14-triaminotriptycene (19):[122]
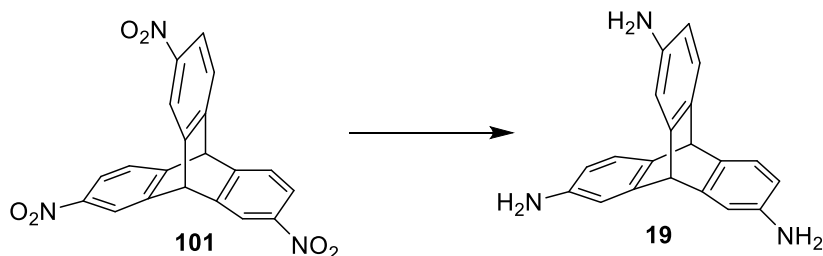
Hydrazine monohydrate (1.5 mL, 47.2 mmol) was added to a mixture of compound **101** (1.0 g, 2.6 mmol), Pd/C (~1.0 g), THF (20 mL) and ethanol (10 mL) under Ar in an ice bath. The mixture was stirred at 0 °C for half an hour at room temperature for a further half an hour. The mixture was heated to 75 °C for 3 hours, cooled to room temperature and then filtered by celite. The filtrate was concentrated by rotary evaporation, and the product was obtained as colourless solid after a column chromatography (silica gel, column: DCM:MeOH = 20:1, R_f = 0.3) with the yield of 80% (0.65 g, 2.08 mmol).

M.p.: 280 °C [Lit.: 279-283 °C].[122]

^{1}H NMR (300 MHz, CDCl$_3$): δ = 3.40 (s, 6H), 4.97 (s, 1H), 5.05 (s, 1H), 6.23 (dd, J = 7.7, 2.1 Hz, 3H), 6.70 (d, J = 7.7 Hz, 3H), 7.03 (d, J = 2.1 Hz, 3H) ppm.

Analytical data are in accordance with those previously reported.[122]

5.3.1.35 Synthesis of Cage compound 104:
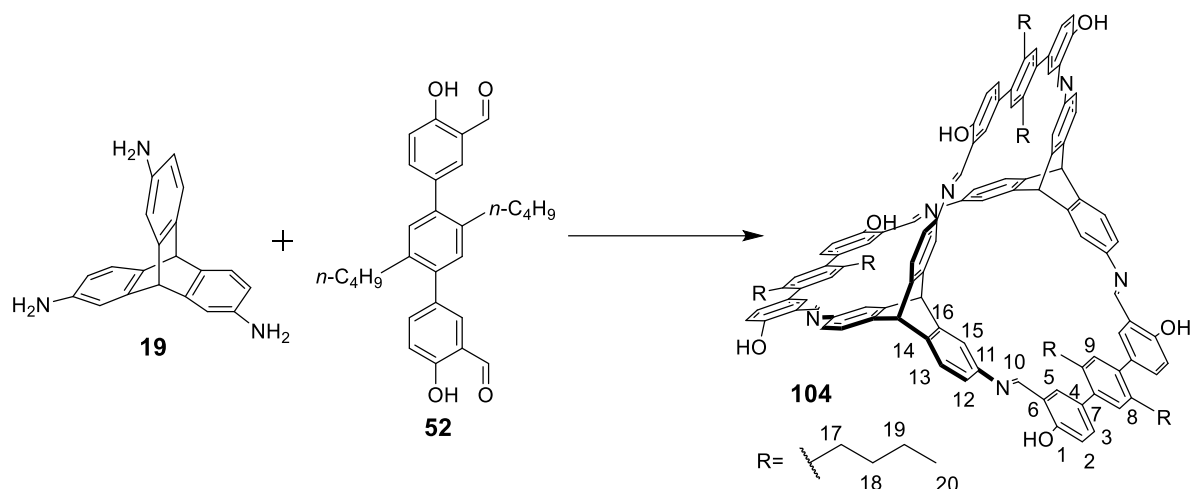
Triaminotriptycene **19** (46.39 mg,0.15 mmol) and aldehyde **52** (100 mg, 0.23 mmol) were dissolved in DMF (15 mL) in a screw cap vessel under Ar. TFA solution (0.1 mol/L, in DMF, 60 µL) was added to the solution. The mixture was heated to 100 °C for 2 days. After cooling to room temperature, the mixture was concentrated to 5 mL under reduced pressure. The remaining reaction mixture was dropped into methanol (20 mL) and stirred for 1 h. The orange precipitates were filtered then washed with methanol (5 × 5 mL) then pentane (5 × 5 mL) to obtain the product as an orange solid with a yield of 68 % (95 mg, 0.051 mmol). Crystals were obtained by diffusing methanol into THF solution at room temperature.

M.p.: >400 °C.

^{1}H NMR (500 MHz, THF-d$_8$) δ = 13.13 (s, 6H, -OH), 9.15 (s, 6H, 10-H), 7.82 (d, J = 1.6 Hz, 6H, 15-H), 7.55 (d, J = 7.8 Hz, 6H, 13-H), 7.41 (d, J = 2.0 Hz, 6H, 5-H), 7.39 (dd, J = 8.2, 2.1 Hz, 6H, 3-H), 7.22 (dd, J = 7.8, 1.8 Hz, 6H, 12-H), 7.13 (s, 6H, 9-H), 7.00 (d, J = 8.2 Hz, 6H, 2-H), 5.71(s, 2H, Bridgehead-H), 5.63 (s, 2H, Bridgehead-H),2.70 – 2.56 (m, 12H, 17-H), 1.47 (dt, J = 15.4, 7.7 Hz, 12H, 18-H), 1.26 – 1.12 (m, 12H, 19-H), 0.77 (t, J = 7.4 Hz, 18H, 20-H) ppm.

^{13}C NMR (150 MHz, THF-d$_8$) δ = 160.62 (C-10), 159.98 (C-1), 146.32 (C-16), 144.66 (C-14), 144.16 (C-10), 140.26 (C-7), 137.75 (C-8), 133.72 (C-3), 133.28 (C-5), 133.02 (C-10), 131.18 (C-9), 125.12 (C-12), 124.93 (C-13), 119.32 (C-10), 116.84 (C-2), 111.04 (C-15), 55.52 (Bridgehead-C), 52.86 (Bridgehead-C), 33.91 (C-17), 32.51 (C-18), 22.71 (C-19), 13.53 (C-20) ppm.

IR (ATR): $\tilde{v}$ = 2953 (w),2926 (w), 2862 (w), 1741 (w), 1624 (s), 1607 (s), 1577 (s), 1474 (s), 1359 (m), 1318 (w), 1278 (s), 1230 (m), 1178 (s), 1129 (m), 957 (m), 886 (m), 856 (s), 829 (s), 790 (s), 747 (s), 725 (s), 690 (s), 656 (s), 588 (s), 538 (s) cm^{-1}.

MS (MALDI-TOF, DCTB): [M+H]$^+$: m/z calcd. For (C$_{124}$H$_{113}$N$_6$O$_6^+$): 1783.30, found 1782.918.

Elemental analysis (%): (C$_{124}$H$_{112}$N$_6$O$_6$ ·H$_2$O) Calcd. C 82.73, H 6.38 N 4.67 found C 82.37, H 6.36 N 4.42.

5.3.1.36 Synthesis of Cage compound 105:
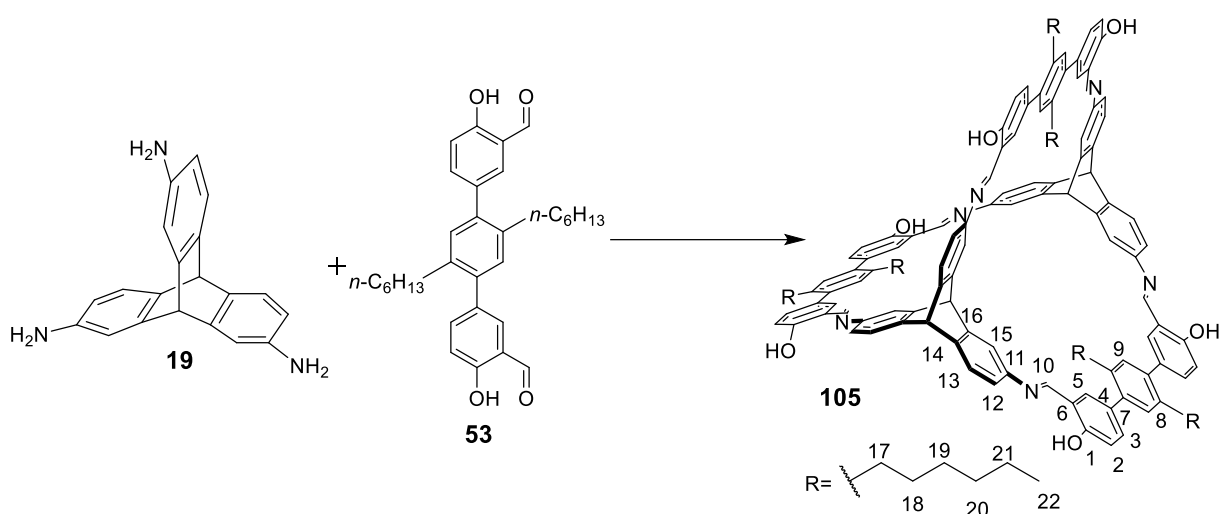
Triaminotriptycene **19** (41.06 mg,0.14 mmol) and aldehyde **53** (100 mg, 0.21 mmol) were dissolved in DMF (15 mL) in a screw cap vessel under Ar. TFA solution (0.1 mol/L, in DMF, 60 μL) was added to the solution. The mixture was heated to 100 °C for 2 days. After cooling to room temperature, the mixture was concentrated to 5 mL under reduced pressure. The remaining reaction mixture was dropped into methanol (20 mL) and stirred for 1 h. The orange precipitates were filtered then washed with methanol (5 × 5 mL) then pentane (5 × 5 mL) to obtain the product as an orange solid with a yield of 78 % (110 mg, 0.054 mmol). Crystals were obtained by diffusing methanol into THF solution.

M.p.: >410 °C.

^{1}H NMR (500 MHz, THF-d$_8$) δ = 13.02 (s, 6H,-OH), 9.04 (s, 6H, 10-H), 7.71 (s, , 6H, 15-H), 7.44 (d, J = 5.0 Hz, 6H, 13-H), 7.30 (s, 6H, 5-H), 7.28 (dd, J = 10.0, 5.0 Hz, 6H, 3-H), 7.12 (dd, J = 10.0, 5.0 Hz, 6H, 12-H), 7.02 (s, 6H, 9-H), 6.90 (d, J = 10.0 Hz, 6H, 2-H), 5.60(s,2H, Bridge-H), 5.51(s, 2H, Bridge-H), 2.51 (t, J = 5.0 Hz, 12H, 17-H), 1.38 (m, 12H,18-H), 1.05 (m, 36H, 19,20,21-H), 0.65 (t, J = 5.0 Hz, 18H,22-H) ppm.

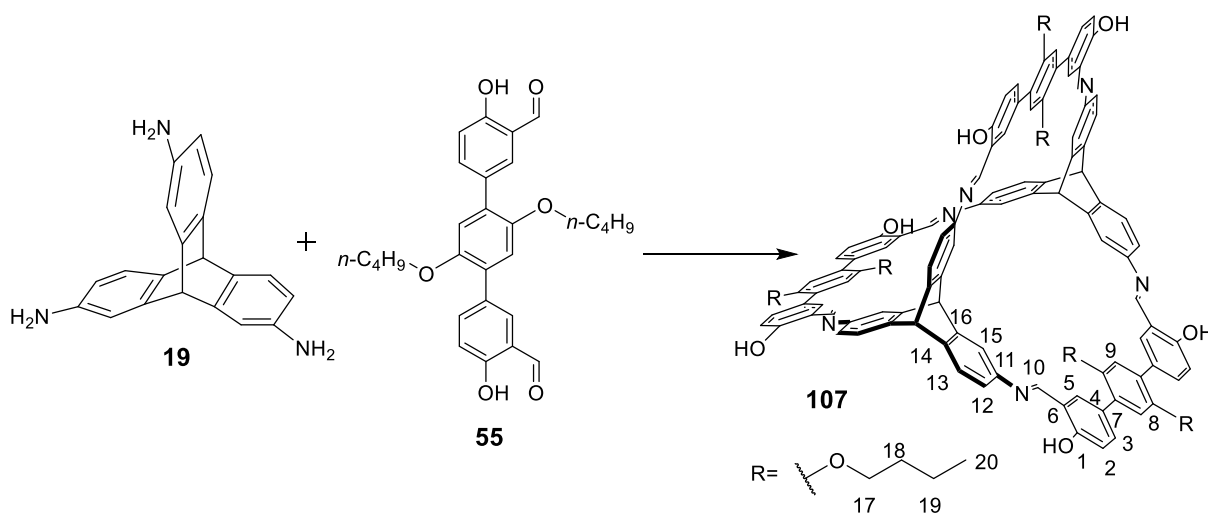^{13}C NMR (150 MHz, THF-d$_8$) δ = 159.98 (C-1), 159.20 (C-10), 145.65 (C-14), 144.03 (C-16), 143.45 (C-11), 139.60 (C-8), 137.20 (C-7), 133.08 (C-6), 132.60 (C-3), 132.36 (C-5), 130.51 (C-9), 124.54 (C-12), 124.30 (C-13), 118.67 (C-4), 116.21 (C-2), 110.29 (C-15), 54.90 (C-Bridgehead), 52.21 (C-Bridgehead), 32.22 (C-17), 31.10 (C-18), 31.02 (C-19), 28.78 (C-20), 22.02 (C-21), 13.04 (C-22) ppm.

IR (ATR): $\tilde{v}$ = 2952 (m), 2923 (m), 2854 (m), 1625 (s), 1607 (s), 1578 (s), 1474 (s), 1381 (m), 1359 (m), 1277 (s), 1230 (m), 1178 (s), 1129 (s), 1087 (w), 957 (s), 887 (s), 856 (s), 829 (s), 791 (s), 724 (s), 657 (s) cm^{-1}.

MS (MALDI-TOF, DCTB): [M+H]$^+$: m/z calcd. For (C$_{136}$H$_{137}$N$_6$O$_6^+$): 1951.62, found 1951.323.

Elemental Analysis (%): (C$_{136}$H$_{136}$N$_6$O$_6$·0.5H$_2$O) Calcd. C 83.30, H 7.07, N 4.29 found C 83.29, H 6.99, N 4.16.

5.3.1.37 Synthesis of Cage compound 106
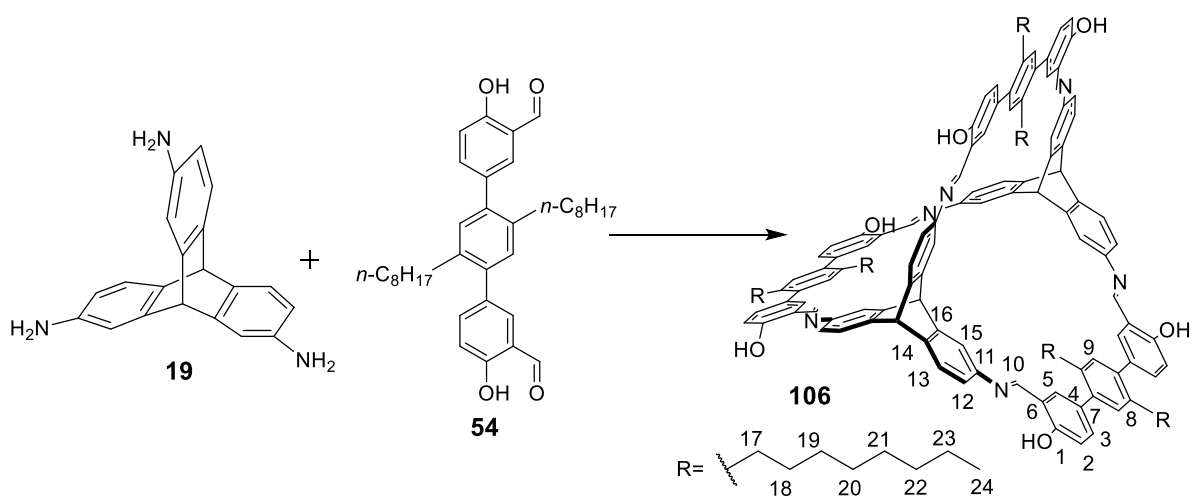
Triaminetriptycene **19** (44.2 mg, 0.15 mmol) and aldehyde **54** (120 mg, 0.22 mmol) were dissolved in DMF (15 mL) in a screw cap vessel under Ar. TFA solution (0.1 mol/L, in DMF, 60 μL) was added to the solution. The mixture was heated to 100 °C for 2 days. After cooling to room temperature, the mixture was concentrated to 5 mL under reduced pressure. The remaining reaction mixture was dropped into methanol (20 mL) and stirred for 1 h. The orange precipitates were filtered then washed with methanol (5 × 5 mL) then pentane (5 × 5 mL) to obtain the product as an orange solid with a yield of 67 % (106 mg, 0.051 mmol). Crystals were obtained by diffusing methanol into THF solution.
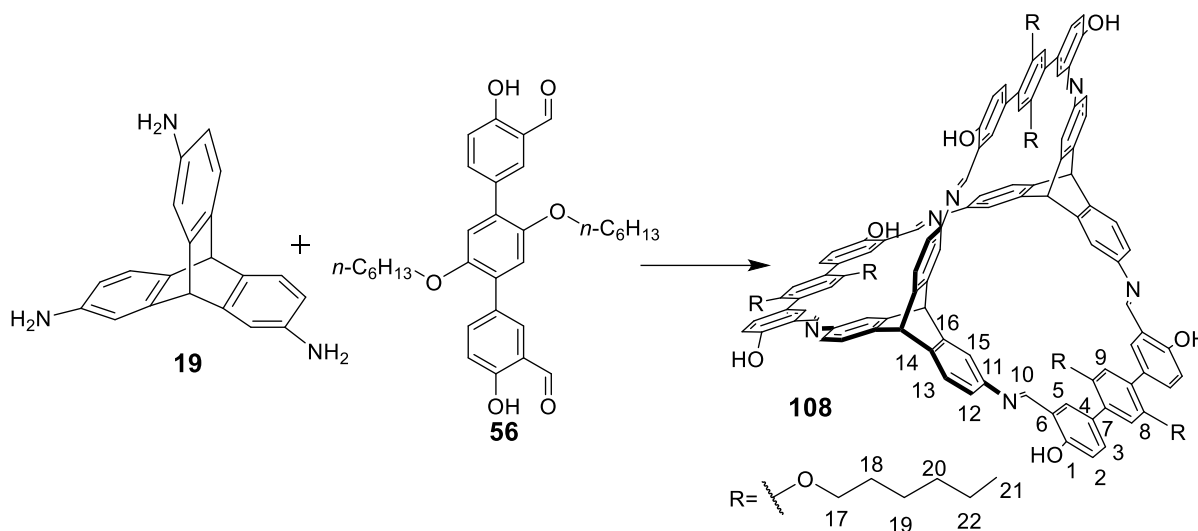
M.p.: >400 °C

^{1}H NMR (500MHz, THF-d$_8$) δ = 13.01 (s, 6H,-OH), 9.03 (s, 5H, 10-H), 7.70 (s, , 6H, 15-H), 7.44 (d, J = 5.0 Hz, 6H, 13-H), 7.30 (s, 6H, 5-H), 7.28 (dd, J = 10.0, 5.0 Hz, 6H, 3-H), 7.12 (dd, J = 10.0, 5.0 Hz, 6H, 12-H), 7.02 (s, 6H, 9-H), 6.90 (d, J = 10.0 Hz, 6H, 2-H), 5.60(s,2H, Bridgehead-H), 5.51(s, 2H, Bridgehead -H), 2.51 (t, J = 5.0 Hz, 12H, 17-H), 1.38 (m, 12H, 18-H), 1.04 (m, 60H,19,20,21,22,23 -H), 0.65 (t, J = 5.0 Hz, 18H, 24-H) ppm.

^{13}C NMR (150 MHz, THF-d$_8$) δ = 158.76 (C-1), 158.00 (C-10), 144.44 (C-14), 142.81 (C-16), 142.26 (C-11), 138.38 (C-8), 135.99 (C-7), 131.86 (C-6), 131.39 (C-3), 131.15 (C-5), 129.32 (C-9), 123.31 (C-12), 123.09 (C-13), 117.44 (C-4), 115.01 (C-2), 109.09 (C-15), 53.68 (C-Bridgehead), 51.03 (C-Bridgehead), 31.00 (C-17), 30.21 (C-18), 29.80 (C-19), 27.85 (C-20), 27.61 (C-21), 27.53 (C-22), 20.94 (C-23), 11.85 (C-24) ppm.

IR(ATR): $\tilde{v}$ = 3007 (w), 2921 (m), 2851 (m), 1741 (s), 1608 (m), 1578 (m), 1477 (s), 1361 (s), 1278 (m), 1215 (s), 1180 (s), 1130 (m), 957 (w), 889 (w), 860 (m), 829 (m), 791 (m), 741 (m), 660 (m), 640 (m) cm^{-1}.

MS (MALDI-TOF, DCTB): [M+H] $^+$: m/z calcd. For (C$_{148}$H$_{161}$N$_6$O$_6$$^+$): 2119.95, found 2119.756.

Elemental Analysis (%): (C$_{148}$H$_{160}$N$_6$O$_6$ ·H$_2$O) Calcd. C 83.18, H 7.64, N 3.95 found C 83.27, H 7.69, N 3.52.

5.3.1.38 Synthesis of Cage compound 107:

Triaminotriptycene **19** (43.2 mg, 0.144 mmol) and aldehyde **55** (100 mg, 0.22 mmol) were dissolved in DMF (15 mL) in a screw cap vessel under Ar. TFA solution (0.1 mol/L, in DMF, 60 µL) was added to the solution. The mixture was heated to 100 °C for 2 days. After cooling to room temperature, the mixture was concentrated to 5 mL under reduced pressure. The

remaining reaction mixture was dropped into methanol (20 mL) and stirred for 1 h. The orange precipitates were filtered then washed with methanol (5 × 5 mL) then pentane (5 × 5 mL) to obtain the product as an orange solid with a yield of 65 % (96 mg, 0.047 mmol). Crystals were obtained by diffusing methanol into THF solution.

M.p.: >400 °C.

^{1}H NMR (600 MHz, THF-d$_8$) δ = 13.17 (s, 6H, -OH), 9.21 (s, 6H, 10-H), 7.90 (d, J = 1.8 Hz, 6H,15-H), 7.75 (d, J = 2.1 Hz, 6H, 13-H), 7.65 (dd, J = 8.2, 2.2 Hz, 6H, 5-H), 7.56 (d, J = 7.8 Hz, 6H, 3-H), 7.23 (dd, J = 7.8, 1.9 Hz, 6H, 12-H), 7.07 (s, 6H, 9-H), 6.98 (d, J = 8.3 Hz, 6H, 2-H), 5.71 (s, 2H, Bridgehead-H), 5.68 (s, 2H, Bridgehead-H), 3.95 (t, J = 6.4 Hz, 12H, 17-H), 1.69 – 1.63 (m, 12H, 18-H), 1.41 (dq, J = 14.7, 7.4 Hz, 12H, 19-H), 0.88 (t, J = 7.4 Hz, 18H, 20-H) ppm.

^{13}C NMR (150 MHz, THF-d$_8$) δ = 160.76 (C-1), 159.83 (C-10), 150.89 (C-8), 146.31 (C-14), 144.67 (C-16), 144.01 (C-11), 134.03 (C-5), 133.70 (C-13), 130.06 (C-4), 129.62 (C-7), 125.29 (C-12), 124.91 (C-3), 119.26 (C-6), 116.56 (C-2), 116.35 (C-9), 110.8 (C-15), 69.52 (C-17), 55.50 (C-Bridgehead), 52.83 (C-Bridgehead), 31.81 (C-18), 19.52 (C-19), 13.43 (C-20) ppm.

IR(ATR): $\tilde{v}$ = 2955 (w), 2930 (w), 2868 (w), 1624 (s), 1606 (s), 1576 (s), 1512 (m), 1469 (s), 1361 (m), 1280 (m), 1227 (s), 1189 (s), 1161 (s), 1130 (m), 1062 (m), 1022 (m), 957 (s), 857 (s), 82 4(s), 791 (s), 743 (s), 658 (s), 587 (s), 534 (s) cm^{-1}.

MS (MALDI-TOF, DCTB): [M] $^+$: m/z calcd. For (C$_{124}$H$_{112}$N$_6$O$_{12}^+$): 1878.29, found 1878.843

Elemental Analysis (%): (C$_{124}$H$_{112}$N$_6$O$_{12}$ ·3H$_2$O) Calcd. C 77.08, H 6.16, N 4.35 found C 77.06, H 6.27, N 3.69.

5.3.1.39 Synthesis of Cage compound 108:

Triaminetriptycene **19** (46.17 mg, 0.15 mmol) and aldehyde **56** (120 mg, 0.23 mmol) were dissolved in DMF (15 mL) in a screw cap vessel under Ar. TFA solution (0.1 mol/L, in DMF, 60 μL) was added to the solution. The mixture was heated to 100 °C for 2 days. After cooling to room temperature, the mixture was concentrated to 5 mL under reduced pressure. The remaining reaction mixture was dropped into methanol (20 mL) and stirred for 1 h. The orange precipitates were filtered then washed with methanol (5 × 5 mL) then pentane (5 × 5 mL) to obtain the product as an orange solid with a yield of 66 % (104 mg, 0.049 mmol). Crystal was obtained by diffusing methanol into THF solution.

M.p.: >400 °C

^{1}H NMR (600 MHz, THF-d$_8$) δ = 13.16 (s, 6H, -OH), 9.21 (s, 6H, 10-H), 7.90 (d, J = 1.8 Hz, 6H, 15-H), 7.74 (d, J = 2.2 Hz, 6H, 13-H), 7.66 (dd, J = 8.2, 2.2 Hz, 6H, 5-H), 7.56 (d, J = 7.8 Hz, 6H, 3-H), 7.23 (dd, J = 7.8, 1.9 Hz, 6H, 12-H), 7.07 (s, 6H, 9-H), 6.98 (d, J = 8.3 Hz, 6H, 2-H), 5.71 (s, 2H, Bridgehead-H), 5.67 (s, 2H, Bridgehead-H), 3.95 (t, J = 6.3 Hz, 12H, 17-H), 1.71 – 1.64 (m, 12H, 18-H), 1.39 (dd, J = 10.1, 4.7 Hz, 12H, 19-H), 1.31 – 1.20 (m, 24H, 20,21-H), 0.82 (t, J = 6.9 Hz, 18H, 22-H) ppm.
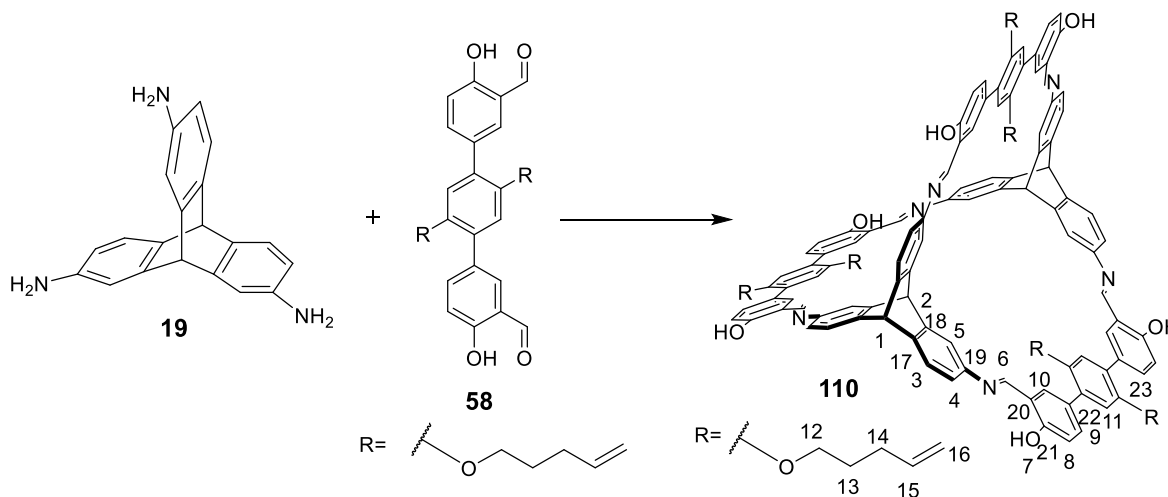
^{13}C NMR (150 MHz, THF-d$_8$) δ = 160.09 (C-10), 159.02 (C-1), 150.22 (C-8), 145.60 (C-7), 144.01 (C-14), 143.26 (C-16), 133.39 (C-5), 133.04 (C-13), 129.39 (C-11), 128.95 (C-4), 124.70 (C-12), 124.28 (C-3), 118.51 (C-6), 115.90 (C-2), 115.64 (C-9), 110.03 (C-15), 69.17 (C-17), 54.98 (C-Bridgehead), 52.16 (C-Bridgehead), 31.06 (C-18), 29.02 (C-19), 25.47 (C-20), 22.17 (C-21), 13.06 (C-22) ppm.

IR (ATR): $\tilde{v}$ = 2927 (m), 2856 (m),1624 (s), 1606 (s), 1578 (s), 1511 (m), 1468 (s), 1377 (m), 1360 (m), 1277 (s), 1226 (s), 1189 (s), 1160 (s), 1131 (s), 1057 (s), 957 (s), 856 (s), 825 (s), 792 (s), 776 (s), 742 (s), 723 (s), 658 (s), 643 (s), 591 (s), 580 (s), 563 (s), 533 (s), 523 (s) cm^{-1}.

MS (MALDI-TOF, DCTB): [M]$^{+}$: m/z calcd. For ($C_{136}H_{136}N_6O_{12}^{+}$): 2046.61, found 2046.297.

Elemental Analysis (%): ($C_{136}H_{136}N_6O_{12}\cdot H_2O$) Calcd. C 78.43, H 6.78, N 4.07 found C 78.81, H 6.59, N 4.16.

5.3.1.40 Synthesis of Cage compound 109:

Triaminotriptycene **19** (43.4 mg,0.15 mmol) and aldehyde **57** (125 mg, 0.21 mmol) were dissolved in DMF (15 mL) in a screw cap vessel under Ar. 0TFA solution (0.1 mol/L, in DMF, 60 µL) was added to the solution. The mixture was heated to 100 °C for 2 days. After cooling to room temperature, the mixture was concentrated to 5 mL under reduced pressure. The remaining reaction mixture was dropped into methanol (20 mL) and stirred for 1 h. The orange precipitates were filtered then washed with methanol (5 × 5 mL) then pentane (5 × 5 mL) to obtain the product as an orange solid with a yield of 67 % (108 mg, 0.050 mmol). Crystals were obtained by diffusing methanol into THF solution.

M.p.: >400 °C

^{1}H NMR (500 MHz, THF-d$_8$) δ = 13.07 (s, 6H, -OH), 9.10 (s, 6H, 10-H), 7.80 (s, 6H, 15-H), 7.63 (d, J = 1.8 Hz, 6H, 13-H), 7.54 (dd, J = 8.3, 2.1 Hz, 6H, 5-H), 7.45 (d, J = 7.8 Hz, 6H, 3-H), 7.12 (dd, J = 7.8, 1.6 Hz, 6H, 12-H), 6.96 (s, 6H, 9-H), 6.87 (d, J = 8.4 Hz, 6H, 2-H), 5.60 (s, 2H, Bridgehead-H), 5.57 (s, 2H, Bridgehead-H), 3.94 (t, J = 6.3 Hz, 12H, 17-H), 1.70 – 1.62

(m, 12H, 18-H), 1.44 – 1.30 (m, 12H, 19-H), 1.28 – 1.05 (m, 48H, 20,21,22,23-H), 0.72 (t, J = 7.0 Hz, 18H, 24-H) ppm.

^{13}C NMR (150 MHz, THF-d$_8$) δ = 160.09 (C-10), 159.02 (C-1), 150.22 (C-8), 145.60 (C-7), 144.01 (C-14), 143.26 (C-16), 133.3 9(C-5), 133.04 (C-13), 129.39 (C-11), 128.95 (C-4), 124.70 (C-12), 124.2 8(C-3), 118.51(C-6), 115.90 (C-2), 115.64 (C-9), 110.0 3(C-15), 69.17 (C-17), 54.98 (C-Bridgehead), 52.16 (C-Bridgehead), 31.33 (C-18), 29.06 (C-19), 28.91 (C-20), 28.85 (C-21), 25.83 (C-22), 22.08 (C-23), 12.98 (C-24) ppm.

IR (ATR): $\tilde{v}$ = 2923 (s), 2853 (m), 1624 (s), 1607 (s), 1577 (s), 1512 (w), 1468 (s), 1378 (m), 1360 (m), 1280 (s), 1195 (s), 1160 (s), 1130 (s), 1056 (m), 1026 (m), 956 (s), 856 (s), 825 (s), 792 (s), 743 (s), 721 (s), 659 (s), 591 (s), 530(s) cm^{-1}.

MS (MALDI-TOF, DCTB): [M+H]$^+$: m/z calcd. For (C$_{148}$H$_{161}$N$_6$O$_{12}{}^+$): 2215.94, found 2215.704.

Elemental Analysis (%): (C$_{148}$H$_{160}$N$_6$O$_{12}$·H$_2$O) Calcd. C 79.61, H 7.31, N 3.76 found C 79.32, H 7.23, N 3.45.

5.3.1.41 Synthesis of Cage compound 110:

Triaminotriptycene **19** (4.1 mg,0.015 mmol), aldehyde **58** (10 mg, 0.021 mmol) were dissolved in DMF (3 mL) in a screw cap vessel under Ar. TFA solution (0.1 mol/L in DMF, 10 μL) was added to the solution. The mixture was heated to 100 °C for 2 days. After cooling to room temperature, the mixture was concentrated to 1 mL under reduced pressure. The remaining reaction mixture was dropped into methanol (5 mL) and stirred for 1 h. The orange precipitates were filtered then washed by methanol (5 × 5 mL) then pentane (5 × 5 mL) to obtain the product

as orange solid with a yield of 77.1 % (10.52 mg, 0.0050 mmol). Crystals were obtained by diffusing methanol into THF solution.

M.p.: >400 °C

^{1}H NMR (600 MHz, THF-d$_8$) δ = 13.50 (s, 6H, H-7), 9.54 (s, 6H, H-6), 8.22 (s, 6H, H10), 8.08 (d, J = 1.8 Hz, 6H, H-8), 7.98 (dd, J = 8.2, 2.1 Hz, 6H, H-11), 7.88 (d, J = 7.8 Hz, 6H, H-9), 7.55 (dd, J = 7.8, 1.7 Hz, 6H, H-4), 7.40 (s, 6H, H-5), 7.31 (d, J = 8.3 Hz, 6H, H-3), 6.10 (ddt, J = 16.9, 10.2, 6.7 Hz, 6H, H-15), 6.02 (d, J = 24.0 Hz, 4H, H-1,2), 5.28 (dd, J = 17.1, 1.6 Hz, 6H, H-16 out of cage), 5.21 (d, J = 10.1 Hz, 6H, H-16 in cage), 4.29 (t, J = 6.2 Hz, 12H, H-12), 2.49 – 2.43 (m, 12H, H-13), 2.13 – 2.07 (m, 12H, H-14) ppm.

^{13}C NMR (150 MHz, THF-d$_8$) δ = 160.79 (C-6), 159.76 (C-7), 146.30 (C-23), 144.68 (C19), 143.97 (C-21), 138.15 (C-15, 22), 134.06 (C-9), 133.70 (C-8), 130.11 (C-3), 129.55 (C-20), 124.93 (C-5), 116.61 (C-4), 116.36 (C-9), 114.69 (C-11,16), 69.12 (C12), 55.54 (C-2), 52.85 (C-1), 30.52 (C-13), 29.04 (C-14) ppm.

IR(ATR): $\tilde{v}$ = 3023 (w), 2968 (w), 1740 (s), 1657 (w), 1620 (m), 1579 (m), 1512 (w), 1473 (s), 1369 (s), 1279 (m), 1209 (s), 1161 (m), 1131 (w), 1055 (w), 1021 (m), 963 (m), 857 (m), 827 (m), 791 (m), 744 (m), 658 (m) cm^{-1}.

MS (MALDI-TOF, DCTB): [M+H]$^+$: m/z calcd. For (C$_{130}$H$_{112}$N$_6$O$_{12}$$^+$): 1950.36, found 1950.408.

Elemental Analysis (%): (C$_{130}$H$_{112}$N$_6$O$_{12}$·6THF) Calcd. C 77.08, H 6.72, N 4.11 found C 77.12, H 6.20, N 3.82.

5.3.1.42 Synthesis of Cage compound 111:

130
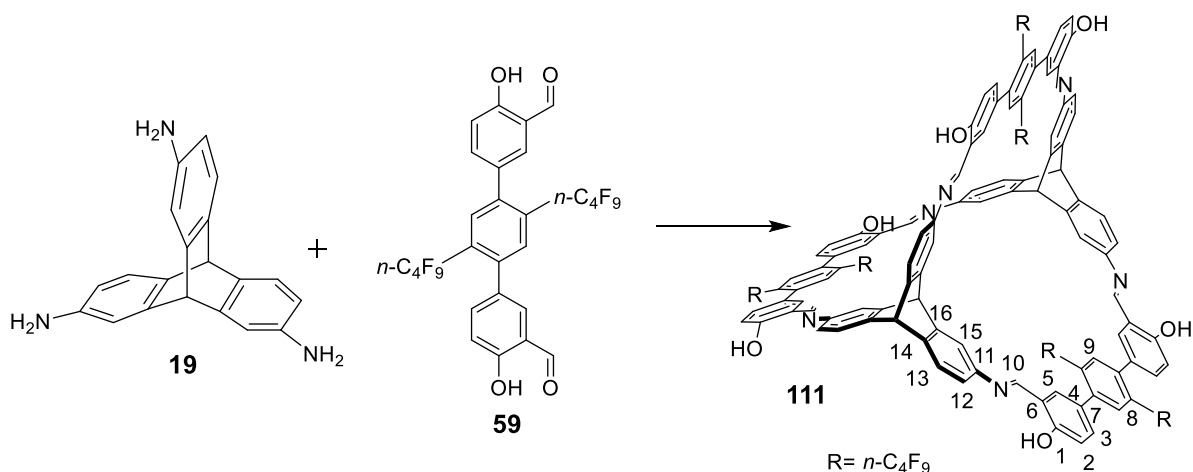
Triaminotriptycene **19** (19.6 mg, 0.07 mmol and aldehyd **59** (74 mg, 0.10 mmol) were dissolved in THF (15 mL) in a screw cap vessel under Ar. TFA solution (0.1 mol/L in THF, 30 µL) was added to the solution. After cooling to room temperature, the mixture was concentrated to 1 mL under reduced pressure. The remaining reaction mixture was dropped into methanol (5 mL) and stirred for 1 h. The yellow precipitates were filtered then washed by methanol (5×5 mL) then pentane (5×5 mL) to obtain the product as yellow solid with a yield of 67 % (45 mg, 0.094 mmol). Crystals were obtained by diffusing methanol into THF solution.

M.p.: >400 °C

C 53.07, H 2.73, N 2.83.

^{1}H NMR (600 MHz, THF-d$_8$) δ = 13.36 (s, 6H, -OH), 9.15 (s, 6H, 10-H), 7.83 (s, 6H,15-H), 7.76 (s, 6H,9-H), 7.56 (d, J = 7.6 Hz, 6H, 13-H), 7.41 (d, J = 7.7 Hz, 6H, 3-H), 7.38 (s, 6H, 5-H), 7.25 (d, J = 7.3 Hz, 6H, 12-H), 7.03 (d, J = 8.1 Hz, 6H, 2-H), 5.72 (s, 2H, Bridgehead-H), 5.57 (s, 2H, Bridgehead-H) ppm.

^{13}C NMR (150 MHz, THF-d$_8$) δ = 159.74 (C-1), 157.30 (C-10), 144.28 (C-16), 142.98 (C-14), 141.79 (C-11), 140.33 (C-7), 132.00 (C-9), 131.68 (C-3), 131.28 (C-5), 127.95 (C-8), 127.34 (C-6), 123.62 (C-12), 123.19 (C-13), 116.98 (C-4), 114.82 (C-2), 108.96 (C-15), 53.78 (Bridgehead-C), 50.97 (Bridgehead-C) ppm.

^{19}F NMR (471 MHz, THF-d$_8$) δ = -82.08, -103.99, -120.86, -126.46 ppm.

IR(ATR): $\tilde{v}$ = 1621 (m), 1581 (m), 1479 (s), 1382 (m), 1349 (m), 1285 (m), 1228 (s), 1172 (s), 1131 (s), 1092 (s), 1009 (m), 953 (m), 860 (s), 821 (s), 797 (s), 739 (s), 680 (s), 593 (m), 534 (m) cm^{-1}.

MS (MALDI-TOF, DCTB): [M+H]$^+$: m/z calcd. For ($C_{124}H_{59}O_6N_6F_{54}^{2+}$): 2755.79, found 2755.259.

Elemental Analysis (%): ($C_{124}H_{58}O_6N_6F_{54} \cdot 4H_2O$) Calcd. C 53.04, H 2.30, N 2.99 found

5.3.1.43 Synthesis of Cage compound 112:
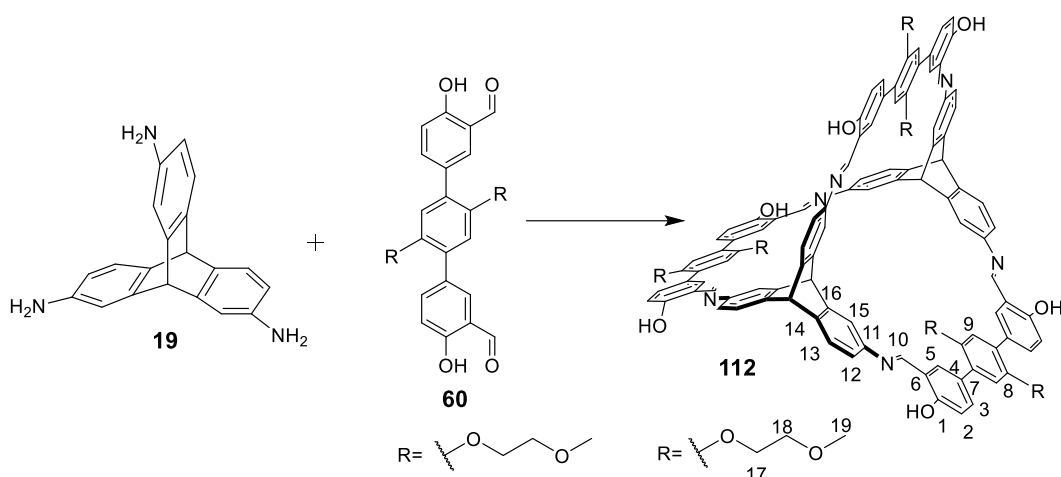
Triaminotriptycene **19** (43.2 mg, 0.14 mmol) and aldehyde **60** (100 mg, 0.21 mmol) were dissolved in DMF (15 mL) in a screw cap vessel under Ar. TFA solution (0.1 mol/L, in DMF, 60 µL) was added to the solution. The mixture was heated to 100 °C for 2 days. After cooling to room temperature, the mixture was concentrated to 5 mL under reduced pressure. The remaining reaction mixture was dropped into methanol (20 mL) and stirred for 1 h. The orange precipitates were filtered then washed with methanol (5 × 5 mL) then pentane (5 × 5 mL) to obtain the product as an orange solid with a yield of 73% (96 mg, 0.05 mmol). The crystals were obtained through the slow cooling of a hot DMF solution (100 °C to 70 °C, 2 °C per hour).

M.p.: >400 °C.

^{1}H NMR (300 MHz, DMSO-d$_6$, 100 °C) δ = 13.07 (s, 6H, -OH), 9.30 (s, 6H, 10-H), 7.99 (d, J = 1.5 Hz, 6H, 15-H), 7.94 (d, J = 2.1 Hz, 6H, 13-H), 7.71 (dd, J = 8.5, 2.1 Hz, 6H, 5-H), 7.61 (d, J = 7.8 Hz, 6H, 3-H), 7.22 (dd, J = 7.7, 1.8 Hz, 6H, 12-H), 7.15 (s, 6H, 9-H), 7.00 (d, J = 8.5 Hz, 6H, 2-H), 5.83 (s, J = 1.8 Hz, 4H, Bridgehead-H), 4.25 – 3.98 (m, 12H, 17-H), 3.74 – 3.51 (m, 12H, 18-H), 3.29 (s, 18H, 19-H) ppm.

^{13}C NMR could not be measured because of the poor solubility.

IR(ATR): $\tilde{v}$ = 2874 (w), 1622 (s), 1607 (s), 1578 (s), 1512 (m), 1473 (s), 138 8(m), 1359 (m), 1277 (s), 1190 (s), 1161 (m), 1125 (m), 1090 (m), 1058 (s), 957 (m), 856 (m), 827 (m), 792 (m), 775 (m), 744 (m), 658 (s), 64 3(s), 583 (s), 551 (m), 541 (m), 535 (m), 525 (m), 515 (m) cm^{-1}.

MS (MALDI-TOF, DCTB): [M]$^+$: m/z calcd. For (C$_{118}$H$_{100}$N$_6$O$_{18}$$^+$): 1889.71, found 1889.767.

Elemental Analysis (%): ($C_{118}H_{100}N_6O_{18}\cdot 4H_2O$) Calcd. C 72.23, H 5.55, N 4.28 found C 72.34, H 5.56, N 4.14.

5.3.1.44 Synthesis of Cage compound 113:

Triaminotriptycene **19** (46 mg, 0.15 mmol and aldehyde **61** (100 mg, 0.023 mmol) were dissolved in DMF (15 mL) in a screw cap vessel under Ar. TFA solution (0.1 mol/L, in DMF, 60 μL) was added to the solution. The mixture was heated to 100 °C for 2 days. After cooling to room temperature, the mixture was concentrated to 5 mL under reduced pressure. The remaining reaction mixture was dropped into methanol (20 mL) and stirred for 1 h. The orange precipitates were filtered then washed with methanol (5 × 5 mL) then pentane (5 × 5 mL) to obtain the product as an orange solid with a yield of 52 % (98 mg, 0.039 mmol). Crystals were obtained by diffusing methanol into THF solution.

M.p.: >400 °C.

^{1}H NMR (500 MHz, THF-d_8) δ = 13.18 (s, 6H, -OH), 9.24 (s, 6H, 10-H), 7.96 (d, J = 1.5 Hz, 6H, 15-H), 7.85 (d, J = 2.0 Hz, 6H, 13-H), 7.74 (dd, J = 8.4, 2.0 Hz, 6H, 5-H), 7.55 (d, J = 7.8 Hz, 6H, 3-H), 7.22 (dd, J = 7.8, 1.8 Hz, 6H, 12-H), 7.12 (s, 6H, 9-H), 6.98 (d, J = 8.4 Hz, 6H, 2-H), 5.73 (s, 2H, Bridgehead-H), 5.70 (s, 2H, Bridgehead-H), 4.20 – 3.99 (m, 17H), 3.73 (dd, J = 8.8, 4.1 Hz, 18H), 3.54 – 3.49 (m, 12H), 3.39 – 3.31 (m, 12H), 3.15 (s, 18H, 23-H) ppm.

^{13}C NMR (100 MHz, THF-d_8) δ = 160.81 (C-10), 160.09 (C-1), 150.86 (C-8), 146.40 (C-7), 144.65 (C-14), 144.01 (C-16), 134.22 (C-5), 133.91 (C-13), 129.81 (C-11), 129.43 (C-4), 125.26 (C-12), 124.85 (C-3), 119.25 (C-6), 116.60 (C-2), 116.22 (C-9), 110.90 (C-15), 72.23

(C-17), 71.04 (C-18), 70.95 (C-19), 70.74 (C-20), 70.00 (C-21), 69.46 (C-22), 58.15 (C-Bridgehead), 55.41 (C-Bridgehead), 52.83 (C-23) ppm.

IR(ATR): $\tilde{v}$ = 2817 (m), 1620 (m), 1576 (s), 1474 (m), 1390 (m), 1356 (m), 1279 (m), 1196 (s), 1162 (s), 1100 (s), 1060 (s), 982 (s), 949 (s), 855 (s), 826 (s), 791 (s), 744 (s), 659 (s), 590 (s), 536 (s) cm^{-1}.

MS (MALDI-TOF, DCTB): [M+H]$^+$: m/z calcd. For ($C_{142}H_{150}N_6O_{30}^+$): 2420.76, found 2420.390.

Elemental Analysis (%): ($C_{142}H_{148}N_6O_{30}\cdot5H_2O$) Calcd. C 67.98, H 6.05, N 3.35 found C 67.98, H 5.85, N 3.52.

5.3.1.45 Synthesis of Cage compound 114:

Triaminotriptycene **19** (46 mg, 0.15 mmol) and aldehyde **62** (100 mg, 0.023 mmol) were dissolved in DMF (15 mL) in a screw cap vessel under Ar. TFA solution (0.1 mol/L, in DMF, 60 µL) was added to the solution. The mixture was heated to 100 °C for 2 days. After cooling to room temperature, the mixture was concentrated to 5 mL under reduced pressure. The remaining reaction mixture was dropped into methanol (20 mL) and stirred for 1 h. The orange precipitates were filtered then washed with methanol (5 × 5 mL) then pentane (5 × 5 mL) to obtain the product as an orange solid with a yield of 78 % (105 mg, 0.058 mmol).

M.p.:>400 °C.

^{1}H NMR (500 MHz, THF-d$_8$) δ = 14.16 (s, 6H, -OH), 9.30 (s, 6H, 9-H), 7.97 (s, 6H, 11-H), 7.72 (m, 24H, 5, 3, 17, 18-H), 7.58 (d, J = 7.7 Hz, 6H, 13-H), 7.26 (dd, J = 7.8, 1.4 Hz, 6H, 12-H), 5.73 (s, 4H, Bridgehead-H), 1.52 (s, 54H, 8-H) ppm.

^{13}C NMR (101 MHz, THF-d$_8$) δ = 160.29 (C-9), 160.13(C-1), 146.12 (C-10), 144.37 (C-15), 143.52 (C-14), 139.04 (C-2), 137.68 (C-4), 130.72 (C-5), 128.82 (C-17), 128.31 (C-18), 126.53 (C-3), 124.85 (C-12), 124.67 (C-13), 119.59 (C-6), 110.58 (C-11), 55.14 (Bridgehead-C), 52.60 (Bridgehead-C), 34.78 (C-7), 28.78 (C-8) ppm.

IR(ATR): $\tilde{v}$ = 2951(m), 1608(s), 1577(s), 1518(w), 1467(s), 1438(s), 1391(m), 1360(m), 1331(m), 1267(s), 1250(s), 1224(m), 1196(m), 1168(s), 1134(m), 1067(m), 959(m), 879(s), 859(s), 828(s), 808(s), 771(s), 734(s), 687(s), 660(w), 624(w) cm^{-1}.

MS (MALDI-TOF, DCTB): [M]$^+$: m/z calcd. For (C$_{124}$H$_{112}$N$_6$O$_6$$^+$): 1781.87, found 1781.861.
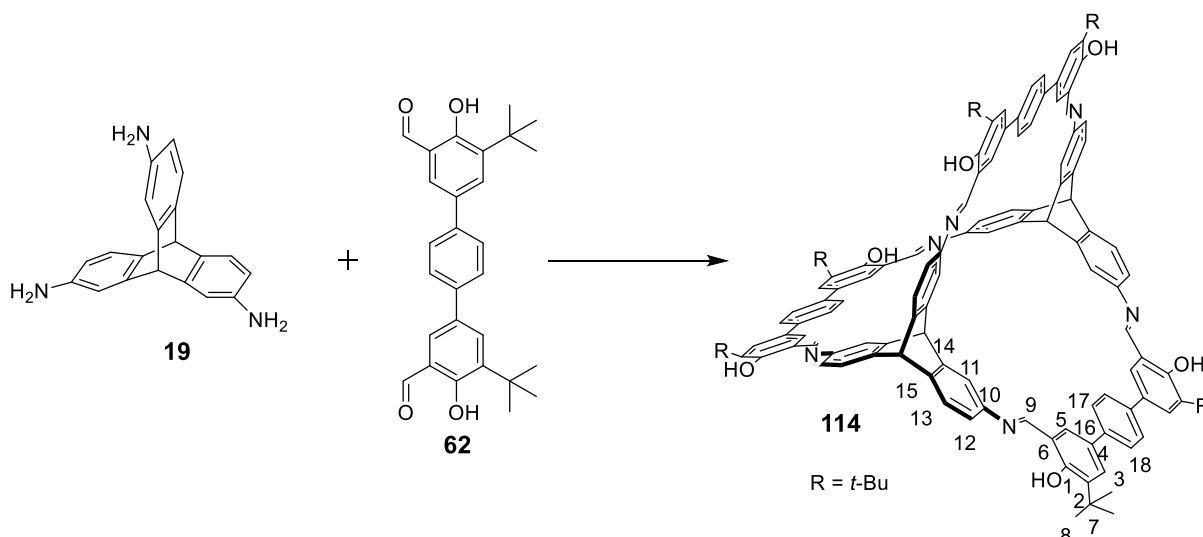
Elemental Analysis (%): (C$_{124}$H$_{112}$N$_6$O$_6$·10H$_2$O) Calcd. C 75.89, H 6.68, N 4.28 found C 75.51, H 6.55, N 4.80.

5.3.2 Compounds of Chapter 3.2

5.3.2.1 Synthesis of Di-*t*-butoxycarbonylamido-tripycene (115):
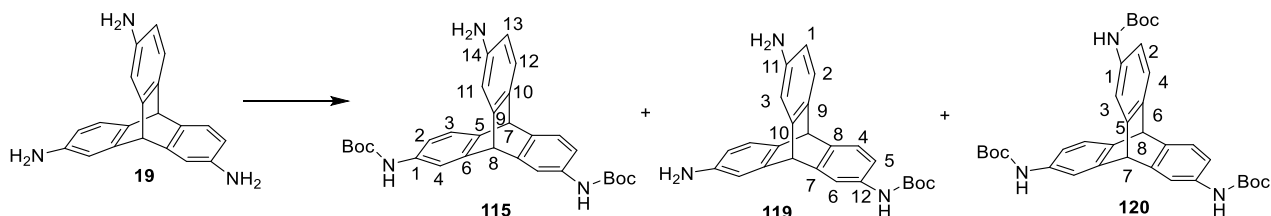
Di-*t*-butyl-dicarbonate (400 mg, 1.8 mmol) and 4-(*N, N*-dimethylamino) pyridine (5 mg, 0.03 mmol) were added to the solution triaminotripycene **19** (300 mg, 0.9 mmol) in ethanol (20 mL) under Ar. The mixture was heated to 50 ˚C for 16 h. The solvent was removed under reduced pressure and the crude product was purified by column chromatography (silica gel, ethyl acetate: petroleum ether = 2:1, R_f = 0.5) to give the product **115** as colourless solid with a yield of 25% (124 mg, 0.225 mmol), product **119** as colourless solid with a yield of 40% (287 mg, 0.72 mmol), product **119** as colourless solid with a yield of 10% (107 mg, 0.18 mmol).

115

M.p.: 174 ºC.

^{1}H NMR (300 MHz, DMSO-d$_6$): δ = 9.16 (s, 2H, -NH-), 7.57 (s, 2H, H-4), 7.15 (s, 1H, H-2), 6.97 (d, J = 5.85 Hz, 1H, H-12), 6.93 (dd, J = 6.0, 1.5 Hz, H-3) 6.70 (d, J = 3 Hz 1H, H-11), 6.12(dd, J = 9,3 Hz, 1H, H-13) 5.23 (s, 1H, Bridgehead-H), 5.19 (s, 1H, Bridgehead-H), 4.83 (s, 2H, -NH2), 1.44 (s, 18H, H-Boc) ppm.

^{13}C NMR (125 MHz, DMSO-d$_6$): δ =153.44 (C-15), 146.31 (C-14), 146.27 (C-9), 146.21 (C-6), 140.90 (C-5), 136.44 (C-1), 133.79 (C-10), 123.77 (C-12), 123.01 (C-3), 114.93 (C-4), 114.64 (C-2), 111.11 (C-11), 109.45 (C-13), 79.26 (C-Boc), 53.80 (C-7), 51.03 (C-8), 28.60 (C-Boc, -CH$_3$) ppm.

IR (ATR): $\tilde{v}$ = 3332 (w), 2976 (w), 1703 (s), 1599 (m), 1520 (s), 1479 (s), 1420 (m), 1392 (m), 1367 (m), 1330 (m), 1289 (m), 1234 (s), 1154 (s), 1097 (w),1050 (s), 1027 (s), 943 (w), 893 (w), 845 (w), 809 (w), 773 (m), 718 (m), 650 (w) cm^{-1}

MS (ESI): [M-H] $^-$: m/z calcd. For (C$_{30}$H$_{32}$N$_3$O$_4$$^-$): 498.24, found 498.10.

Elemental Analysis (%): (C$_{30}$H$_{33}$N$_3$O$_4$) Calcd. C 72.12, H 6.66, N 8.4 found C 71.61, H 6.91, N 7.55.

119

M.p.: 174 ºC.

^{1}H NMR (300 MHz, DMSO-d$_6$): δ = 8.94 (s, 1H, -NH-), 7.33 (s, 1H, 6-H), 7.11 (d, J = 6 Hz, 1H, 5-H), 6.93 (m, 3H, 4, 2-H), 6.66 (s, 2H, 3-H), 6.11(dd, J = 9,3 Hz, 2H, 1-H) 5.05 (s, 1H, Bridgehead-H), 5.03 (s, 1H, Bridgehead-H), 4.78 (s, 4H, NH$_2$-H), 1.45 (s, 9H, Boc-H) ppm

^{13}C NMR (125 MHz, DMSO-d$_6$): δ = 153.24 (Boc, C=O), 146.40 (C-11),145.81 (C-10), 141.56 (C-7), 136.03 (C-8), 134.57 (C-9), 123.32 (C-12), 122.55 (C-4), 114.69 (C-6), 114.34 (C-5), 110.98 (C-3), 109.21 (C-1), 79.17 (Boc-C), 55.24 (Bridgehead-C), 53.85 (Bridgehead-C), 28.49 (Boc, -CH$_3$) ppm.

IR (ATR): $\tilde{v}$ = 3347 (w), 2970 (w), 2928 (w), 1723 (s), 1609 (s), 1522 (s), 1478 (s), 1420 (m), 1367 (s), 1302 (w), 1231 (s), 1155 (s), 1095 (m), 1051 (s), 1027 (m), 945 (w), 895 (w), 843 (m), 807 (m), 773 (m), 658 (m) cm^{-1}.

MS (ESI): [M] $^+$: m/z calcd. For (C$_{25}$H$_{25}$N$_3$O$_2$$^+$): 399.41, found 399.21.

Elemental Analysis (%): (C$_{25}$H$_{25}$N$_3$O$_2$) Calcd. C 74.16, H 6.31, N 10.52 found C 74.24, H 6.63, N 10.19.

120

M.p.: 172 °C.

^{1}H NMR (300 MHz, DMSO-d$_6$): δ = 9.19 (s, 3H, -NH-), 7.62 (s, 3H, 3-H), 7.21 (d, J = 6 Hz 3H, 4-H), 6.93 (dd, J = 9,3 Hz, 3H, 2-H), 5.42 (s, 1H, Bridgehead-H), 5.34 (s, 1H, Bridgehead-H), 1.44 (s, 27H, Boc-H) ppm.

^{13}C NMR (100 MHz, DMSO-d$_6$): δ = 153.42 (C-Boc-C=O), 146.13 (C-5), 140.11 (C-6), 136.71 (C-1), 123.44 (C-4), 115.02 (C-3), 114.75 (C-2), 79.32 (Boc-C), 53.58 (Bridgehead-H), 51.13 (Bridgehead-C), 28.57 (C-Boc-CH$_3$) ppm.

IR (ATR): $\tilde{v}$ = 3321 (w), 2976 (w), 2932 (w), 1701 (s), 1598 (m), 1519 (s), 1479 (s), 1416 (m), 1392 (m), 1331 (s), 1287 (m), 1231 (s), 1154 (s), 1098 (m), 1050 (s), 956 (m), 896 (s), 847 (s), 812 (m), 773 (s), 649 (s) cm^{-1}.

MS (ESI): [M+Na] $^{+}$: m/z calcd. For (C$_{35}$H$_{41}$N$_3$O$_6$Na^{+}): 622.72, found 622.04.

Elemental Analysis (%): (C$_{35}$H$_{41}$N$_3$O$_6$) Calcd. C 70.10, H 6.89, N 7.01 found C 69.70, H 6.98, N 6.33.

5.3.2.2 Synthesis of tetra-tert-butyl ((9s,9's,10s,10's)-((pyridine-2,6-dicarbonyl) bis(azanediyl)) bis (9,10-dihydro-9,10- [1,2] benzenoanthracene-15,2,7-triyl)) tetracarbamate (117):
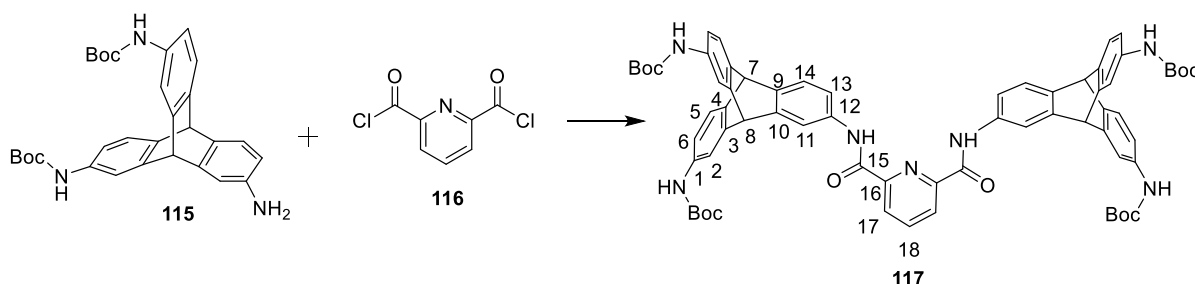
A solution of pyridine carbonyl dichloride **116** (20 mg, 0.49 mmol) in THF (2 mL) was added slowly to a solution of di-*t*-butoxycarbonylamido-tripycene **115** (100 mg, 0.2 mmol) in THF (8 mL), The solution was stirred at room temperature for 2 h. The solvent was removed under reduced pressure and the crude solid was washed with water and dried under vacuum to obtain the product as a colourless solid in a yield of 86% (99 mg, 0.086 mmol)

M.p.:353 °C (dec)

^{1}H NMR (300 MHz, DMSO-d$_6$) δ = 10.91 (s, 2H, -NH-pyridine), 9.22 (s, 4H, -NH-Boc), 8.36 (d, J = 6.0 Hz, 2H, H-17), 8.31 – 8.23 (m, 1H, H-18), 8.09 (s, 2H, H-11), 7.67 (s, 4H, H-13, 14), 7.44 (s, 4H, H-5), 7.27 (d, J = 9.0 Hz, 4H, H-2), 6.99 (d, J = 9.0 Hz, 4H, H-6), 5.60 (s, 2H, Bridgehead-H), 5.47 (s, 2H, Bridgehead-H), 1.45 (s, 36H) ppm.

MS (ESI): [M+Na] $^+$: m/z calcd. For (C$_{67}$H$_{67}$N$_7$O$_{10}$Na$^+$): 1152.48, found 1152.48.

IR (ATR): $\tilde{v}$ = 3329 (m), 2977 (m), 1696 (s), 1599 (m), 1521 (s), 1478 (s), 1416 (s), 1392 (s), 1367 (s), 1337 (s), 1303 (m), 1232 (s), 1155 (s), 1096 (w), 1051 (s), 1025 (s), 958 (m), 895 (s), 847 (m), 810 (s), 773 (s), 681 (m), 650 (m), 610 (m) cm^{-1}.

5.3.2.3 Synthesis of *N2, N6*-bis((9r,10r)-7,15-diamino-9,10-dihydro-9,10-[1,2] benzenoanthracen-2-yl)pyridine-2,6-dicarboxamide (118):
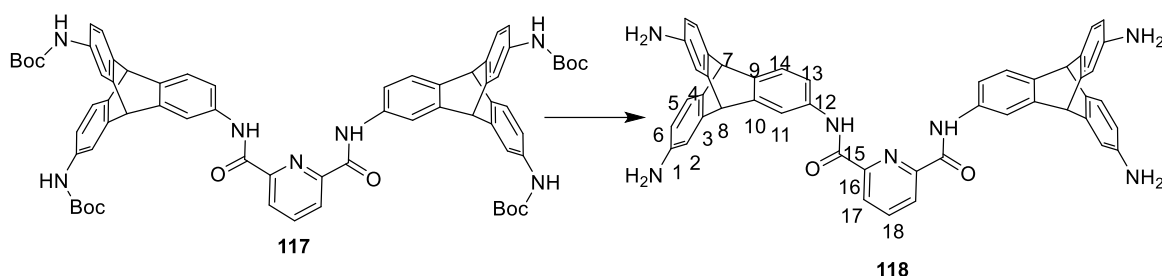
TFA (1 mL) was added to the solution of compound **117** (120.8 mg 0.11 mmol) in CH$_2$Cl$_2$ (10 mL), and stirred at room temperature for 4 h. After the reaction, the solution was poured in conc. NaHCO$_3$ solution (40 mL) and the solid was filtered. The solid was washed with water and dried under vacuum to give compound **118** as a colorless solid with a yield of 98% (79 mg, 0.107 mmol).

M.p.: 307 ºC.

^{1}H NMR (300 MHz, DMSO-d$_6$): δ = 10.87 (s, 2H, -NH-), 8.35 (m, 2H, H-17), 8.29-8.24 (m, 1H, H-18), 8.00 (s, 2H, H-11), 7.41 (dd, J = 7.8, 1.7 Hz, 2H, H-13), 7.33 (d, J = 7.9 Hz, 2H, H-14), 6.98 (d, J = 7.8 Hz, 4H, H-5), 6.71 (s, 4H, H-2), 6.13 (dd, J = 7.8, 1.7 Hz, 4H, H-6) 5.23 (s, 2H, Bridgehead-H), 5.15 (s, 2H, Bridgehead-H), 4.82 (s, 8H, -NH$_2$) ppm.

^{13}C NMR (125 MHz, DMSO-d6) δ = 161.92 (C-15), 149.45 (C-16), 146.65 (C-10), 146.44 (1-C-1), 146.07 (C-3), 144.02 (C-9), 140.32 (C-18), 134.66 (C-12), 134.43 (C-4), 125.62 (C-17), 123.58 (C-5), 122.77 (C-14), 117.70 (C-3), 117.44 (C-11), 111.11 (C-2), 109.40 (C-6), 53.78 (Bridgehead-C), 51.31 (Bridgehead-C) ppm

IR (ATR): $\tilde{v}$ = 3354 (m), 2958 (w), 2887 (w), 2606 (w), 2359 (w), 1669 (s), 1608 (s), 1531 (s), 1498 (s), 1478 (s), 1449 (s), 1423 (s), 1332 (m), 1258 (m), 1199 (s), 1182 (s), 1131 (s), 999 (w), 946 (w), 884 (w), 843 (s), 801 (s), 776 (s), 749 (m), 720 (s), 684 (s), 649 (m), 618 (m) cm^{-1}.

MS (MALDI-TOF, DCTB): [M]$^+$: m/z calcd. For ($C_{47}H_{35}N_7O_2^+$): 729.29, found 729.267.

Elemental Analysis (%): ($C_{47}H_{35}N_7O_2 \cdot 3H_2O$) Calcd. C 72.01, H 5.27, N 12.51 found C 72.44, H 5.05, N 12.64.

5.3.2.4 Synthesis of 5,5'-methylenebis(2-hydroxybenzaldehyde) (121):[169]
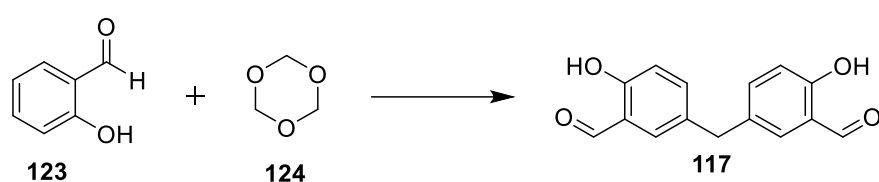
A solution of trioxane **124** (0.9 g, 0.009 mol) in a mixture of concentrated sulfuric acid (0.12 mL) and glacial acetic acid (0.6 mL) was added slowly to a solution of salicylaldehyde **123** (10 g, 0.08 mol) in glacial acetic acid (12.5 mL) under Ar. The reaction mixture was heated to 90 °C for 22 h. The reaction mixture was allowed to stand in an ice bath overnight. The precipitate was filtered, dissolved in methanol and poured into water. The precipitate was filtrated and recrystallized from acetone (40 mL) to give the product as a colourless solid with a yield of 43% (4.83 g, 0.017 mol).

M.p.: 142 °C [Lit.: 142-143 °C].[169]

^{1}H NMR (300 MHz, CDCl$_3$): δ =10.84 (s, 2H), 9.78 (s, 2H), 7.19-7.29 (m, 4H), 6.8 (d, J =7.5 Hz, 2H), 3.89 (s, 2H) ppm.

Analytical data are in accordance with those previously reported.[169]

5.3.2.5 Synthesis of 1,2-bis(4-methoxyphenyl) ethane (126):[49b]
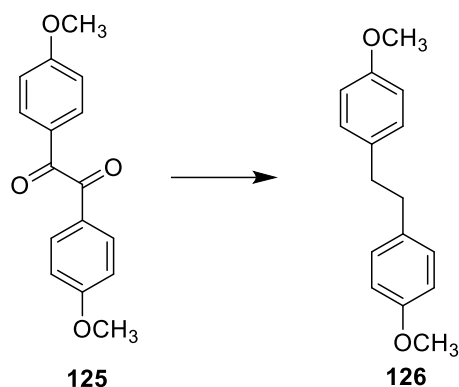
Zinc dust (20.0 g, 0.31 mol) and mercury (II) chloride (2.00 g, 7.37 mmol) were suspended in water (34 mL) and hydrochloric acid (0.7 mL) and stirred for 5 min at room temperature. The aqueous phase was decanted and the residue was washed with water (50 mL).

The amalgamated zinc was added to the suspension of Anisil **125** (6.00 g, 22.2 mmol) in hydrochloric acid solution (6 mol/L, 70 mL) and heated to reflux for 5 h. Concentrated hydrochloric acid was added to the reaction mixture at a rate of 4 mL per hour. After cooling to room temperature, DCM (50 mL) was added to the reaction mixture, the solid was filtered and the filtrate was washed with a saturated sodium bicarbonate solution (50 mL) and a saturated sodium chloride solution (50 mL). The organic phase was dried over Na_2SO_4. The solvent was removed under reduced pressure, and the residue was recrystallized from ethanol to obtain the product as a colourless solid with a yield of 89% (4.79 g, 19.7 mmol).

M.p.: 126 °C [Lit.: 126-127 °C].[49b]

^{1}H-NMR (300 MHz, CDCl$_3$): δ = 7.10 – 7.07 (m, 4H), 6.84-6.81 (m, 4H), 3.79 (s, 6H), 2.83 (s, 4H) ppm.

Analytical data are in accordance with those previously reported.[49b]

5.3.2.6 Synthesis of 5,5'-(ethane-1,2-diyl) bis(2-methoxybenzaldehyde) (123):[49b]

126   127
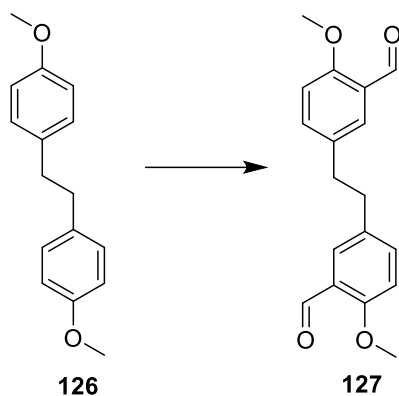
1,2-Bis(4-anisyl) ethane **126** (1.5 g, 6.2 mmol) and hexamethylentetramine (3.47 g, 24.8 mmol) were dissolved under argon in anhydrous trifluoroacetic acid (25 mL) and stirred for 24 h at 110 °C. After cooling to room temperature, the solution was poured into a mixture of 4 mol/L hydrochloric acid (100 mL) and dichloromethane (100 mL) and stirred overnight. The aqueous layer was extracted with dichloromethane (3×75 mL). The combined organic layers were washed with 4 mol/L hydrochloric acid (2×100 mL), water (100 mL), brine (100 mL) and dried over Na_2SO_4. The solvent was removed under reduced pressure. The crude product was purified by column chromatography (silica gel, dichloromethane, $R_f = 0.1$) to give the pure product as a colourless solid with a yield of 56% (1.12 g, 3.42 mmol).

M.p.: 155 °C [Lit.: 155 °C].[49b]

^{1}H NMR (300 MHz, CDCl$_3$): $\delta = 10.37$ (s, 2H, -CHO), 7.55 (d, $J = 2.1$ Hz, 2H,), 7.22 (dd, $J = 8.5, 2.1$ Hz, 2H, Aryl-5,5'-H), 6.83(d, $J = 8.5$ Hz, 2H,), 3.84 (s, 6H), 2.80 ppm (s, 2H)

Analytical data are in accordance with those previously reported.[49b]

5.3.2.7 Synthesis of 5,5'-(ethane-1,2-diyl) bis(2-hydroxybenzaldehyde) (22):[49a]

127   22
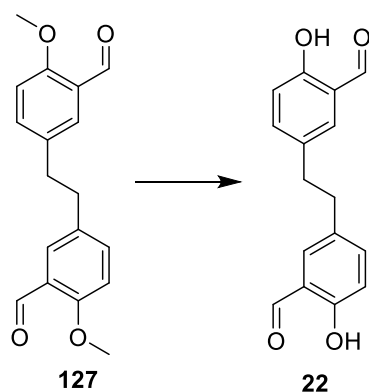
1,2-Bis(3-formyl-4-anisyl) ethane **127** (1.79 g, 6.00 mmol) was dissolved in abs. dichloromethane (30 mL) under argon and cooled to -20 ℃ (acetone/ dry ice). BBr$_3$ (1.25 mL, 13.2 mmol) was added and the mixture was stirred for 30 min at -20 ℃. The reaction mixture was allowed to warm up to room temperature for 3 h. A saturated sodium hydrogen carbonate solution (20 mL) was added to the reaction mixture, followed by ethyl acetate (30 mL). The aqueous layer was extracted with ethyl acetate (3 × 40 mL). The combined organic layers were washed with a saturated sodium hydrogencarbonate solution (50 mL) and brine (50 mL), and dried over Na$_2$SO$_4$. The solvent was removed under reduced pressure and the crude product was purified by column chromatography (silica gel, dichloromethane, R_f = 0.36) to give the product as a colourless solid with a yield of 73% (1.12 g, 4.38 mmol).

M.p.: 180 ℃ [Lit: 181 ℃].[49a]

^{1}H NMR (300 MHz, CDCl3): δ = 10.80 (s, 2H), 9.77 (s, 2H), 7.24 – 7.17 (m, 4H), 6.85 (m, 2H), 2.84 ppm (s, 4H) ppm.

Analytical data are in accordance with those previously reported.[49a]

5.3.2.8 Synthesis of 4,4''-dihydroxy-[1,1':4',1''-terphenyl] -3,3''-dicarbaldehyde (102):[49b]
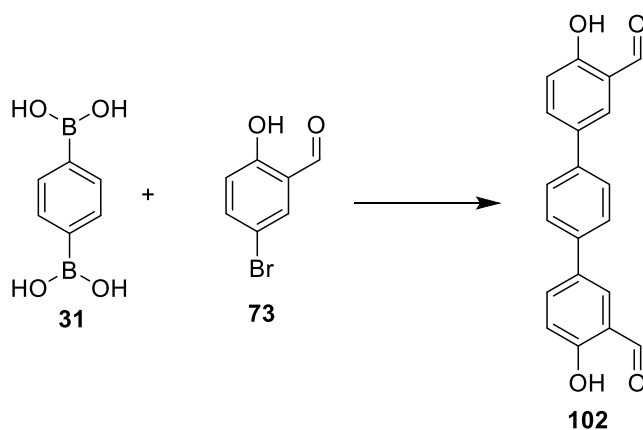
Benzene-1,4-diboronic acid **31** (0.5 g, 3.02 mmol), 4-bromosalicyladehyde **73** (1.3 g, 6.04 mmol) and Pd(PPh$_3$)$_4$ (100 mg) were added to a mixture of THF (15 mL) and 2 M potassium carbonate solution (10 mL) under Ar. The mixture was heated to 85 °C for 24 h. After cooling to room temperature, the reaction mixture was poured in 150 mL water. The aqueous layer was extracted with dichloromethane (3 × 10 mL). The combined organic layers were washed with water and dried over NaSO$_4$. The solvent was removed under reduced pressure and the residue

was purified by column chromatography (silica gel, toluene, $R_f = 0.25$) to give a yellow solid with a yield of 32% (300 mg, 0.96 mmol).

M.p.: 234 ºC [Lit.: 234 ºC].[49b]

^{1}H NMR (300 MHz, CDCl$_3$): δ =10.87 (s, 2H, -OH), 10.34 (s, 2H, -CHO), 7.98 (d, J = 2.4 Hz, 2H), 7.91 (dd, J = 8.6, 2.4 Hz, 2H), 7.74 (s, 4H,),7.11 (d, J = 8.6 Hz, 2H) ppm.

Analytical data are in accordance with those previously reported.[49b]

5.3.2.9 Synthesis of 4,4'- biphenyldiboronic acid dipinacol ester (128):[170]

128
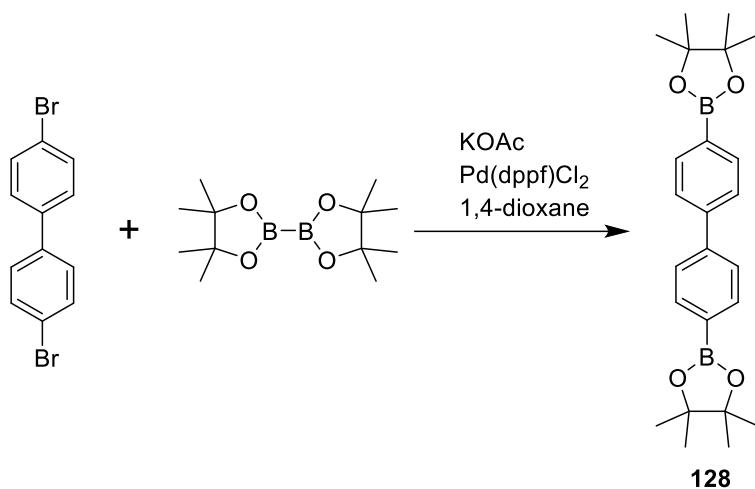
4,4' – dibromobiphenyl (1.56 g, 5 mmol), bis(pinacolato)diboron (2.66 g, 10.5 mmol) and 1,4-dioxane (40 mL) were placed in a flask under argon and then Pd(dppf)Cl$_2$ (50 mg) was added to the flask. The mixture was degassed three times and refluxed overnight (~12 h). The mixture was poured in 100 mL of water and extracted with dichloromethane (3 × 30 mL). The organic layers were dried over NaSO$_4$ and evaporated. The crude product was dissolved in dichloromethane (100 mL) and passed through a short pad of silica gel. After evaporation of the solvent, the residue was crystallized from acetone to give the pure product with a yield of 56 % (1.2 g, 2.8 mmol).

M.p.: 247 °C

^{1}H NMR (300 MHz, CDCl$_3$) δ = 7.88 (d, J = 8.2 Hz, 4H), 7.63 (d, J = 8.2 Hz, 4H), 1.36 (s, 24H) ppm.

^{13}C NMR (125 MHz, CDCl$_3$) δ = 143.68, 135.26, 126.52, 83.84, 24.67 ppm.

Analytical data are in accordance with those previously reported.[170]

5.3.2.10 Synthesis of *t*-Bu-quarterphenyl salicyl aldehyde (122):
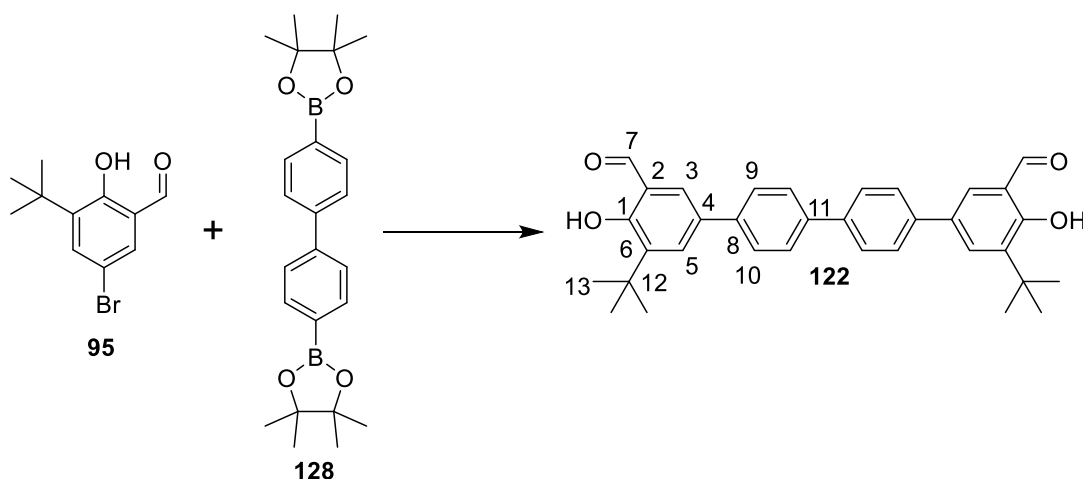
Compound **95** (146.2 mg, 0.57 mmol) and boronic ester **128** (92.4 mg, 0.22 mmol) and [(*t*-Bu)$_3$PH]BF$_4$ (14.5 mg, 0.05 mmol) were suspended into THF (2 mL) and K$_2$CO$_3$ solution (2 mol/L, 0.5 mL) in a screw cap vessel. The suspension was stirred under Ar for 5 min. Pd$_2$(dba)$_3$ (11.5 mg, 0.02 mmol) was added to the reaction mixture and then the suspension was heated to 90 °C for 16 h. After cooling to room temperature, the suspension was poured in water (5 mL), and extracted with CH$_2$Cl$_2$ (3 × 10 mL). The combined organic layers were washed with water (3 × 10 mL), and dried over Na$_2$SO$_4$. The solvent was removed under reduced pressure and the crude product was purified by column chromatography (silica gel, DCM:PE = 1:1, R_f = 0.5) to give the product as a yellow solid with a yield of 34% (40 mg, 0.078 mmol).

M.p.:276 °C.

^{1}H NMR (300 MHz, CDCl$_3$) δ = 11.82 (s, 2H, -OH), 9.99 (s, 2H, H-7), 7.83 (d, J = 2.2 Hz, 2H, H-3), 7.76 (s, 2H, H-5), 7.73 (s, 2H, H-9), 7.66 (m, 6H), 1.50 (s, 18H, H-13) ppm.

^{13}C NMR (125 MHz, CDCl$_3$) δ = 197.27 (C-7), 160.76 (C-1), 139.37 (C-8), 139.21 (C-11), 138.90 (C-6), 133.06 (C-5), 131.88 (C-2), 129.9 (C-4), 127.52 (C-3), 127.16 (C-10), 120.81 (C-9), 35.10 (C-12), 29.27 (C-13) ppm.

IR (ATR): $\tilde{v}$ = 2959 (w), 2856 (w), 1643 (s), 1610 (w), 1502 (w), 1481 (w), 1463 (w), 1442 (s), 1421 (m), 1391 (m), 1367 (w), 1333 (w), 1294 (w), 1267 (w), 1253 (w), 1221 (w), 1199 (w), 1166 (s), 1074 (w), 1002 (w), 957 (w), 934 (w), 884 (w), 855 (w), 822 (s), 801 (w), 757 (s), 711 (s), 621 (w) cm^{-1}.

MS (ESI): [M-H]$^-$: *m/z* calcd. For (C$_{34}$H$_{33}$O$_4$$^-$): 505.24, found 505.2384.

Elemental Analysis (%): ($C_{34}H_{34}O_4$) Calcd. C 80.60, H 6.76 found C 80.32, H 6.81.

5.3.2.11 Synthesis of Cage compound 129:
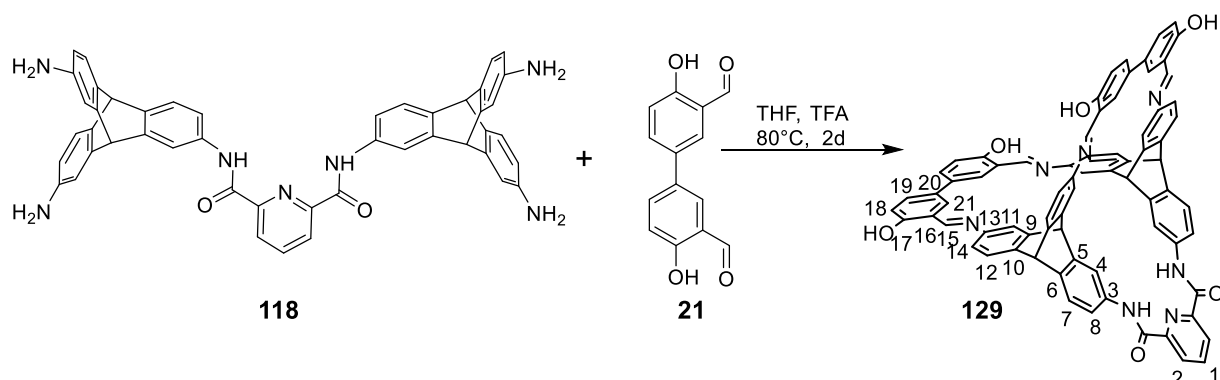
Amine **114** (36.5 mg, 0.05 mmol) and biphenyl disalicyaldehyde **21** (24.3 mg, 0.1 mmol) were dissolved in DMF (10 mL). TFA solution (0.1 mol/L in DMF, 10 µL) was added and stirred under Ar for 10 min. The reaction mixture was heated to 90 °C for 2 days. After cooling to room temperature, the reaction mixture was concentrated to 5 mL, dropped into methanol (5 mL) and stirred for 30 min. The precipitates were filtered and washed with THF (3 × 10 mL) then pentane (3 × 10 mL) to obtain the product as an orange solid in a yield of 36% (21 mg, 0.018 mmol). Crystals were obtained by diffusing methanol into a DMF solution.

M.p.: >400 °C.

^{1}H NMR (600 MHz, THF-d$_8$) δ = 11.66 (s, 4H, -OH), 10.04 (s, 2H, -NH-), 9.12 (s, 4H, 15-H), 8.54 (dd, J = 8.1, 1.6 Hz, 2H, 2-H), 8.51 (d, J = 7.7 Hz, 2H, 7-H), 8.16 (t, J = 7.7 Hz, 1H, 1-H), 8.00 (d, J = 1.7 Hz, 4H, 21-H), 7.76 (s, 4H, 11-H), 7.73 (dd, J = 8.4, 2.1 Hz, 4H, 18-H), 7.58 (s, 2H, 4-H), 7.57 (d, J = 7.9 Hz, 4H, 12-H), 7.50 (d, J = 8.2 Hz, 2H, 8-H), 7.21 (dd, J = 7.9, 1.6 Hz, 4H, 14-H), 7.00 (d, J = 8.3 Hz, 4H, 19-H), 5.72 (d, J = 3.2 Hz, 2H, Bridgehead-H) ppm.

^{13}C NMR (150 MHz, THF-d$_8$) δ = 161.11 (C=O), 160.86 (C-15), 158.96 (C-C=O), 149.42 (C-17), 145.92 (C-5), 145.80 (C-13), 144.95 (C-10), 144.01 (C-9), 140.63 (C-3), 138.74 (C-1), 135.68 (C-6), 130.30 (C-16), 130.22 (C-21), 129.04 (C-18), 125.53 (C-7), 124.09 (C-8), 123.82 (C-12), 122.03 (C-14), 119.96 (C-20), 116.52 (C-19), 116.15 (C-2), 114.42 (C-4), 112.61 (C-11), 54.82 (Bridgehead-C), 51.88 (Bridgehead-C) ppm.

IR (ATR): $\tilde{v}$ = 3049 (w), 2953 (m), 2921 (s), 2852 (s), 1649 (s), 1586 (s), 1476 (s), 1387 (m), 1342 (m), 1316 (s), 1274 (s), 1224 (s), 1167 (s), 1126 (m), 899 (m), 839 (s), 730 (s), 668 (s), 634 cm^{-1}

MS (ESI): [M+H]$^+$: *m/z* calcd. For ($C_{75}H_{48}N_7O_6^+$): 1142.24, found 1142.403.

Elemental Analysis (%): ($C_{75}H_{47}N_7O_6·6H_2O$) Calcd. C 72.05, H 4.76, N 7.84 found C 72.40, H 5.10, N 7.70.

5.3.3 Compounds of Chapter 3.3

5.3.3.1 Syntheisis of 4,4'-dihydroxy-[1,1'-biphenyl]-3,3'-dicarbaldehyde (21):[49a]
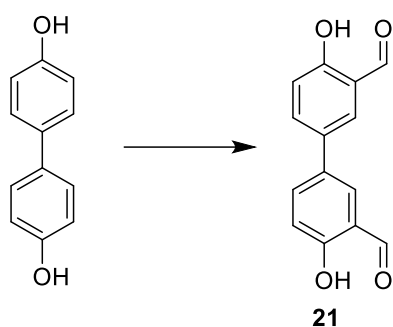
4,4'-Dihydroxybiphenyl (3 g, 16 mmol) and hexamethylenetetraamine (5.06 g, 36 mmol) were dissolved under argon in anhydrous trifluoroacetic acid (35 mL) and stirred at 110 °C for 3 h. After cooling to room temperature, the solution was poured into 4 N hydrochloric acid (350 mL) and stirred overnight. The yellow solid was collected by filtration, washed with water (3 × 100 mL) and dried under vacuum. The crude product was purified by column chromatography (silica gel, dichloromethane, R_f = 0.27) to give the pure product as a yellow solid with a yield of 31% (1.23 g, 4.96 mmol).

M.p.: 231 ºC [Lit 49: 231 °C].[49a]

^{1}H NMR (300 MHz, DMSO): δ = 10.84 (s, 2H), 10.32 (s, 2H), 7.89 (d, J = 2.5 Hz, 2H), 7.82 (dd, J = 8.6, 2.5 Hz, 2H), 7.09 ppm (d, J = 8.6 Hz, 2H) ppm.

Analytical data are in accordance with those previously reported.[49a]

5.3.3.2 Synthesis of [2+3] bisphenyl imine cage (24):[49a]
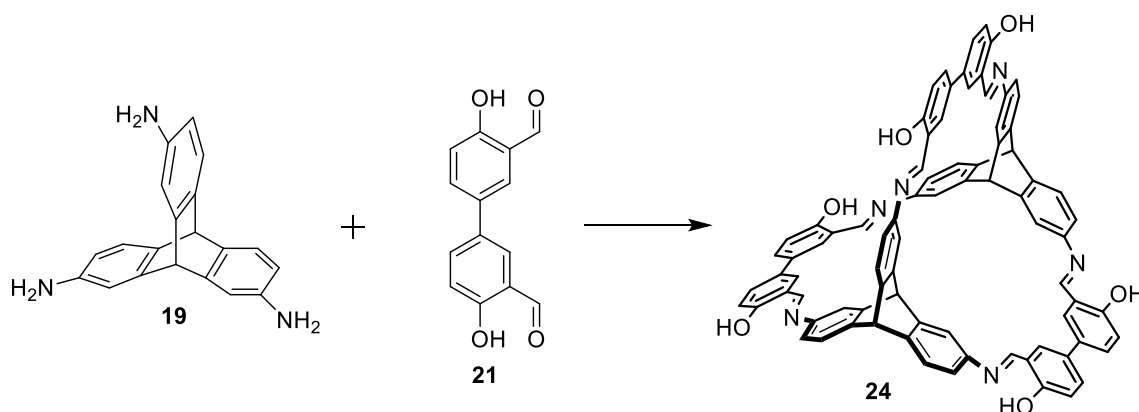
Triptycene triamine **19** (76.5 mg, 0.26 mmol) and aldehyde **21** (92.9 mg, 0.38 mmol) were dissolved in dry THF (40 mL) under argon and TFA (6.4 µL, 2 mol%) was added. The yellow solution was refluxed for 2 d at 90 ℃. After cooling the reaction mixture to room temperature, the solid was collected by filtration. The product was obtained by adding n-pentane (40 mL) to the filtrate. The precipitate was collected and washed with n-pentane (5 mL) to give cage compound **24** as an orange solid with the yield of 56% (88 mg, 0.073 mmol).

M.p.: > 410 ℃ [Lit.: >410 °C].[49a]

^{1}H NMR (THF, 500 MHz): δ = 12.69 (s, 6H), 9.16 (s, 6H,), 7.82 (d, J = 2.0 Hz, 6H), 7.75 (d, J = 2.3 Hz, 6H), 7.66 (dd, J = 8.5, 2.4 Hz, 6H), 7.57 (d, J = 7.8 Hz, 6H), 7.21 (dd, J = 7.8, 2.0 Hz, 6H), 7.01 (d, J = 8.5 Hz, 6H), 5.75 (s, 2H), 5.72 (s, 2H) ppm.

Analytical data are in accordance with those previously reported.[49a]

5.3.3.3 Synthesis of [2+3] bisphenyl amine cage (130).
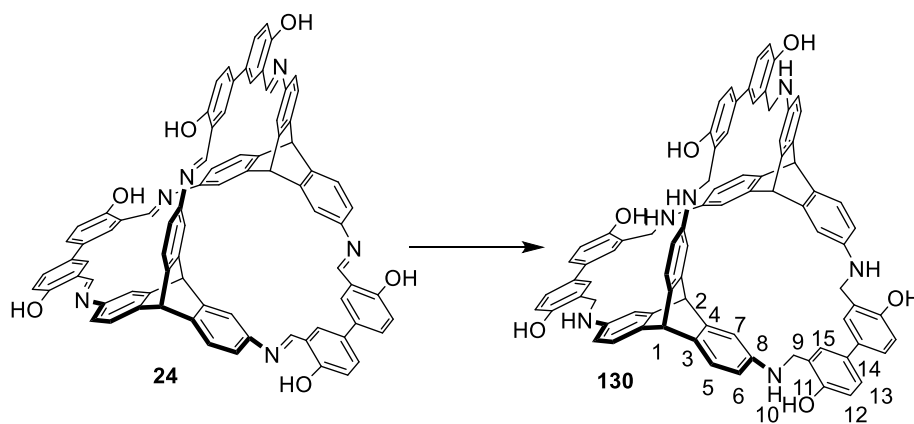
Cage **24** (30 mg, 0.02 mmol) was suspended in a mixture of methanol (5 mL) and THF (5 mL) and then NaBH₄ (40 mg,1.05 mmol) was added to the solution. The suspension was stirred for

15 h at room temperature. Methanol and THF were removed by rotary evaporation. The white solid was suspended in water (10 mL) and extracted with ethyl acetate (3 × 10 mL). The combined organic phase was dried with Na_2SO_4 and the solvent removed by rotary evaporation. The solid was dried in vacuum at 90 °C, giving **130** as a light yellow solid with a yield of 54% (16 mg, 0.108 mmol).

M.p.: >410 °C.

^{1}H NMR (300 MHz, DMSO-d$_6$): δ = 9.38 (s, 6H, -OH), 7.61 (d, J = 0.9 Hz, 6H, 15-H), 7.24 (dd, J = 6, 1.2 Hz, 6H, 13-H), 7.00 (br s, 6H, 7-H), 6.96 (d, J = 9 Hz, 6H, 5-H), 6.78 (d, J = 6 Hz, 6H, 12-H), 6.16 (d, J = 9 Hz, 6H, 6-H), 5.39 (s, 6H, -NH), 5.32 (s, 2H, Bridgehead-H), 4.98 (s, 2H, Bridgehead-H), 4.15 (d, J = 3 Hz, 12H, 9-H) ppm.

^{13}C NMR (DMSO-d$_6$, 125 MHz, 373.15K): δ = 154.69 (s, C-11), 146.91 (s, C-4), 146.53 (s, C-3), 136.02 (s, C-8), 131.61 (s, C-14), 127.41 (s, C-15), 126.73 (s, C-10), 125.67 (s, C-13), 123.20 (s, C-5), 116.19 (s, C-12), 110.14 (s, C-7), 108.45 (s, C-6), 55.62 (s, Bridgehead-C), 51.14 (s, Bridgehead-C), 43.62 (s, C-9) ppm.

IR(ATR): $\tilde{v}$ = 3341 (w, br), 2921 (w), 2868 (w), 1655 (m), 1608 (s), 1486 (s), 1442 (m), 1384 (m), 1345 (m), 1243 (s), 1183 (s), 1150 (m), 1116 (m), 1093 (m), 1058 (m), 991 (m), 940 (w), 813 (s), 775 (m), 668 (w) cm^{-1}.

MS (MALDI-TOF, DCTB): [M]$^+$: m/z calcd. For ($C_{82}H_{64}N_6O_6^+$): 1229.45, found 1229.495.

Elemental Analysis (%): ($C_{82}H_{64}N_6O_6 \cdot 4H_2O$) Calcd. C 75.67, H 5.58, N 6.46, found C 75.51, H 5.52, N 6.45.

5.3.3.4 Synthesis of [2+3] bisphenyl carbamate cage (131):
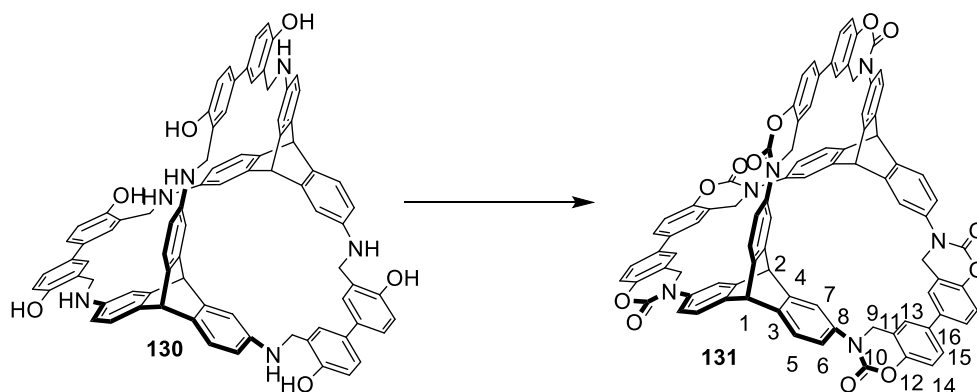
Cage **130** (30 mg, 0.024 mmol) and carbonyldiimidazole (70 mg, 0.43 mmol) were dissolved in dry DMF (3 mL) and the reaction mixture stirred for two days at room temperature. DMF was removed by rotary evaporation. The crude product was suspended in 0.1 mol/L NaOH solution and stirred for 1 h. The precipitate was collected by filtration and washed with water (3 × 10 mL). The crude product was purified by short column chromatography (silica gel, chloroform) and dried in vacuum to give pure cage compound **131** with a yield of 62% (20 mg, 0.015 mmol) as a white solid. Crystal A was obtained by diffusing methanol into DMF solution. Crystal B was obtained by dropping hot DMSO solution into acetone.

M.p. > 410 °C.

^{1}H NMR (300 MHz, DMSO-d$_6$): δ = 7.56 (d, J = 12 Hz, 6H, 6-H), 7.45 (dd, J = 12,1.8 Hz, 6H, 15-H), 7.33 (d, J = 1.8 Hz, 6H, 13-H), 7.30 (dd, J = 12, 1.8 Hz, 6H, 5-H), 7.21 (m, 12H), 5.85 (s, 2H, Bridgehead-H), 5.54 (s, 2H, Bridgehead-H), 4.85 (s, 12H, 9-H) ppm.

^{13}C NMR (DMSO-d$_6$, 125 MHz, 373.15K): δ = 150.61 (s, C-12), 150.32 (s, C-11), 146.83 (s, C-3), 144.12 (s, C-4), 139.07 (s, C-8), 137.72 (s, C-16), 128.07 (s, C-15), 125.88 (s, C-13), 124.54 (s, C-5), 124.27 (s, C-6), 122.39 (s, C-11), 121.04 (s, C-7), 116.54 (s, C-14), 53.43 (s, Bridgehead-C), 52.07 (s, Bridgehead-C), 50.73 (s, C-9) ppm.

IR (ATR): $\tilde{v}$ = 1729 (s), 1609 (w), 1478 (m), 1437 (m), 1385 (m), 1236 (s), 1216 (m), 1177 (s), 1159(s), 1106 (s), 1000 (m), 922 (m), 881(w), 830 (m), 790 (w), 773 (w), 750 (m), 679 (w), 630 (w) cm^{-1}

MS (MALDI-TOF, DCTB): [M]$^+$: m/z calcd. For (C$_{88}$H$_{52}$N$_6$O$_{12}^+$): 1385.41, found 1385.367.

Elemental Analysis (%): (C$_{82}$H$_{52}$N$_6$O$_{12}$·3H$_2$O·DMF) Calcd. C 72.26, H 4.33, N 6.48, found C 72.10, H 4.25, N 6.43.

6 Reference

[1] a) W. Cullen, M. C. Misuraca, C. A. Hunter, N. H. Williams, M. D. Ward, *Nat. Chem.* **2016**, *8*, 231–236. b) M. Yoshizawa, J. K. Klosterman, M. Fujita, *Angew. Chem., Int. Ed*. **2009**, *48*, 3418–3438.

[2] S. Das, P. Heasman, T. Ben, S. Qiu, *Chem. Rev*., **2017**, *117*, 1515-1563.

[3] P. Muller, *Pure Appl. Chem.,* **1994**, *66*, 1077.

[4] W. Zhang, Y. Jin, *Dynamic Covalent Chemistry: principles, reactions, and applications.* Wiley, 2017.

[5] K. S. Iyer, M. Norret, S. J. Dalgarno, J. L. Atwood, C. L. Raston, *Angew. Chem., Int. Ed.* **2008**, *47*, 6362–6366.

[6] a) S. J. Dalgarno, N. P. Power, J. L. Atwood, *Coord. Chem. Rev*. **2008**, *252*, 825–841. b) Z. Laughrey, B. C. Gibb, *Chem. Soc. Rev*. **2011**, *40*, 363–386.

[7] a) K. Suzuki, M. Tominaga, M. Kawano, M. Fujita, *Chem. Commun*., **2009**, 1638-1640. b) M. Tominaga, K. Suzuki, M. Kawano, T. Kusukawa, T. Ozeki, S. Sakamoto, K. Yamaguchi, M. Fujita, Angew. Chem. Int. Ed., 2004, 43, 5621–5625. c) Q.-F. Sun, J. Iwasa, D. Ogawa, Y. Ishido, S. Sato, T. Ozeki, Y. Sei, K. Yamaguchi, and M. Fujita, *Science*, **2010**, *328*, 1144–1147.

[8] a) M. Yoshizawa, M. Tamura, and M. Fujita, *Science*, **2006**, *312*, 251–254. b) D. Fujita, K. Suzuki, S. Sato, M. Yagi-Utsumi, Y. Yamaguchi, N. Mizuno, T. Kumasaka, M. Takata, M. Noda, S. Uchiyama, K. Kato, and M. Fujita, *Nat. Commun*., **2012**, *3*, 1093.

[9] a) N. Nishimura, K. Kobayashi, *J. Org. Chem.*, **2010**, *75*, 6079–6085. b) P. Mal, B. Breiner, K. Rissanen, J. R. Nitschke*, Science* **2009**, *324*, 1697–1699.

[10] G. Zhang, M. Mastalerz, *Chem. Soc. Rev.* **2014**, *43*, 1934–1947.

[11] M. Mastalerz, *Angew. Chem., Int. Ed*. **2010**, *49*, 5042–5053

[12] P. E. Eaton, T. W. Cole, *J. Am. Chem. Soc.*, **1964**, *86*, 3157–3158.

[13] a) L. A. Paquette, R. J. Ternansky, D. W. Balogh, G. Kentgen, *J. Am. Chem. Soc*., **1983**, *105*, 5446. b) W.-D. Fessner, B. A. R. C. Murty, J. Wörth, D. Hunkler, H. Fritz, H. Prinzbach, W. D. Roth, P. v. R. Schleyer, A. B. McEwen, W. F. Maier, *Angew. Chem., Int. Ed. Engl.,* **1987**, *26*, 452.

[14] B. Dietrich, J. M. Lehn, J. P. Sauvage, *Tetrahedron Lett*., **1969**, *10*, 2885–2888.

[15] W. Kiggen, F. Vögtle, *Angew. Chem., Int. Ed. Engl*., **1984**, *23*, 714–715.

[16] D. J. Cram, S. Karbach, Y. H. Kim, L. Baczynskyj, G. W. Kalleymeyn, *J. Am. Chem. Soc.*, **1985**, *107*, 2575–2576.

[17] J. D. Evans, C. J. Sumby, C. J. Doonan, *Chem. Lett*. **2015**, *44*, 582–588.

[18] Z. Wu, S. Lee, J. S. Moore, *J. Am. Chem. Soc.*, **1992**, *114*, 8730–8732.

[19] a) A. Avellaneda, P. Valente, A. Burgun, J. D. Evans, A. W. Markwell-Heys, D. Rankine, D. J. Nielsen, M. R. Hill, C. J. Sumby, C. J. Doonan, *Angew. Chem., Int. Ed.* **2013**, *52*, 3746–3749. b) M. M. Naseer, D. X. Wang, L. A. Zhao, Z. T. Huang, M. X. Wang, *J. Org. Chem.* **2011**, *76*, 1804–1813.

[20] a) F. Ebmeyer, F. Vögtle, *Angew. Chem., Int. Ed. Engl.*, **1989**, *28*, 79–81. b) A. Wallon, J. Peter-Katalinića, U. Wener, W. M. Müller, F. Vögtle, *Chem. Ber.*, **1990**, *123*, 375–379.

[21] T. J. McMurry, S. J. Rodgers, K. N. Raymond, *J. Am.Chem. Soc.*, **1987**, *109*, 3451-3453.

[22] T. J. Ryan, G. Lecollinet, T. Velasco, A. P. Davis, *Proc. Natl. Acad. Sci. U. S. A.*, **2002**, *99*, 4863–4866.

[23] J. L. Katz, K. J. Selby, R. R. Corny, *Org. Lett.*, **2005**, *7*, 3505-3507.

[24] F. Vögtle, J. Gross, C. Seel and M. Nieger, *Angew. Chem., Int. Ed. Engl.*, **1992**, *31*, 1069–1071.

[25] H.-E. Hoegberg, O. Wennerstroem, *Acta Chem. Scand., Ser. B,* **1982**, *B36*, 661–667.

[26] P. R. Ashton, N. S. Isaacs, F. H. Kohnke, G. S. D'Alcontes, J. F. Stoddart, *Angew. Chem., Int. Ed. Engl.*, **1989**, *28*, 1261–1263.

[27] P. T. Corbett, J. Leclaire, L. Vial, K. R. West, J. L. Wietor, J. K. M. Sanders, S. Otto, *Chem. Rev.*, **2006**, *106*, 3652–3711.

[28] a) S. J. Rowan, S. J. Cantrill, G. R. L. Cousins, J. K. M. Sanders, J. F. Stoddart, *Angew. Chem. Int. Ed.* **2002**, *41*, 898–952. b) Y. Jin, C. Yu, R. J. Denman, W. Zhang, *Chem. Soc. Rev.* **2013**,*42*, 6634–6654.

[29] a) A. Martinez-Castaneda, H. Rodriguez-Solla, C. Concellon, V. del Amo, *Org. Biomol. Chem.*, **2012**, *10*, 1976–1981. b) P. Vongvilai, M. Angelin, R. Larsson, O. Ramstrom, *Angew. Chem., Int. Ed.,* **2007**, *46*, 948–950.

[30] C. D. Gutsche, D. E. Johnston, D. R. Stewart, *J. Org. Chem.*, **1999**, *64*, 3747–3750.

[31] M. E. Belowich, J. F. Stoddart, *Chem. Soc. Rev.*, **2012**, *41*, 2003–2024.

[32] R. Nishiyabu, Y. Kubo, T. D. James, J. S. Fossey, *Chem. Commun.*, **2011**, *47*, 1124–1150.

[33] a) M. Mastalerz, *Acc. Chem. Res.* **2018**, *51*, 2411–2422. b) Q. Wang, C. Yu, H. Long, Y. Du, C. Zhang, S. Azarnoush, Y. Jin, W. Zhang, *Chem. Sci.* **2016**, *7*, 3370–3376.

[34] a) K. Severin, *Dalton Trans.*, **2009**, 5254–5264. b) R. Nishiyabu, Y. Kubo, T. D. James, J. S. Fossey, *Chem. Commun.*, **2011**, *47*, 1124–1150.

[35] a) M. E. Belowich, J. F. Stoddart, *Chem. Soc. Rev.*, **2012**, *41*, 2003–2024.

[36] M. L. Quan, D. J. Cram, *J. Am. Chem. Soc.* **1991**, *113*, 2754–2755.

[37] S. Ro, S. J. Rowan, A. R. Pease, D. J. Cram, J. F. Stoddart, *Org. Lett.* **2000**, *2*, 2411–2414.

[38] X. Liu, Y. Liu, G. Li, R. Warmuth, *Angew. Chem. Int. Ed*, **2006**, *45*, 901–904.

[39] Y. Liu, X. Liu, R. Warmuth, *Chem. Eur. J.* **2007**, *13*, 8953–8959.

[40] X. Liu, R. Warmuth, J. Am. Chem. Soc. 2006, 128, 14120–14127.

[41] M. E. Briggs, A. I. Cooper, *Chem. Mater*. **2017**, *29*, 149–157.

[42] P. Skowronek, J. Gawronski, *Org. Lett*, **2008**, *10*, 4755–4758.

[43] T. Tozawa, J. T. A. Jones, S. I. Swamy, S. Jiang, D. J. Adams, S. Shakespeare, R. Clowes, D. Bradshaw, T. Hasell, S. Y. Chong, C. Tang, S. Thompson, J. Parker, A. Trewin, J. Bacsa, A. M. Z. Slawin, A. Steiner, A. I. Cooper, *Nature Mater*., **2009**, *8*, 973–978.

[44] K. E. Jelfs, E. G. B. Eden, J. L. Culshaw, S. Shakespeare, E. O. Pyzer-Knapp, H. P. G. Thompson, J. Bacsa, G. M. Day, D. J. Adams, A. I. Cooper, *J. Am. Chem. Soc.*, **2013**, *135*, 9307–9310.

[45] M. Mastalerz, *Chem. Commun.*, **2008**, 4756–4758.

[46] M. W. Schneider, I. M. Oppel, H. Ott, L. G. Lechner, H.-J. S. Hauswald, R. Stoll, M. Mastalerz, *Chem. Eur. J.*, **2012**, *18*, 836–847.

[47] M. Mastalerz, M. W. Schneider, I. M. Oppel, O. Presly, *Angew. Chem. Int. Ed.*, **2011**, *50*, 1046–1051.

[48] M. W. Schneider, H. S. Hauswald, R. Stoll, M. Mastalerz, *Chem. Commun.*, **2012**, *48*, 9861–9863.

[49] a) M. W. Schneider, I. M. Oppel, M. Mastalerz, *Chem. Eur. J.*, **2012**, *18*, 4156–4160. b) Markus Willibald Schneider, PhD thesis 2015, Universität Ulm

[50] F. Beuerle, B. Gole, *Angew. Chem. Int. Ed*. **2018**, 57, 4850–4878.

[51] G. Zhang, O. Presly, F. White, I. M. Oppel, M. Mastalerz, *Angew. Chem. Int. Ed*, **2014**, *53*, 1516–1520.

[52] G. Zhang, O. Presly, F. White, I. M. Oppel, M. Mastalerz, *Angew. Chem. Int. Ed*, **2014**, *53*, 5126–5130.

[53] S. M. Elbert, N. I. Regenauer, D. Schindler, W.-S. Zhang, F. Rominger, R. R. Schröder, M. Mastalerz, *Chem. Eur. J.* **2018**, *24*, 11438–11443.

[54] S. Klotzbach, F. Beuerle, *Angew. Chem. Int. Ed.*, **2015**, *54*,10356–10360.

[55] a) C. Zhang, Q. Wang, H. Long, W. Zhang, *J. Am. Chem. Soc.*, **2011**, *133*, 20995–21001. b) S. Lee, A. Yang, T. P. Moneypenny, J. S. Moore, *J. Am. Chem. Soc.*, **2016**, *138*, 2182–2185. c) Q. Wang, C. Zhang, B. C. Noll, H. Long, Y. Jin, W. Zhang, *Angew. Chem. Int. Ed.*, **2014**, *53*, 10663–10667.

[56] a) K. R. West, K. D. Bake, S. Otto, *Org. Lett*., **2005**, *7*, 2615–2618. b) F. Brégier, O. Hudeček, F. Chaux, M.-J. Penouilh, J.-C. Chambron, P. Lhoták, E. Aubert, E. Espinosa, *Eur.*

J. Org. Chem., **2017**, 3795–3811. c) Y.-C. Horng, T.-L. Lin, C.-Y. Tu, T.-J. Sung, C.-C. Hsieh, C.-H. Hu, H. M. Lee, T.-S. Kuo, *Eur. J. Org. Chem*., **2009**, 1511–1514.

[57] R.-C. Brachvogel, F. Hampel, M. von Delius, *Nat. Commun.*, **2015**, *6*, 7129.

[58] A. Burgun, P. Valente, J. D. Evans, D. M. Huang, C. J. Sumby, C. J. Doonan, *Chem. Commun.* **2016**, *52*, 8850–8853.

[59] P. S. Reiss, M. A. Little, V. Santolini, S. Y. Chong, T. Hasell, K. E. Jelfs, M. E. Briggs, A. I. Cooper, *Chem. Eur. J.* **2016**, *22*, 16547–16553.

[60] a) D. Xu, R. Warmuth, *J. Am. Chem. Soc.*, **2008**, *130*, 7520-7521. b) T. Hasell, M. A. Little, S. Y. Chong, M. Schmidtmann, M. E. Briggs, V. Santolini, K. E. Jelfs, A. I. Cooper, *Nanoscale*, **2017**, *9*, 6783–6790.

[61] D. Beaudoin, F. Rominger, M. Mastalerz, *Angew. Chem. Int. Ed.* **2017**, *56*, 1244–1248.

[62] a) X. Wang, Y. Wang, H. Yang, H. Fang, R. Chen, Y. Sun, N. Zheng, K. Tan, X. Lu, Z. Tian, X. Cao, *Nat. Commun.* **2016**, *7*,12469. b) Y. Wang, H. Fang, W. Zhang, Y. Zhuang, Z. Tian, X. Cao, *Chem. Commun.* *2017*, **53**, 8956–8959.

[63] Y. Wang, H. Fang, I. Tranca, H. Qu, X. Wang, A. J. Markvoort, Z. Tian, X. Cao, *Nat. Commun.* **2018**, *9*,488.

[64] H. Qu, Y. Wang, Z. Li, X. Wang, H. Fang, Z. Tian, X. Cao, *J. Am. Chem. Soc*. **2017**, *139*, 18142–18145.

[65] a) S. M. Cohen, *Chem. Rev.*, **2012**, *112*, 970–1000. b) 9 K. K. Tanabe, S. M. Cohen, *Chem. Soc. Rev.*, **2011**, *40*, 498–519.

[66] P. S. Lakshminarayanan, D. K. Kumar, P. Ghosh, *J. Am. Chem. Soc.*, **2006**, *128*, 9600–9601.

[67] M. W. Schneider, I. M. Oppel, A. Griffin, M. Mastalerz, *Angew. Chem. Int. Ed*., **2013**, *52*, 3611–3615.

[68] J. L. Culshaw, G. Cheng, M. Schmidtmann, T. Hasell, M. Liu, D. J. Adams, A. I. Cooper, *J. Am. Chem. Soc*. **2013**, *135*, 10007–10010.

[69] K. Acharyya, P. S. Mukherjee, *Chem. Eur. J.* **2015**, *21*, 6823–6831.

[70] T. P. Moneypenny, N. P. Walter, Z. Cai, Y.-R. Miao, D. L. Gray, J. J. Hinman, S. Lee, Y. Zhang, J. S. Moore, *J. Am. Chem. Soc*., **2017**, *139*, 3259–3264.

[71] a) T. Hasell, A. I. Cooper, *Nat. Rev. Mater*, **2016**, 1, 16053. b) S. Kitagawa*, Angew. Chem. Int. Ed*, **2015**, *54*, 10686–10687.

[72] M. E. Davis*, Nature,* **2002**, *417*, 813-821.

[73] H. Furukawa, K. E. Cordova, M. O'Keeffe, O. M. Yaghi, *Science*, **2013**, *341*, 1230444.

[74] C. S. Diercks, O. M. Yaghi, *Science*, **2017**, *355*, eaal1585.

[75] O. K. Farha, I. Eryazici, N. C. Jeong, B. G. Hauser, C. E. Wilmer, A. A. Sarjeant, R. Q. Snurr, S. T. Nguyen, A. Ö. Yazaydın, J. T. Hupp, *J. Am. Chem. Soc.* **2012**, *134*, 15016–15021.

[76] P. Nugent, Y. Belmabkhout, S. D. Burd, A. J. Cairns, R. Luebke, K. Forrest, T. Pham, S. Ma, B. Space, L. Wojtas, M. Eddaoudi, M. J. Zaworotko, *Nature*, **2013**, *495*, 80–84.

[77] a) Y. Hou, X. Zhang, J. Sun, S. Lin, D. Qi, R. Hong, D. Li, X. Xiao, J. Jiang, *Microporous Mesoporous Mater.*, **2015**, *214*, 108–114. b) P. Pachfule, M. K. Panda, S. Kandambeth, S. M. Shivaprasad, D. D. Diaz, R. Banerjee, *J. Mater. Chem. A*, **2014**, *2*, 7944–7952. c) H. Xu, J. Gao, D. L. Jiang, *Nat. Chem.*, **2015**, *7*, 905–912. d) C. Perego, A. Carati, Zeolites: From model materials to industrial catalysts, ed. J. J. Cejka, J. Paréz-Pariente and W. J. Roth, 2008, 357–389.

[78] R. Rostami, A. Jonidi Jafari, *J. Environ. Health Sci. Eng.*, **2014**, *12*, 89.

[79] a) N. B. McKeown, J. Mater. Chem., 2010, 20, 10588-10597. b) J. Tian, P. K. Thallapally, B. P. McGrail, CrystEngComm, 2012, 14, 1909–1919.

[80] P. M. Budd, B. S. Ghanem, S. Makhseed, N. B. McKeown, K. J. Msayib, C. E. Tattershall, *Chem, Commun*, **2004**, 230–231.

[81] J. R. Holst, A. Trewin, A. I. Cooper, *Nat. Chem.* **2010**, *2*, 915–920.

[82] M. I. Hashim, C.-W. Hsu, H. T. M. Le, O. Miljanić, *Synlett*, **2016**, *27*, 1907-1918.

[83] a) X. Wang, M. Simard, J. D. Wuest. *J. Am. Chem. Soc.*, **1994**, *116*, 12119-12120. b) P. Brunet, M. Simard, J. D. Wuest, *J. Am. Chem. Soc.*, **1997**, *119*, 2737–2738. c) R. V. Afonso, J. Durao, A. Mendes, A. M. Damas, L. Gales, *Angew. Chem., Int. Ed.*, **2010**, *49*, 3034−3036.

[84] M. Mastalerz, *Angew. Chem. Int. Ed.*, **2012**, *51*, 584–586.

[85] a) C. H. Görbitz, *Chem. Eur. J.*, **2007**, *13*, 1022-1031. b) R. V. Afonso, J. Durão, A. Mendes, A. M. Damas, L. Gales, *Angew. Chem. Int. Ed.*, **2010**, *49*, 3034–3036.

[86] a) A. L. Sisson, V. del Amo Sanchez, G. Magro, A. M. E. Griffin, S. Shan, J. P. H. Charmant, A. P. Davis, *Angew. Chem. Int. Ed.*, **2005**, *44*, 6878–6881. b) R. Natarajan, J. P. H. Charmant, A. G. Orpen, A. P. Davis, Angew. Chem. Int. Ed., 2010, 49, 5125–5129. c) R. Natarajan, G. Magro, L. N. Bridgland, A. Sirikulkajorn, S. Narayanan, L. E. Ryan, M. F. Haddow, A. G. Orpen, J. P. H. Charmant, A. J. Hudson, A. P. Davis, *Angew. Chem. Int. Ed.*, **2011**, *50*, 11386–11390. d) R. Natarajan, L. Bridgland, A. Sirikulkajorn, J. Lee, M. F. Haddow, G. Magro, B. Ali, S. Naroyanan, P. Strickland, J. P. H. Charmant, A. G. Orpen, N. B. McKeown, C. G. Bezzu, A. P. Davis, *J. Am. Chem. Soc.*, **2013**, *135*, 16912−16925. e) L. Travaglini, L. N. Bridgland, A. P. Davis, *Chem. Commun.*, **2014**, *50*, 4803−4805.

[87] J. C. Bellows, P. N. Prasad, *J. Chem. Phys.*, **1977**, *66*, 625–631.

[88] T. Hasell, A. I. Cooper, *Nat. Rev. Mater.*, **2016**, *1*, 16053.

[89] a) S. Jiang, J. T. A. Jones, T. Hasell, C. E. Blythe, D. J. Adams, A. Trewin, A. I. Cooper, *Nat. Commun.*, **2011**, *2*, 207. b) S. Jiang, K. E. Jelfs, D. Holden, T. Hasell, S. Y. Chong, M. Haranczyk, A. Trewin, A. I. Cooper, *J. Am. Chem. Soc.*, **2013**, *135*, 17818–17830. c) M. W. Schneider, L. G. Lechner, M. Mastalerz, *J. Mater. Chem.*, **2012**, *22*, 7113–7116.

[90] J. T. A. Jones, D. Holden, T. Mitra, T. Hasell, D. J. Adams, K. E. Jelfs, A. Trewin, D. J. Willock, G. M. Day, J. Bacsa, A. Steiner, A. I. Cooper, *Angew. Chem., Int. Ed.*, **2011**, *50*, 749–753.

[91] S. Mintova, M. Jaber, V. Valtchev, *Chem. Soc. Rev.* **2015**, *44*, 7207–7233.

[92] T. Hasell, S. Y. Chong, M. Schmidtmann, D. J. Adams, A. I. Cooper, *Angew. Chem. Int. Ed.*, **2012**, *51*, 7154–7157.

[93] L. Smart, E. A. Moore, *Solid State Chemistry: An Introduction*, Taylor & Francis Group, 2012.

[94] a) C. Zhang, Q. Wang, H. Long, W. Zhang, *J. Am. Chem. Soc.*, **2011**, *133*, 20995−21001. b) J.-H. Zhang, S.-M. Xie, L. Chen, B.-J. Wang, P.-G. He, L.-M. Yuan, *Anal. Chem.*, **2015**, *87*, 7817−7824.

[95] a) T. Mitra, X. Wu, R. Clowes, J. T. A. Jones, K. E. Jelfs, D. J. Adams, A. Trewin, J. Bacsa, A. Steiner, A. I. Cooper, *Chem. Eur. J.* **2011**, *17*, 10235−10240. b) S. M. Elbert, F. Rominger, M. Mastalerz, *Chem. Eur. J.* **2014**, *20*, 16707–16720.

[96] A. Galan, P. Ballester, *Chem. Soc. Rev*, **2016**, *45*, 1720−1737.

[97] M. Tagliabue, D. Farrusseng, S. Valencia, S. Aguado, U. Ravon, C. Rizzo, A. Corma, C. Mirodatos. *Chem. Eng. J.* **2009**, *155*, 553−566.

[98] C. Zhang, Z. Wang, L. X. Tan, T. L. Zhai, S. Wang, B. Tan, Y. S. Zheng, X. L. Yang, H. B. Xu, *Angew. Chem., Int. Ed.*, **2015**, *54*, 9244–9248.

[99] T. Mitra, K. E. Jelfs, M. Schmidtmann, A. Ahmed, S. Y. Chong, D. J. Adams, A. I. Cooper, *Nat. Chem.*, **2013**, *5*, 276–281.

[100] L. Chen, P. S. Reiss, S. Y. Chong, D. Holden, K. E. Jelfs, T. Hasell, M. A. Little, A. Kewley, M. E. Briggs, A. Stephenson, K. M. Thomas, J. A. Armstrong, J. Bell, J. Busto, R. Noel, J. Liu, D. M. Strachan, P. K. Thallapally, A. I. Cooper, *Nat. Mater.*, **2014**, *13*, 954–960.

[101] H. Feng, Y. Yuan, J. Xiong, Y. Zheng, B. Z. Tang, *Chem. Soc. Rev.*, **2018**, *47*, 7452–7476.

[102] B. Xiong, J.-H. Wang, B. Li, C. Zhang, B. Tan Y.-S. Zheng, *Org. Lett.*, **2018**, *20*, 321–324.

[103] N. O. Reilly, N. Giri, S. L. James, *Chem. Eur. J.* **2007**, *13*, 3020–3025.

[104] a) N. Giri, C. E. Davidson, G. Melaugh, M. G. Del Popolo, J. T. A. Jones, T. Hasell, A. I. Cooper, P. N. Horton, M. B. Hursthouse, S. L. James, *Chem. Sci.* **2012**, *3*, 2153–2157. b) G. Melaugh, N. Giri, C. E. Davidson, S. L. James, M. G. Del Popolo, *Phys. Chem. Chem. Phys*. **2014**, *16*, 9422–9431.

[105] N. Giri, M. G. Del Plpolo, G. Melaugh, R. L. Greenaway, K. Rtzke, T. Koschine, L. Pison, M. F. C. Gomes, A. I. Coopers. L. James, *Nature*, **2015**, *527*, 216–220.

[106] a) C. Godoy-Alcantar, A. K. Yatsimirsky, J.-M. Lehn, *J. Phys. Org. Chem*., **2005**, *18*, 979–985. b) T. Hirashita, Y. Hayashi, K. Mitsui, S. Araki, *J. Org. Chem*., **2003**, *68*, 1309–1313.

[107] M. Liu, M. A. Little, K. E. Jells, J. T. A. Jones, M. Schmidtmann, S. Y. Chong, T. Hasell, A. I. Cooper, *J. Am Chem. Soc.*, **2014**, *136*, 7583–7586.

[108] M. Brutschy, M. W. Schneider, M. Mastalerz, S. R. Waldvogel, *Adv. Mater*., **2012**, *24*, 6049–6052.

[109] a) K. Tamao, K. Sumitani, M. Kumada, *J. Am. Chem. Soc*., **1972**, *94*, 4374−4376. b) M. Skaisgirski, X, Guo, O. S. Wenger, *Inorg. Chem.* **2017**, *56*, 2432−2439.

[110] A. M. Bowen, M. W. Jones, J. E. Lovett, T. G. Gaule, M. J. McPherson, J. R. Dilworth, C. R. Timmel and J. R. Harmer, *Phys. Chem. Chem. Phys*., **2016**, *18*, 5981.

[111] T. Ishiyama, M. Murata, N. Miyaura, *J. Org. Chem*., **1995**, *60*, 7508–7510.

[112] D. Reinhard, W.-S. Zhang, F. Rominger, R.Curticean, I. Wacker, R.R. Schroeder, M. Mastalerz. *Chem. Eur.J.* **2018**, *24*,11433–11437.

[113] a) N. Miyaura, K. Yamada, A. Suzuki, *Tetra. Lett*. **1979**, *36*, 3437-3440. b) N. Miyaura, A. Suzuki, *Chem. Comm*., **1979**, 866-867.

[114] a) K. Shen, L. Qin, H.-G. Zheng, *Dalton Trans*., **2016**, *45*, 16205–16210. b) A. Williamson, *Philos, Mag. Series 3*, **1850**, *37*, 350–356.

[115] a) F. J. Uribe-Romo, D. Vazquez-Molina, J.K. Harper, US 2016-62361139, Jul 12, 2016. b) C.-H. Chiang, D. Pangeni, E. E. Nesterov, *Macromolecules* **2017**, *50*, 6961−6966.

[116] H. J. Jeon, R. Matsuda, P. Kanoo, H. Kajiro, L. Li, H. Sato, Y. Zheng, S. Kitagawa, *Chem. Commun.,* **2014**, *50*, 10861.

[117] X.-G. Guo, S. Qiu, X. Chen, Y. Gong, X. S, *Inorg. Chem.* **2017**, *56*, 12357−12361.

[118] D. Wang, M. R. Talipov, M. V. Ivanov, R. Rathore, *J. Am. Chem. Soc.* **2016**, *138*, 16337−16344.

[119] A. Sen, T. W. Lai, *Inorg. Chem*., **1984**, *23*, 3257–3258.

[120] T, Kitamura, M.Yamane, K. Inoue, M. Todaka, N. Fukatsu, Z. Meng, Y. Fujiwara, *J. Am. Chem. Soc.* **1999**, *121*, 11674−11679.

[121] S. M. Elbert, Masterarbeit, Universität Ulm, Ulm (Germany), **2013**.

[122] C. Zhang, C.-F. Chen, *J. Org. Chem.*, **2006**, *71*, 6626–6629.

[123] a) P. Metrangolo, F. Meyer, T. Pilati, G. Resnati, G. Terraneo, *Angew. Chem. Int. Ed.,* **2008**, *47*, 6114–6127. b) L. C. Gilday, S. W. Robinson, T. A. Barendt, M. J. Langton, B. R. Mullaney, P. D. Beer, *Chem. Rev.*, **2015**, *115*, 7118–7195. c) A. Mukherjee, S. Tothadi, G. R. Desiraju, *Acc. Chem. Res*., **2014**, *47*, 2514–2524. d) Y. Lu, T. Shi, Y. Wang, H. Yang, X. Yan, X. Luo, H. Jiang, W. Zhu, *J. Med. Chem.* **2009**, *52*, 2854–2862.

[124] Z. Han, G. Czap, C. Chiang, C. Xu, P. J. Wagner, X. Wei, Y. Zhang, R. Wu, W. Ho, *Science*, **2017**, *358*, 206–216.

[125] F. Rouquerol, J. Rouquerol, K.S.W. Sing, P. Llewellyn, G. Maurin, Adsorption by powders and porous solid: priciples, methodology and application. Elsevier, 2014.

[126] K.S.W. Sing, *Colloid. Surf*., **1989**, *38*, 113–124.

[127] a) K.S.W. Sing, D.S.H. Everett, R.A.W. Haul, L. Moscou, R. A. Pierotti, J. Rouquerol, T. Siemieniewska, *Pure & Appl. Chem.* **1985**, *57*, 503–619. b) J. Rouquerol, D. Avnir, C. W. Fairbridge, D. H. Everett, J. H. Haynes, N. Pernicone, J. D. F. Ramsay, K. S. W. Sing, K. K. Unger, *Pure & Appl. Chem.* **1994**, *66*, 1739–1758.

[128] Z. A. A. L. Othman, *Materials*, **2012**, *12,* 2874–2902.

[129] S. Brunauer, L. S. Deming, W. S. Deming, E. Teller, *J. Am. Chem. Soc.*, **1940**, *62*, 1723–1732.

[130] I. Langmuir, *J. Am. Chem. Soc.* **1918**, *40*, 1361–1403.

[131] F. Rouquerol, J. Rouquerol, K.S.W. Sing, P. Llewellyn, G. Maurin, *Adsorption by powders and porous solid: priciples, methodology and application*. Elsevier, 2014.

[132] S. Brunauer, P. H. Emmett, E. Teller, *J. Am. Chem. Soc.* **1938**, *60*, 309–319.

[133] J. T. A. Jones, T. Hasell, X. Wu, J. Bacsa, K. E. Jelfs, M. Schmidtmann, S. Y. Chong, D. J. Adams, A. Trewin, F. Schiffman, F. Cora, B. Slater, A. Steiner, G. M. Day, A. I. Cooper, *Nature*, **2011**, *474*, 367–371.

[134] A. R. Ravishankara, S. Solomon, R. F. Warren, *Science*, **1993**, *259*,194–199.

[135] M, Rigby, J. Mühle, B. Miller, R. Prinn, P. Krummel, L. Steele, P. Fraser, P. Salameh, Harth, *Atmos. Chem. Phys*., **2010**, *10*, 10305–10320.

[136] a) M. J. Elrod, *J. Chem. Educ*., **1999**. *76*, 1702. b) U. S. Energy Information Administration. *Glossary: Global warming potential (GWP)*. Retrieved 2011-04-26.

[137] X.K. Fang, X. Hu, G. Janssens-Maenhout, J. Wu, J.R. Han, S.S. Su, J.B. Zhang, J.X. Hu, *Environ. Sci. Technol*., **2013**, *47*, 3848–3855.

[138] M. Kim, S. J. Lee, C.Y. Lee, Y.S. Bae, *Microporous Mesoporous Mater.* **2014**, *190*, 356

[139] T. Hasell, M. Miklitz, A. Stephenson, M. A. Little, S. Y. Chong, R. Clowes, L. Chen, D. Holden, G. A. Tribello, K. E. Jelfs and A. I. Cooper, *J. Am. Chem. Soc.*, **2016**, *138*, 1653–1659.

[140] M. Kim, T. Yoon, D. Hong, S. Kim, S. Lee, S. Kim, S. Lee, J. Chang, Y. Bae*, Chem. Eng. J.,* **2015**, *276*, 315.

[141] M. Toyoda, H. Murase, T. Imai, H. Naotsuka, A. Kobayashi, K. Takano, K. Ohkuma, *IEEE Trans. Power Delivery.*, **2003**, *18*, 442

[142] P.-J. Kim, Y.-W. You, H. Park, J.-S. Chang, Y.-S. Bae, C.-H. Lee, J.-K. Suh, *Chem. Eng. J.*, **2014**, *262*, 683–690.

[143] A. L. Myers, J. M. Prausnitz, *AIChE J*. **1965**; *11*, 121–127.

[144] a) R. Babarao, Z. Q. Hu, J. W. Jiang, S. Chempath, S. I. Sandler, *Langmuir*, **2007**, *23*, 659; b) J. Chen, L. S. Loo, K. Wang, *J. Chem. Eng. Data*, **2011**, *56*, 1209–1212

[145] E. D. Shchukin, A. V. Pertsov, E. A. Amelina, A. S. Zelenev, *Colloid and Surface Chemistry*, Volume 12, Elsevier, 2001.

[146] H. Freundlich, Kapillarchemie–Eine Darstellung der Chemie derKolloide und verwandter Gebiete, Akademische Verlagsgesellschaft, Leipzig, 1909.

[147] J. Toth, *Acta Chim. Acad. Sci. Hung*. **1971**, *69*, 311.

[148] a) K. Sumida, D. L. Rogow, J. A. Mason, T. M. McDonald, E. D. Bloch, Z. R. Herm, T.-H. Bae, J. R. Long, *Chem. Rev*. **2012**, *112*, 724–781. b) H. Murase, T. Imai, T. Inohara, M. Toyoda, *IEEE Trans. Dielectr. Electr. Insul.* **2004**, *11*, 166.

[149] M. Koppen, A. Dhakshinamoorthy, A. K. Inge, O. Cheung, J. Angstrom, P. Mayer, N. Stock, *Eur. J. Inorg. Chem.*, **2018**, 3496–3503.

[150] D. M. Ruthven, I. H. Doetsch, *J. Chem. Soc., Faraday Trans. 1*, **1976**, *72*, 1043−1050.

[151] A. Isidro-Llobet, M. Álvarez, F. Albericio, *Chem. Rev.*, **2009**, *109*, 2455−2504.

[152] C. Schotten, *Ber. Dtsch. Chem. Ges.*, **1884**, *17*, 2544–2547, b) E. Baumann, *Ber. Dtsch. Chem. Ges.*, **1886**, *19*, 3218–322.

[153] X.-G. Guo, S.Qiu, X. Chen, Y. Gong, X. S, *Inorg. Chem.* **2017**, *56*, 12357−12361.

[154] E. Clemmensen, *Chemische Berichte*, **1913**, *46*, 1837−1843.

[155] Y. Cohen, L. Avram, L. Frish, *Angew. Chem. Int. Ed.*, **2005**, *44*, 520–554.

[156] A. Einstein, *Ann. Phys.*, **1905**, *322*, 549–560.

[157] H. C. Chen, S. H. Chen, *J. Phys. Chem.*, **1984**, *88*, 5118–5121.

[158] Yaws, C. L. Thermophysical properties of chemicals and hydrocarbons. (William Andrew Inc. New York, 2008)

[159] J. Peterson, H. Cooper, C. Baukal, *Hydrocarbon processing*, **2017**, 111−115.

[160] a) S. Hong, M. R. Rohman, J. Jia, Y. Kim, D. Moon, Y. Kim, Y. H. Ko, E. Lee, K. Kim, *Angew. Chem., Int. Ed.*, **2015**, *54*, 13241–13244. b) S. Bera, A. Basu, S. Tothadi, B. Garai, S. Banerjee, K. Vanka, R. Banerjee, *Angew. Chem., Int. Ed.*, **2017**, *56*, 2123–2126.

[161] P. Larkin, Infrared and Raman Spectroscopy: Priciples and Spectral Interpretation. Elsevier, 2012.

[162] Yaws, C. L. Thermophysical properties of chemicals and hydrocarbons. (William Andrew Inc. New York, 2008)

[163] P. Wessig, M. Gerngroß, D. Freyse, P. Bruhns, M. Przezdziak, U. Schilde, A. Kelling, *J. Org. Chem.* **2016**, *81*, 1125−1136.

[164] D. Mossinger, S. S. Jester, E. Sigmund, U. Muller, S. Hoger, *Macromolecules*, **2009**, *42*, 7974-7978.

[165] W.Y. Huang, W. Cao, T.K. Kwei, Y. Okamoto, *Macromolecules* **2001**, *34*, 1570–1578

[166] A. M. Bowen, M. W. Jones, J. E. Lovett, T. G. Gaule, M. J. McPherson, J. R. Dilworth, C. R. Timmel and J. R. Harmer, *Phys. Chem. Chem. Phys.*, **2016**, *18*, 5981.

[167] K. T. Nielsen, H. Spanggaard, F. C. Krebs, *Macromolecules* **2005**, *38*, 1180–1189.

[168] R. M. Pankow, N. S. Gobalasingham, J. D. Munteanu, B. C. Thompson, *J. Polym. Sci. A.* **2017**, *55*, 3370-3380.

[169] M. Wang, R. Jeng, C.H. Lin, *RSC Adv.*, **2016**, *6*, 18678–18684

[170] D. Wang, M. R. Talipov, M. V. Ivanov, R. Rathore, *J. Am. Chem. Soc. 2016*, *138*, 16337−16344.

[171] X.-Y. Hu, W.-S. Zhang, F. Rominger, I. Wacker, R. R. Schroder, M. Mastalerz, *Chem. Commun.*, **2017**, *53*, 8616−8619.

7 Spectra

7.1 NMR Spectra

The following section contains the NMR spectra of unpublished compounds.

-Spectra of compounds **130** and **131** in reference [171].
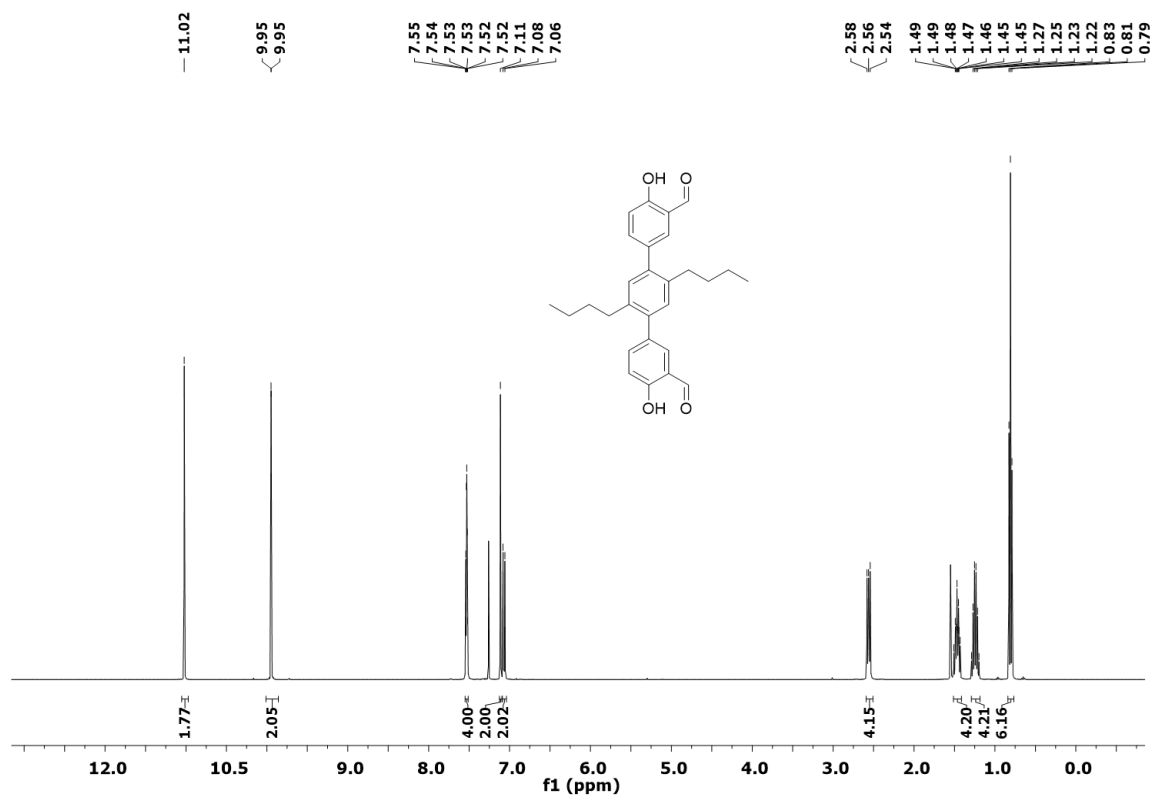
Figure 58. ^{1}H NMR spectrum of compound **52** in CDCl$_3$ (500 MHz).
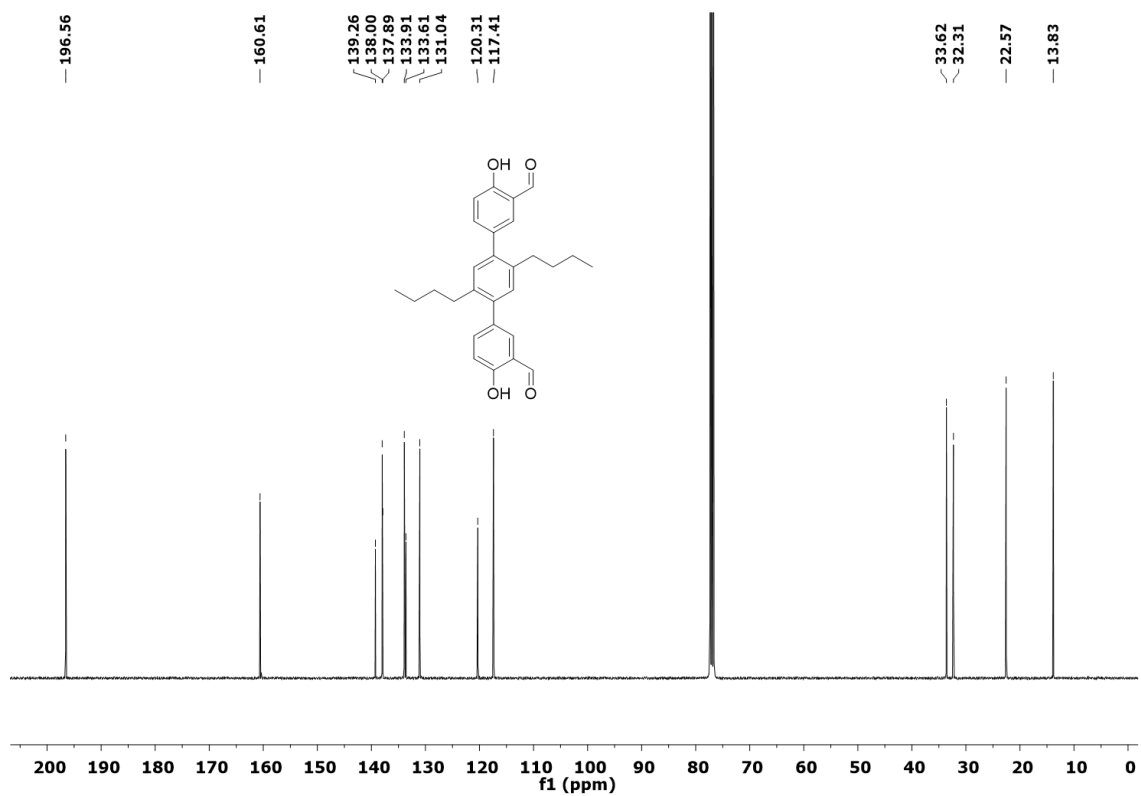
Figure 59. ^{13}C NMR spectrum of compound **52** in CDCl$_3$ (125 MHz).
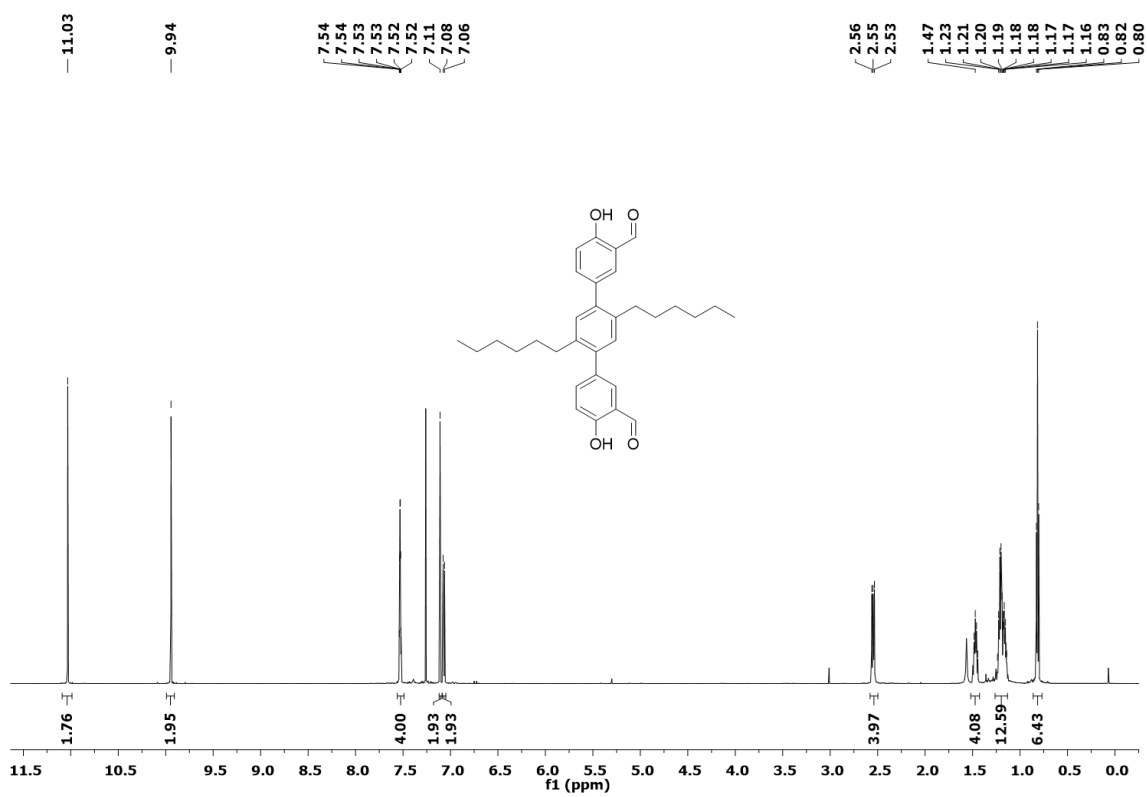
Figure 60. ^{1}H NMR spectrum of **53** in CDCl$_3$ (500 MHz).
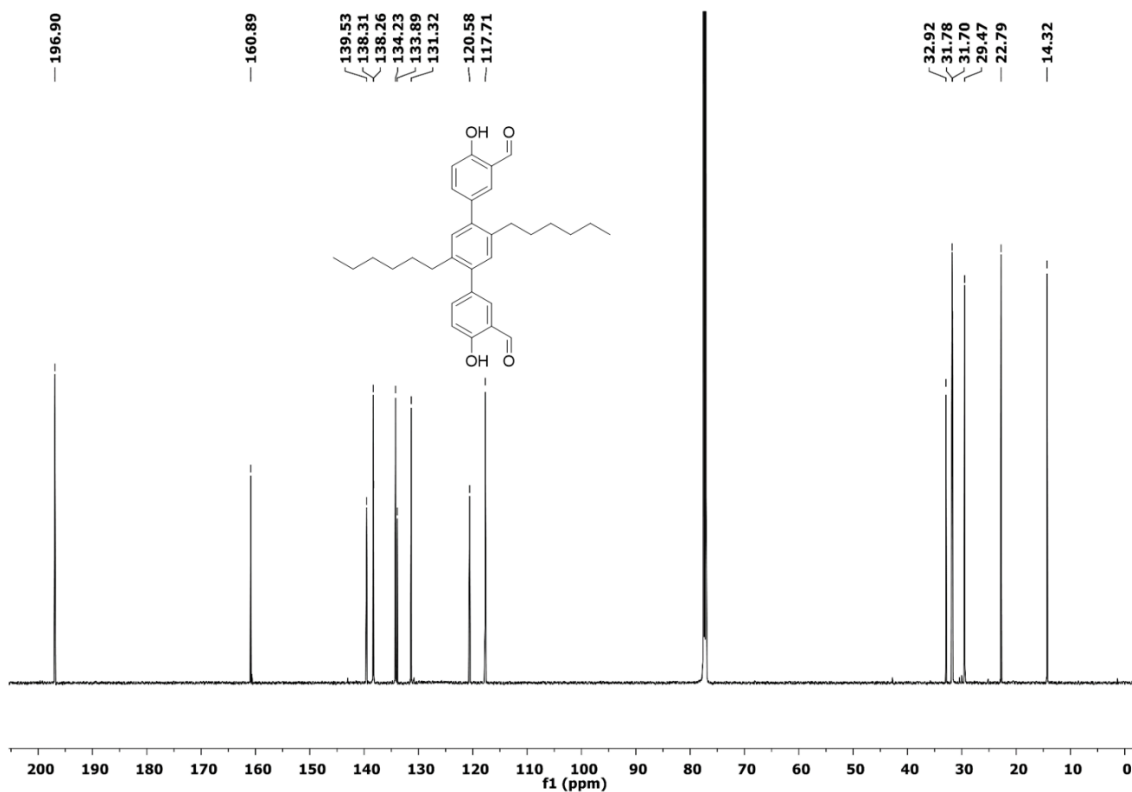
Figure 61. ^{13}C NMR spectrum of **53** in CDCl$_3$ (125 MHz).
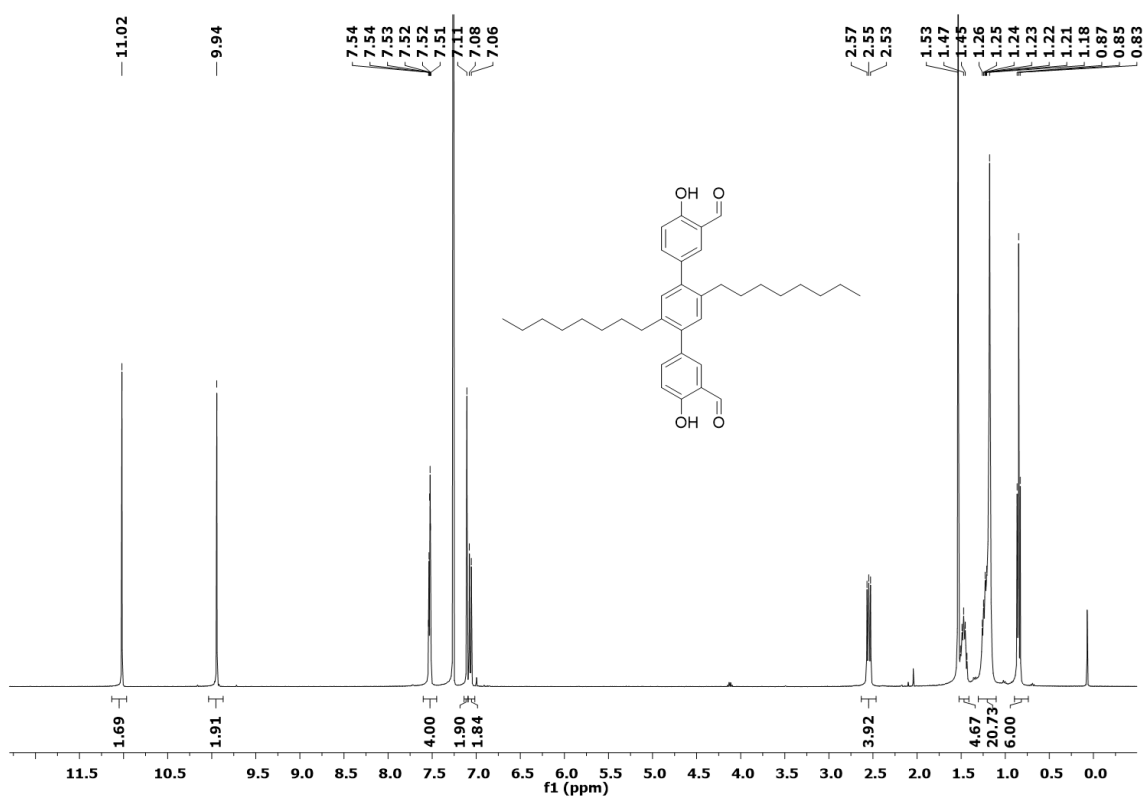
Figure 62. ^{1}H NMR spectrum of **54** in CDCl$_3$ (500 MHz).
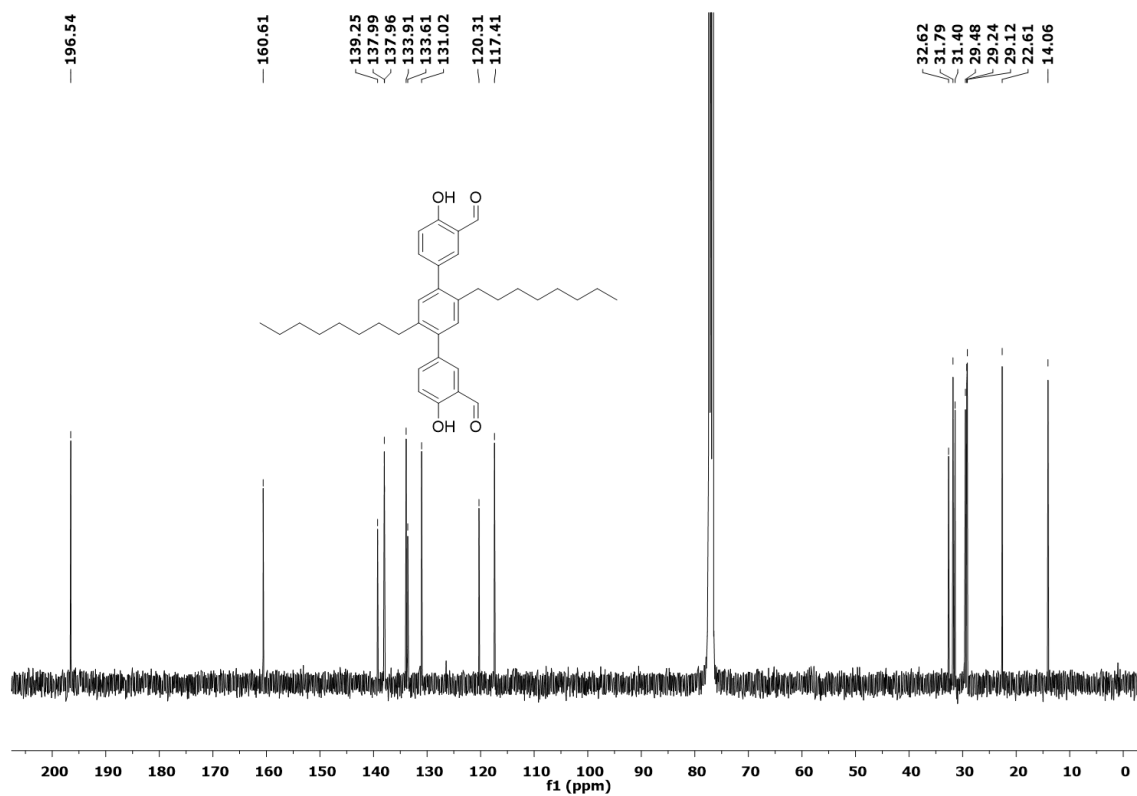
Figure 63. ^{13}C NMR spectrum of **54** in CDCl$_3$ (125 MHz).
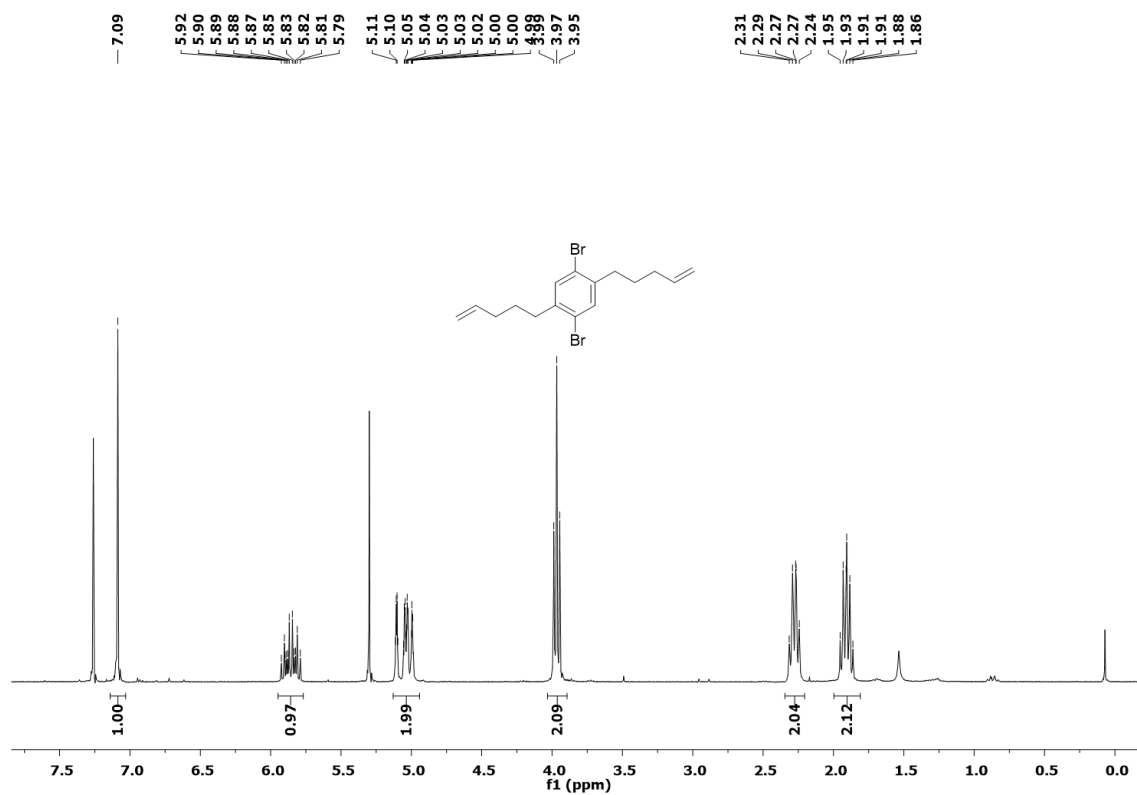
Figure 64. ^{1}H NMR spectrum of **83** in CDCl$_3$ (300 MHz).
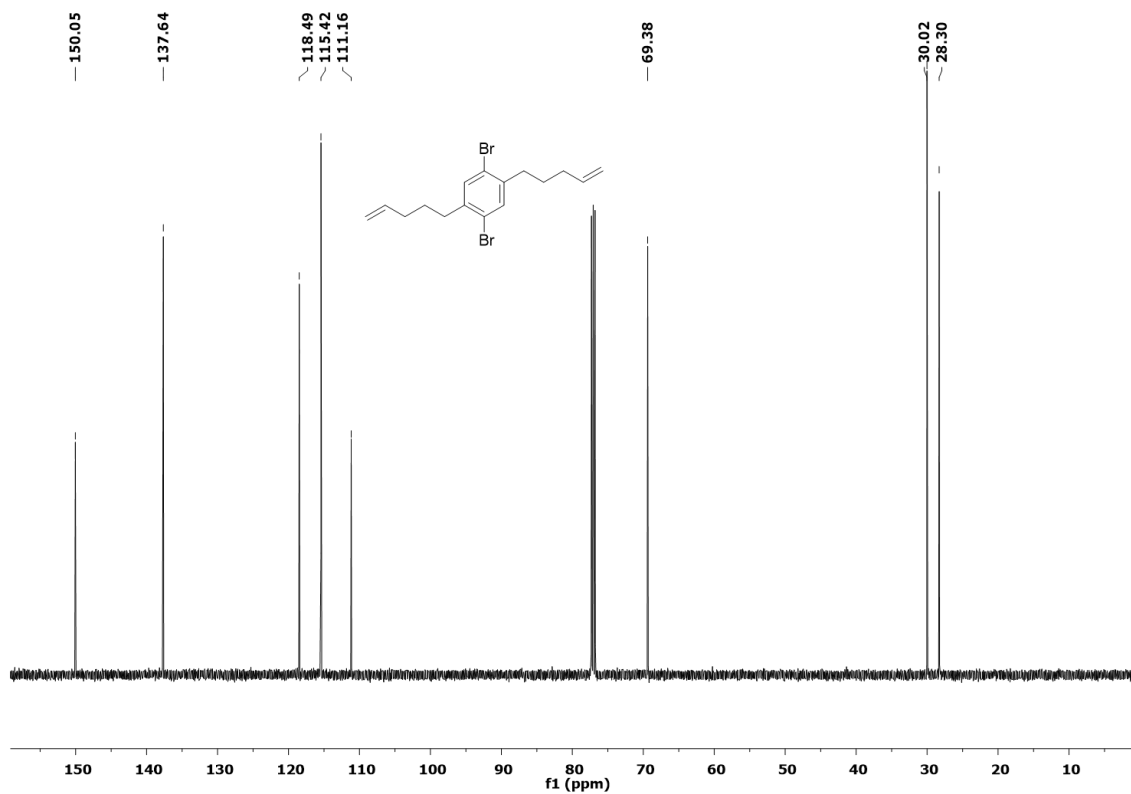
Figure 65. ^{13}C NMR spectrum of **83** in CDCl$_3$ (125MHz).
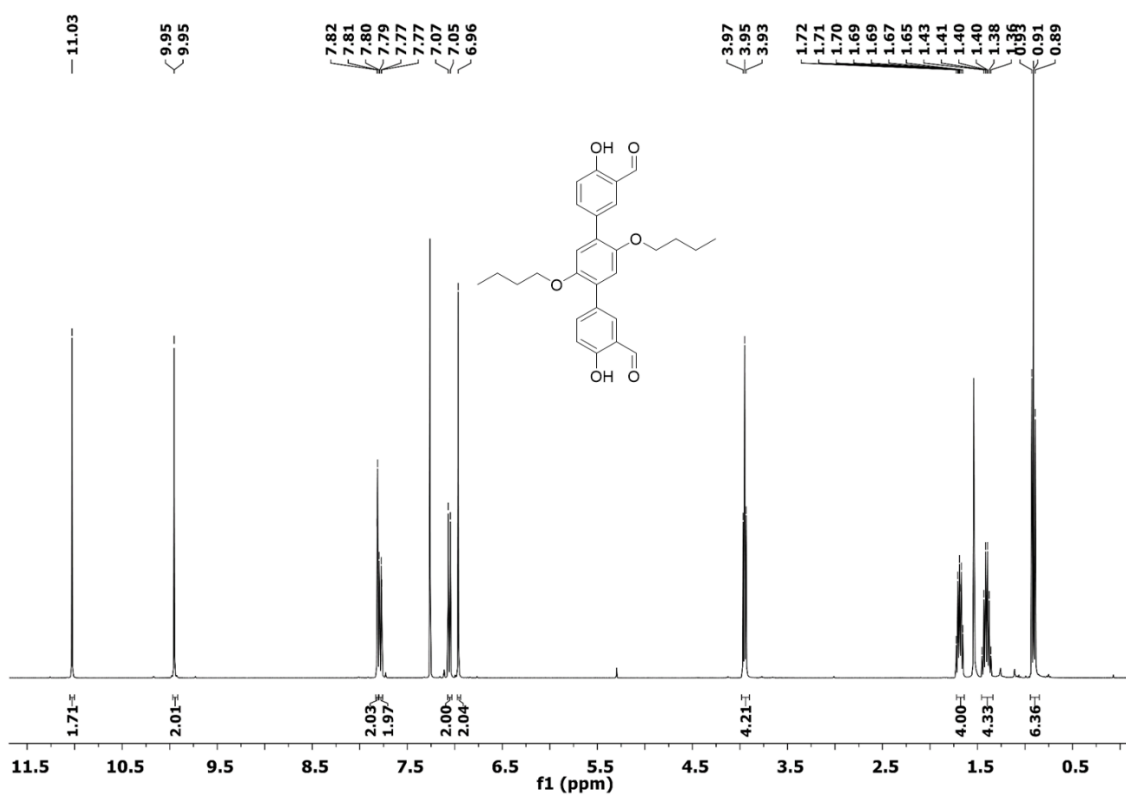
Figure 66. ^{1}H NMR spectrum of **55** in CDCl$_3$ (300 MHz).

Figure 67. ^{13}C NMR spectrum of **55** in CDCl$_3$ (125 MHz).

Figure 68. ^{1}H NMR spectrum of **56** in CDCl3 (300 MHz). # is the peak of remaining DCM.
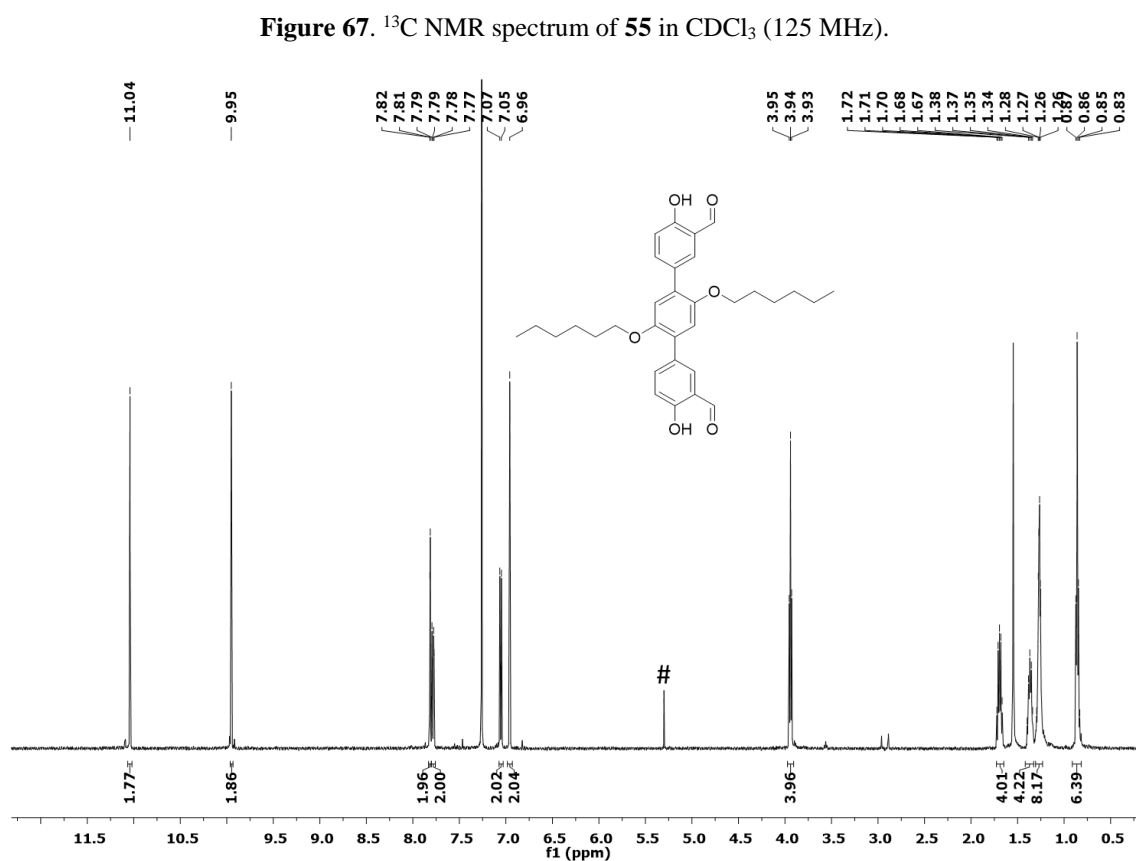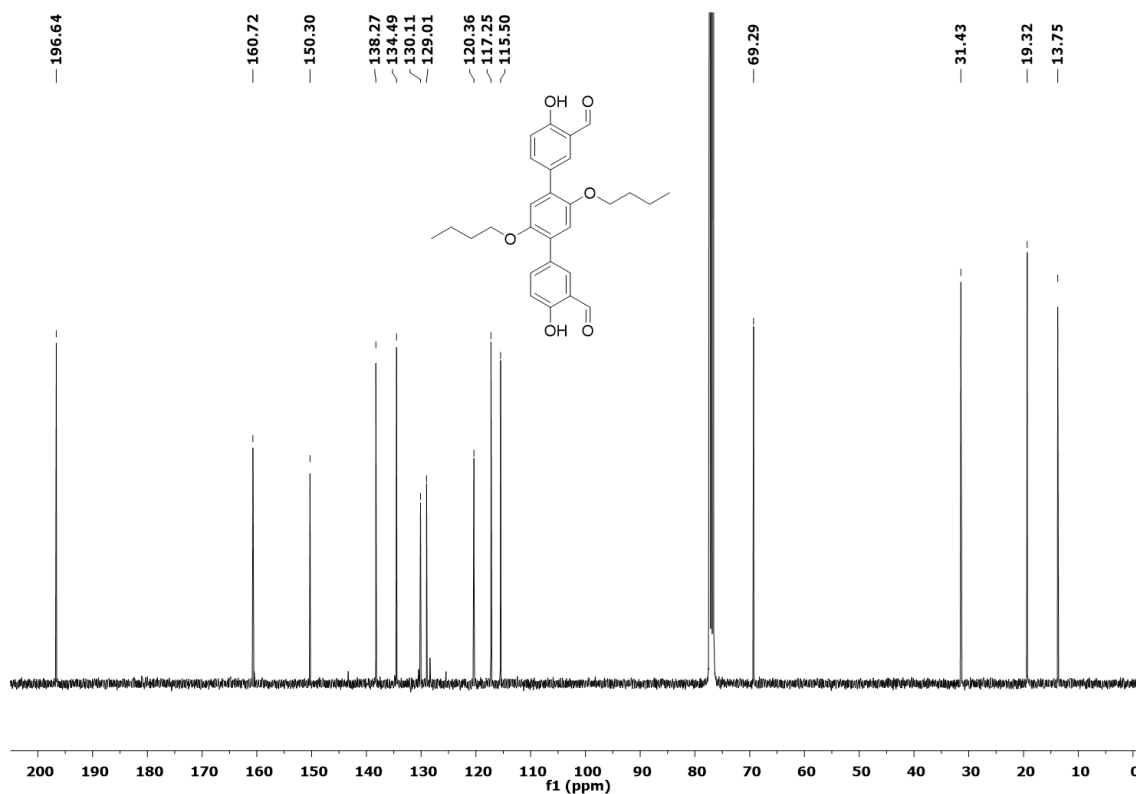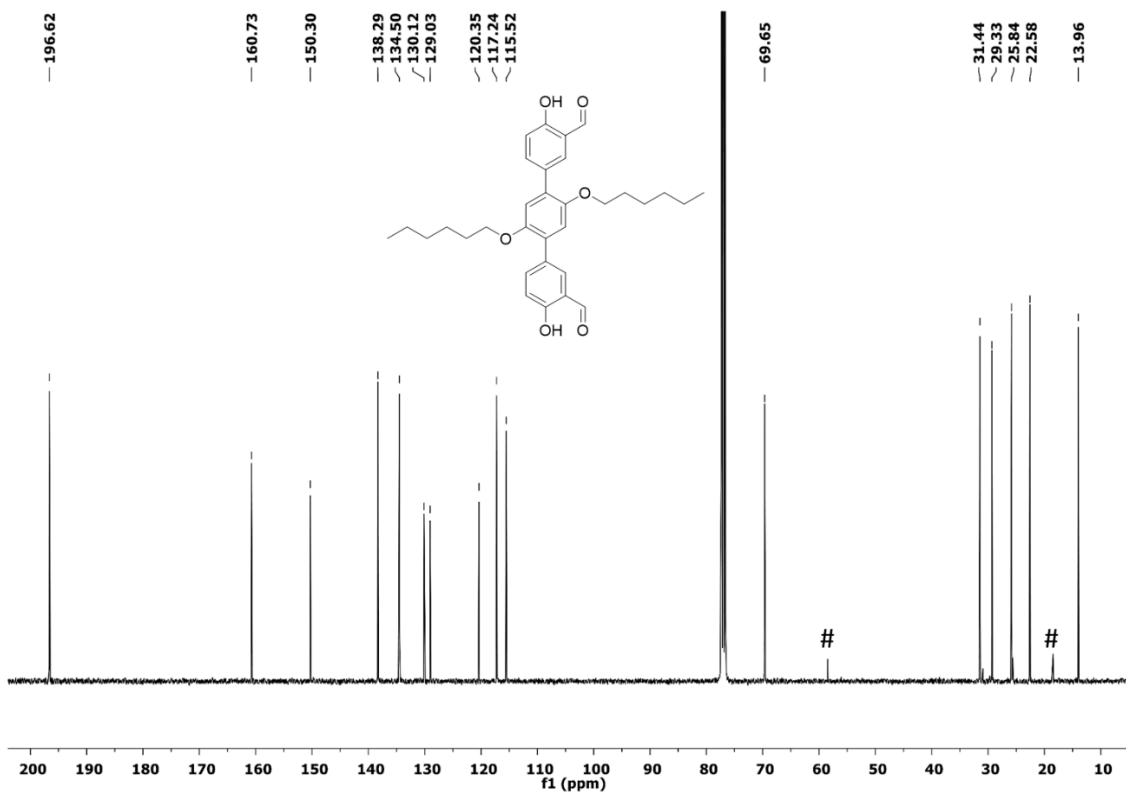
Figure 69. ^{13}C NMR spectrum of **56** in CDCl$_3$ (125 MHz). # is the peak of remaining ethanol.
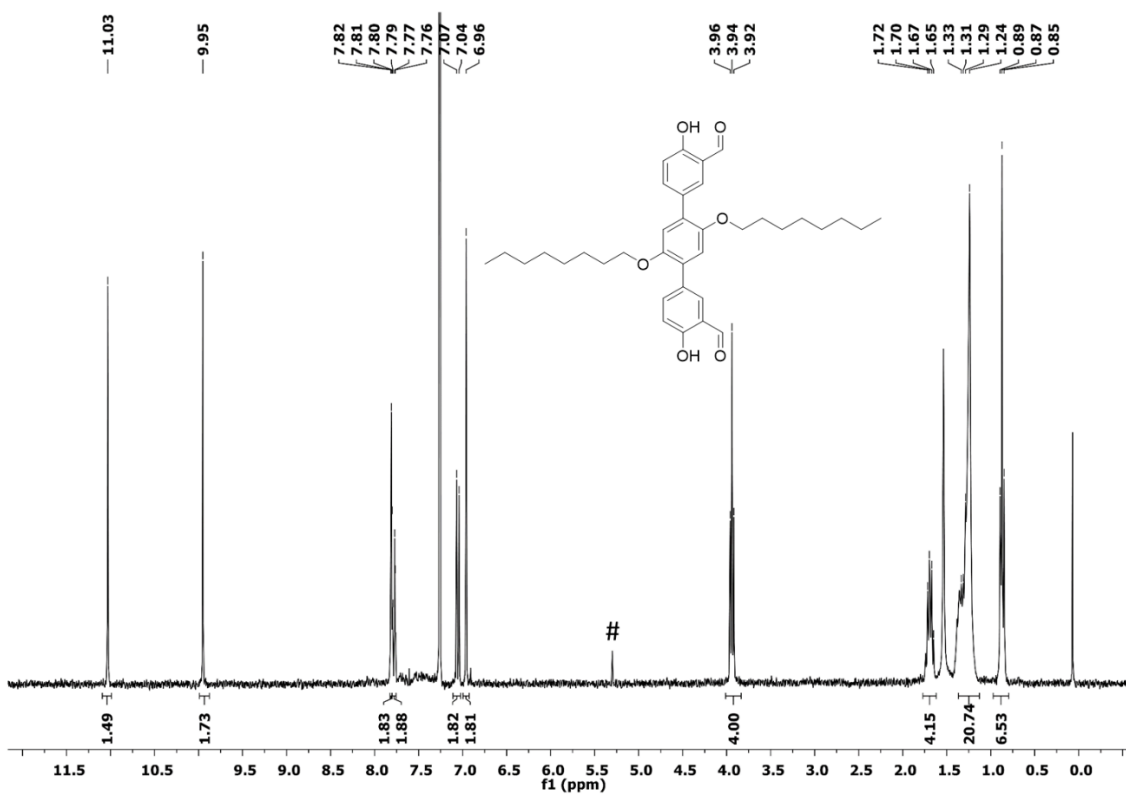
Figure 70. ^{1}H NMR spectrum of **57** in CDCl$_3$ (300 MHz). # is the peak of remaining DCM.
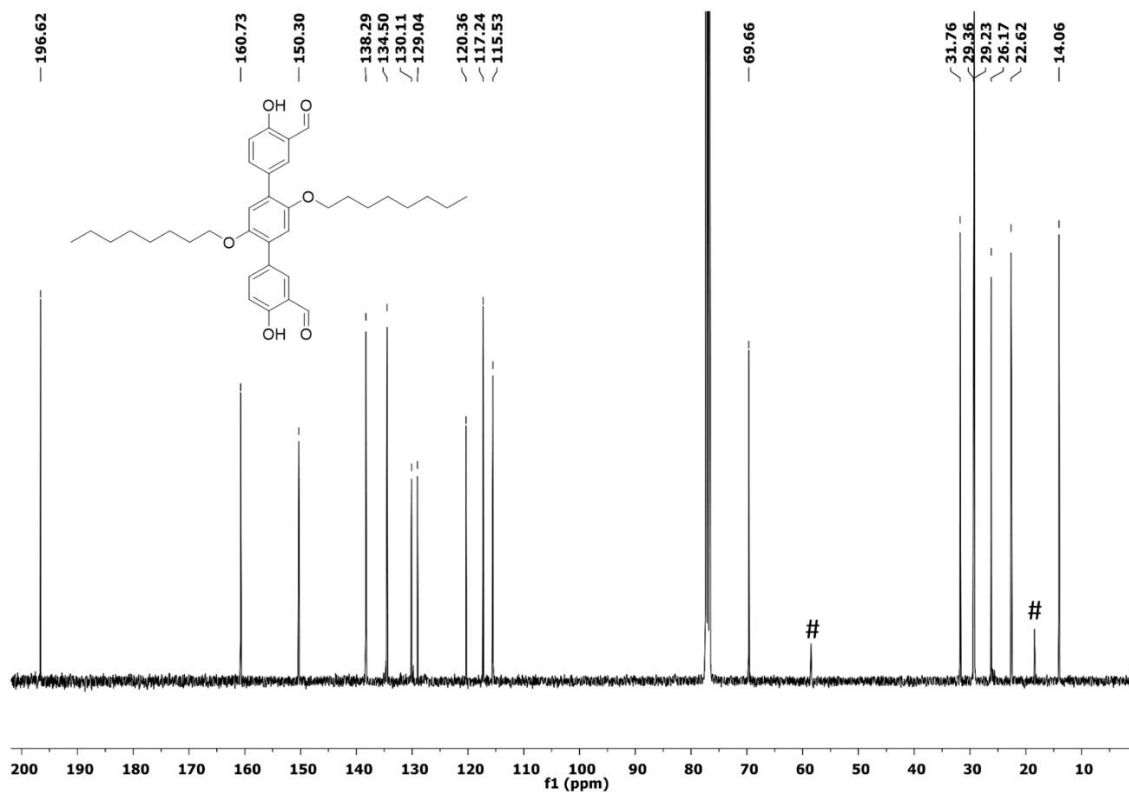
Figure 71. ^{13}C NMR spectrum of **57** in CDCl$_3$ (125 MHz). # is the peak of remaining ethanol.
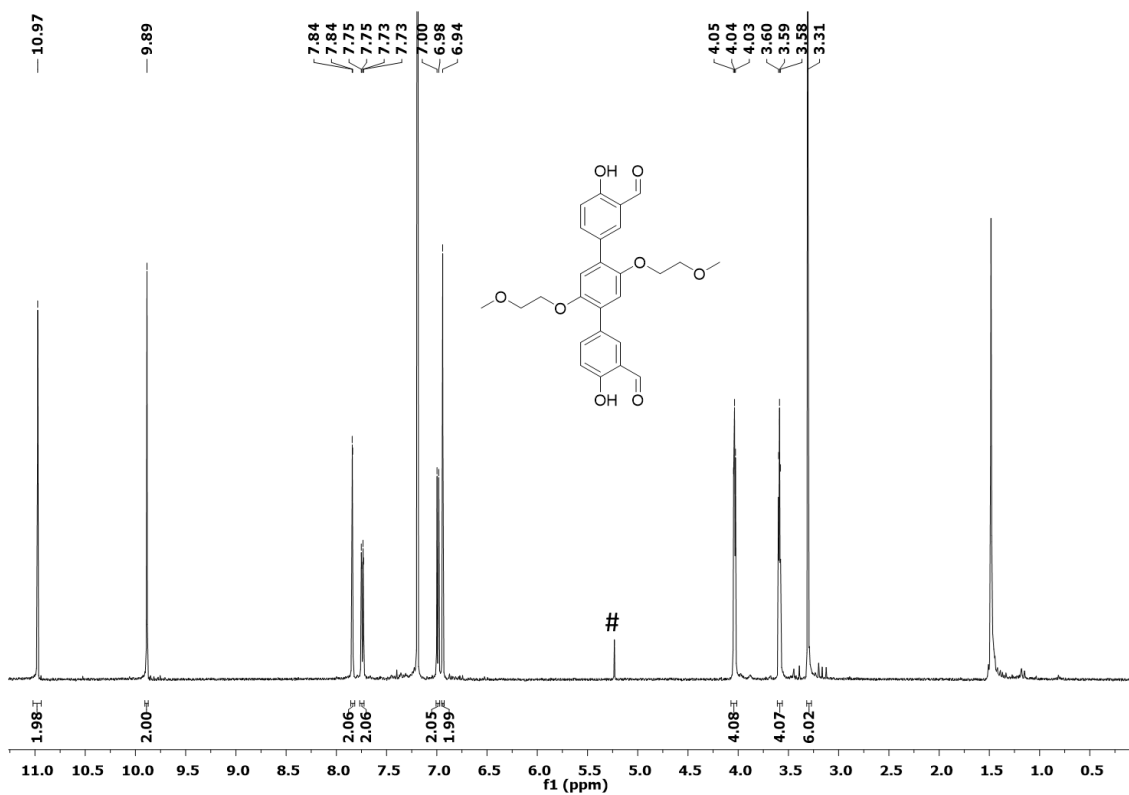
Figure 72. ^{1}H NMR spectrum of **60** in CDCl$_3$ (500 MHz). # is the peak of remaining DCM.

167

Figure 73. ^{13}C NMR spectrum of **60** in CDCl$_3$ (125 MHz).

Figure 74. ^1H NMR spectrum of **61** in CDCl$_3$ (300 MHz).
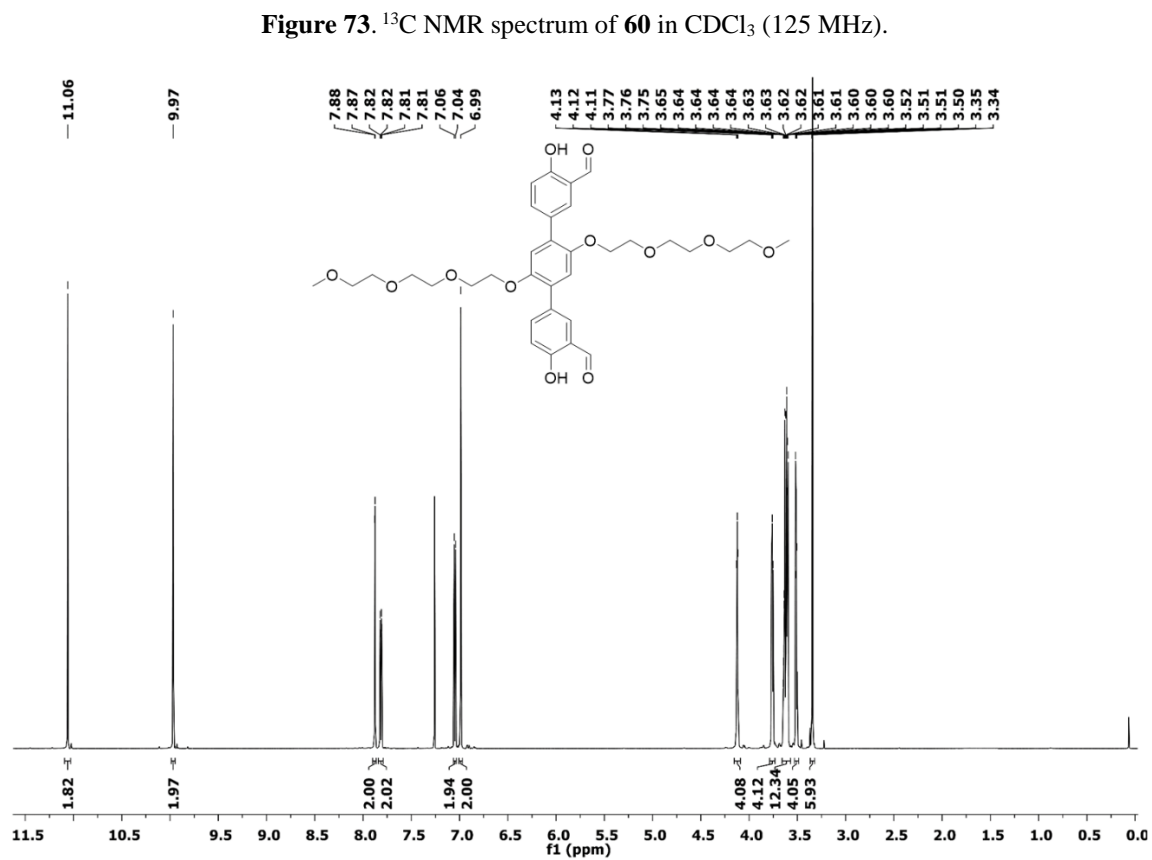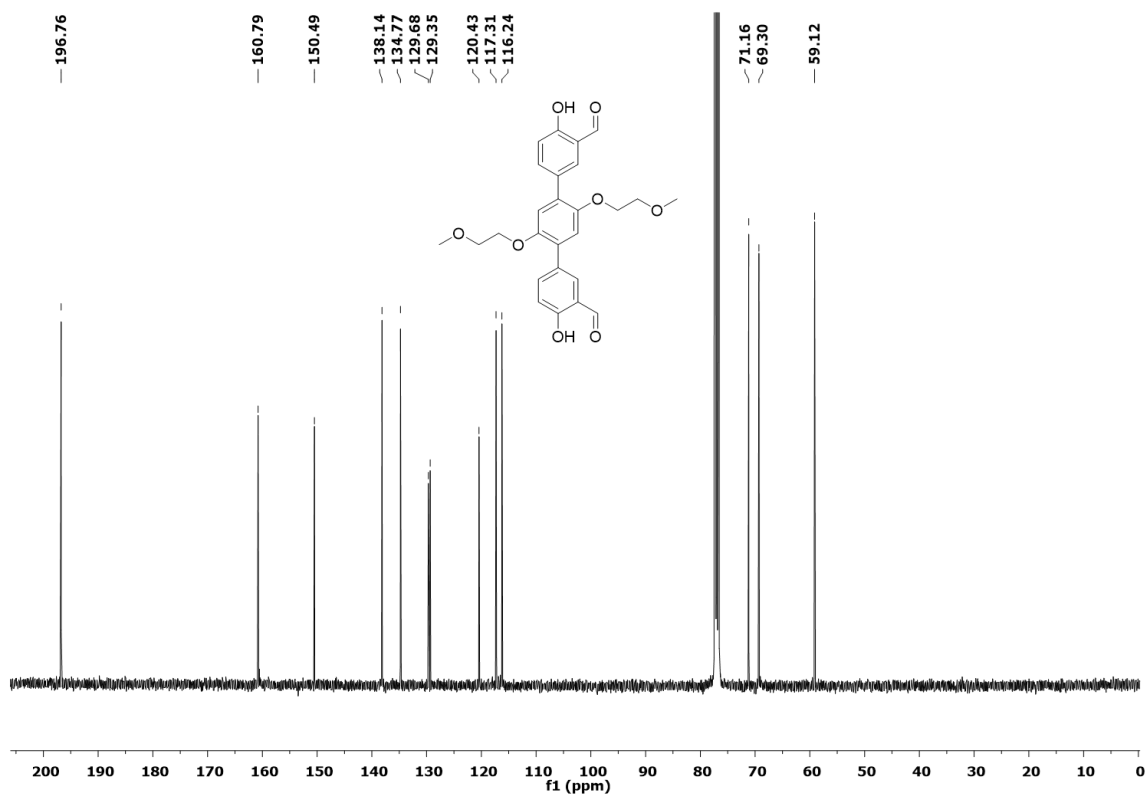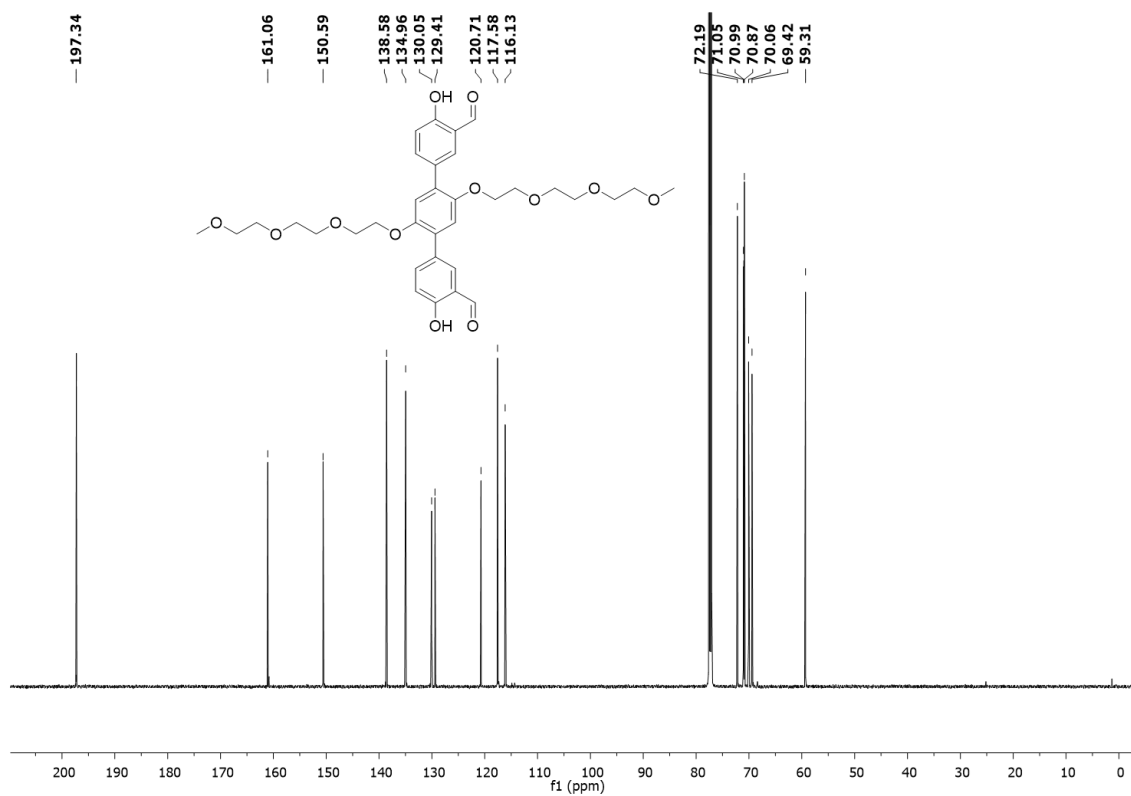
Figure 75. ^{13}C NMR spectrum of **61** in CDCl$_3$ (125 MHz).
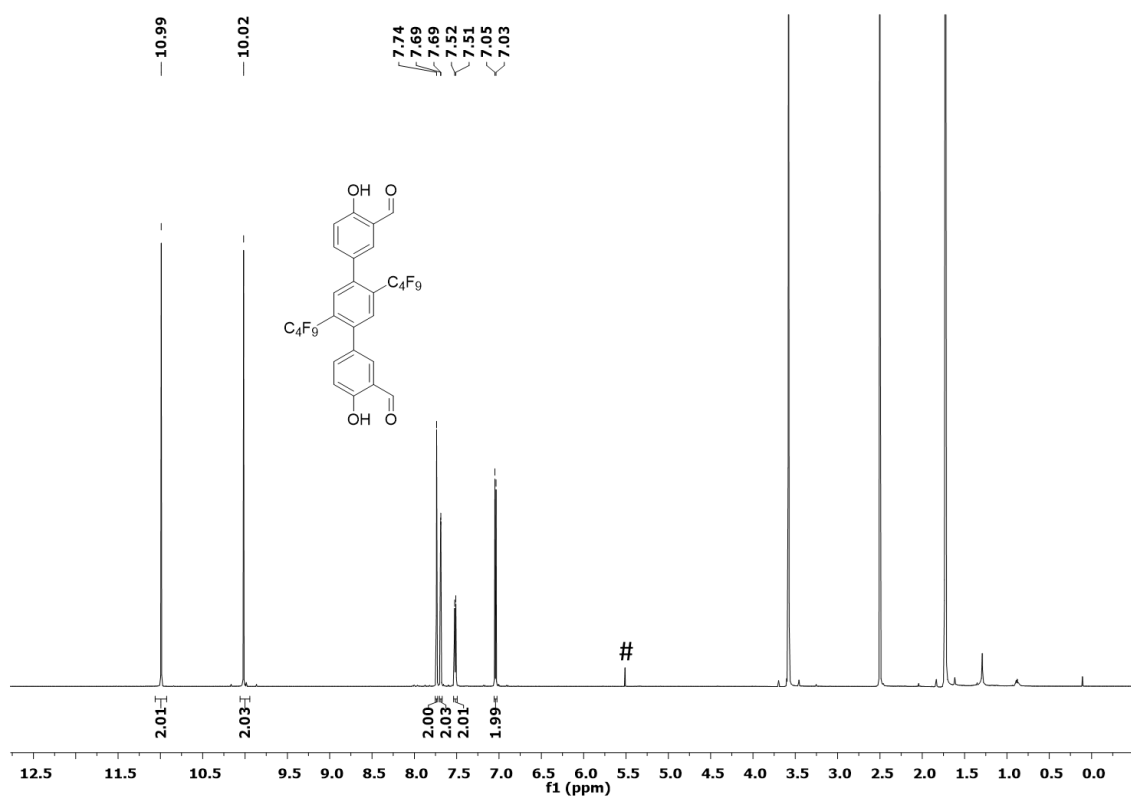
Figure 76. ^{1}H NMR spectrum **59** in THF-d$_8$ (500 MHz). # is the peak of remaining DCM
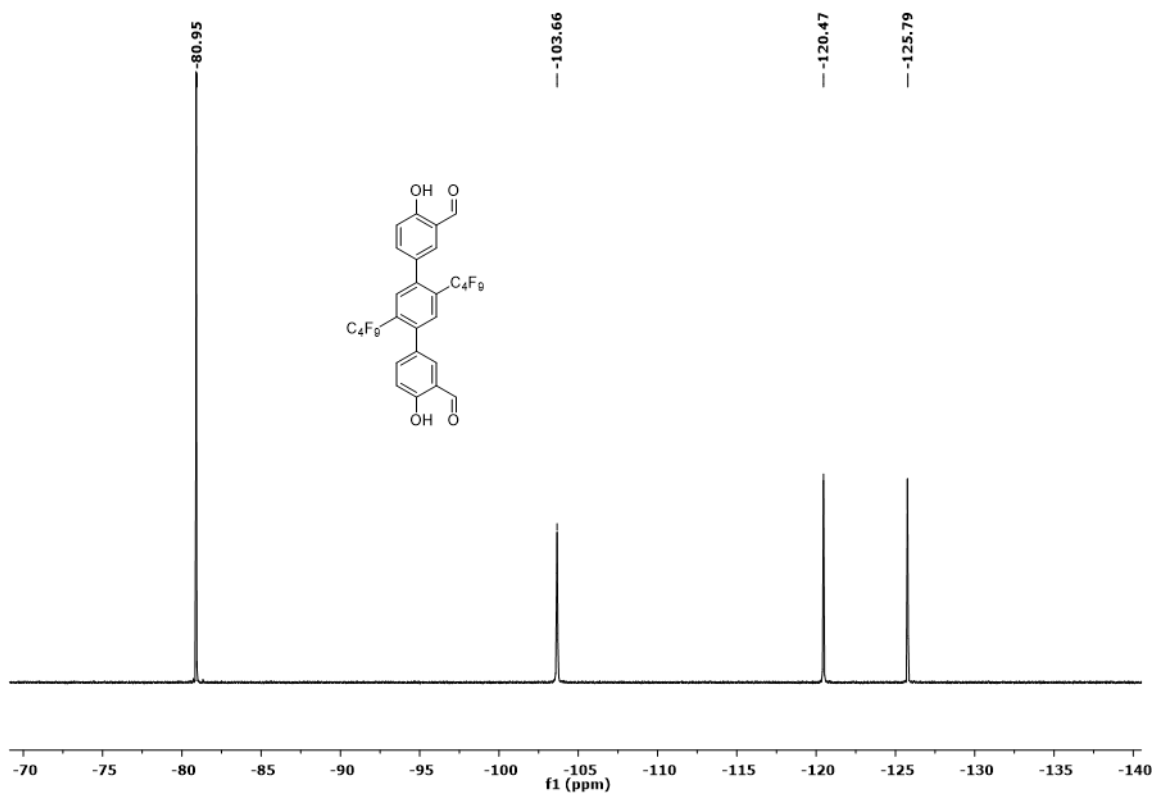
Figure 77. ^{19}F NMR spectrum of **59** in CDCl$_3$ (283 MHz).
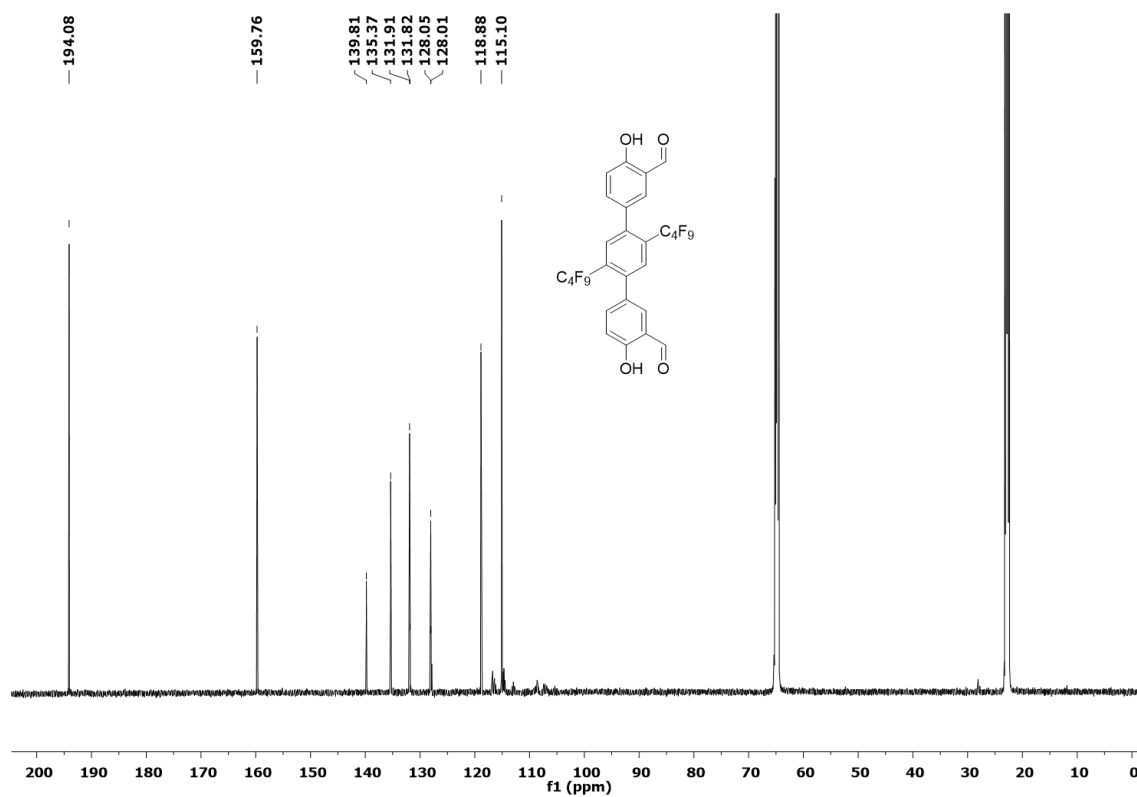
Figure 78. ^{13}C NMR spectrum of **59** in THF-d$_8$ (125 MHz).
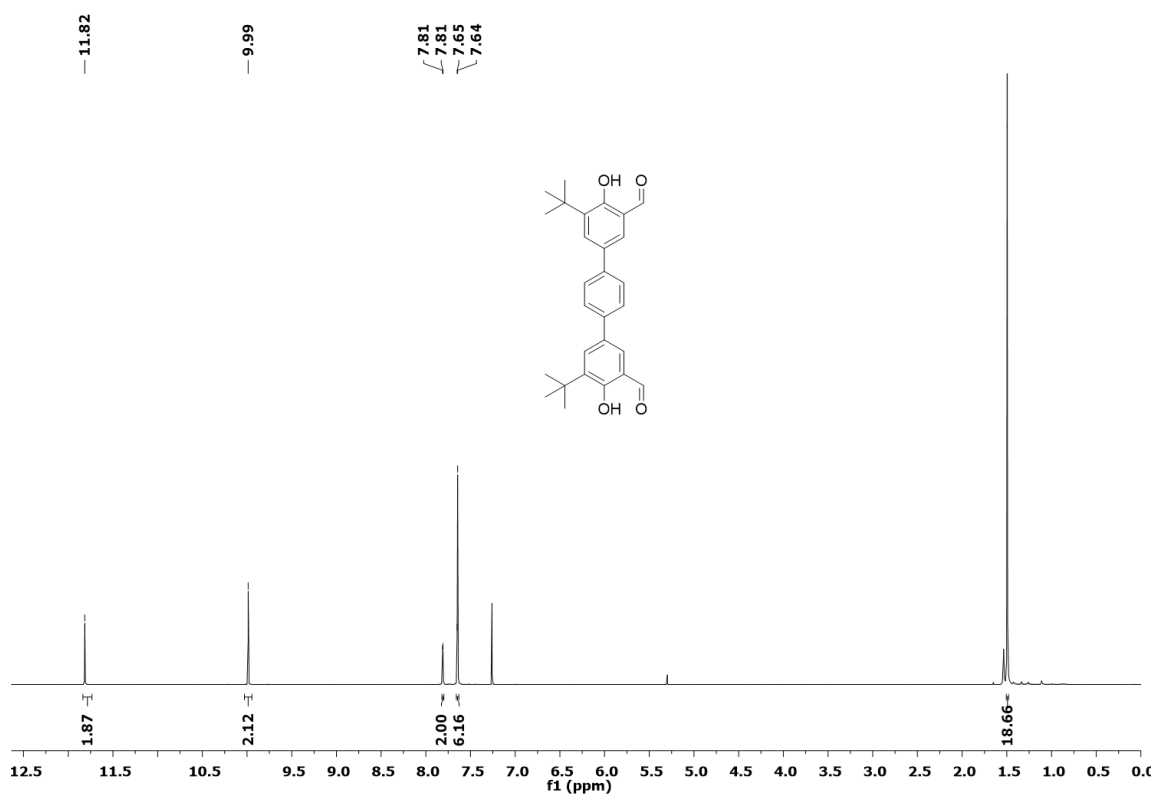
Figure 79. ^{1}H NMR spectrum of **62** in CDCl$_3$ (500 MHz).
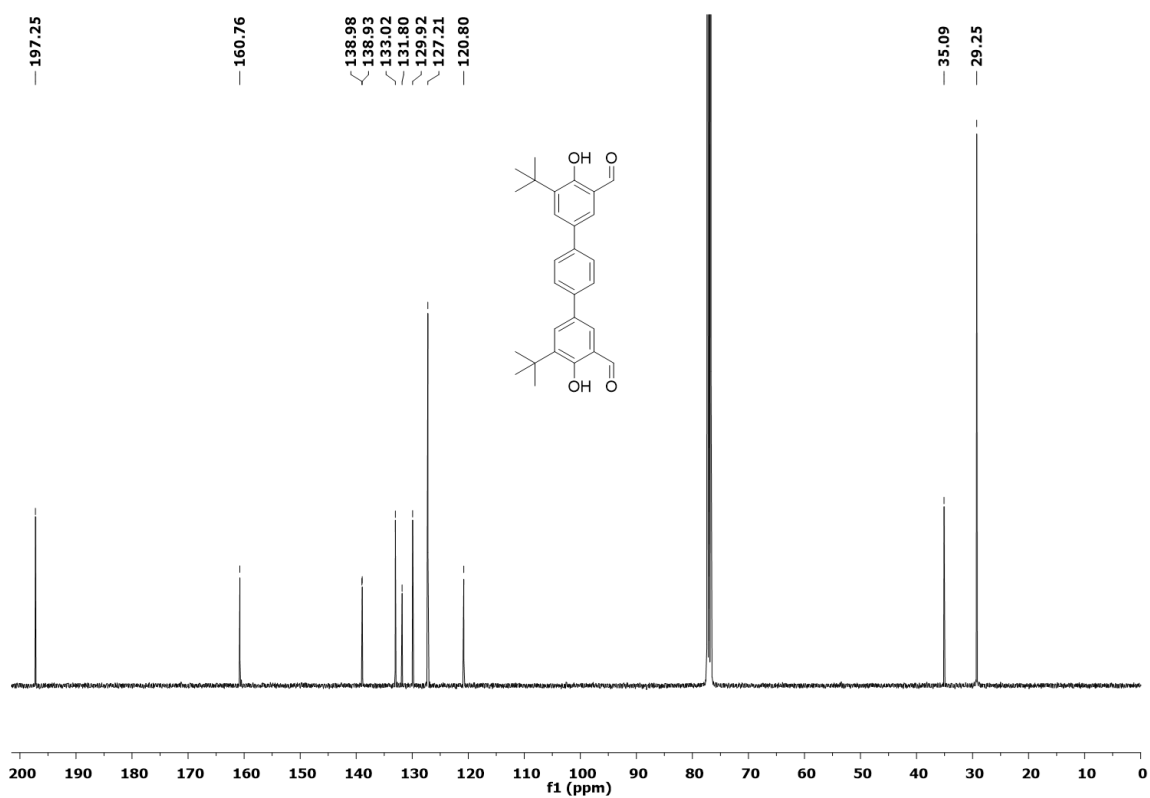
Figure 80. ^{13}C NMR spectrum of **62** in CDCl$_3$ (125 MHz).
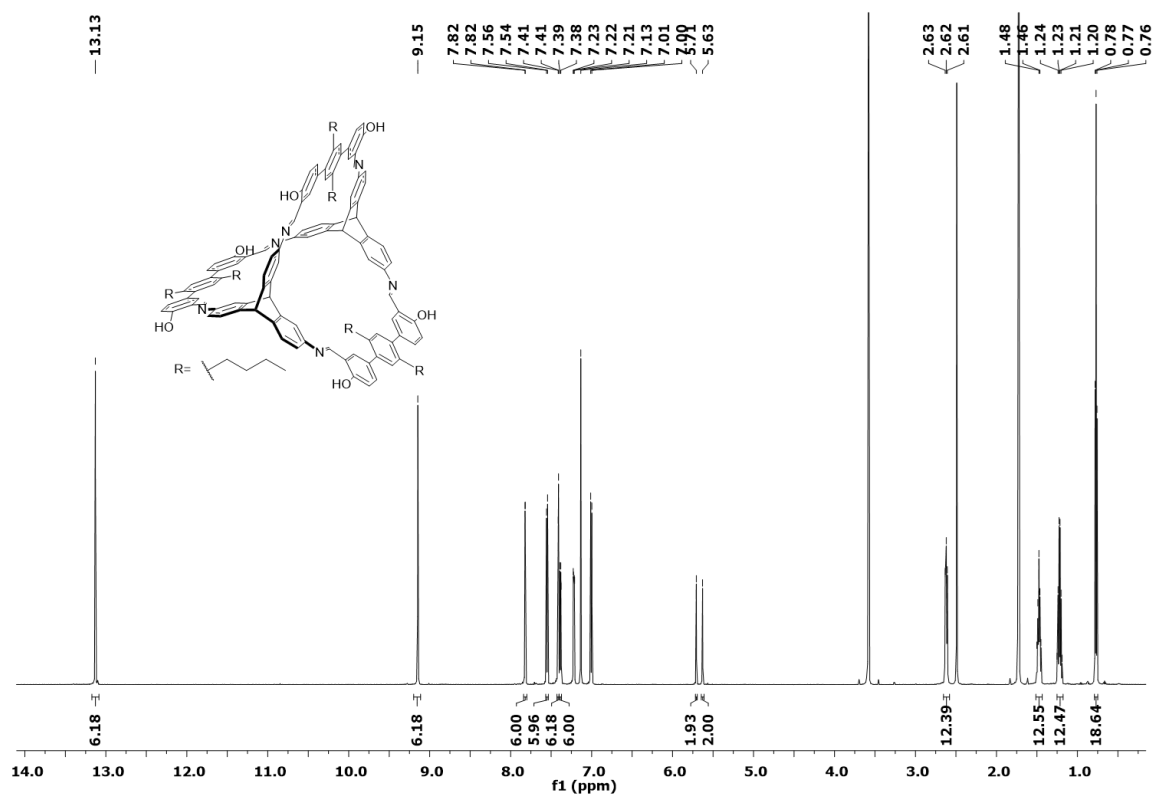
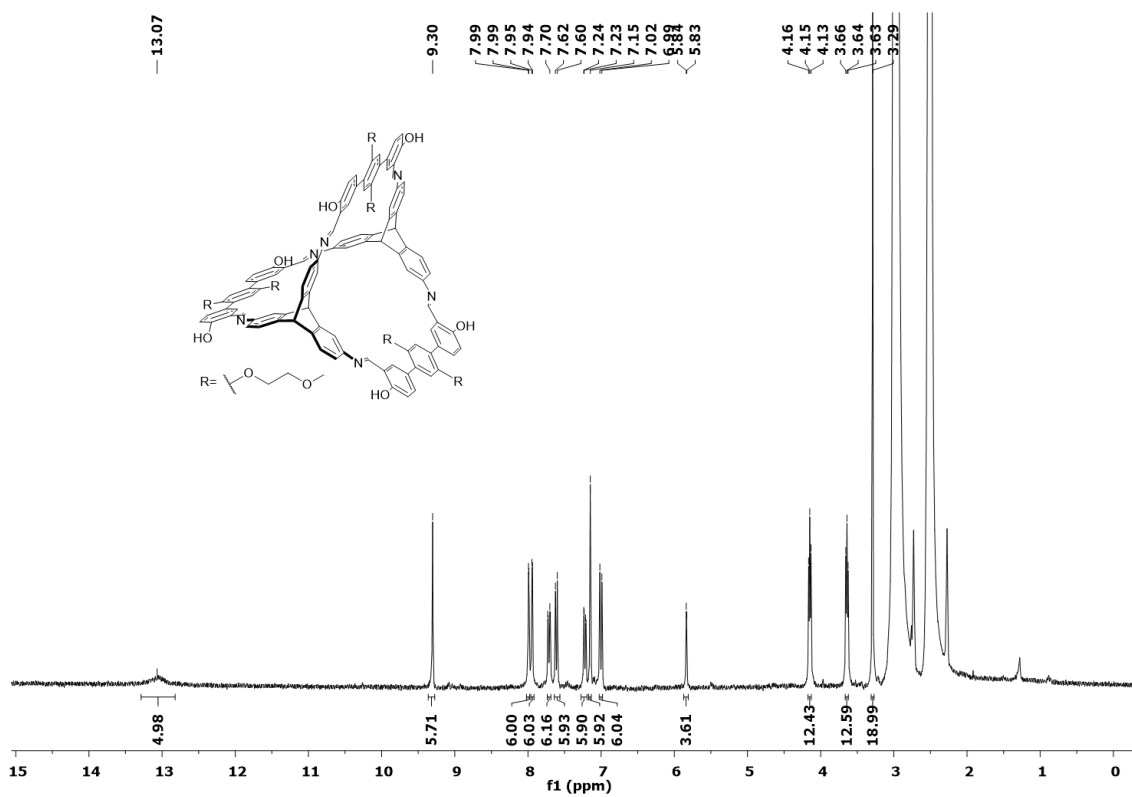**Figure 81**. ^{1}H NMR spectrum of cage compound **104** in THF-d$_8$ (500 MHz).
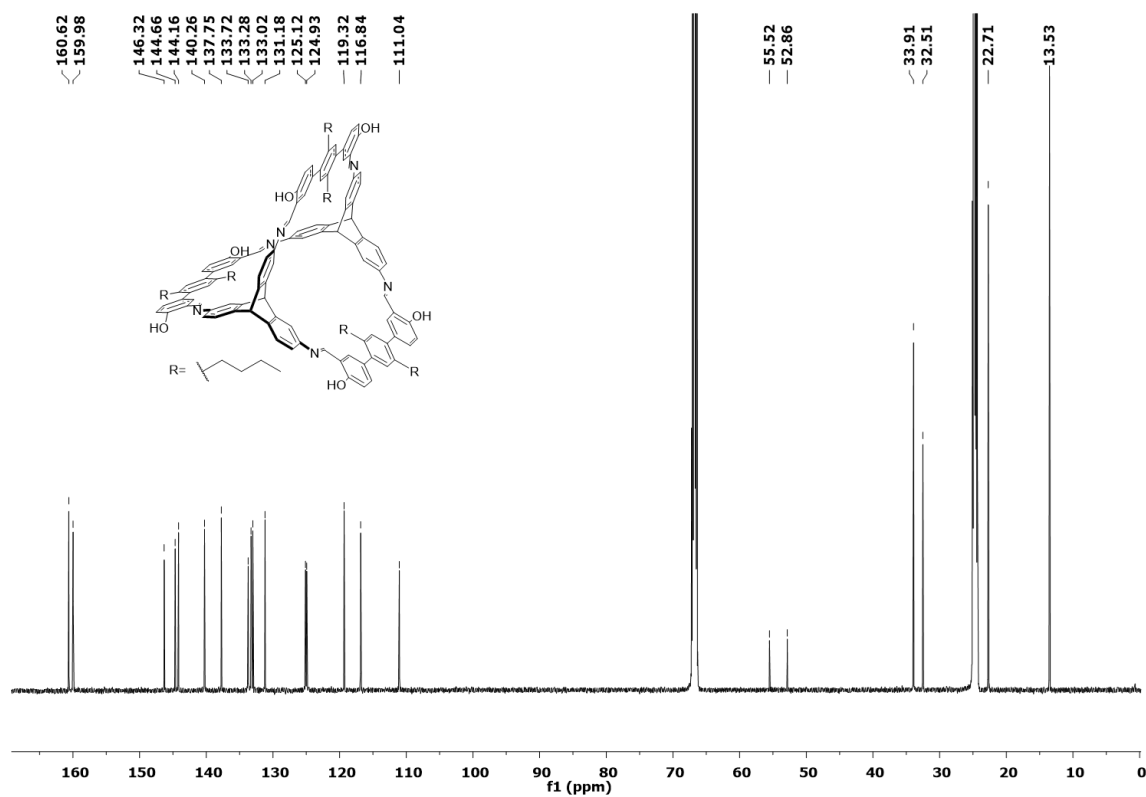
Figure 82. ^{13}C NMR spectrum of cage compound **104** in THF-d$_8$ (125 MHz).
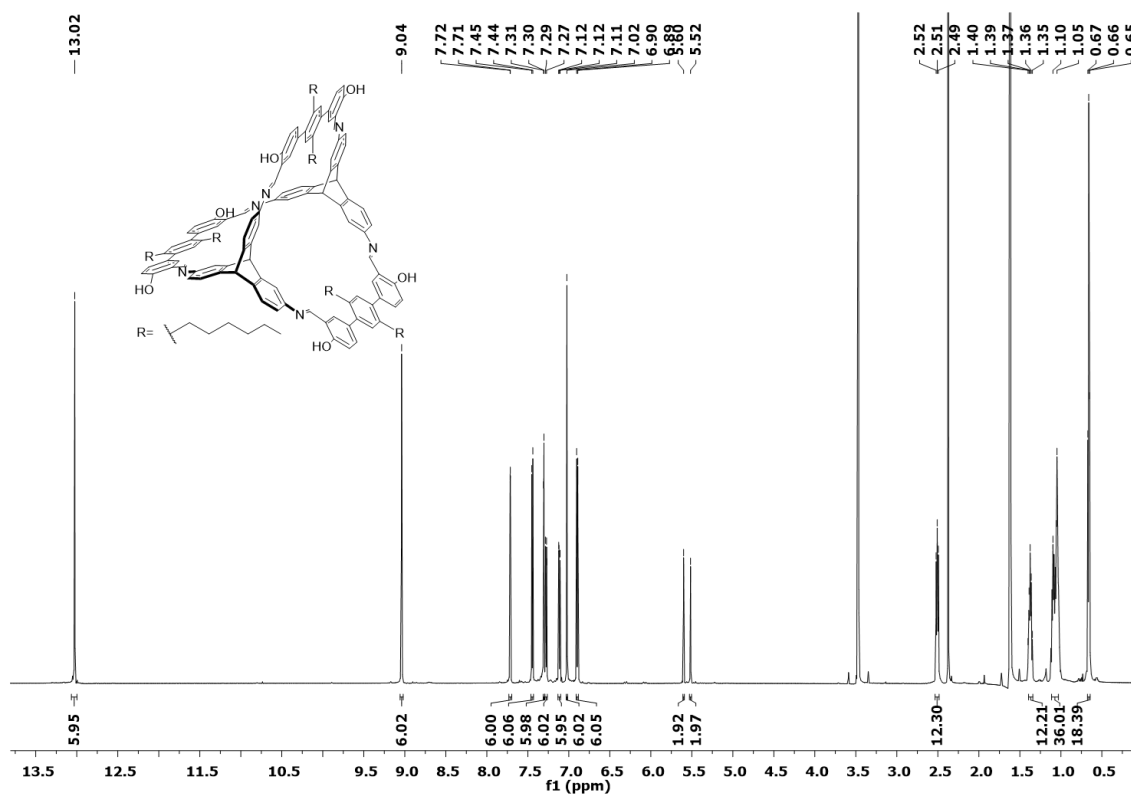
Figure 83. ^{1}H NMR spectrum of cage compound **105** in THF-d$_8$ (500 MHz).
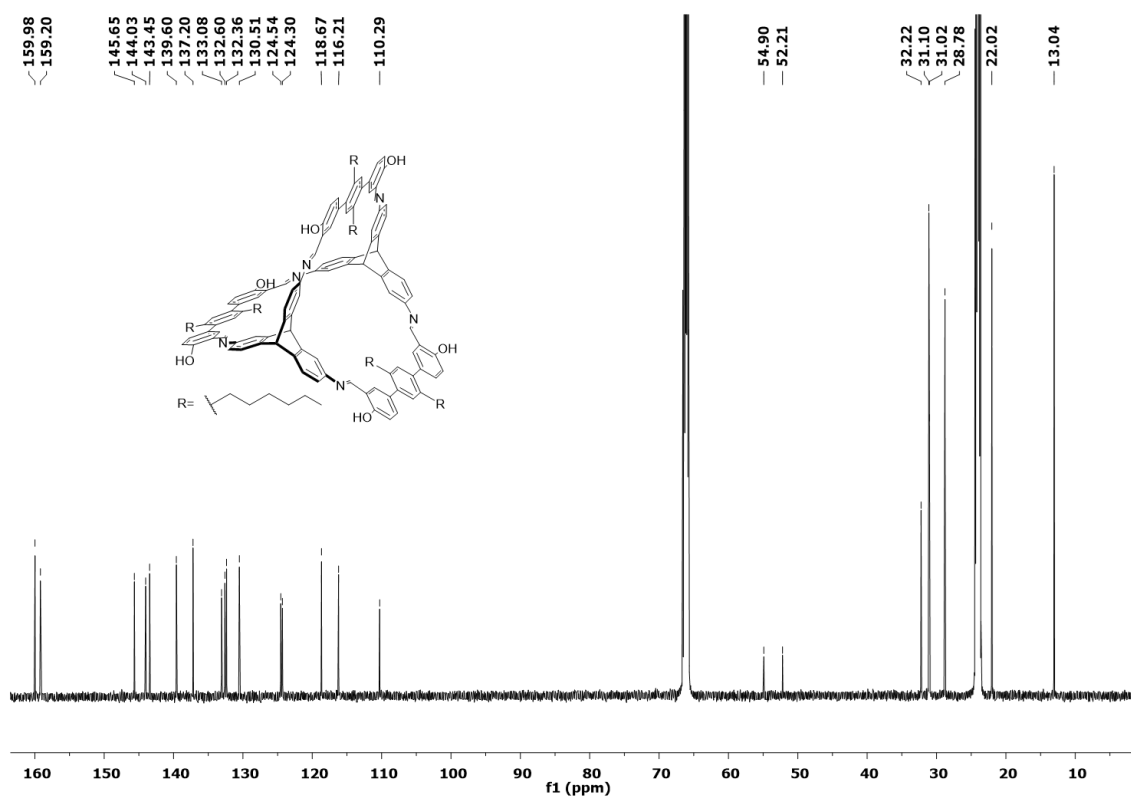
Figure 84. ^{13}C NMR spectrum of cage compound **105** in THF-d$_8$ (125 MHz).
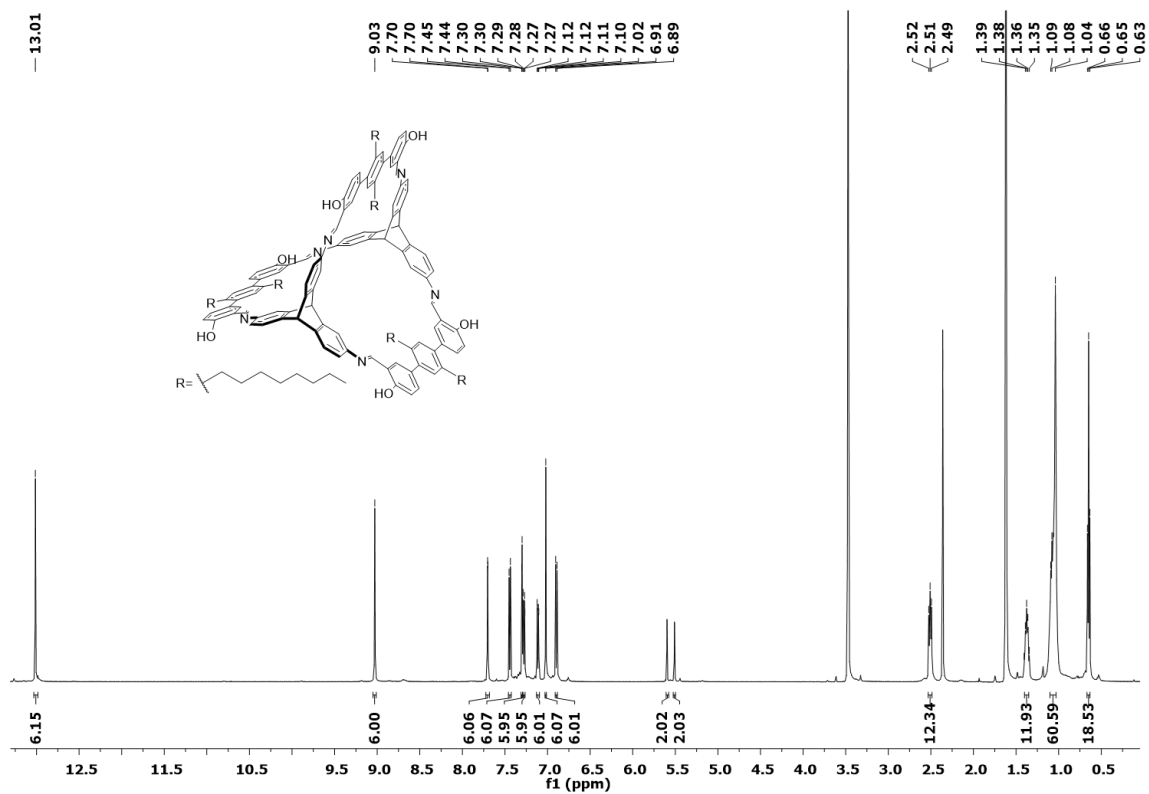
Figure 85. ^{1}H NMR spectrum of cage compound **106** in THF-d$_8$ (500 MHz).
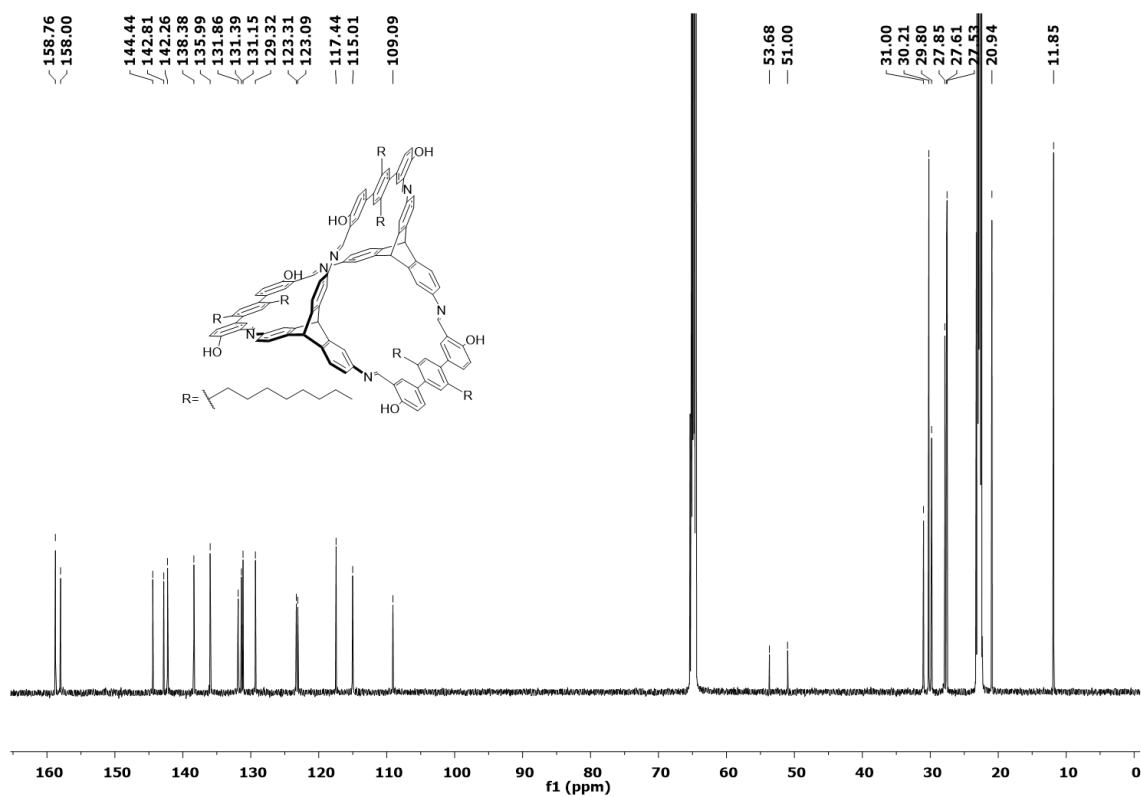
Figure 86. ^{13}C NMR spectrum of cage compound **106** in THF-d$_8$ (125 MHz).
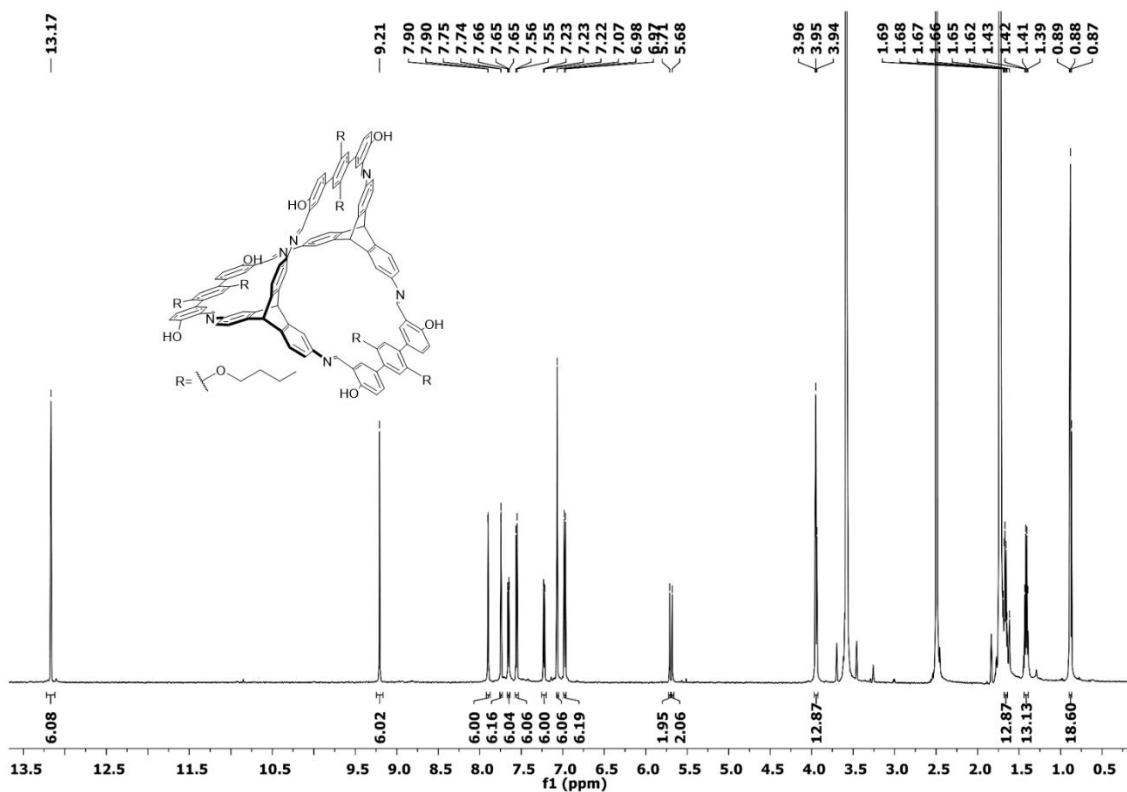
Figure 87. ^{1}H NMR spectrum of cage compound **107** in THF-d$_8$ (500 MHz).
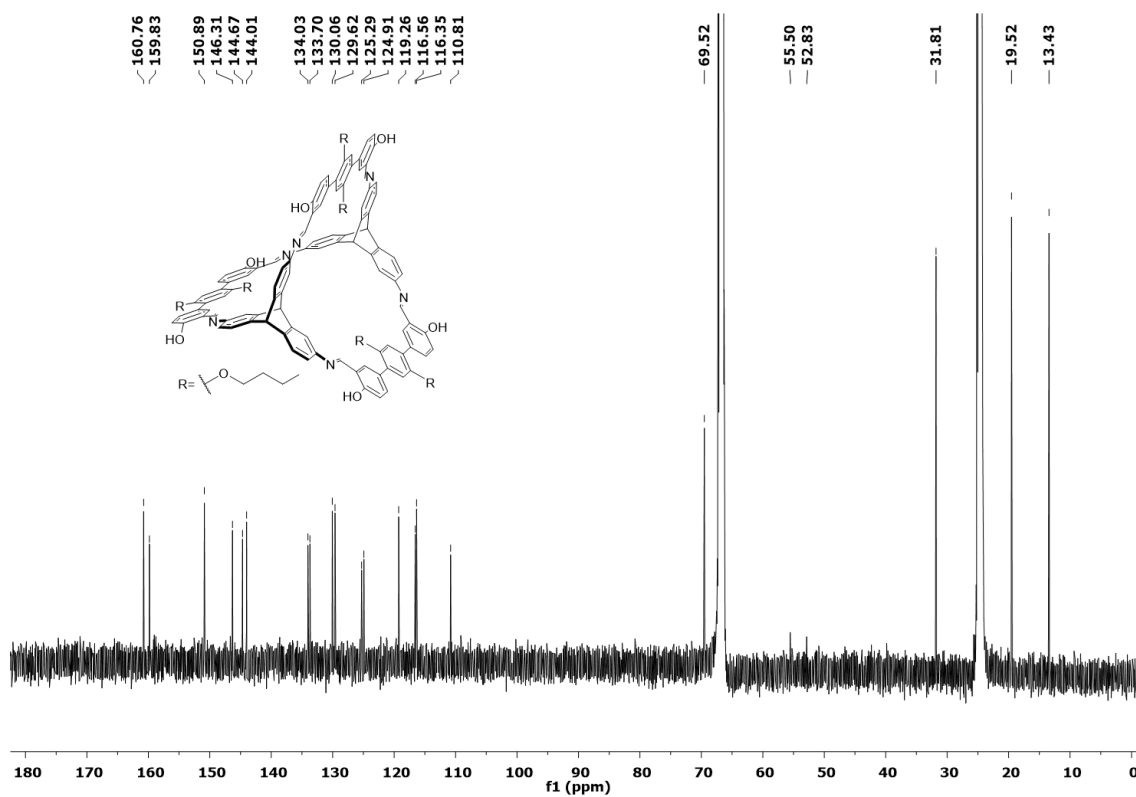
Figure 88. ^{13}C NMR spectrum of cage compound **107** in THF-d$_8$ (125 MHz).
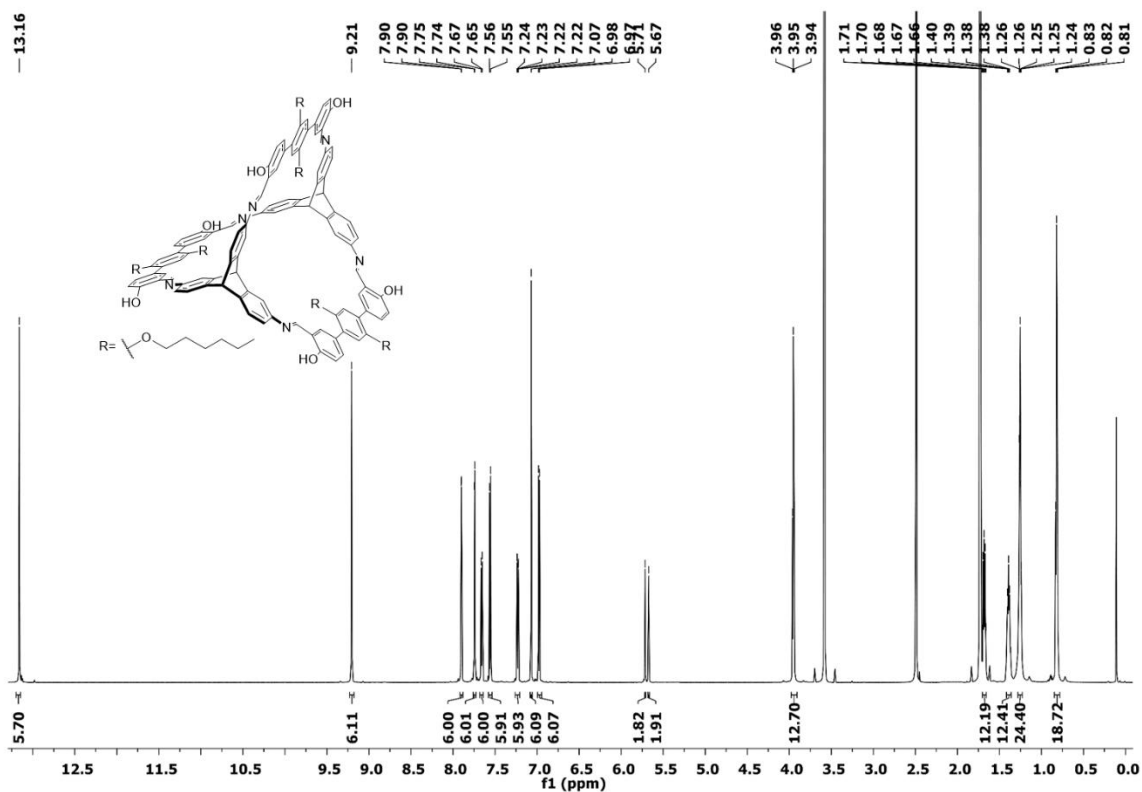
Figure 89. ^{1}H NMR spectrum of cage compound **108** in THF-d$_8$ (500 MHz).
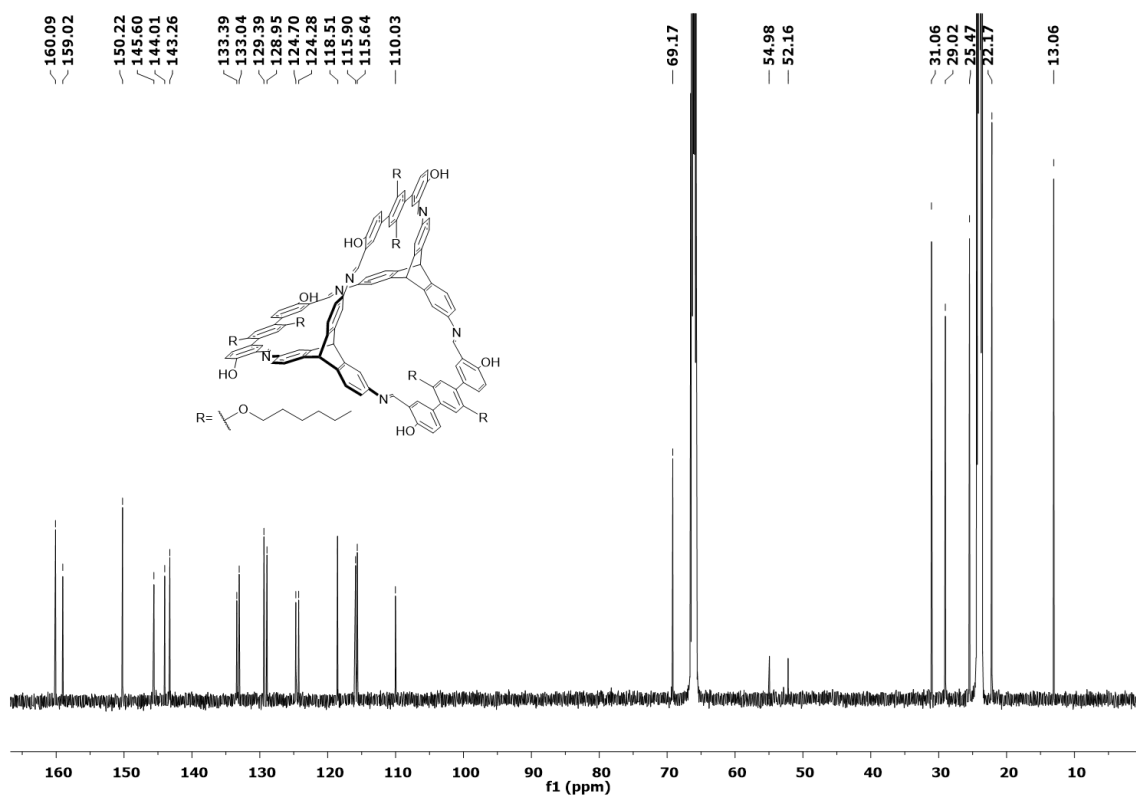
Figure 90. ^{13}C NMR spectrum of cage compound **108** in THF-d$_8$ (125 MHz).
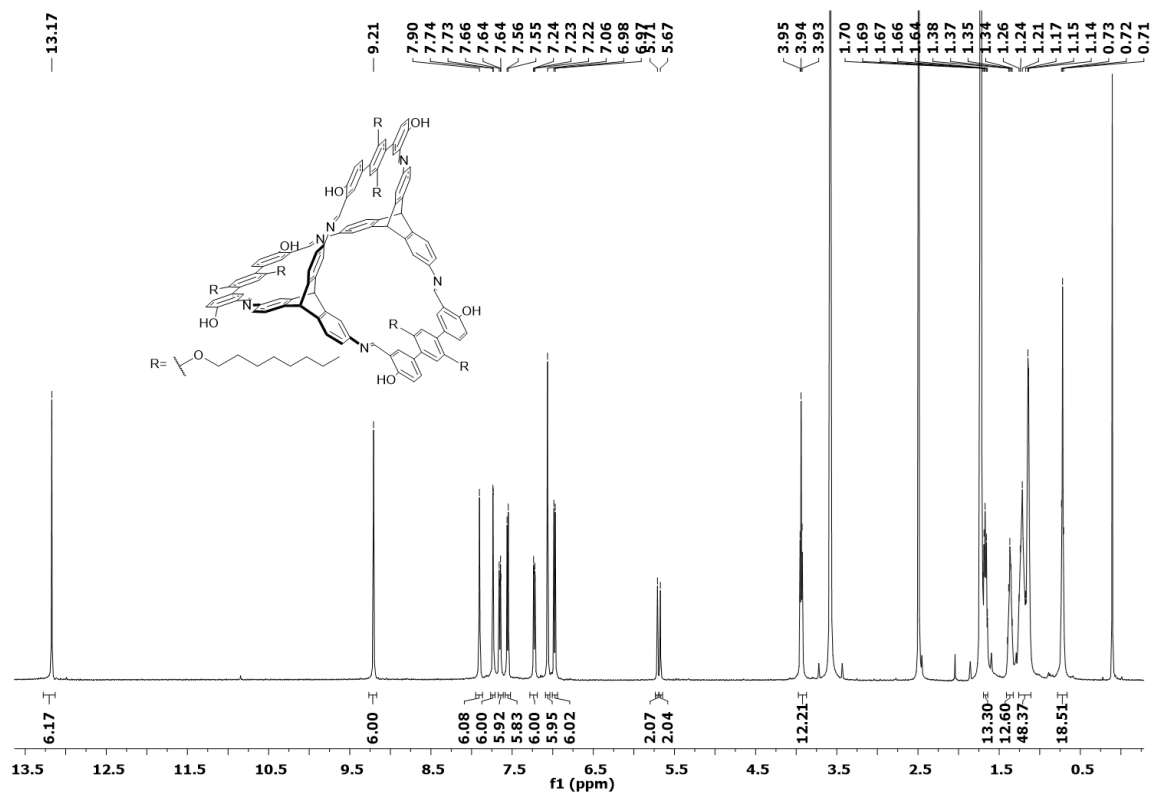
Figure 91. ^{1}H NMR spectrum of cage compound **109** in THF-d[8] (500 MHz).
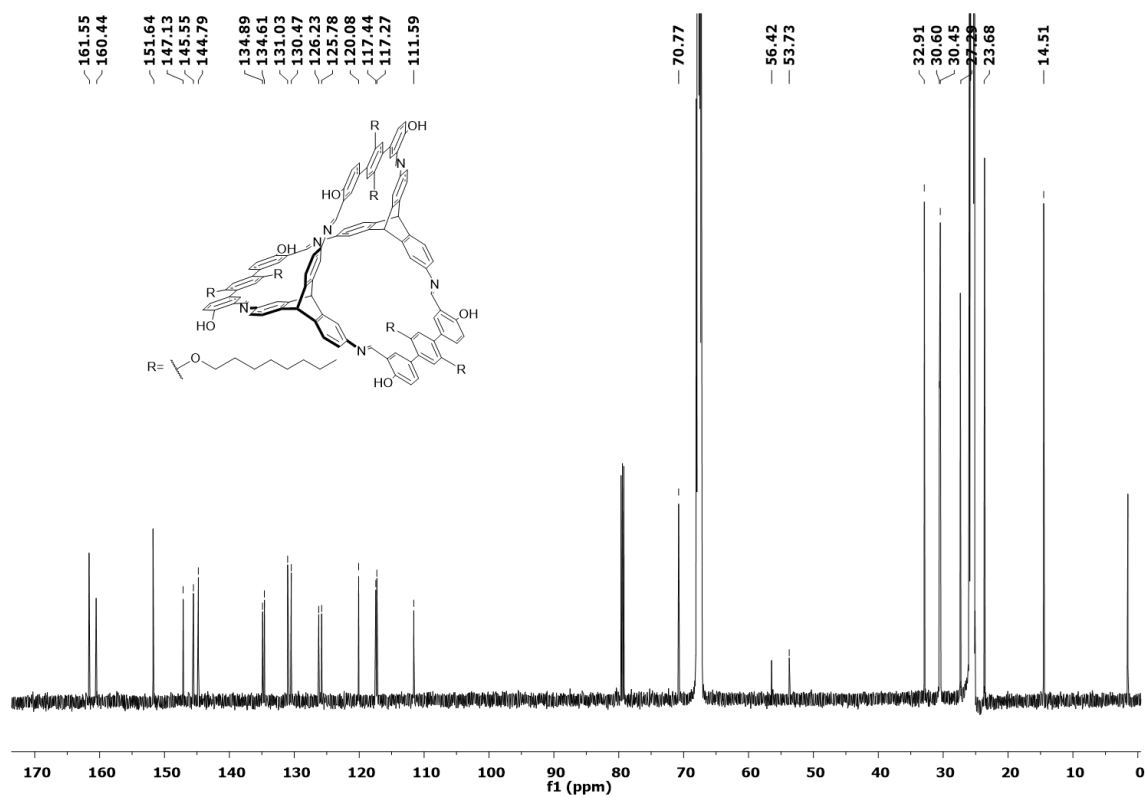
Figure 92. ^{13}C NMR spectrum of cage compound **109** in THF-d[8] (125 MHz).
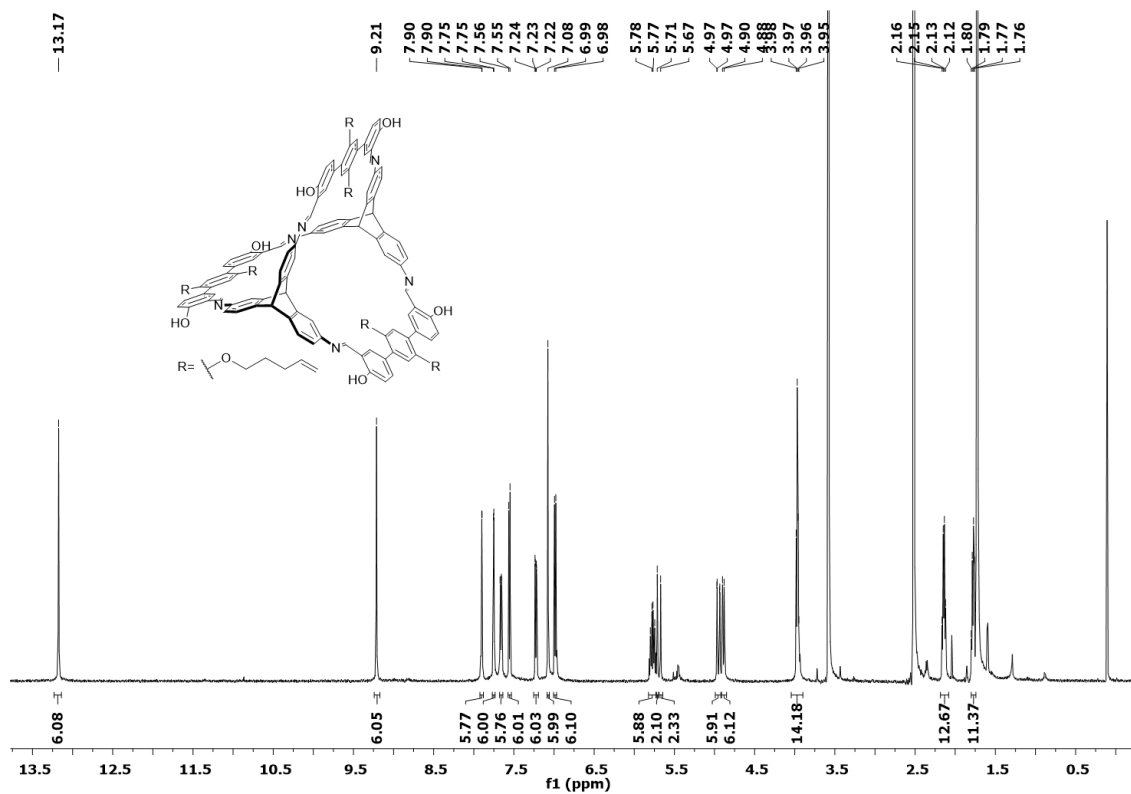
Figure 93. ^{1}H NMR spectrum of cage compound **110** in THF-d$_8$ (500 MHz).
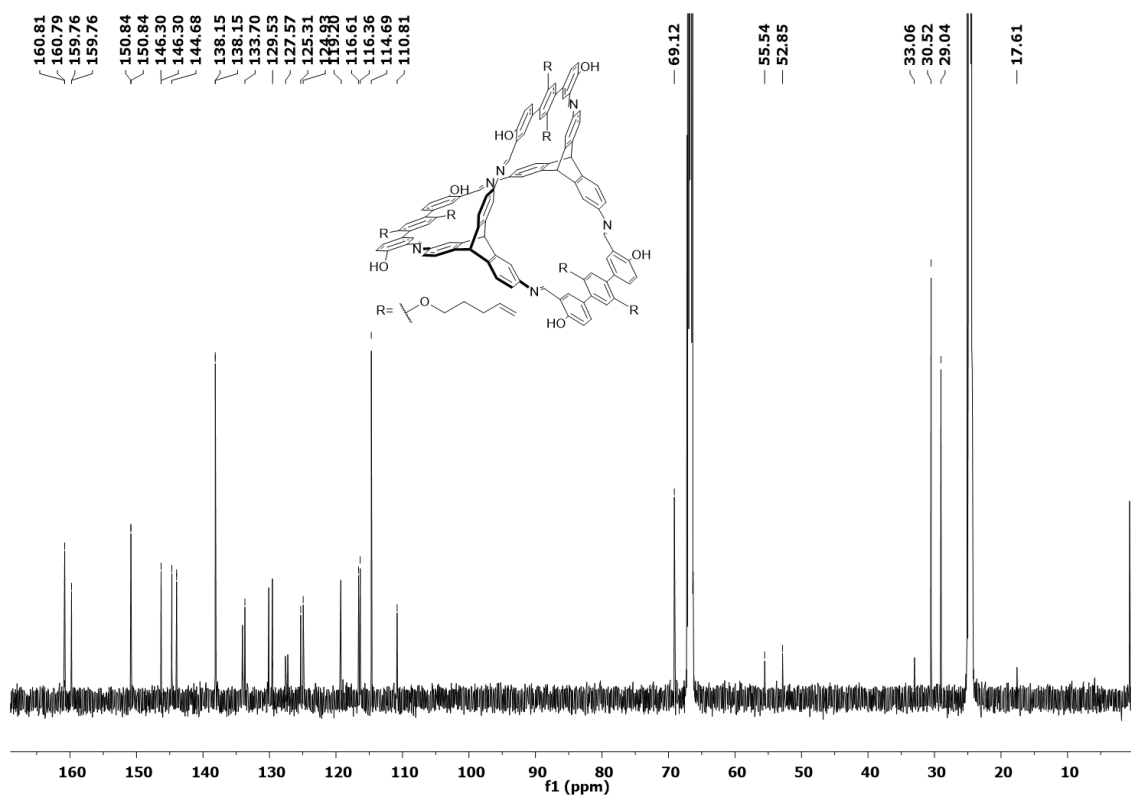
Figure 94. ^{13}C NMR spectrum of cage compound **110** in THF-d$_8$ (125 MHz).
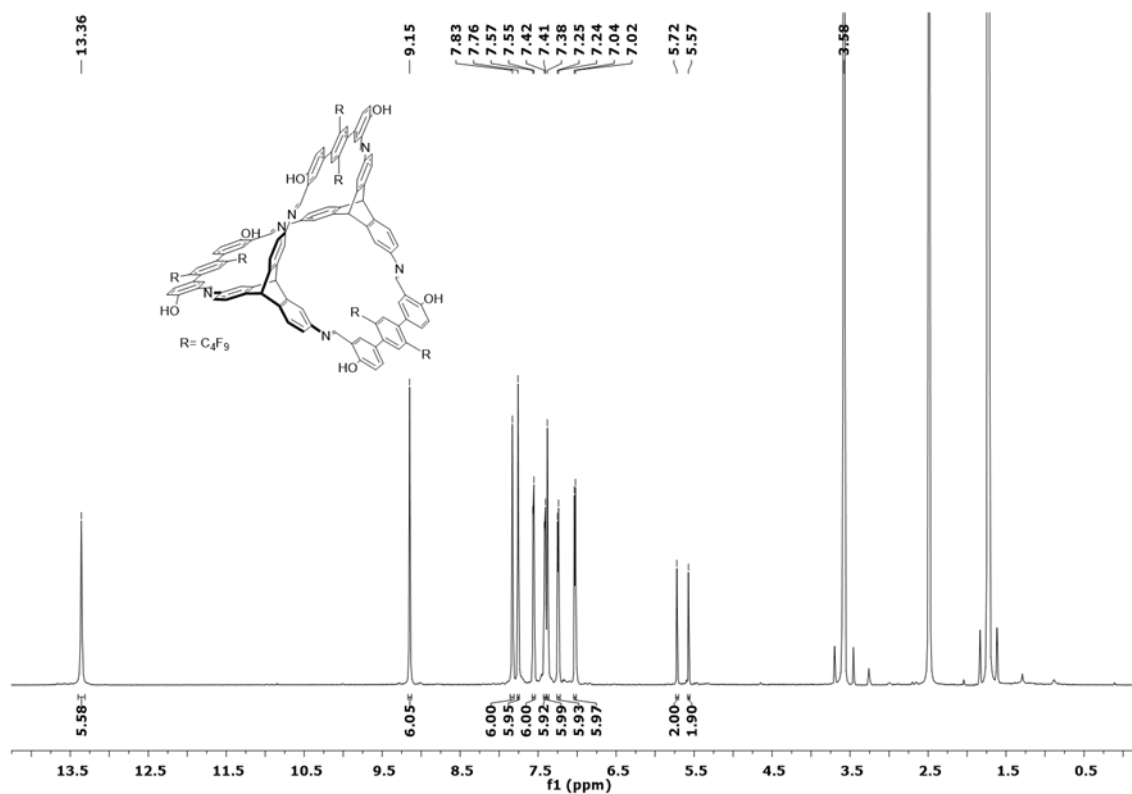
Figure 95. ^{1}H NMR spectrum of cage compound **111** in THF-d$_8$ (500 MHz).
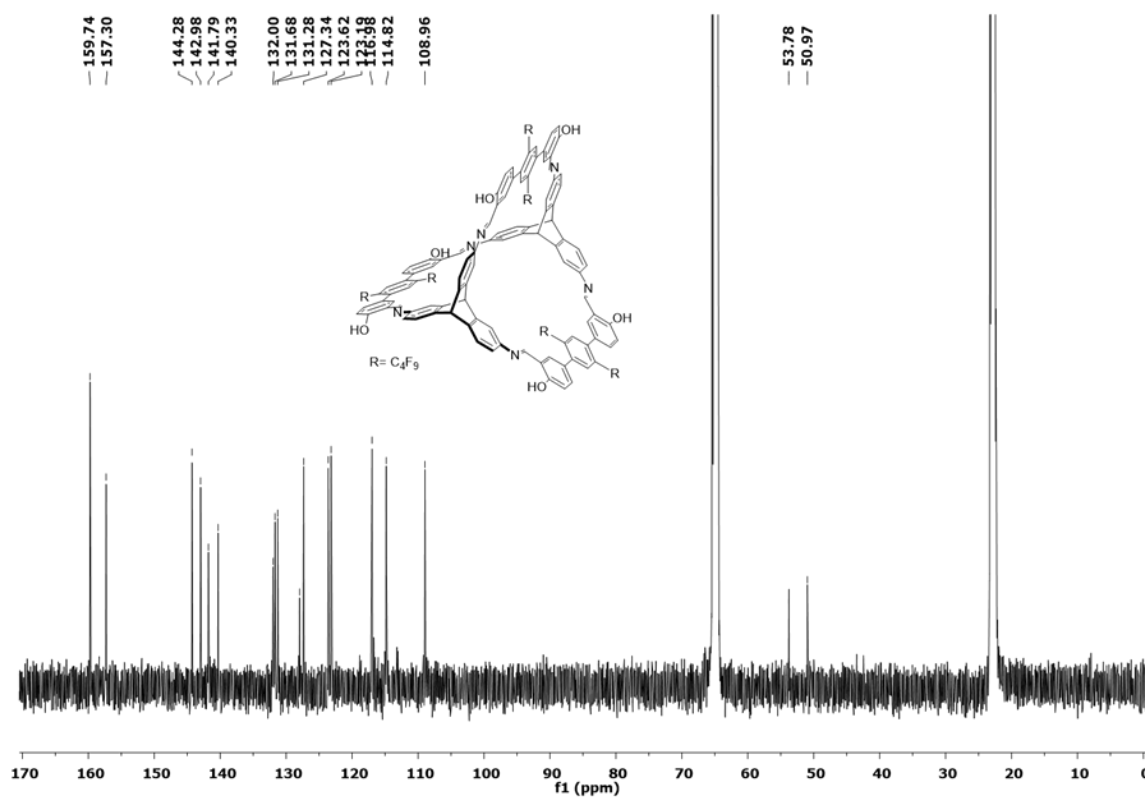
Figure 96. ^{13}C NMR spectrum of cage compound **111** in THF-d$_8$ (125 MHz).
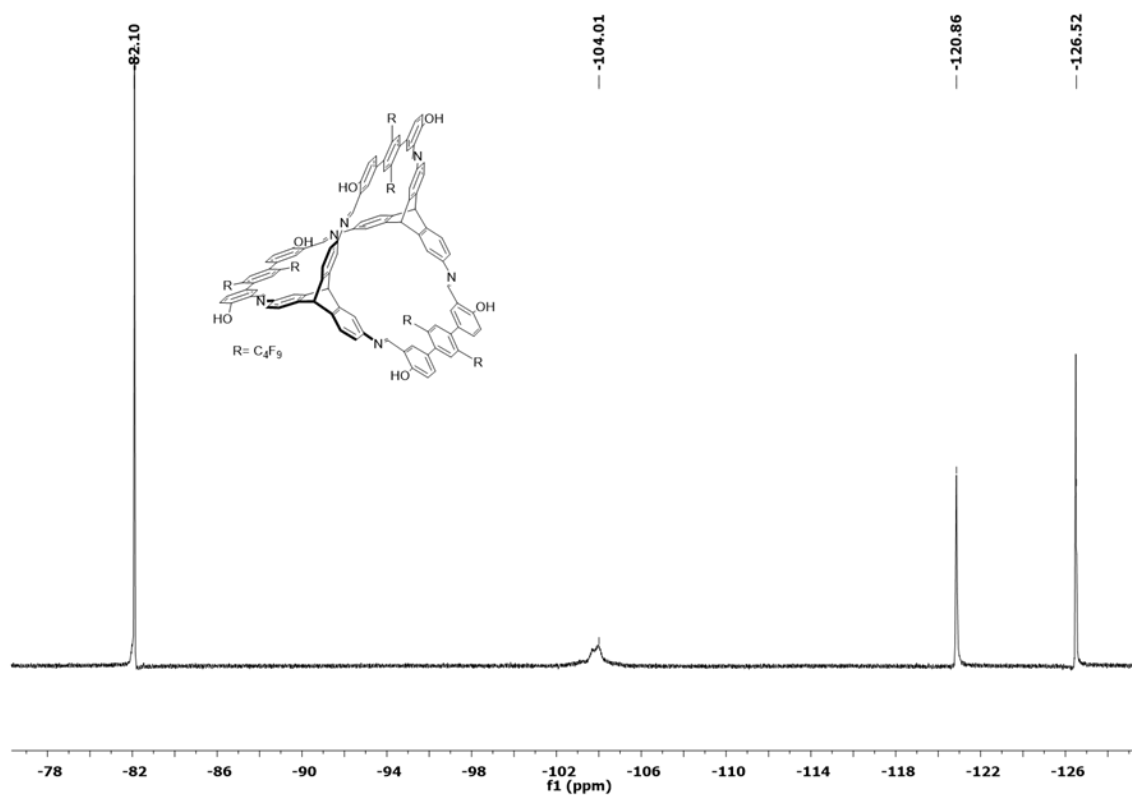
Figure 97. ^{19}F NMR spectrum of cage compound **111** in THF-d_8 (471 MHz).

Figure 98. ^1H NMR spectrum of cage compound **112** in DMSO-d_6 (500 MHz, 100 °C).
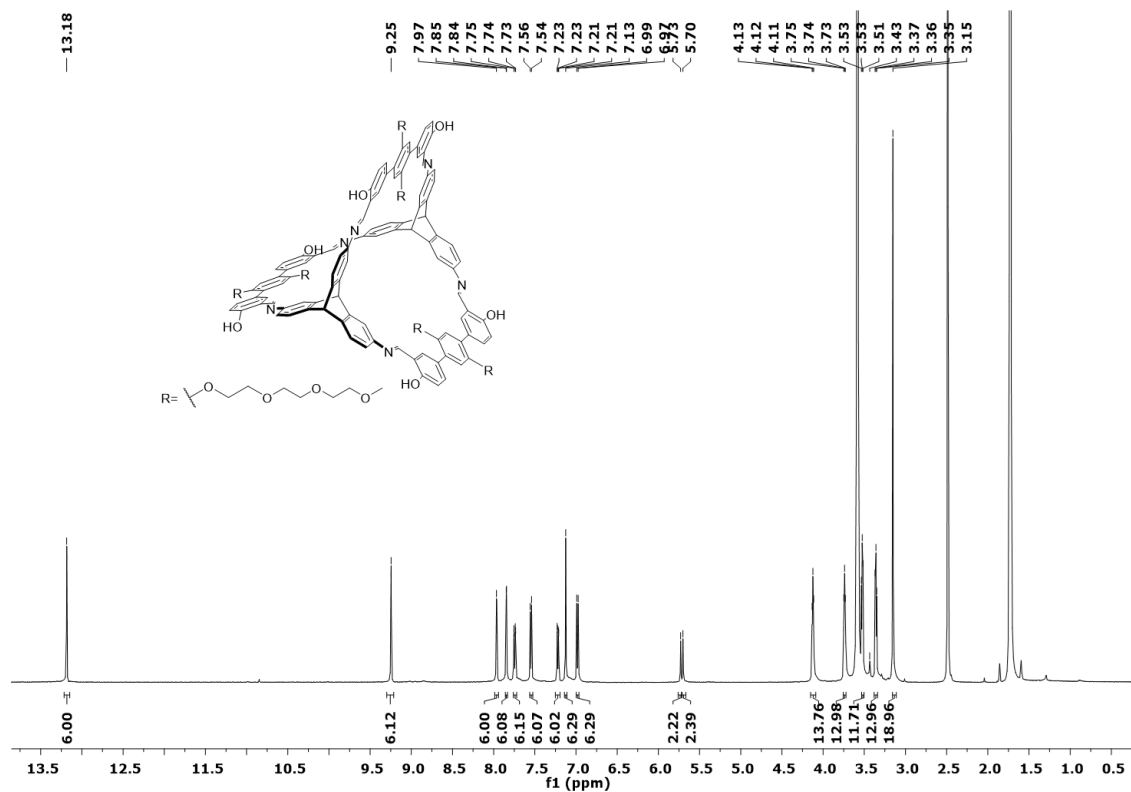
Figure 99. ^{1}H NMR spectrum of cage compound **113** in THF-d$_8$ (500 MHz).
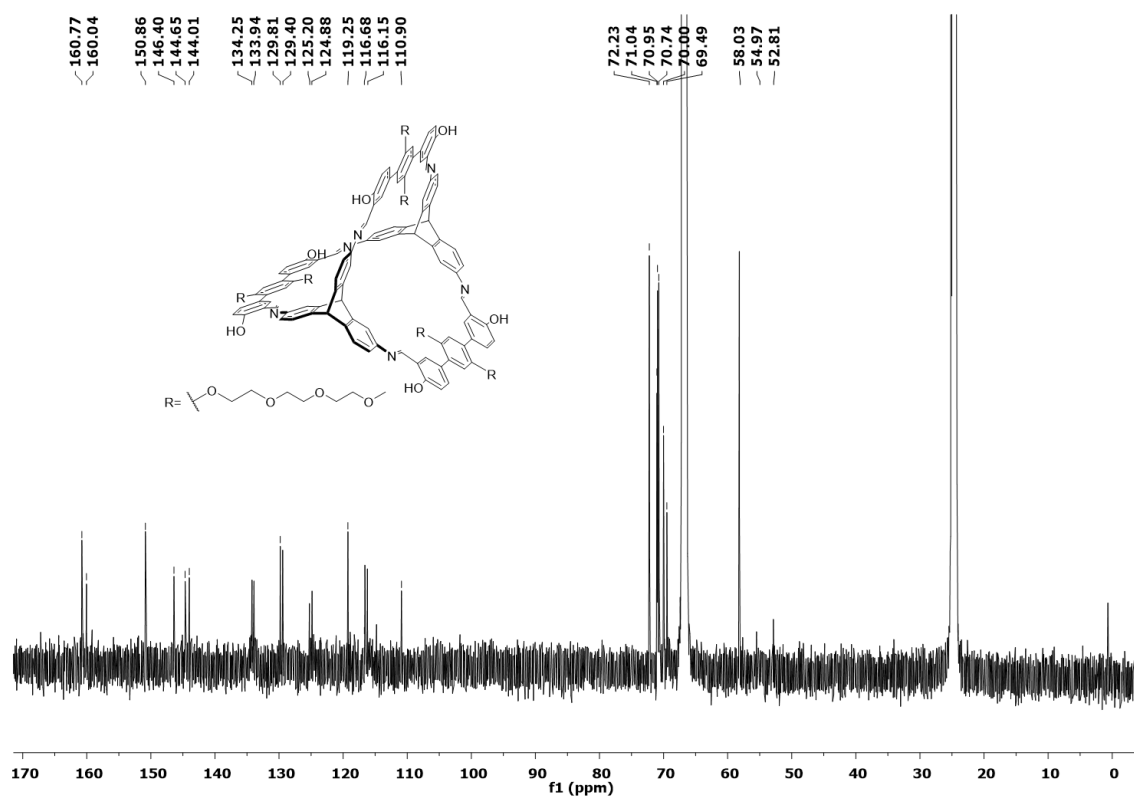
Figure 100. ^{13}C NMR spectrum of cage compound **113** in THF-d$_8$ (125 MHz).
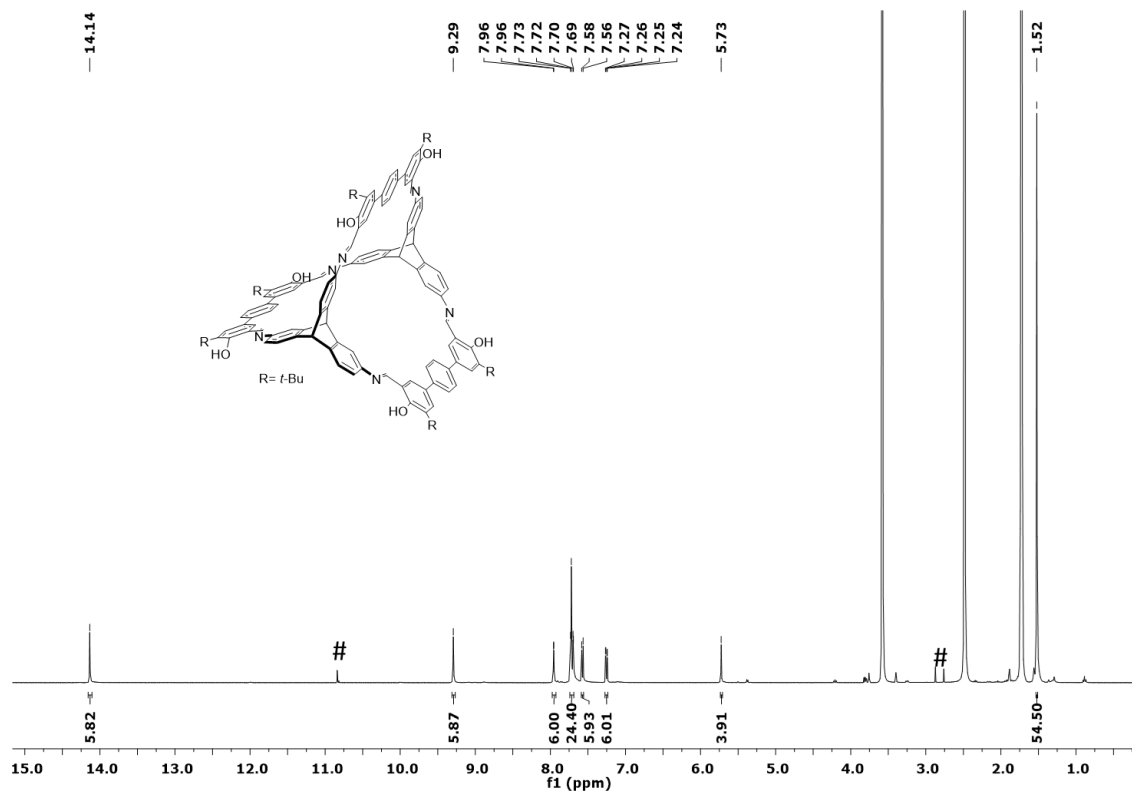
Figure 101. ^{1}H NMR spectrum of cage compound **114** in THF-d$_8$ (500 MHz). # is the peak of remaining DMF.
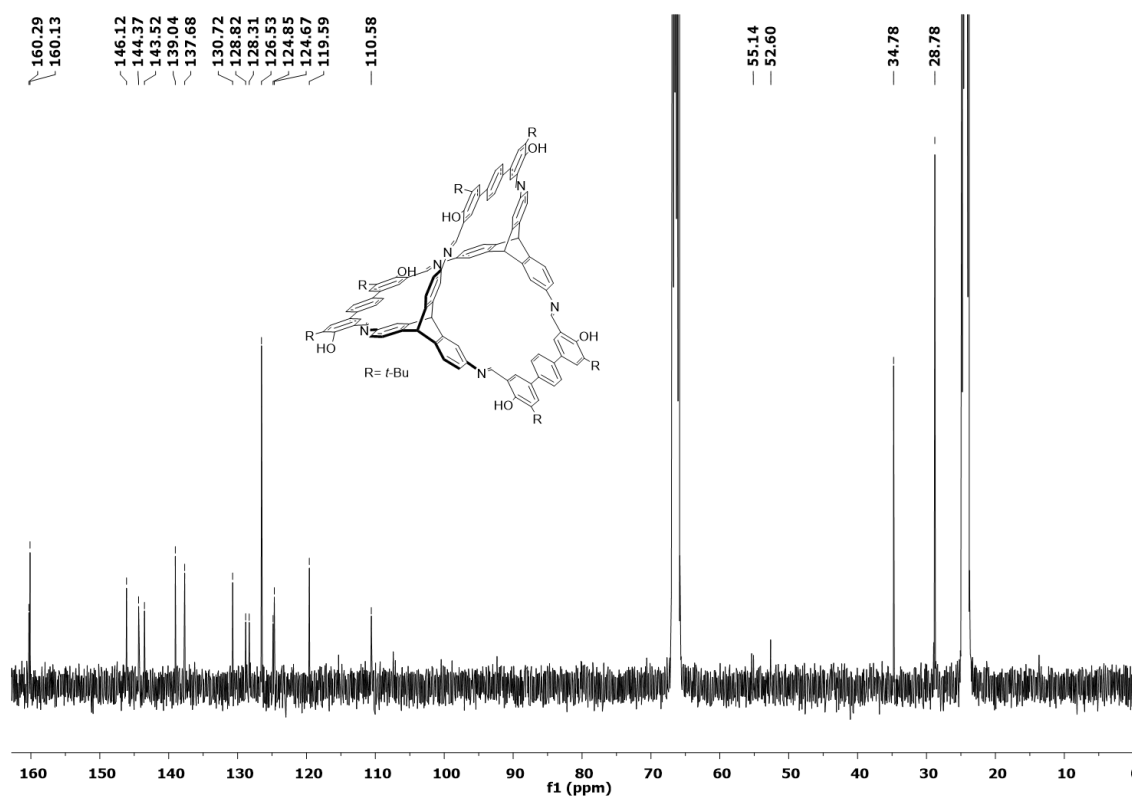
Figure 102. ^{13}C NMR spectrum of cage compound **114** in THF-d$_8$ (125 MHz).
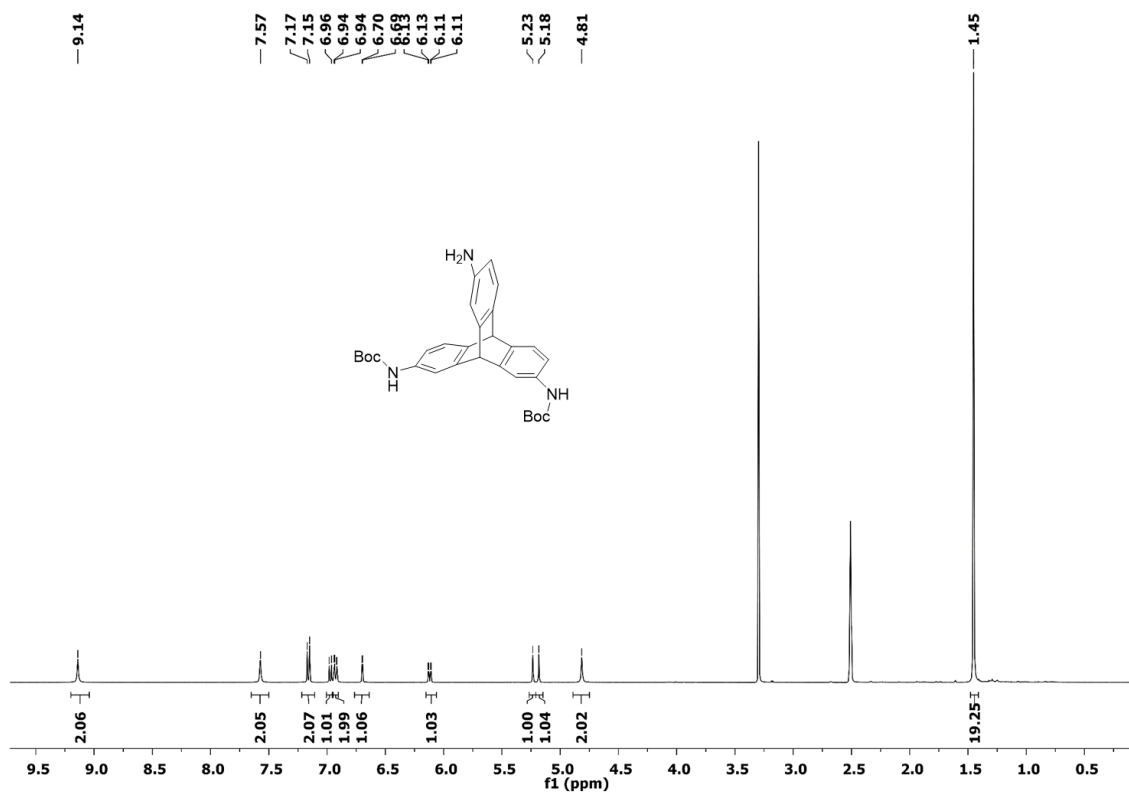
Figure 103. ^{1}H NMR spectrum of **115** in DMSO-d$_6$ (300 MHz).
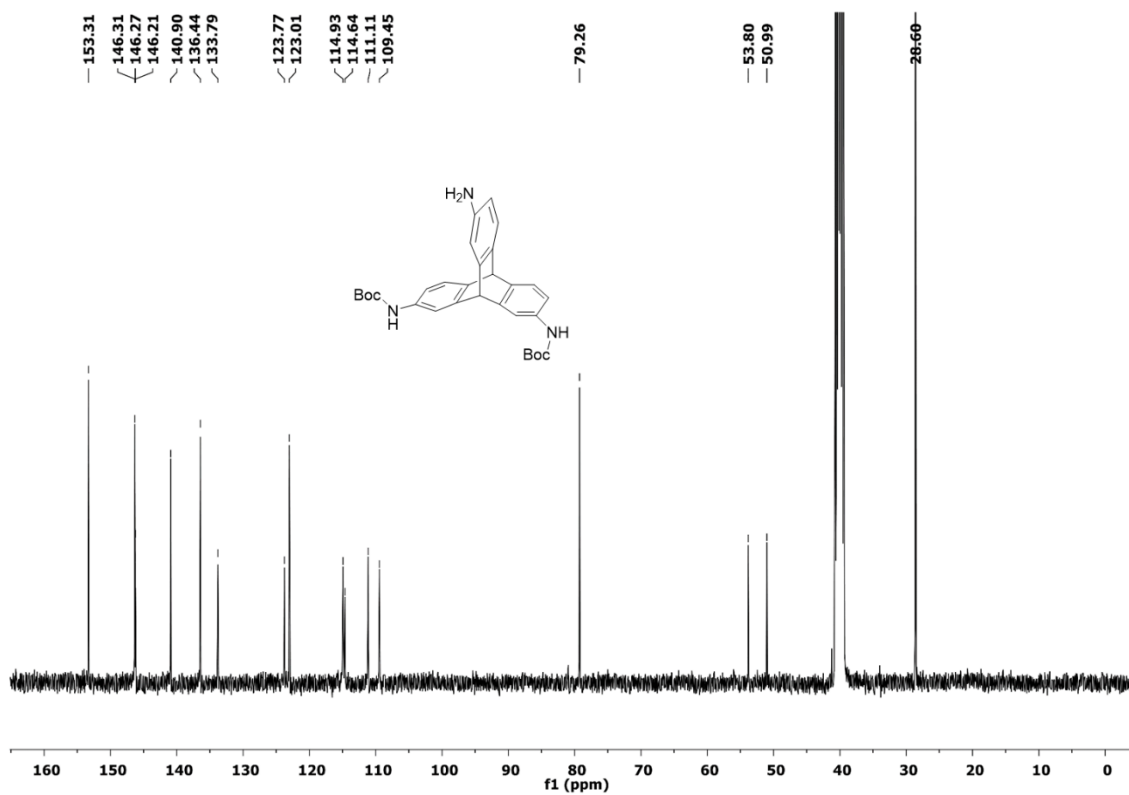
Figure 104. ^{13}C NMR spectrum of **115** in DMSO-d$_6$ (125 MHz).

Figure 105. ^{1}H NMR spectrum of **119** in DMSO-d_6 (300 MHz).
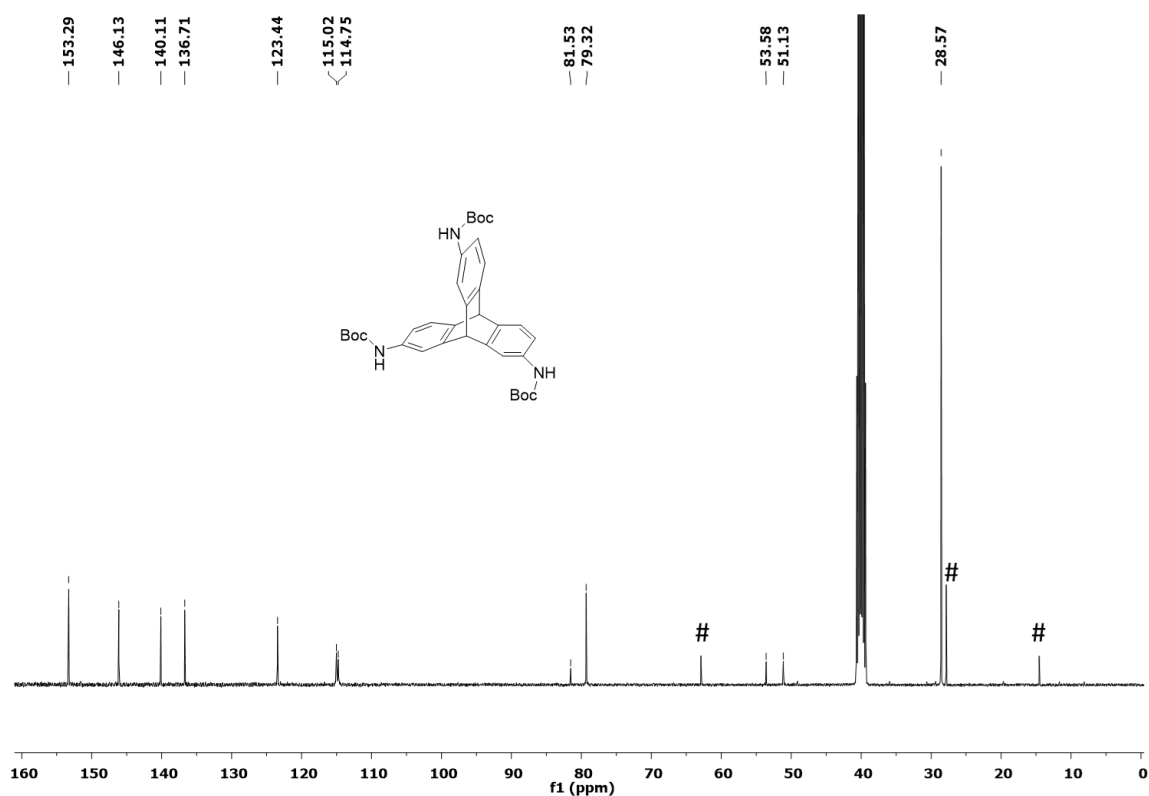

Figure 106. ^{13}C NMR spectrum of **119** in DMSO-d_6 (125 MHz).
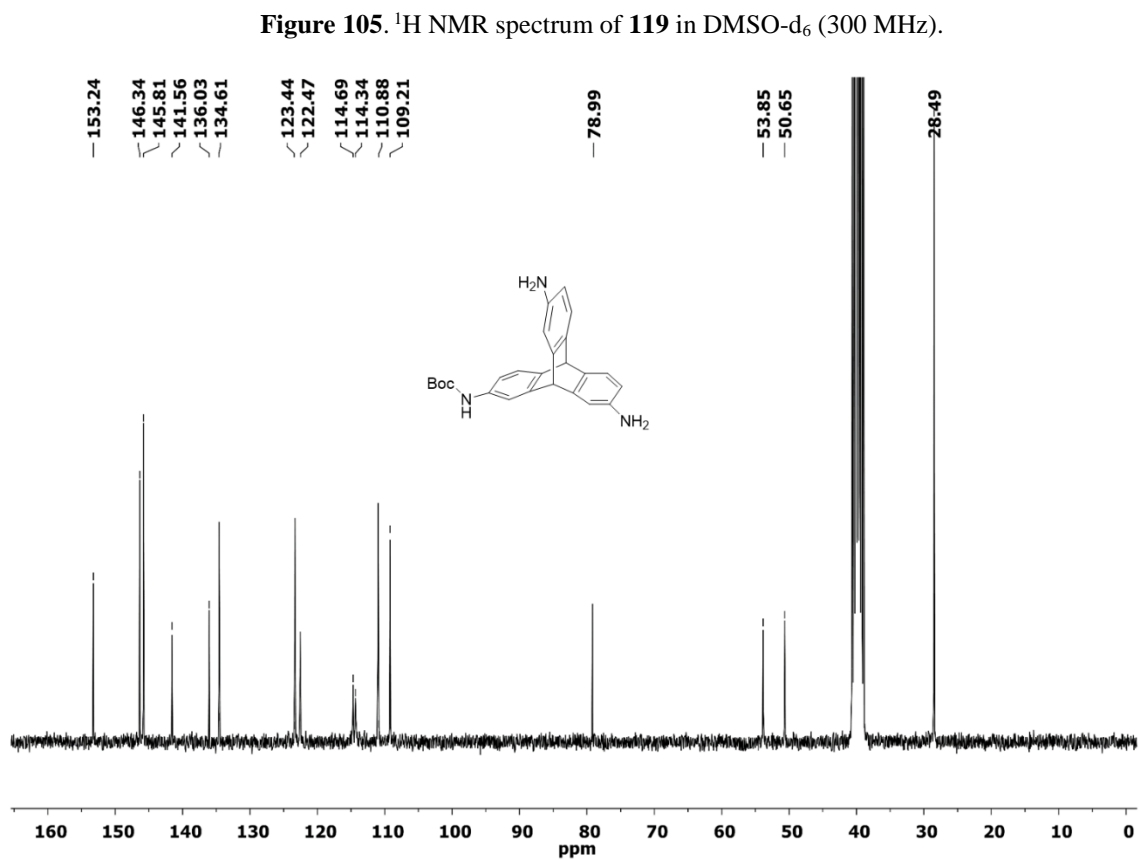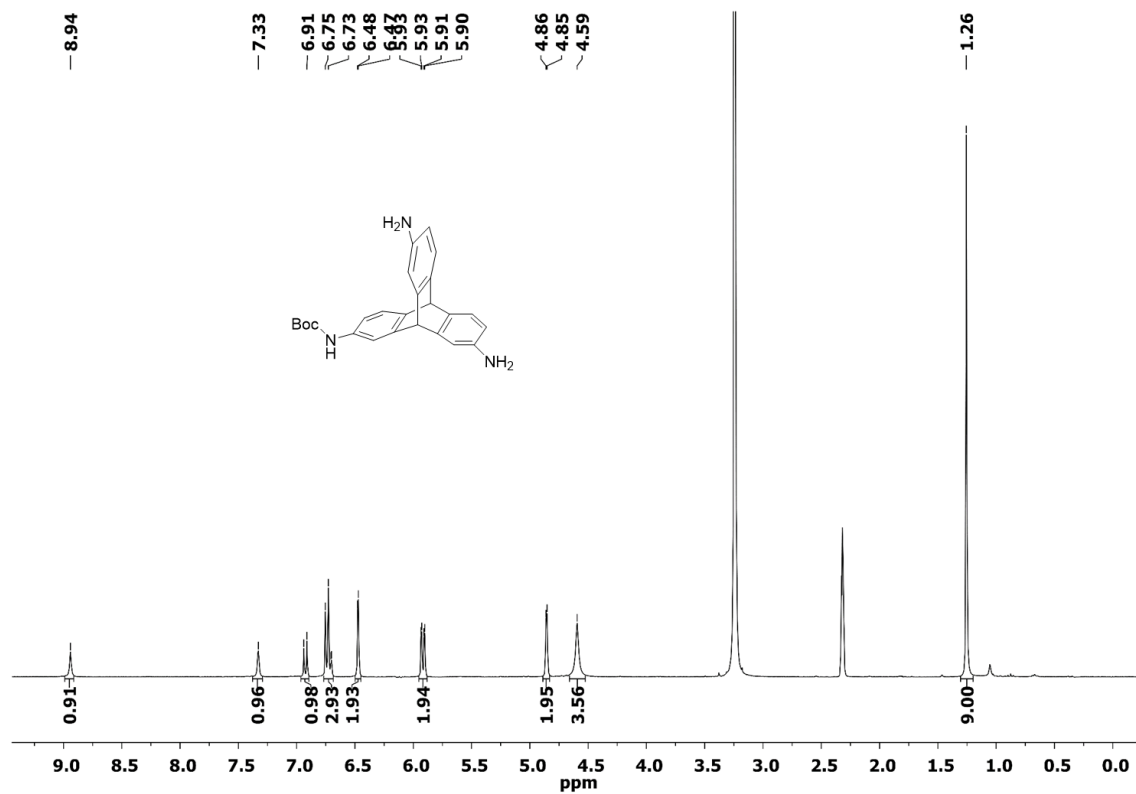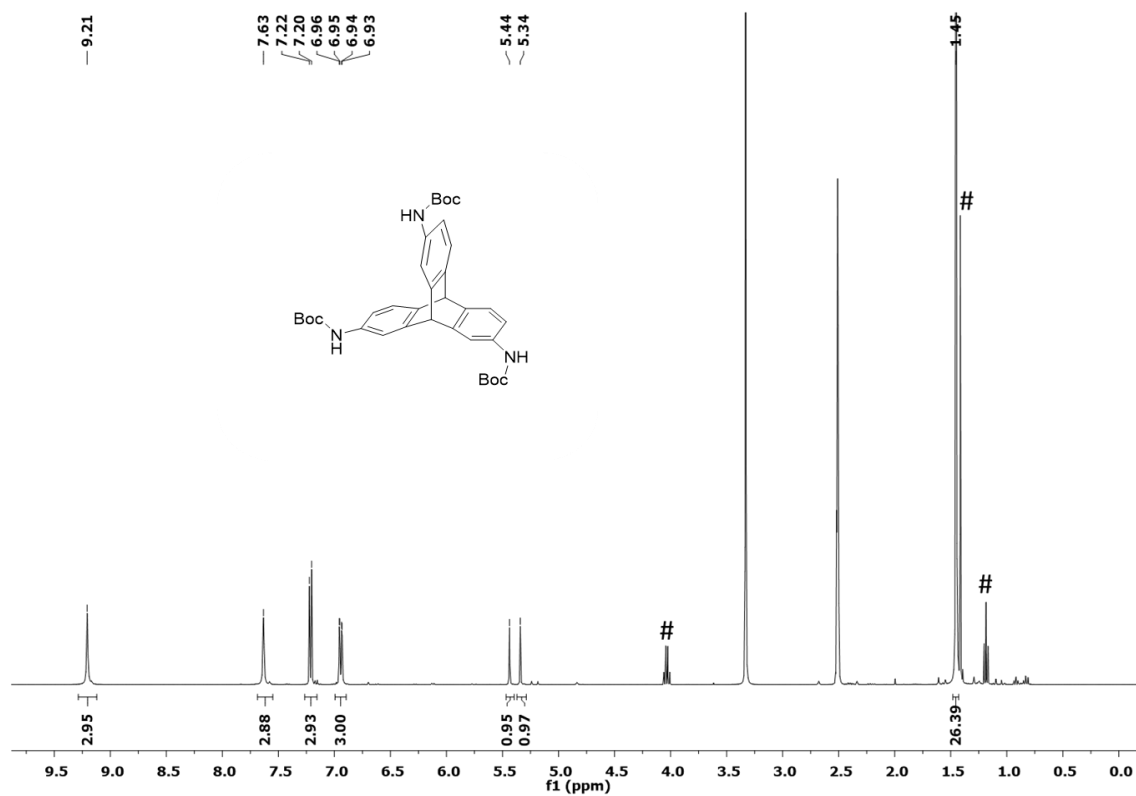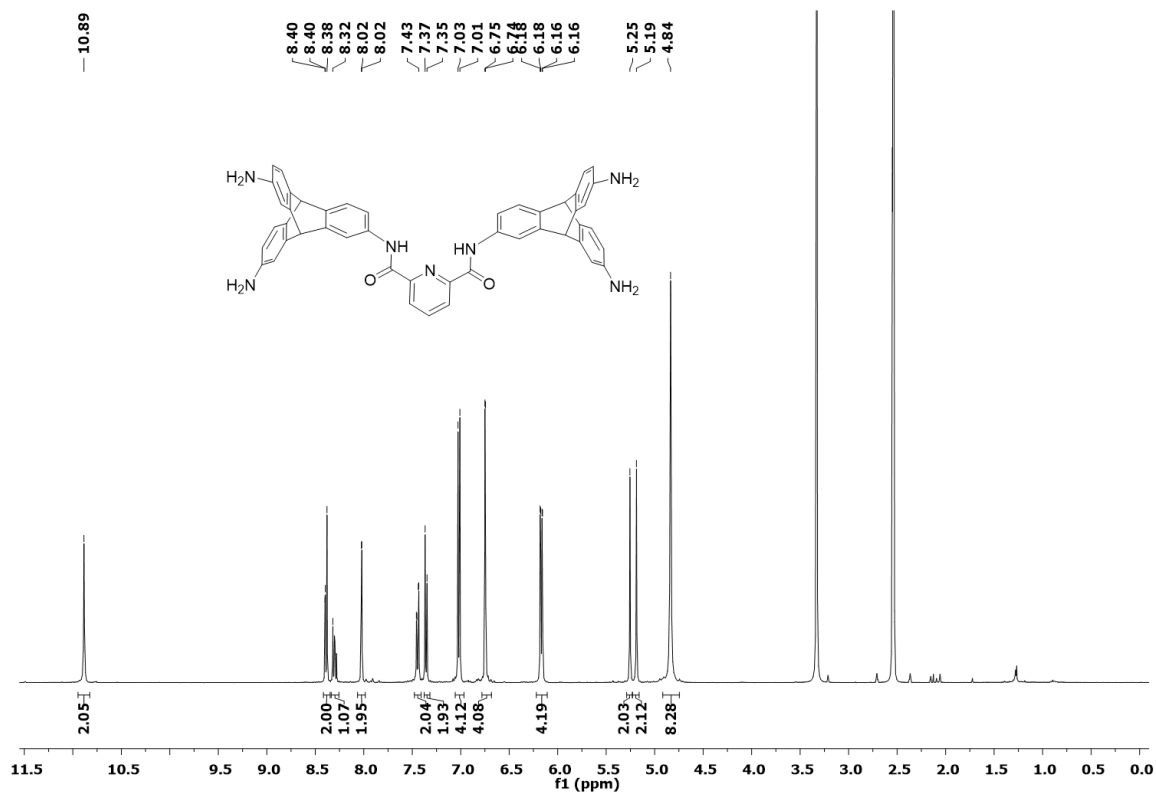
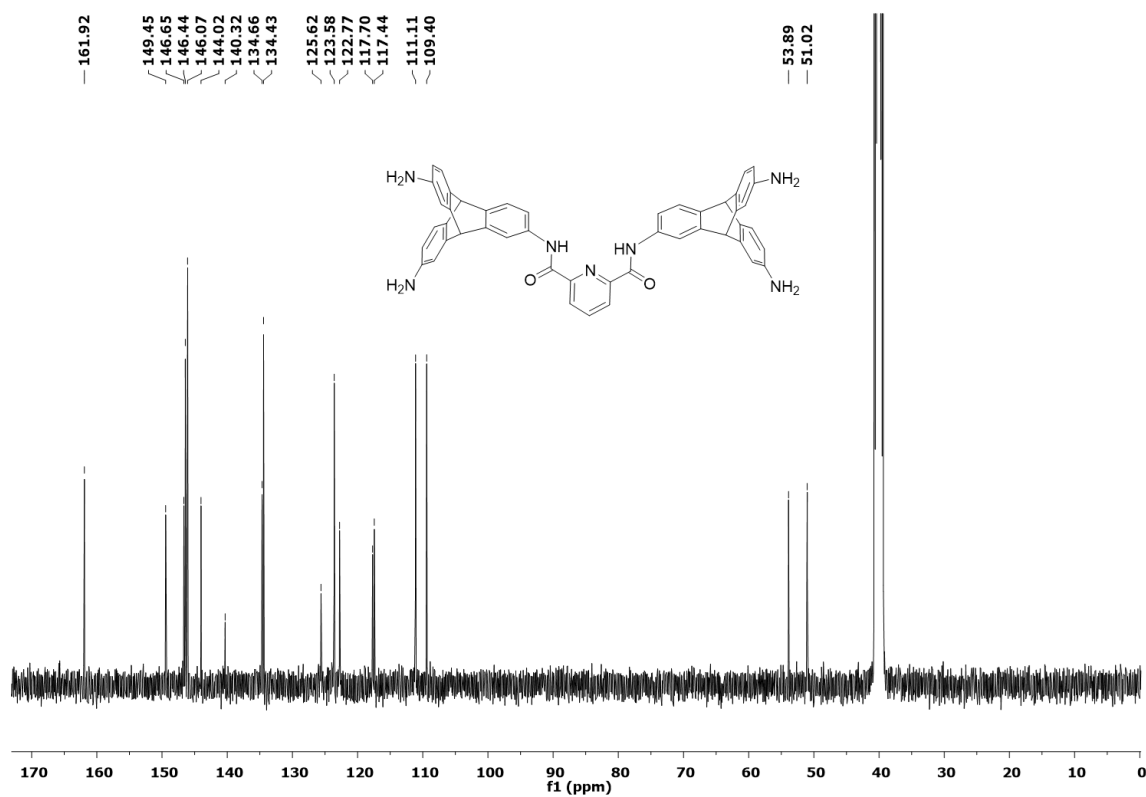**Figure 107**. ^{1}H NMR spectrum of **120** in DMSO-d$_6$ (300 MHz). # is the peak of remaining ethyl acetate.

Figure 108. ^{13}C NMR spectrum of **120** in DMSO-d$_6$ (125 MHz). # is the peak of remaining ethyl acetate.

Figure 109. [^1]H NMR spectrum of **118** in DMSO-d$_6$ (500 MHz).

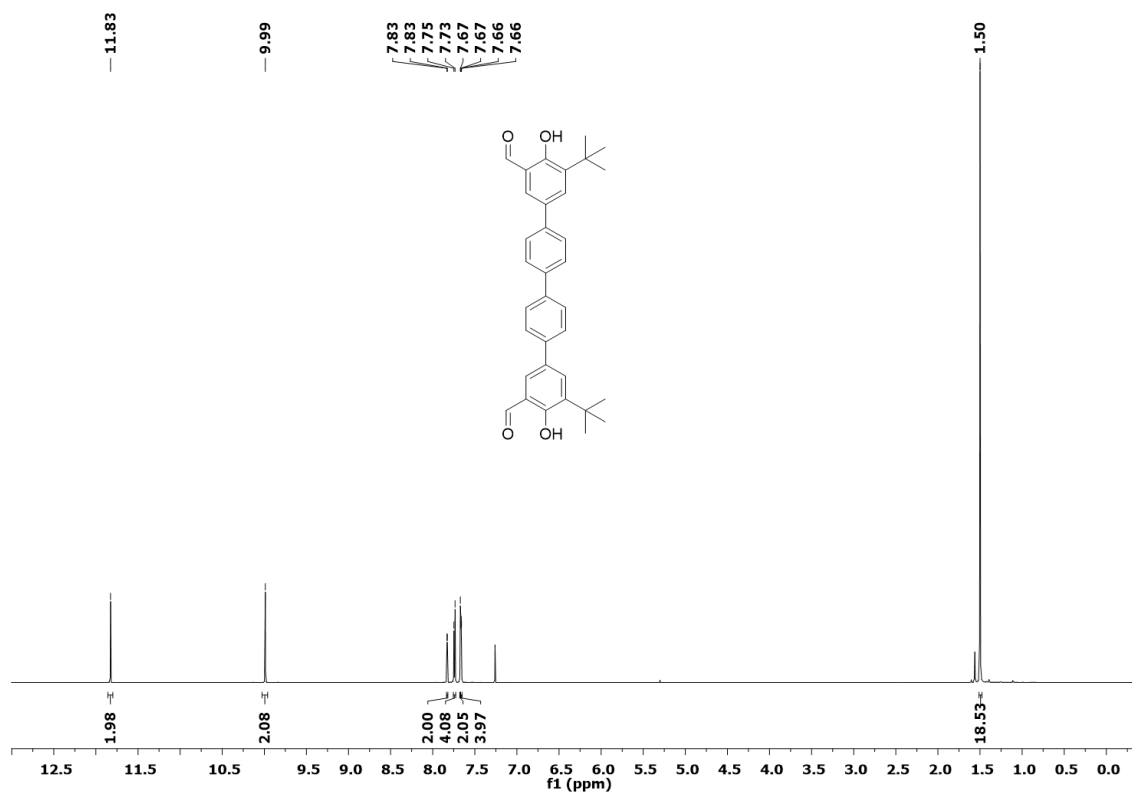**Figure 110**. [^13]C NMR spectrum of **118** in DMSO-d$_6$ (125 MHz).

Figure 111. ^{1}H NMR spectrum of **122** in CDCl$_3$ (400 MHz).
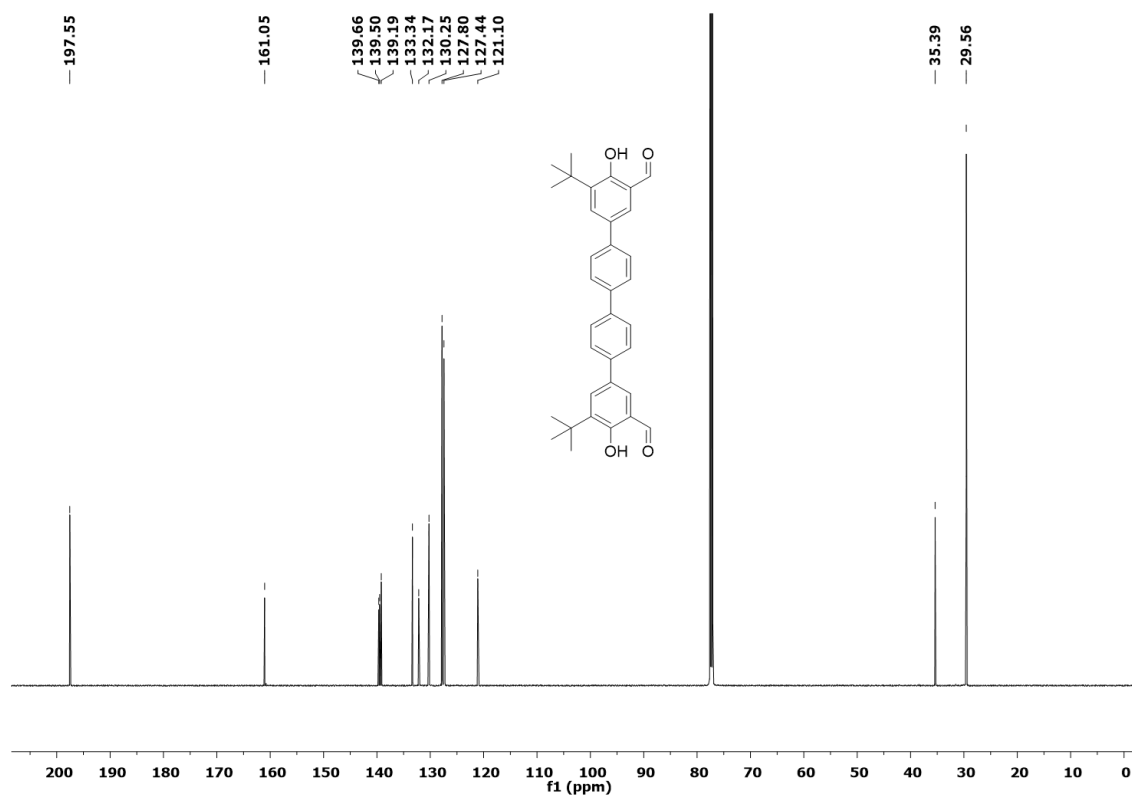
Figure 112. ^{13}C NMR spectrum of **122** in CDCl$_3$ (100 MHz).
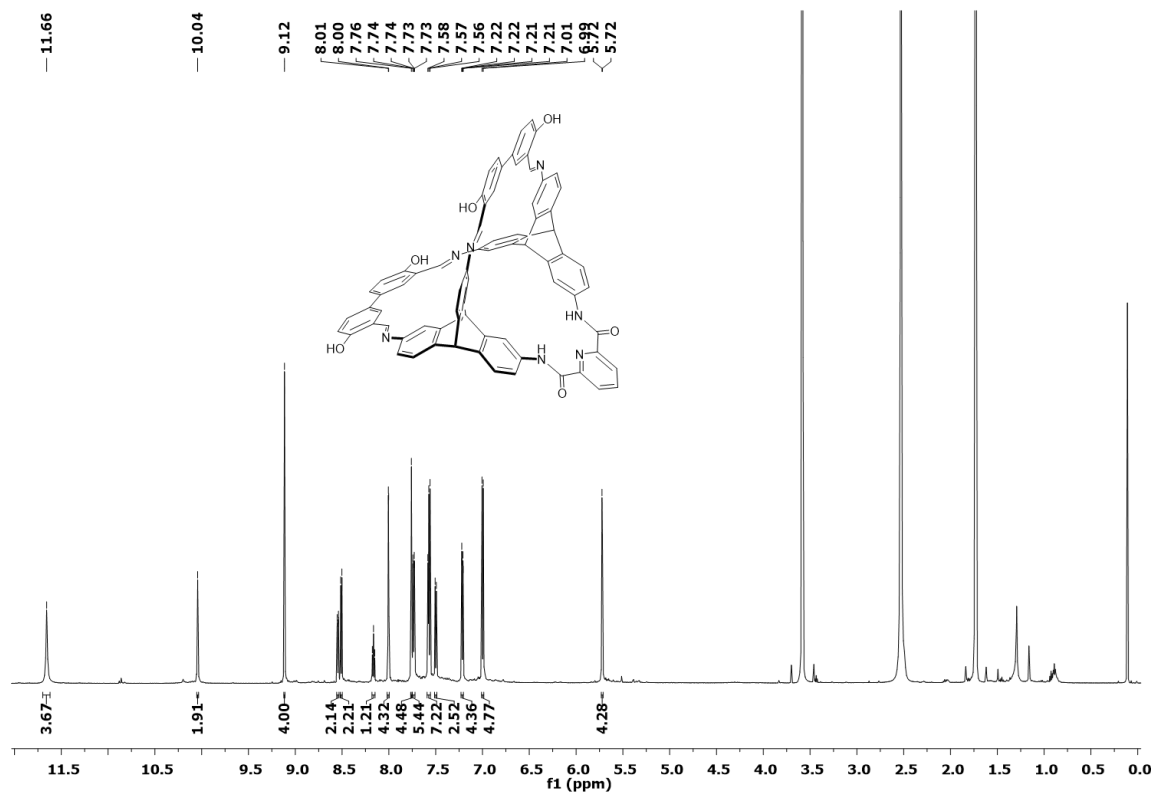
Figure 113. ^{1}H NMR spectrum of **129** in THF-d$_8$ (400 MHz).
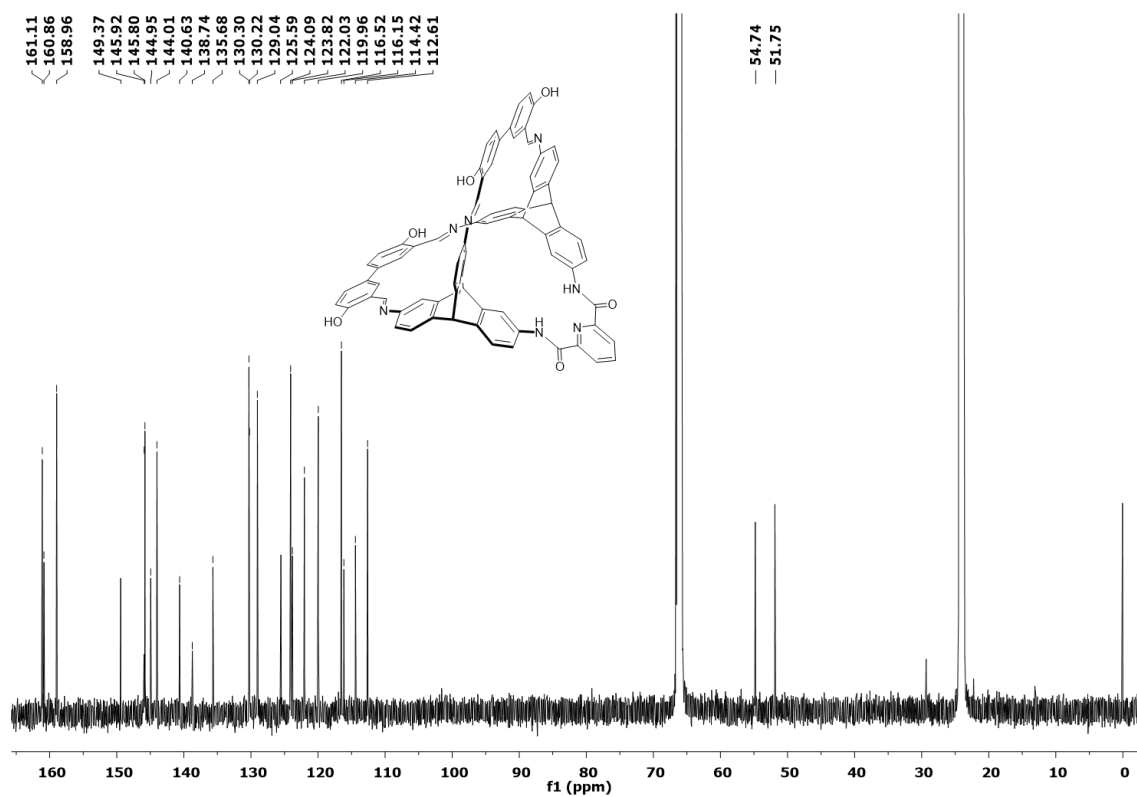
Figure 114. ^{13}C NMR spectrum of **129** in THF-d$_8$ (400 MHz).

7.2 MS spectra

Figure 115. Mass spectrum of cage 104 (MALDI-TOF, matrix: DCTB)

Figure 116. Mass spectrum of cage **105** (MALDI-TOF, matrix: DCTB).

Figure 117. Mass spectrum of cage **106** (MALDI-TOF, matrix: DCTB).

Figure 118. Mass spectrum of cage **107** (MALDI-TOF, matrix: DCTB).

Figure 119. Mass spectrum of cage **108** (MALDI-TOF, matrix: DCTB).

Figure 120. Mass spectrum of cage **109** (MALDI-TOF, matrix: DCTB).

Figure 121. Mass spectrum of cage **111** (MALDI-TOF, matrix: DCTB).

Figure 122. Mass spectrum of cage **112** (MALDI-TOF, matrix: DCTB).

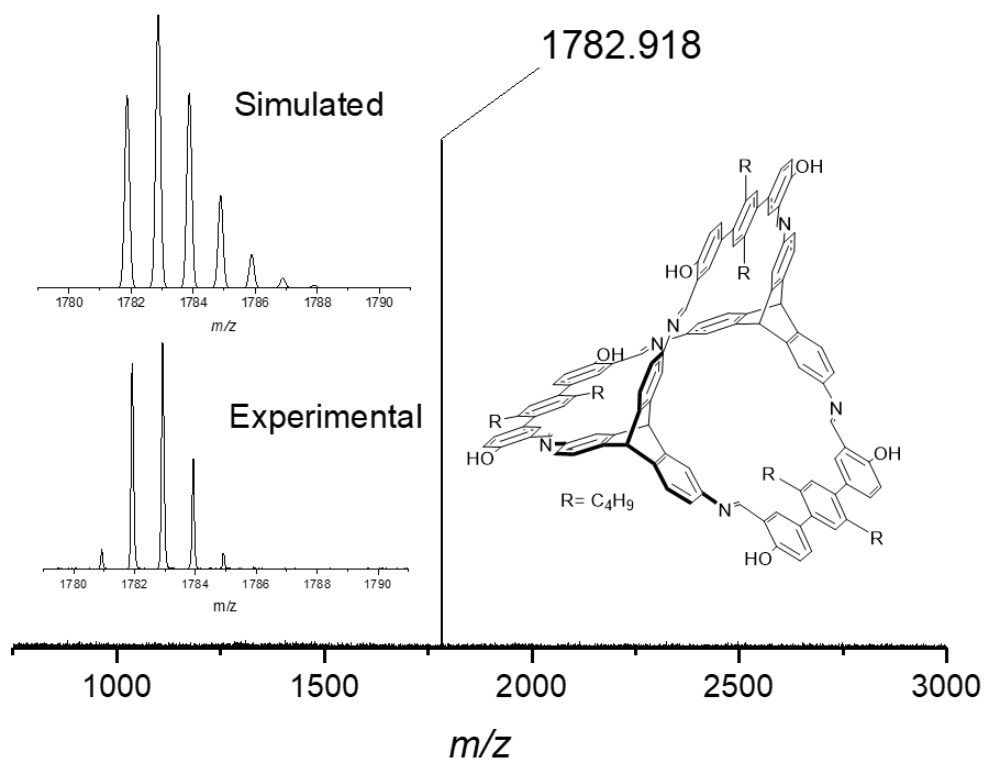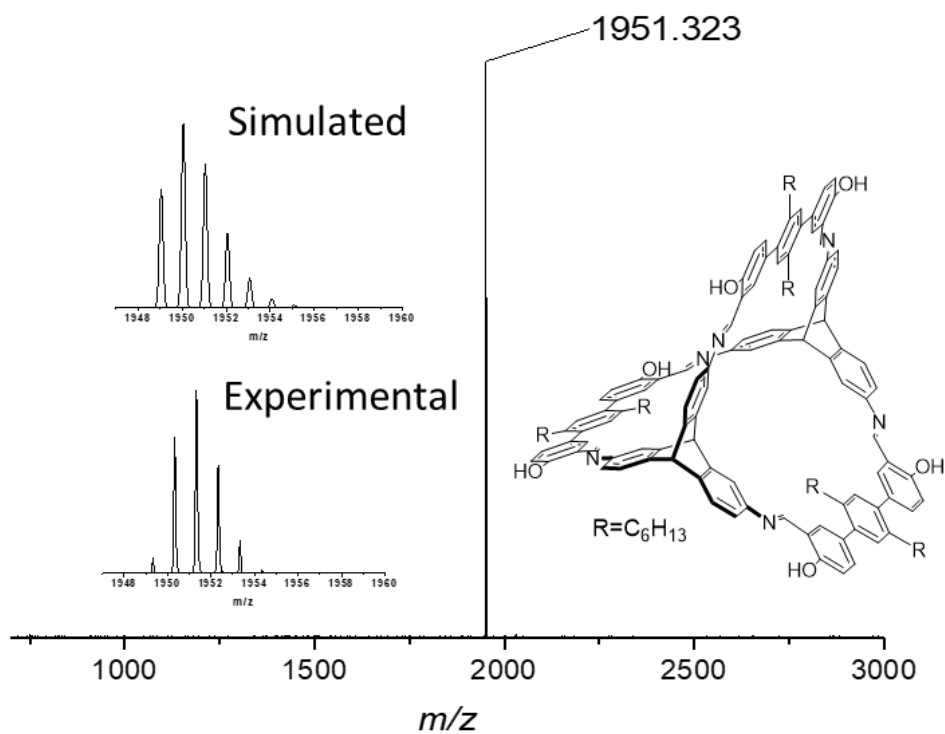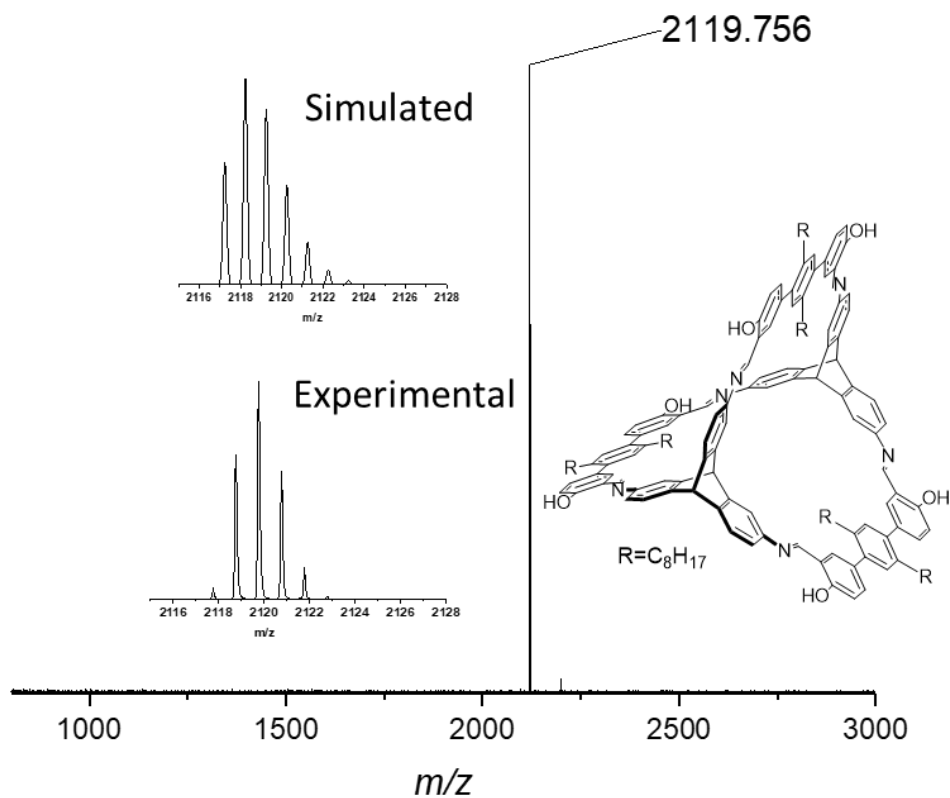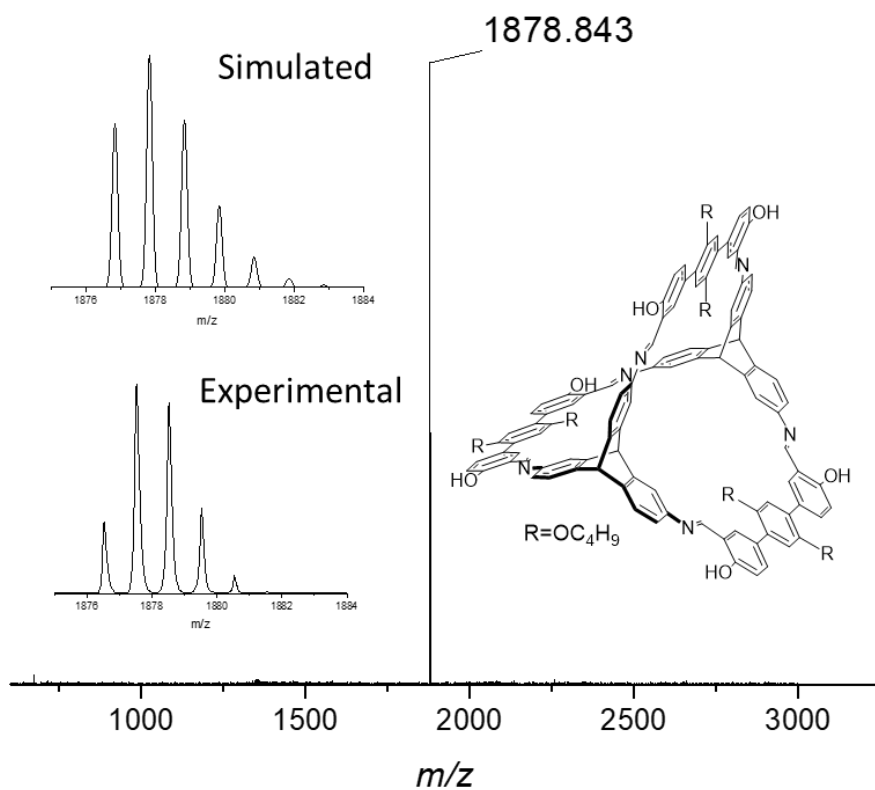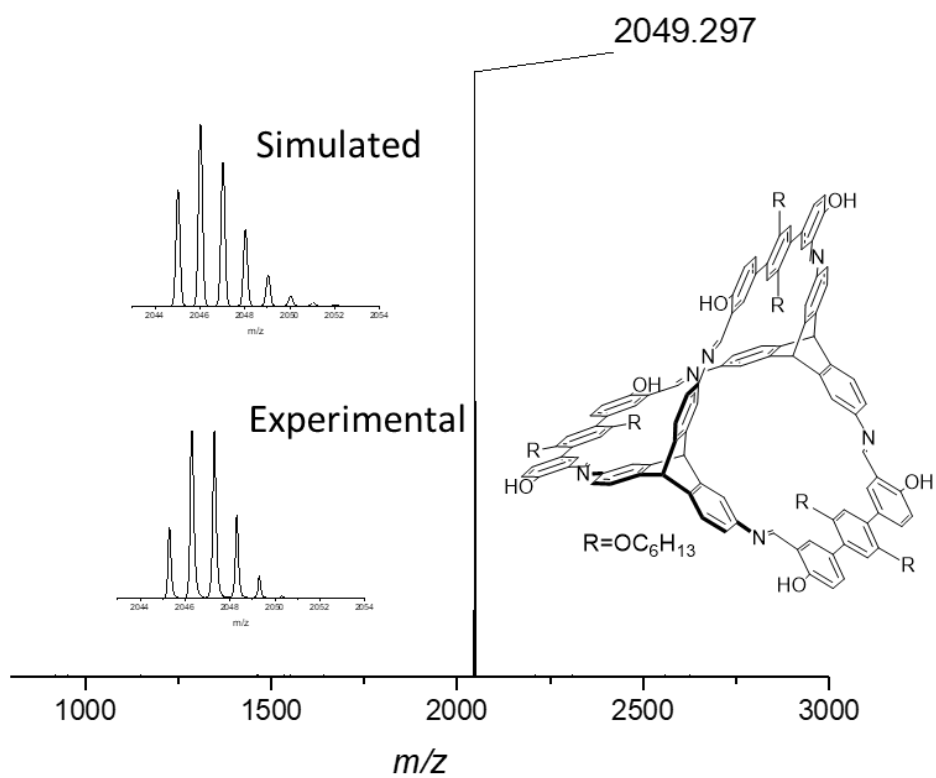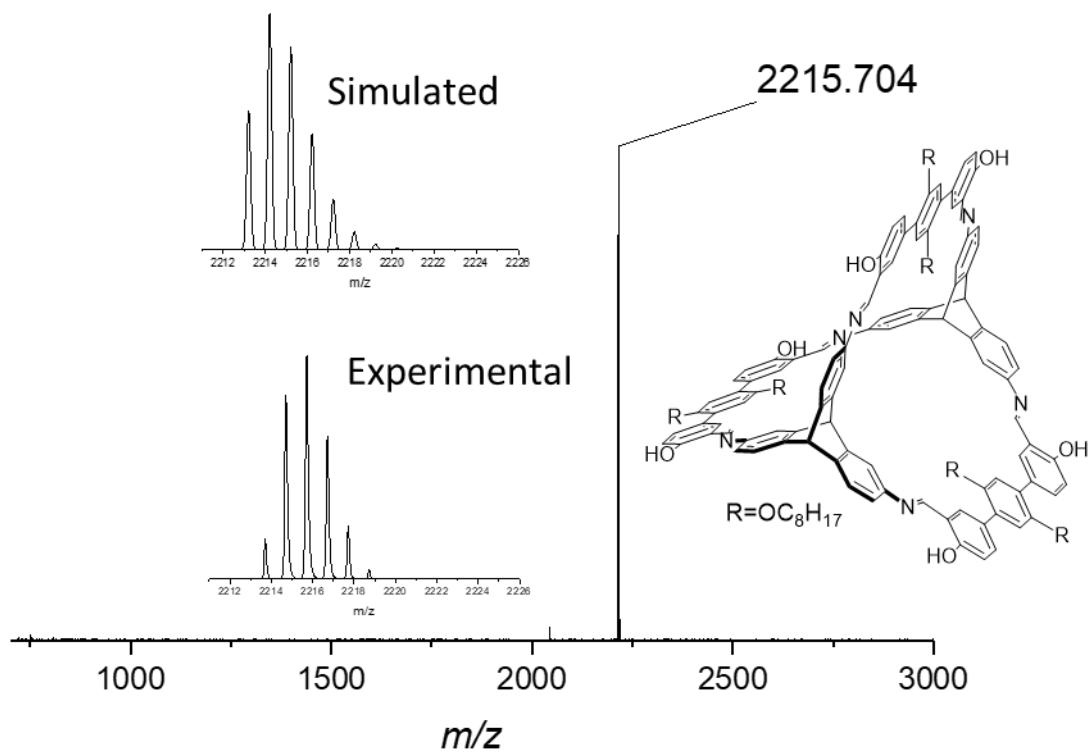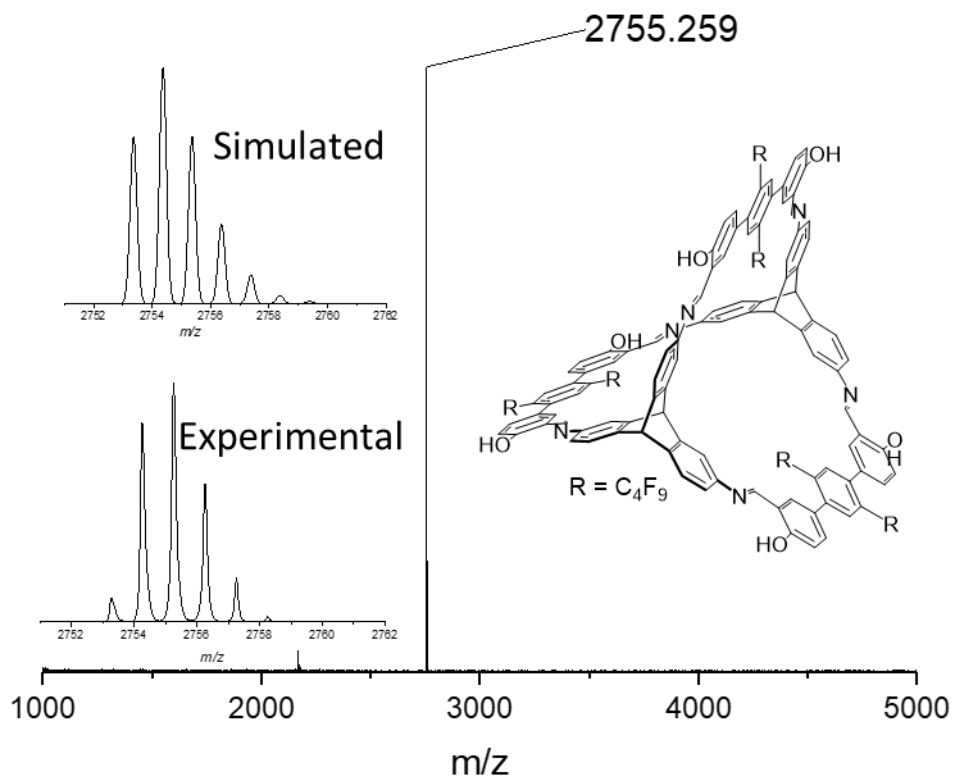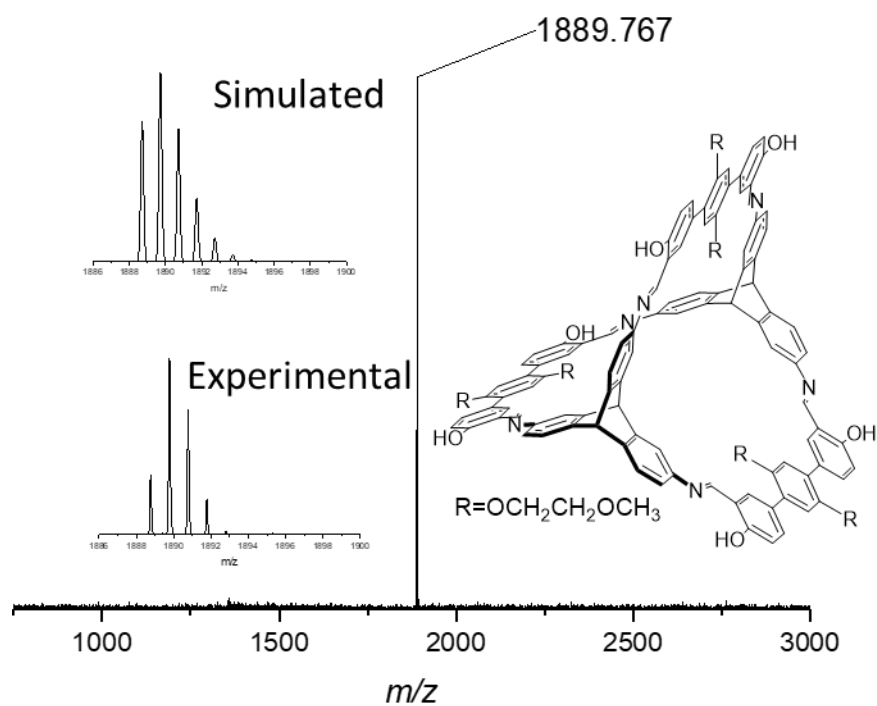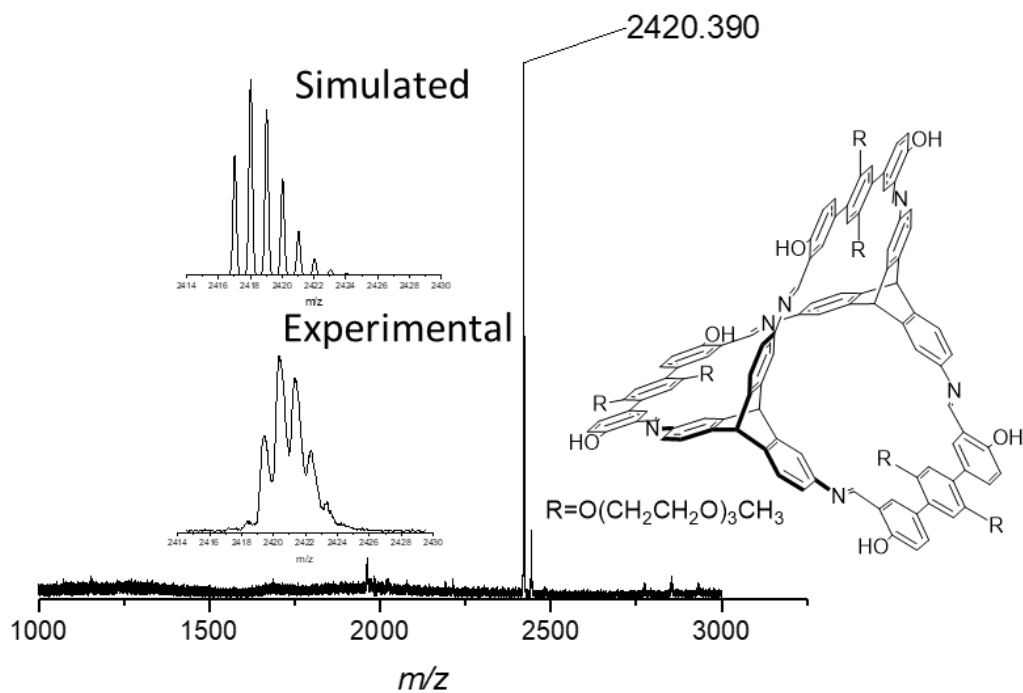**Figure 123**. Mass spectrum of cage **113** (MALDI-TOF, matrix: DCTB).
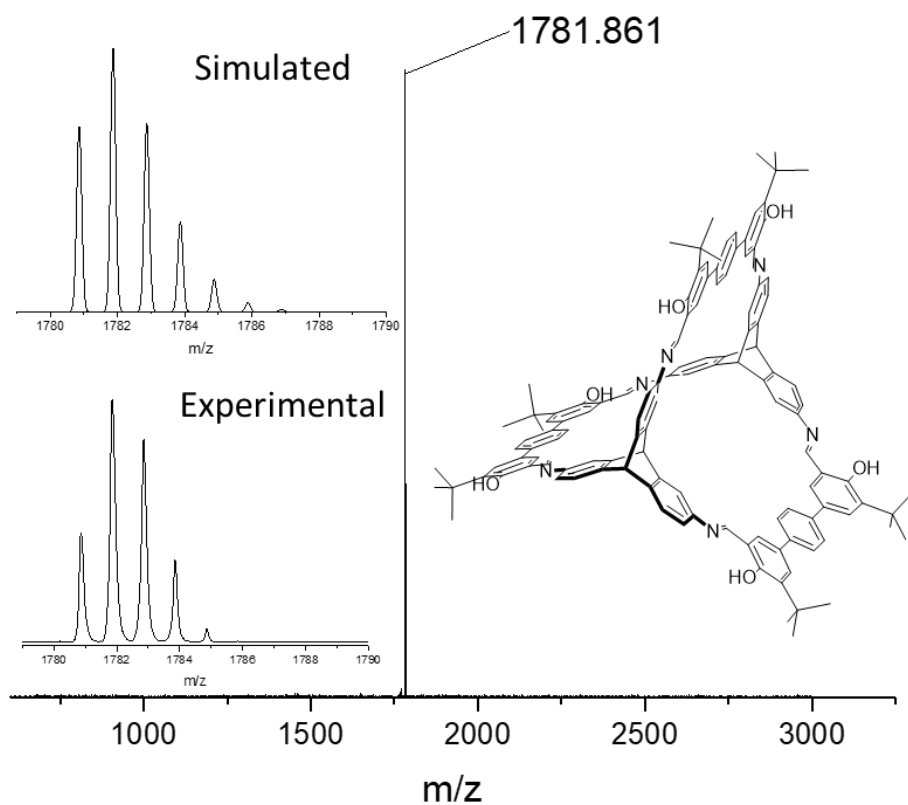
Figure 124. Mass spectrum of cage **114** (MALDI-TOF, matrix: DCTB).

7.3 Single Crystal Structure X-ray Data

Compound **131**
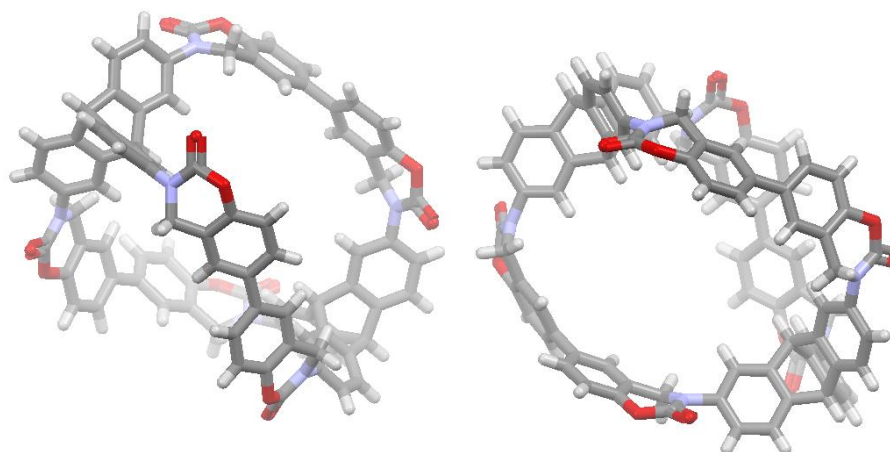
Table 12. Crystal data and structure refinement for **131**

Identification code	xh1sq
Empirical formula	$C_{88}H_{52}N_6O_{12}$
Formula weight	1385.35
Temperature	100(2) K
Wavelength	1.54178 Å
Crystal system	triclinic
Space group	P $\bar{1}$
Z	4
Unit cell dimensions	a = 18.7671(3) Å α = 76.070(2) deg.
	b = 19.4091(4) Å β = 87.338(2) deg.
	c = 27.7570(6) Å γ = 84.030(2) deg.
Volume	9757.6(3) Å^3
Density (calculated)	0.94 g/cm^3
Absorption coefficient	0.52 mm^{-1}
Crystal shape	needle
Crystal size	0.270 x 0.050 x 0.050 mm^3
Crystal colour	colourless
Theta range for data collection	2.4 to 68.6 deg.
Index ranges	-18≤h≤22, -23≤k≤19, -31≤l≤33
Reflections collected	99968
Independent reflections	34263 (R(int) = 0.0454)
Observed reflections	25908 (I > 2σ(I))
Absorption correction	Semi-empirical from equivalents
Max. and min. transmission	1.69 and 0.56
Refinement method	Full-matrix least-squares on F^2
Data/restraints/parameters	34263 / 5643 / 1909
Goodness-of-fit on F^2	1.11
Final R indices (I>2sigma(I))	R1 = 0.071, wR2 = 0.190
Largest diff. peak and hole	0.36 and -0.27 eÅ^{-3}

Compound **131**
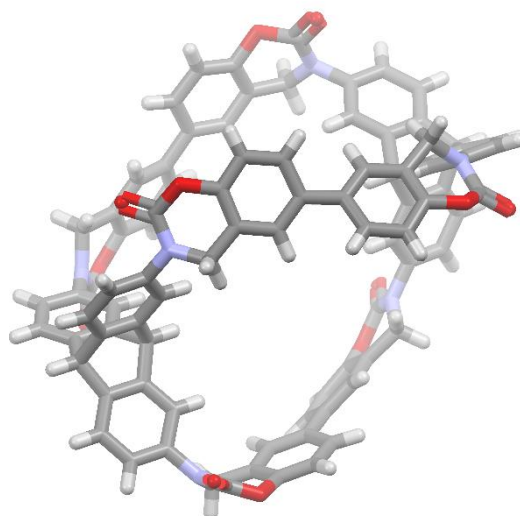
Table 13.Crystal data and structure refinement for **131**

Identification code	xh4sq
Empirical formula	$C_{88}H_{52}N_6O_{12}$
Formula weight	1385.35
Temperature	100(2) K
Wavelength	1.54178 Å
Crystal system	triclinic
Space group	P $\bar{1}$
Z	2
Unit cell dimensions	a = 15.638(3) Å $\quad \alpha =$ 83.365(13) deg.
	b = 16.513(3) Å $\quad \beta =$ 68.721(13) deg.
	c = 18.346(3) Å $\quad \gamma =$ 72.264(12) deg.
Volume	4204.6(13) Å^3
Density (calculated)	1.09 g/cm^3
Absorption coefficient	0.60 mm^{-1}
Crystal shape	needle
Crystal size	0.140 x 0.010 x 0.010 mm^3
Crystal colour	colourless
Theta range for data collection	4.7 to 44.5 deg.
Index ranges	$-14 \leq h \leq 14, -12 \leq k \leq 15, -16 \leq l \leq 16$
Reflections collected	22088
Independent reflections	6581 (R(int) = 0.2517)
Observed reflections	2555 (I I > 2$\square$(I))
Absorption correction	Semi-empirical from equivalents
Max. and min. transmission	1.70 and 0.59
Refinement method	Full-matrix least-squares on F^2
Data/restraints/parameters	6581 / 828 / 425
Goodness-of-fit on F^2	1.02
Final R indices (I>2sigma(I))	R1 = 0.125, wR2 = 0.279
Largest diff. peak and hole	0.35 and -0.31 eÅ^{-3}

Compound **105**
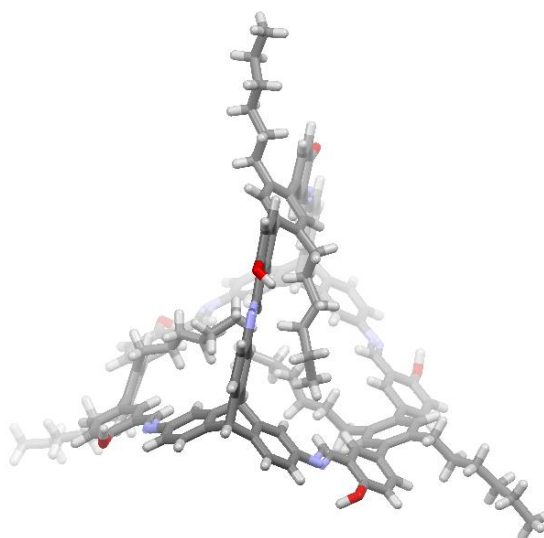
Table 14.Crystal data and structure refinement for **105**

Identification code	xh8sq
Empirical formula	$C_{136}H_{136}N_6O_6$
Formula weight	1950.50
Temperature	100(2) K
Wavelength	1.54178 Å
Crystal system	hexagonal
Space group	$P6_3/m$
Z	2
Unit cell dimensions	a = 19.6363(11) Å $\quad$ α = 90 deg.
	b = 19.6363(11) Å $\quad$ β = 90 deg.
	c = 27.033(2) Å $\quad$ γ = 120 deg.
Volume	9026.9(12) Å^3
Density (calculated)	0.72 g/cm^3
Absorption coefficient	0.34 mm^{-1}
Crystal shape	irregular
Crystal size	0.250 x 0.130 x 0.100 mm^3
Crystal colour	orange
Theta range for data collection	4.5 to 39.9 deg.
Index ranges	$-16 \leq h \leq 16, -16 \leq k \leq 14, -22 \leq l \leq 22$
Reflections collected	26337
Independent reflections	1861 (R(int) = 0.2757)
Observed reflections	927 (I > 2σ (I))
Absorption correction	Semi-empirical from equivalents
Max. and min. transmission	1.96 and 0.45
Refinement method	Full-matrix least-squares on F^2
Data/restraints/parameters	1861 / 493 / 277
Goodness-of-fit on F^2	1.47
Final R indices (I>2sigma(I))	R1 = 0.136, wR2 = 0.374
Largest diff. peak and hole	0.40 and -0.22 eÅ^{-3}

Compound **106**
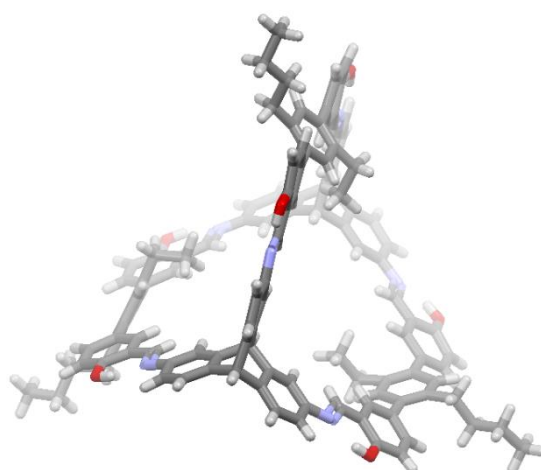
Table 15.Crystal data and structure refinement for **106**

Identification code	xh11sq
Empirical formula	$C_{148}H_{160}N_6O_6$
Formula weight	2118.81
Temperature	100(2) K
Wavelength	1.54178 Å
Crystal system	hexagonal
Space group	$P6_3$
Z	2
Unit cell dimensions	a = 19.697(3) Å α = 90 deg.
	b = 19.697(3) Å β = 90 deg.
	c = 26.904(5) Å γ = 120 deg.
Volume	9040(3) Å^3
Density (calculated)	0.78 g/cm^3
Absorption coefficient	0.36 mm^{-1}
Crystal shape	brick
Crystal size	0.197 x 0.149 x 0.146 mm^3
Crystal colour	orange
Theta range for data collection	7.1 to 36.7 deg.
Index ranges	-15≤h≤15, -12≤k≤15, -16≤l≤20
Reflections collected	20432
Independent reflections	2527 (R(int) = 0.1154)
Observed reflections	1339 (I I > 2σ (I))
Absorption correction	Semi-empirical from equivalents
Max. and min. transmission	1.71 and 0.65
Refinement method	Full-matrix least-squares on F^2
Data/restraints/parameters	2527 / 65 / 177
Goodness-of-fit on F^2	1.19
Final R indices (I>2sigma(I))	R1 = 0.097, wR2 = 0.281
Absolute structure parameter	-0.5(10)
Largest diff. peak and hole	0.27 and -0.34 eÅ^{-3}

Compound **110**
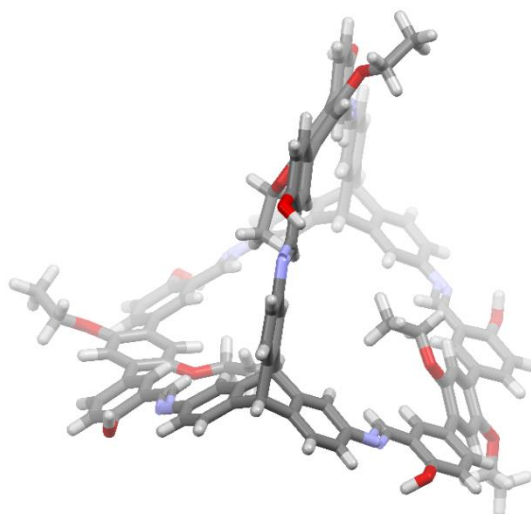
Table 16.Crystal data and structure refinement for **110**.

Identification code	xh14sq
Empirical formula	$C_{115}H_0N_6O_6$
Formula weight	1561.21
Temperature	100(2) K
Wavelength	1.54178 Å
Crystal system	hexagonal
Space group	$P6_3/m$
Z	2
Unit cell dimensions	a = 20.0491(14) Å α = 90 deg.
	b = 20.0491(14) Å β = 90 deg.
	c = 23.410(3) Å γ = 120 deg.
Volume	8149.2(15) Å^3
Density (calculated)	0.64 g/cm^3
Absorption coefficient	0.32 mm^{-1}
Crystal shape	brick
Crystal size	0.129 x 0.109 x 0.096 mm^3
Crystal colour	orange
Theta range for data collection	3.2 to 41.2 deg.
Index ranges	-15≤h≤17, -17≤k≤15, -17≤l≤20
Reflections collected	16148
Independent reflections	1852 (R(int) = 0.1881)
Observed reflections	1039 (I > 2σ (I))
Absorption correction	Semi-empirical from equivalents
Max. and min. transmission	2.41 and 0.53
Refinement method	Full-matrix least-squares on F^2
Data/restraints/parameters	1852 / 207 / 241
Goodness-of-fit on F^2	1.28
Final R indices (I>2sigma(I))	R1 = 0.107, wR2 = 0.316
Largest diff. peak and hole	0.26 and -0.25 eÅ^{-3}

Compound **111**
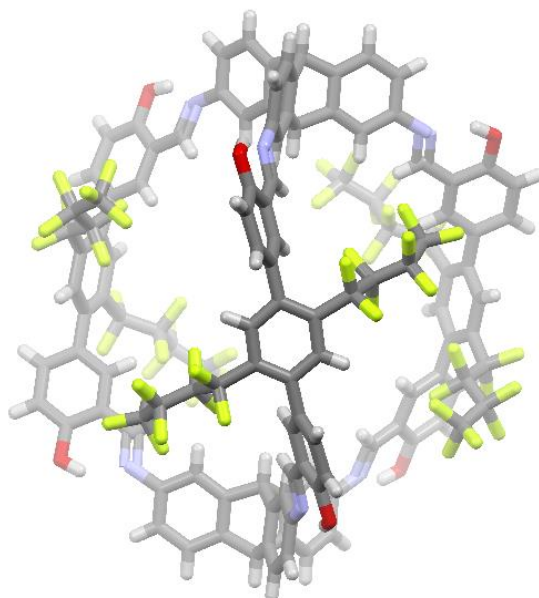
Table 17.Crystal data and structure refinement for **111**.

Identification code	xh13sq
Empirical formula	$C_{124}H_{58}F_{54}N_6O_6$
Formula weight	2753.76
Temperature	100(2) K
Wavelength	1.54178 Å
Crystal system	trigonal
Space group	R $\bar{3}$ c
Z	6
Unit cell dimensions	a = 19.0156(4) Å α = 90 deg.
	b = 19.0156(4) Å β = 90 deg.
	c = 64.026(2) Å γ = 120 deg.
Volume	20049.6(11) Å^3
Density (calculated)	1.37 g/cm^3
Absorption coefficient	1.23 mm^{-1}
Crystal shape	brick
Crystal size	0.143 x 0.134 x 0.098 mm^3
Crystal colour	yellow
Theta range for data collection	3.0 to 57.9 deg.
Index ranges	-20≤h≤20, -20≤k≤16, -70≤l≤56
Reflections collected	23997
Independent reflections	3106 (R(int) = 0.0757)
Observed reflections	1851 (I > 2σ (I))
Absorption correction	Semi-empirical from equivalents
Max. and min. transmission	1.97 and 0.64
Refinement method	Full-matrix least-squares on F^2
Data/restraints/parameters	3106 / 1091 / 392
Goodness-of-fit on F^2	2.88
Final R indices (I>2sigma(I))	R1 = 0.150, wR2 = 0.404
Largest diff. peak and hole	0.78 and -0.50 eÅ^{-3}

Compound **112**
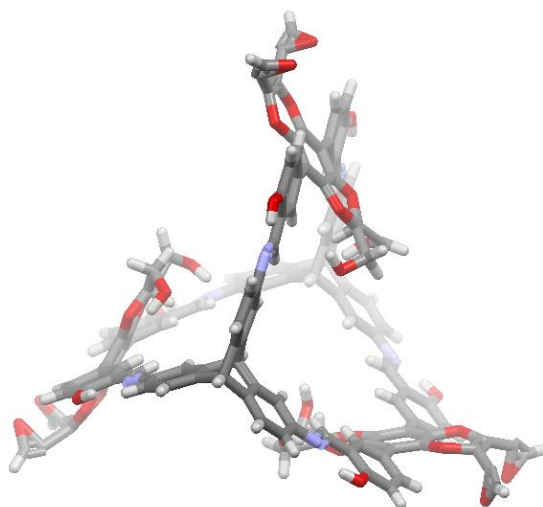
Table 18. Crystal data and structure refinement for **112.**

Identification code	xh15sq
Empirical formula	$C_{118}H_{100}N_6O_8$
Formula weight	1730.03
Temperature	100(2) K
Wavelength	1.54178 Å
Crystal system	hexagonal
Space group	$P6_3/m$
Z	2
Unit cell dimensions	$a = 19.2235(6)$ Å $\alpha = 90$ deg.
	$b = 19.2235(6)$ Å $\beta = 90$ deg.
	$c = 26.6855(11)$ Å $\gamma = 120$ deg.
Volume	8540.3(6) Å^3
Density (calculated)	0.67 g/cm^3
Absorption coefficient	0.33 mm^{-1}
Crystal shape	brick
Crystal size	0.221 x 0.102 x 0.076 mm^3
Crystal colour	orange
Theta range for data collection	2.7 to 51.1 deg.
Index ranges	$-17 \leq h \leq 19$, $-19 \leq k \leq 19$, $-26 \leq l \leq 15$
Reflections collected	23365
Independent reflections	3164 (R(int) = 0.0525)
Observed reflections	2021 ($I > 2\sigma(I)$)
Absorption correction	Semi-empirical from equivalents
Max. and min. transmission	1.35 and 0.67
Refinement method	Full-matrix least-squares on F^2
Data/restraints/parameters	3164 / 398 / 251
Goodness-of-fit on F^2	1.88
Final R indices (I>2sigma(I))	R1 = 0.133, wR2 = 0.442
Largest diff. peak and hole	0.51 and -0.36 eÅ^{-3}

Compound **118**
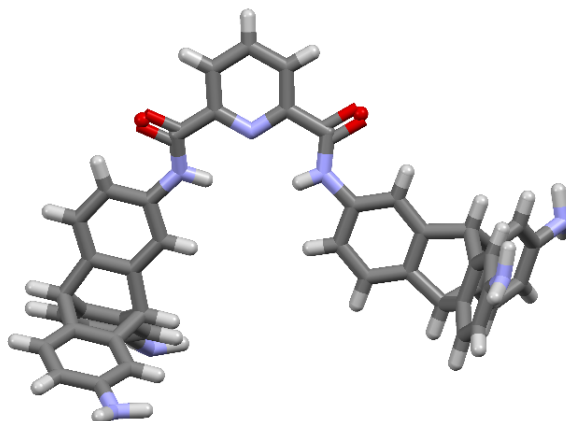
Table 19.Crystal data and structure refinement for **118**.

Identification code	xh2
Empirical formula	$C_{57}H_{55}N_7O_{4.50}$
Formula weight	910.08
Temperature	200(2) K
Wavelength	0.71073 Å
Crystal system	monoclinic
Space group	C2/c
Z	8
Unit cell dimensions	a = 23.5123(11) Å α = 90 deg.
	b = 18.7580(9) Å β = 110.5677(13) deg.
	c = 22.9427(11) Å γ = 90 deg.
Volume	9473.7(8) Å^3
Density (calculated)	1.28 g/cm^3
Absorption coefficient	0.08 mm^{-1}
Crystal shape	shim
Crystal size	0.440 x 0.080 x 0.070 mm^3
Crystal colour	colourless
Theta range for data collection	1.4 to 22.7 deg.
Index ranges	$-25 \le h \le 23, -20 \le k \le 20, -24 \le l \le 24$
Reflections collected	24533
Independent reflections	6372 (R(int) = 0.0489)
Observed reflections	3853 (I > 2σ (I))
Absorption correction	Semi-empirical from equivalents
Max. and min. transmission	0.96 and 0.89
Refinement method	Full-matrix least-squares on F^2
Data/restraints/parameters	6372 / 782 / 726
Goodness-of-fit on F^2	1.03
Final R indices (I>2sigma(I))	R1 = 0.061, wR2 = 0.153
Largest diff. peak and hole	0.23 and -0.17 eÅ^{-3}

8 Abbreviations

Ac	acetyl
Ar	aryl
ATR	attenuated total refraction
BET	Brunauer, Emmett and Teller model
Boc	*t*-Butyloxy carbonyl
Bu	butyl
Calcd.	calculated
COF	covalent organic framework
d	day
DCC	Dynamic covalent chemistry
DCM	Dichlormethane
DMF	Dimethylformamide
DMSO	Dimethyl sulfoxide
DOSY	diffusion-ordered spectroscopy
EA	Ethylacetate
EI	Electron Ionization
Eq	equivalents
ESI	electrospray ionization
EtOH	ethanol
g	gram
h	hours
Hex	hexyl
HMTA	Hexamethylenetetramine
HR	High resolution
IAST	ideal adsorbed solution theory
IR	infrared spectroscopy
IUPAC	International Union of Pure and Applied Chemistry
M.p.	melting point
MALDI	matrix-assisted laser ionization
MeCN	acetonitrile
MeOH	methanol

min	minutes
MS	mass spectra
NBS	*N*-bromo succinimide
NMR	Nuclear magnetic resonance
nm	Nanometer
Oct	octyl
ppm	parts per million
PXRD	Power X-Ray Diffraction
R_f	ratio of fronts
RT	room temperature
SEC	Size Exclusion Chromatography
SEM	Scanning Electron Microscope
t	*tert*
TGA	Thermogravimetric analysis
THF	tetrahydrofuran
TLC	Thin layer chromatography
TOF	Time of flight
TFA	Trifluoroacetic acid